A STUDY OF DROPLET BEHAVIOUR IN A CENTRIFUGAL CONTACTOR

by

M.J. AHMED

A thesis submitted to the University of Aston in Birmingham

for the degree of Doctor of Philosophy

Department of Chemical Engineering,
University of Aston in Birmingham

December 1976

SUMMARY

A study has been made of droplet hydrodynamics in a single stage, liquid-liquid centrifugal contactor. The literature describing the droplet formation mechanisms, droplet velocities and droplet sizes under both gravity and centrifugal conditions has been reviewed.

A single stage centrifugal contactor with transparent end-plates was designed and operated with four typical liquid-liquid systems covering a range of 1.5 cp to 38.37 cp viscosity values. Operational characteristics, e.g. flooding curves, hold-up and discharge rates were measured. Droplet phenomena were analysed using high speed cine photography.

Droplets were formed either by single drop detachment, jetting or spray; the regime could be predicted in terms of a dimensionless group $(\frac{\rho_d U_N}{\Delta\rho\,\omega R})$. Three types of flooding were observed, that is shaft flooding, rim flooding and capacity flooding, dependent on the phase ratios and the back pressure.

Mathematical models were derived to predict,

(a) droplet volumes,

and (b) droplet velocities.

Experimental values gave reasonable agreement with the values obtained from models.

Recommendations are made for the application of the results to practical design.

CONTENTS

LIST OF FIGURES

ACKNOWLEDGEMENTS

The author wishes to acknowledge the assistance of the following:

Professor G.V. Jeffreys for allowing me to pursue the project in the Department of Chemical Engineering and for his guidance and supervision throughout the duration of the work;

Dr. G.J. Mumford for his continual invaluable assistance during the project;

My father, Captain S.S. Khan, for his guidance and inspiration throughout my life.

I am also indebted to the:-

(i) Members of the Technical Staff and Photographic Section of the Department, in particular Mrs. Melling.

(ii) S.R.C. for the scholarship during 1973-74.

(iii) Miss Freeman for the typing of the thesis.

1. INTRODUCTION

1.1 LIQUID-LIQUID EXTRACTION

Liquid-liquid extraction is a method of affecting the separation of two components of a liquid phase by the addition of another immiscible liquid. As a developed technique it is of recent origin although Goerring[1] described a process for the production of acetic acid from dilute solution by extraction with a suitable solvent, much earlier. Advantages of using this method of separation have been comprehensively discussed elsewhere[2]: the principle ones being:-

(1) As an alternative to direct methods where these are more expensive. Examples of this are:

(a) Separation of close-boiling liquids.

(b) Separation of liquids possessing poor relative volatility.

(c) As a less expensive alternative to the separation of high-boiling point liquids where high-vacuum, or molecular distillation is necessary.

(d) As a substitute for evaporation, and

(e) As a substitute for fractional crystallisation.

(2) As an alternative means of separating liquids where direct methods fail. This includes:

(a) The separation of heat-sensitive substances.

(b) The separation of azeotropic mixtures, and

(c) The separation according to chemical type, where boiling points overlap.

(3) As an alternative means of separation to the expensive chemical methods.

1.2 CLASSIFICATION OF EXTRACTION EQUIPMENT

Because a wide variety of devices have been proposed, studied and developed, an exact classification of extraction equipment is not possible. Arnold[3] observes that the parameter, rate of energy input per unit volume of the continuous phase, can be used to classify the contactors. However, the most acceptable classification involves division into those in which the process is continuous, and those in which the extraction takes place in discrete stages.

(i) Stagewise In this type of equipment the liquids are mixed, extracted and separated in discrete stages. Examples are the mixer settlers, plate columns and some centrifugal extractors. (Chapter 2).

(ii) Differential In the case of differential equipment all the operations are achieved by continuous countercurrent contact between the liquids in one equipment containing any number of stages. A further sub-classification of differential extracting equipment is often made. This is as shown in Fig.1.1. The classification in Fig.1.1 is based on the type of force employed to disperse a liquid as droplets in the other, i.e. gravitational or centrifugal.

The classification into differential and stagewise, like the classification reported by Arnold[3], however, leads to centrifugal extractors being classified in both categories. Thus the Podbielniak variant is a differential type, whereas the Robotel can be classified

as stagewise. This is discussed further in Chapter 2.

1.2.1 Stagewise Extractors

Although some of these form the oldest type of extraction equipment, they offer some advantages compared with the other types and have, therefore, remained popular over the years. The essential operations in this type of equipment are:-

(i) Contacting of the immiscible liquids to enable transfer of solute to occur - the driving force being the deviation from equilibrium, and

(ii) The separation of the resulting liquids by settling and coalescence.

If the operation is batchwise, both the contacting and settling may be achieved in the same vessel. On a continuous basis, it is customary, though not essential, to have two vessels, hence the term 'mixer-settlers'. In stagewise centrifugal extractors there are two separate chambers, one for contacting and the other for the settling. This is discussed in Chapter 2 in greater detail.

Industrial separations generally require more than one extraction stage and this leads to the establishment of a cascade by connecting together a number of stages.

1.2.2 Differential Extractors

This type of extractor provides continuous counter-current contact between the two immiscible liquids. The equivalent of many stages may be built into one piece of equipment, without the intermediate removal of the phases. Parallel or co-current flow is conceivable, but if the latter were used, the device would provide at best the equivalent of one

ideal stage and fall into the category of line-mixers. Since multistage effects are generally required, counter-current flow is the rule.

Counter-current flow of the liquids occurs by virtue of the difference in densities. When flow is by gravity the equipment takes the form of towers with the light-liquid entering at the bottom and flowing upwards, and heavy-liquid entering at the top and flowing downwards. Alternatively, if centrifugal force is the driving force then the direction of flow is radial with respect to the axis of revolution, which may be either horizontal or vertical dependent on the type of extractor.

1.2.2.1 Types of Differential Extractors

There are essentially three types of differential extractor:-

(i) Non-mechanically Dispersed

This variety of column represents the simplest class of extractor for liquid-liquid extraction. Their initial cost is relatively low and maintenance is negligible, provided they do not require frequent cleaning. However, despite requiring a low floor area, they are relatively low in efficiency and are most suitable where the number of theoretical stages required is low. The principal examples of this class of equipment are the baffle plate, spray, packed and perforated columns.

(ii) Mechanical Agitated

With non-mechanical agitated extractors the energy available for break-up of the dispersed phase, is limited to the potential energy at entry, and hence to the difference in density between the phases.

The degree of dispersion, and consequently the performance, can therefore be considerably enhanced by the expenditure of a relatively small amount of mechanical energy. However, this type of extractor has the disadvantage of high maintenance costs, particularly where handling corrosive liquids. The main examples of this class of equipment are the rotary agitated and pulsed columns.

(iii) Centrifugal

Whereas in the two preceding cases the flow is maintained by gravity, in this type of extractor centrifugal forces are used to induce very rapid flow of the phases. The magnitude of such forces, up to 10,000 g's, enables very high velocities to be achieved and increased settling rates. The centrifugal extractor is by comparison with other equipment a relatively recent innovation and consequently its mode of operation is not well understood.

1.3 CENTRIFUGAL EXTRACTORS

The centrifugal extractor despite being a new type of extraction equipment, offers several advantages over other extractors. Although originally developed for the pharmaceutical industry[4] the centrifugal extractor has diversified into other industries, e.g. Nuclear industry[5].

1.3.1 Advantages and Disadvantages of Centrifugal Extractors

The main advantages of the centrifugal extractor can be summarised as:-

(i) Space-saving. Because of its comparatively small size there is substantial saving in space.

(ii) Inventory of solvents and associated losses are reduced. Generally the solvents are expensive and any reduction is, therefore, desirable.

(iii) Continuous extraction processes reach steady-state quickly with relatively little of the raffinate requiring reprocessing to bring it to final specifications.

(iv) Short residence time. This may be an essential requirement as in the processing of anti-biotics and uzanium separation, where chemical and physical degradation can occur if the residence time is large.

(v) Phases with very small density differences can be separated and the extractor can work over a wide range of phase ratios and viscosities.

(vi) Operations at low or high temperatures are easily handled.

(vii) The equipment can be operated at above atmospheric pressure and since it is hemetically sealed, there are no losses due to evaporation or diffusion, and no contamination due to atmospheric pollutants.

(viii) Hazardous liquids, corrosive or radioactive, liquids are safely processed.

(ix) There is no air in the equipment to cause oxidation of process liquids.

The chief disadvantages of centrifugal extractors are:-

(i) Because it is a precision built unit the capital cost is higher than other extractors: the extent to which this is so can be judged from Table 1.1.

(ii) The operating and maintenance costs also compare less favourably with most other types of extractor, and

(iii) The volumetric capacity is lower than other types of extractor.

1.3.2 Comparison with Other Extractors

The comparison of the centrifugal extractor with other extractors given above is very qualitative. However, Table 1.1 shows that it compares very favourably with the other extractors[6].

Although the first commercial application of a centrifugal extractor was in the anti-biotic field[4],[7],[8],[9],[10],[11], it is increasingly being used in other fields. One such is the processing of radioactive materials where its performance has been highly acclaimed [5],[12],[13],[14]. Another is in chemical and refinery applications [15],[16],[17]. Fox[18] has reported that for lube oil extraction the centrifugal extractor compares favourably with gravity towers.

1.3.3 Mechanism of Centrifugal Extractor Operations

Despite their usage over 40 years there is little data on operating mechanisms beyond that which is available in manufacturers catalogues[19] and basic patents[20-41]. Some workers, notably Ponikarovetal[42] and Garfullin et al[43] have provided a little data on the internal hydrodynamics of centrifugal extractors. However, this has been limited to flow discharges in centrifugal fields that is up to 3000 g's, whereas in commercial extractors it is often in the range 4000 - 10,000 g's. Fundamental work on the centrifugal extractor has been confined to:-

(i) Flow discharges in centrifugal fields[42],[43].

(ii) Operational characteristics[44], and

(iii) Comparison[14],[45] with other liquid extraction equipment using the same system in each case.

Droplet phenomena i.e. drop formation, drop velocities and drop size distribution, and mass transfer coefficients in centrifugal extractors have not been investigated hitherto. For example, the only data on droplet

TABLE 1.1

COMPARISON OF EXTRACTORS[6]

size in a centrifugal extractor is given by Fox[18] who postulates that it should be forty to seventy times less than that found in gravity towers. No correlation of drop size exists, nor any mechanism of drop formation at orifices and nozzles in centrifugal fields.

There is no reliable concept of a 'theoretical stage' of a centrifugal extractor: the present day concept renders it to be dependent, among other factors, on:-

(i) The liquid system used, and

(ii) Speech of rotation,

for the same machine.

1.4 SCOPE OF THIS WORK

In view of the paucity of basic data regarding centrifugal extractor operation an attempt has been made in this work to elucidate the hydrodynamics. The primary objectives can be summarised as:-

(i) Designing, developing and commissioning of a centrifugal extractor of Podbielniak variant, and

(ii) Conducting hydrodynamic studies on the extractor using various liquid systems.

2. CENTRIFUGAL EXTRACTORS

2.1 HISTORICAL REVIEW

Centrifugal extractors are a relatively new type of liquid-liquid contactor. The earliest description of a centrifugal extractor was given by Placek[31],[32] who obtained U.S. patents in 1933. (Fig.2.1). The device covered by these patents contained a spiral passageway through which the liquids and vapours flowed countercurrently. In the first of these two patents, the device was described as a distillation and fractionation apparatus: in the second it was described as a means of carrying out physical and chemical changes.

Cautor[27],[28] and Podbielniak[20] also obtained U.S. patents for centrifugal apparatus but which were never built. The practical application of the patents came as a result of the second World War, because of problems arising in the production of pencillin in large quantities. Miner[4] exploited the potential of a centrifugal extractor for pencillin production and the first model was built in co-operation with Podbielniak Inc. in 1945.

Since then many variants have appeared[29],[30],[33-41],[46-47], some of which are novel whilst others differ only in the country of manufacture. Leaving aside those extractors used only for research, the main commercial contactors are:-

(i) Podbielniak

(ii) Quadronic

(iii)Alfa-Laval

(iv) Robatel

(v) Lurgi-westafalia

FIG. 2.1. PLACEK'S SPIRAL PASSAGEWAY DESIGN (31)

(vi) Luwesta

(vii) Savannah River

Of these extractors the data available in the literature is only derived from Podbielniak (pup model) or the Quadronic designs. By data is meant the operational characteristics, i.e. flooding, hold-up and pressure of the inlet/outlet streams. Also included is information on the 'theoretical stages' concept.

2.2 PODBIELNIAK

2.2.1 Mechanical Design

Although the Podbielniak extractor has undergone many modifications, the earliest design consisted of a cylindrical drum 26" in diameter with two spirally grooved end-plates to accommodate a 50.29m metal strip (0.00038 m thick and 0.1524 m wide). The metal strip were wound into the grooves of the end-plates to form an unperforated passageway of thirty turns through which the liquid streams were able to flow counter-currently. The cylindrical drum was rotated on a horizontal axis at a speed of 5000 r.p.m. with the liquids entering through mechanical seals. The total combined stream capacity was 3 gal/min. The next modification contained perforations in the spiral passageway and doubled the capacity.

Other variants followed and the present day Podbielniak machines have evolved through three stages:-

(i) With spiral passageway

(ii) With perforated spiral passageway, and

(iii) With perforated concentric cylinders.

The most recent design is given in Fig.2.3.

FIG. 2.2. WALTER J. PODIELNIAK CONICAL CENTRIFUGAL COUNTER CURRENT CONTRACTOR [20]

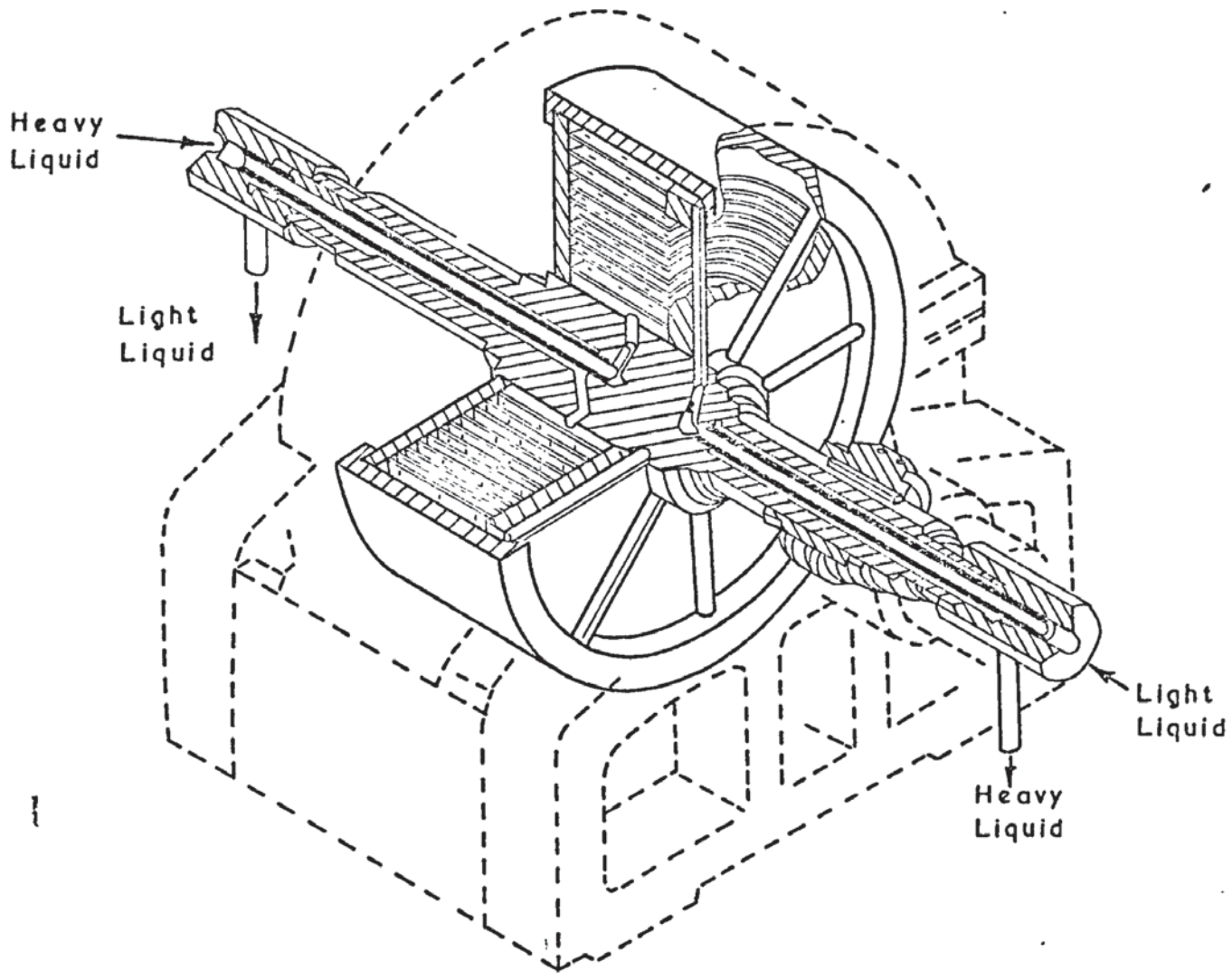

FIG. 2.3. PODBIELNIAK EXTRACTOR

2.2.2 Mode of Operation

The mode of operation of all Podbielniak extractors is similar, despite their having different internals. The heavy liquid is fed axially through the rotary seals at one end of the extractor so that it enters the contacting section of the rotor near the axis. The light liquid is fed through a similar seal at the opposite end of the extractor and into a small channel. From this channel the liquid is conducted to the periphery of the rotor. Centrifugal force acting on the heavy liquid causes it to be thrown towards the periphery and the light liquid to be thrown inwardly to the centre. The heavy liquid leaves the rotor near the periphery from which it is conducted to the axis and then out of the extractor; the light liquid leaves from the shaft and out of the extractor.

2.3 QUADRONIC

The Quadronic extractor, another member of the continuous differential class, bears a strong external resemblance to the Podbielniak in that its axis of rotation is horizontal and the means of affecting transportation of liquids to and from the extractor are similar, as is the general assembly. However, there is a fundamental difference in the internals which are better designed.

All the centrifugal extractors are usually 'tailor made', in that they are designed for a specific process. This renders such extractors inflexible. The Quadronic extractor is claimed to combine the functions of counter-current pluri-stage extractor and that of countercurrent pluri-stage phase separators[33-36]. It is also claimed[37-39] to be versatile in that it can perform complex functions, such as quadruple

component extraction, equally well as the single phase separations.

The basic Quadronic design is illustrated in Fig.2.3.

2.4 α-LAVAL CONTACTOR[48]

Like the Podbielniak extractor this continuous-differential extractor had its origins in the manufacture of pencillin. However, it differs in that it employs a vertically rotating shaft. Although both types were initially employed in the antibiotics field subsequent models have diversified in other branches of industry[48].

2.4.1 Mechanical Design

The detailed construction is shown in Fig.2.4. Within the main shell of the bowl there are a series of concentric cylinders each fitted with helical guides on the outside. These threads have an opposite pitch on alternate cylinders to cause the liquid to channel alternately from the top to the bottom and vice versa, between successive cylinders. Between each cylindrical space there are holes which allow the liquids to pass from one cylinder to the next; the light phase flows inward and heavy phase flows outward. These transfer holes are alternately at the top or bottom corresponding to the upward and downward threads on the cylinders.

The cylinders rest on a bottom-plate and are capped by a top-plate and the whole rotating unit is completed by a hood and the main locking ring.

2.4.2 Mode of Operation

Fig.2.5. illustrates the liquid path through a cross-section of

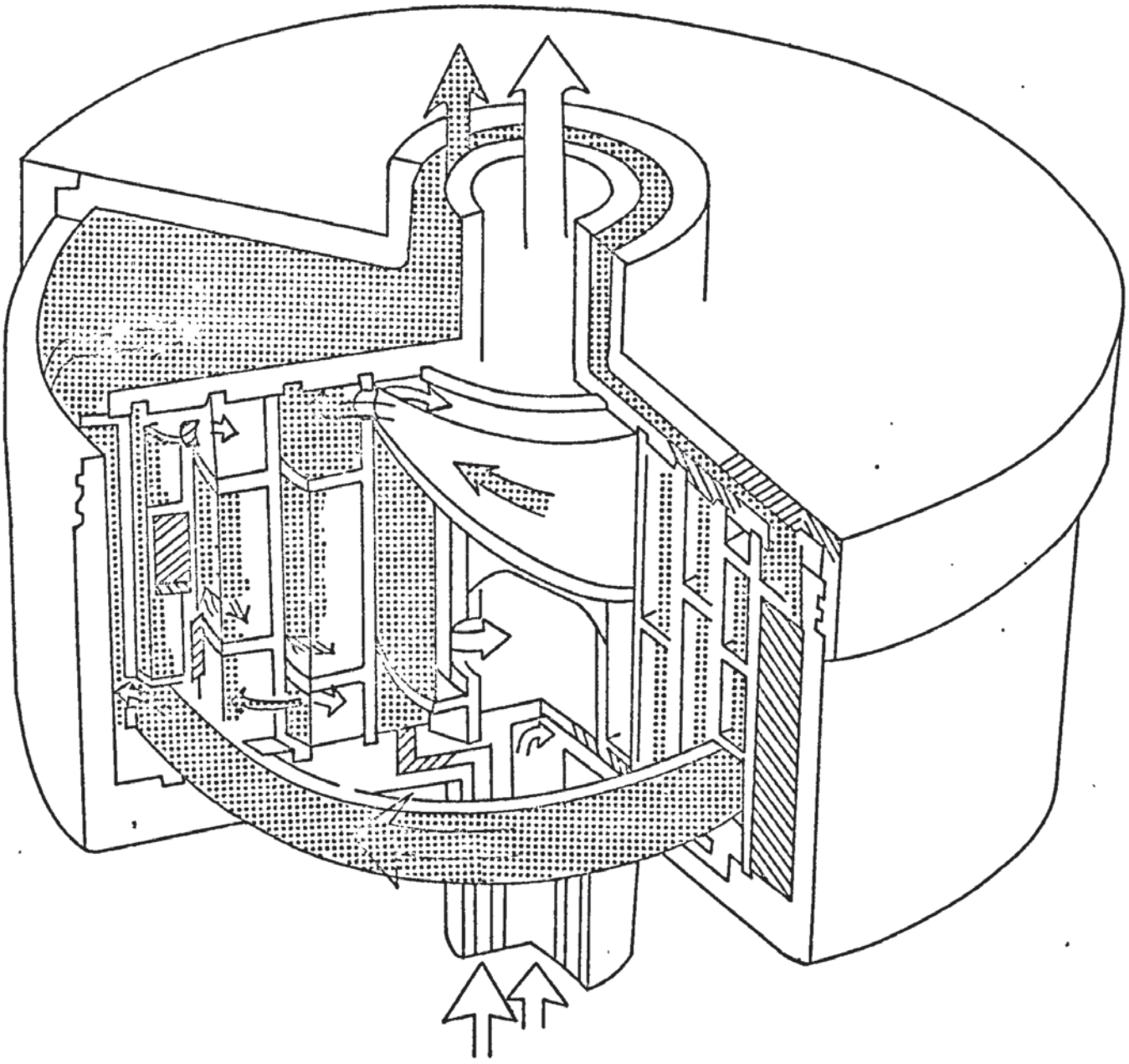

FIG·2.4· ∝-LAVAL CENTRIFUGAL EXTRACTOR.

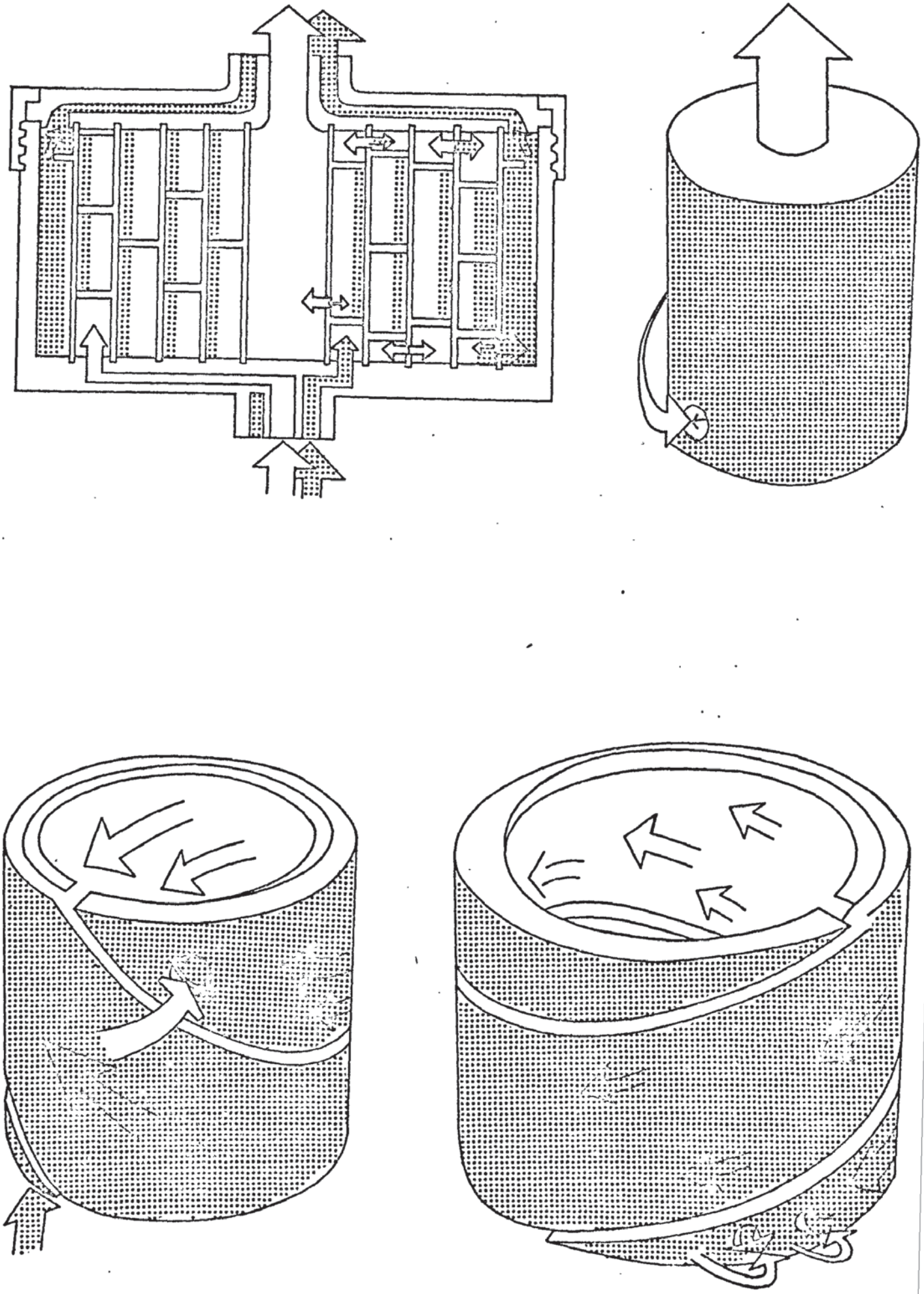

FIG. 2.5. . ∝-LAVAL EXTRACTOR SHOWING LIQUID PATH

the extractor. The heavy phase liquid is fed to the bowl by means of an annular fed tube and enters the extraction bowl near the centre of rotation. The light phase also enters via the hollow feed spindle, and by means of channels in the bottom-plate, is conducted to the outside of the bowl. Under the action of centrifugal force the heavy phase liquid will be displaced outwards, and conversely the light phase will be displaced inwards to the centre. Mass transfer takes place in the holes by mixing, and in the transfer channels by combined shear force and turbulence in the interface. The flow paths are illustrated by Fig.2.5.

After the main solute transfer has occurred, the stream enters the separating zone where further transfer takes place to remove the last traces of heavy phase. The light liquid is then discharged through the exit.

The heavy phase enters the outside compartment where the last traces of solvent are stripped. It then passes over the top of the upper plate and to the heavy phase outlet.

2.5 ROBATEL EXTRACTOR

2.5.1 Mechanical Design

The Robatel extractor differs from the other centrifugal extractors in its similarity to gravity-mixer-settlers. It consist of two separate chambers, each performing differing functions, i.e. mixing and settling. Of the two sections, the settling chamber has a volume considerably greater than the mixing chamber ($\simeq$ 5:1). Because of presence of two chambers, this extractor is clearly a development from bowl centrifuges.

Essentially the extractor comprises a vertically rotating bowl,

FIG. 2.6. FIVE STAGE NON NUCLEAR CENTRIFUGAL EXTRACTOR LX. 525 TYPE ( )

located in a round casing. (Fig.2.6). All fixed and rotating parts and discs are removable via the top: the drum is fixed to a cover plate bearing instrumentation and the complete assembly and the motor are supported on a large base plate.

The physical stages in the extractor number up to seven in conventional extractors, and up to eight in the nuclear models. Each stage consists of an annular part including the two separate chambers. The smaller mixing section contains a circular groove located between ranges of radial blades; the larger separating sections act as a normal centrifuge.

2.5.2 Mode of Operation

In operation, the radial blades in the mixing section act as a centrifugal two stage pump, while the brake effect of the fixed disc represents the intermediate return part. This induces simultaneously a general pumping effect of the liquids from the other adjoining stages to the annular settling chamber, and intense turbulent mixing in the liquid due to the difference in relative velocities between fixed and moving surfaces.

In order to maintain suitable levels, the setting annular chamber is terminated by a circular over-flow which is the outlet of the light phase to the next stage. The heavy phase outlet consists of a series of axial and radial channels, drilled into the periphery of the cylinders so as to lead the liquid up to a second overflow at the entrance to the preceding stage,located on a slightly larger diameter.

2.6 AKTIEBOLOGET EXTRACTOR[41]

The Aktiebologet extractor, invented in Sweden, bears some similarity

FIG. 2.7.1. AKTIEBOLOGET EXTRACTOR [41]

FIG. 2.7.2.

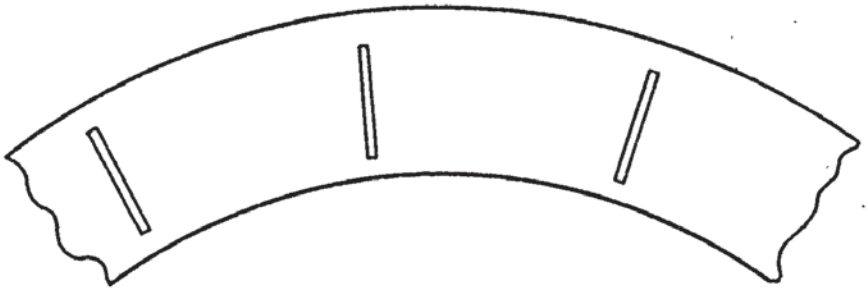

FIG. 2.7.3.

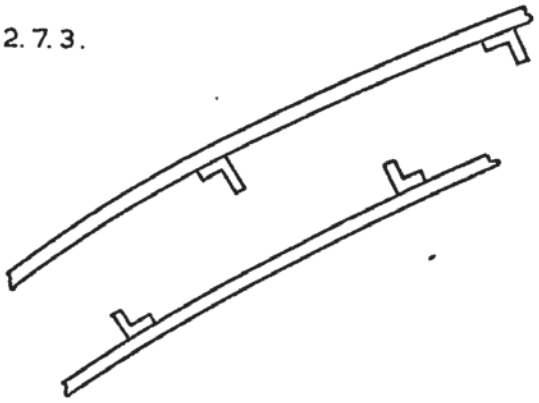

FIG. 2.7.4.

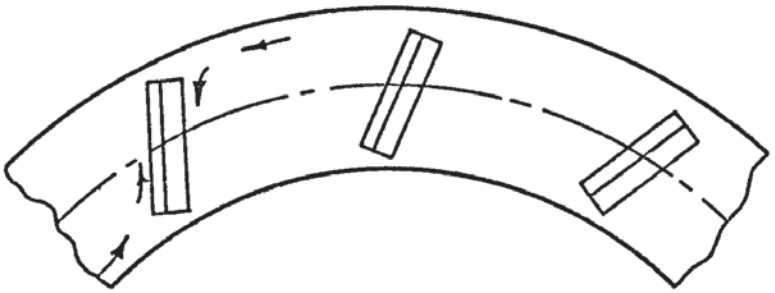

to both the Podbielniak and Robatel extractors. A number of cylindrical mantels, in the interior of the rotor, are fitted in between the end parts and at mutual distances decreasing towards the periphery of the rotor. Interfaces existing between the cylinders communicate with others by means of holes at their end. It is claimed[41] that extraction efficiencies are improved by providing the channel walls with means to create whirls in the fluid flowing through the channels. These means are the employment of obliquely and axially angled protrusions, and the holes in channel walls, as shown by Figs.2.7.2, 2.7.3 and 2.7.4.

The mode of liquid feeding is similar to that employed in other vertically rotating centrifugal extractors, i.e. by means of a hollow spindle. The distinguishing factors are the direction of rotation, and the existence of the differently angled protrusions.

2.7 OTHER COMMERCIAL TYPES OF CENTRIFUGAL EXTRACTOR

2.7.1 Luwesta Extractor

The Luwesta extractor is characterised by a vertical flexible shaft, by annular weirs with or without skimmers used for liquid withdrawals according to the usual centrifugal clarifier practice, and by use of three completely discrete mechanical stages to mix and settle liquids in countercurrent flow. Thus the Luwesta is analgous to a countercurrent cascade of three gravitational mixer-settlers. The rated output is 50 gal/min. It is also reported[49] that the number of stages is approximately three times the efficiency factor of the machine, which is known to vary with liquid systems used.

2.7.2 Lurgi-Westfalia

This is reported[50] to be a stagewise extractorwith two or three discrete mechanical stages, where mixing and separations are accomplished

separately. No mass transfer or hydrodynamic data have been published.

2.7.3 Russian/Czechoslovak Models

A Russian equivalent of the Luwesta extractor has been reported[47]. This is reported to have only two mechanical stages in comparison with three in the Luwesta. No performance data are available. Furthermore, two Podbielniak types of extractor have also been reported[51,52]. (Fig.2.8).

Use of a Czechoslovakian[46] extractor has also been reported for the production of pencillin. It appears, however, to be a copy of early models of the Podbielniak extractor used for antibiotic processing. No further details are available.

2.7.4 Savannah River Model

This single stage extractor is discussed in 2.8.1.

2.8 RESEARCH CENTRIFUGAL EXTRACTORS

2.8.1 Nuclear Processing Models

The separation and recovery of highly radioactive substances by solvent extraction is often limited by the solvent degradation products formed during the extraction process. An extractor with a residence time of seconds rather than minutes is, therefore, necessary. Two centrifugal extractors have been developed that achieve this requirement

(i) Jenning[12] has developed a mini-centrifugal extractor for the separation of uranium and plutonium from other fission products. As in Robatel extractor, the prototype of the mini-centrifugal extractor comprises mixing and settling chambers of 5/8" dia. and 1.0" dia. respectively. The unit housing was made of 'Plexiglass'

FIG. 2.8. A RUSSIAN CENTRIFUGAL EXTRACTOR[51]

to permit observations of internal phenomena.

A standard 4-bladed paddle and baffle arrangement was used in the design of the mixing chamber. The two liquids are fed near the centre of the shaft and the mixed phases are discharged through a duct into the centrifuge bowl. In the latter they are separated into clear zones, the heavy phase near the wall and the light phase near the rotor. The light phase overflows the circular weir near the axis and is conducted via a radial duct to the next stage. The heavy phase passes through ports near the periphery of the bowl into the heavy-phase weir. The heavy phase overflows the weir and is discharged to the next stage.

Residence times of 3-6 seconds per stage are claimed for the prototype at a mixer speed of 5000 r.p.m. and centrifuge bowl speed of 2500 - 7000 r.p.m. For the final design, consisting of 16 stages, a residence time of 2 seconds/stage and a hold-up of 10 ml/stage are reported. Efficiencies of 90 - 95% are claimed[53,54] for both the prototype and final design.

(ii) Webster-Clark[13] report a stage-wise countercurrent centrifugal extractor for the processing of natural or enriched uranium.

Initial[53,54] research centrifugal extractors with 4 and 5 inch diameter bowls, have led[13] to the development of a 10 inch diameter centrifugal extractor. The extractor comprises a bowl, 10 inches in diameter and 18 inches in length, suspended inside a casing beneath the driver motor. The motor shaft extends through the bottom of the bowl and ends in a 4-blade mixing paddle, 6 inches in diameter. The upper 4½ inches of the bowl contain the centrifugal weir and discharge ports. From this

FIG. 2.10 SECTION VIEW OF THE 10 - INCH CENTRIFUGAL CONTACTOR

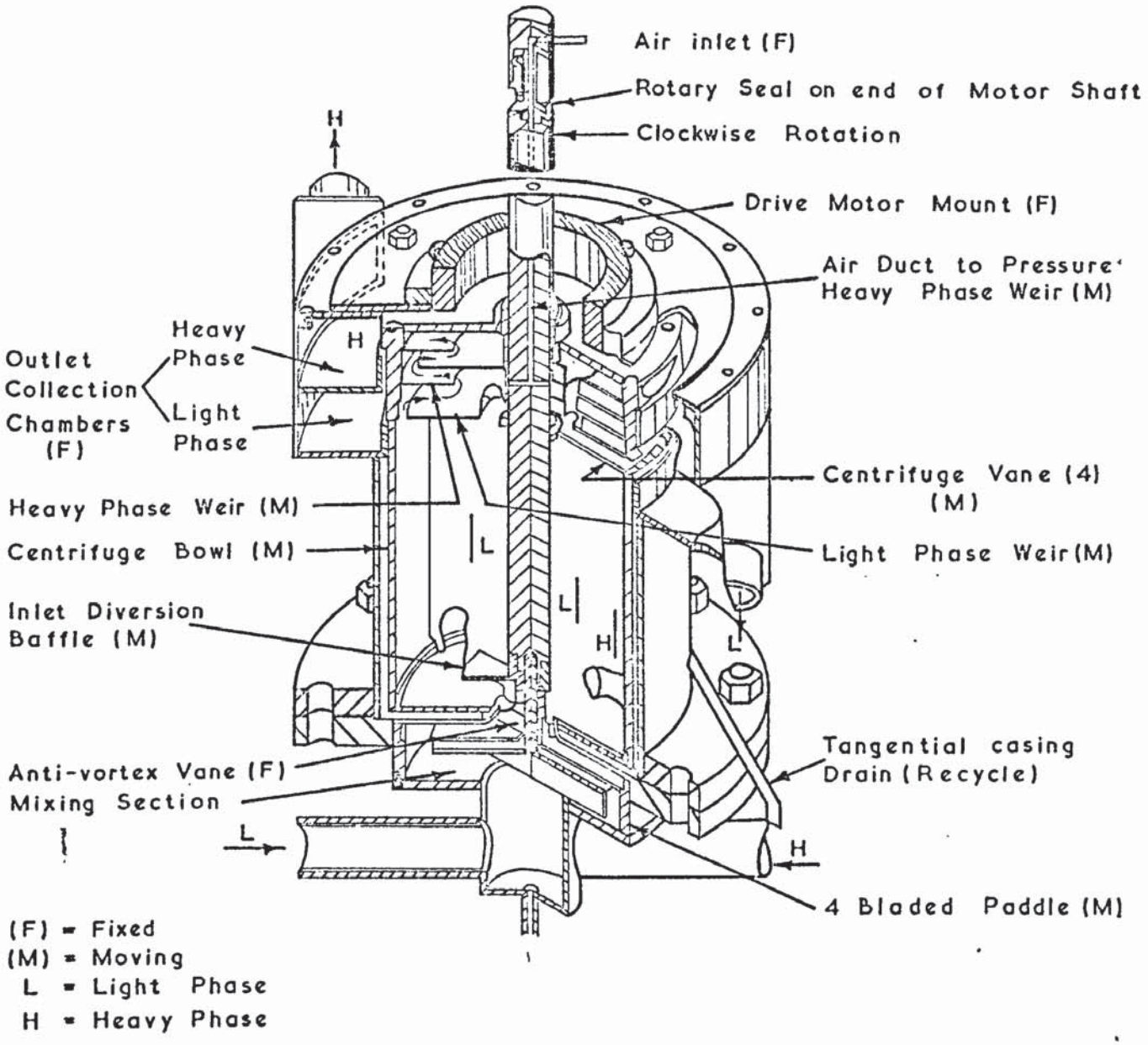

FIG. 2.9 SECTION VIEW OF THE 10 - INCH CENTRIFUGAL CONTACTOR

section to the base of the bowl comprises the settling section.

Excellent efficiency is claimed with uranium total flows of at least 40 g.p.m.

The extractor design is as shown in Fig.2.9

2.8.2 Non-Nuclear Research Centrifugal Extractors

The only known extractor of this type is of Russian origin [43]. It is of Podbielniak type but with portholes for the observation of droplet phenomena inside the rotor. No detailed diagrams are available.

However, due to its particular relevance to this work a more detailed discussion of this extractor is given in Chapter6 .

2.9 COMPARISON AND CRITICAL REVIEW OF CENTRIFUGAL EXTRACTORS

2.9.1 Classification

The above centrifugal extractors can be classified into the following categories:-

(a) Continuous Differential. viz, those involving no discrete mechanical stages. Examples are the Podbielniak, Quadronic and Alfa-Laval extractors.

(b) Stagewise, viz, those in which the processes of mixing and settling are carried out in separate chambers. This generally results in the use of weirs and a liquid seal. Examples are the Luwesta, Robatel and Savannah River extractors.

(c) Hybrid, viz, those in which characteristics of both (a) and (b) are exhibited. An example is the Aktiebologet extractor.

(d) Research Extractors for investigative studies only.

Since the last type includes (a), (b) and (c) it is only necessary to compare these types. The most important difference between the three types is in the internals and the classification has been made on this basis.

2.9.2 Comparison/Discussion

Comparison of the various designs is restricted since the amount of data available is small and covers certain designs only.

Since the basic principles of centrifugal extraction, that is the utilisation of centrifugal force to mix and then separate two liquid streams, is common to all contactors differences only arise from the varying geometrical configurations. Thus the different types are not necessarily mere imitations with sufficient modifications to circumvent the Patent Laws. However, Podbielniak reports that a Russian model is an imitation of a Podbielniak extractor.

The continuous differential type (e.g. the Podbielniak) can be considered as an extraction column, such as the perforated tray or other gravitational extractors, wrapped around a shaft and rotated to expose its contents to centrifugal force. Like the countless tray design variations which have been invented for the gravitational columns, many variants of elements have been proposed for use in a centrifugal extractor. The original extractor used unperforated spiral sheets, which were succeeded by perforated sheets and then, for reasons of greater flexibility, ease of fabrication and efficiency, by perforated concentric cylinders. In summary, the different variants of the continuous differential type of centrifugal extractor may be regarded as fundamentally similar but with different geometrical arrangements in the search for greater efficiency,

better volumetric capacity and lower cost. Another factor is the desirability of achieving short residence times per stage. This is analogous to the wide variety of agitated Rotating Disc Contactor (R.D.C.) column designs.

Stagewise countercurrent centrifugal extractors can be considered as analogous to a mixer and a settler wrapped around a shaft with separation being accelerated by the action of centrifugal force.

Most of the stagewise centrifugal extractors employ annular weirs and skimmers whereas the differential variants have mechanical seals. This has a direct bearing on the limitations of any particular centrifugal extractor. In the former case the heavy and light liquids enter the rotor at or near the centre of the shaft, with little pressure required. The weir overflow or skim-off radius for the heavy liquid must be mechanically adjusted according to the density difference of the two liquids; the overflow radius for the light-liquid must similarly be adjusted mechanically, both according to the density difference and according to desired location of the principal interface within the rotor. Effluent streams are also ejected with little pressure.

In the differential type of extractor, introduction and withdrawal of all liquids are affected via mechanical, rotory seals which results in a hermetically tight rotor. The advantages of operating under hermetic conditions are principally concerned with pressure balances of the extractor. Such conditions are also reported[49] to improve extraction processes carried out at high temperatures.

3. DROPLET FORMATION AND THEIR VELOCITIES

3.1 INTRODUCTION

Mass transfer in a centrifugal contactor occurs by process of diffusion and for practical contactors is estimated from the expression,

$$N = K A_i . \Delta C \qquad (3.1)$$

To affect greater mass transfer for a given ΔC, the interfacial area A_i needs to be increased. In practical contactors this is achieved by converting the dispersed phase into droplet form in the continuous phase. The behaviour of the droplet, therefore, is of great importance in understanding of liquid-liquid contactors. Whereas various aspects of droplet phenomena for gravity towers have been extensively studied, this is not the case for centrifugal contactors. As a result of this, the basic fundamentals of single/multiple droplet/(s) behaviour under gravity conditions are reviewed - the intention being that they may be extended to centrifugal conditions.

3.2 DROPLET FORMATION AT ORIFICE/NOZZLES

3.2.1 General

The design of orifice, or nozzle, and the wettability of the materials of construction with respect to the dispersed phase are important factors governing the formation of droplets at an orifice. If the orifice is a hole drilled through a plate which is preferentially wetted by the dispersed phase, at low velocities the latter will spread to form a pool. The droplets then break away from the pool at a rate dependent upon the rate of flow. At higher velocities the behaviour is similar to the more common case where the dispersed phase

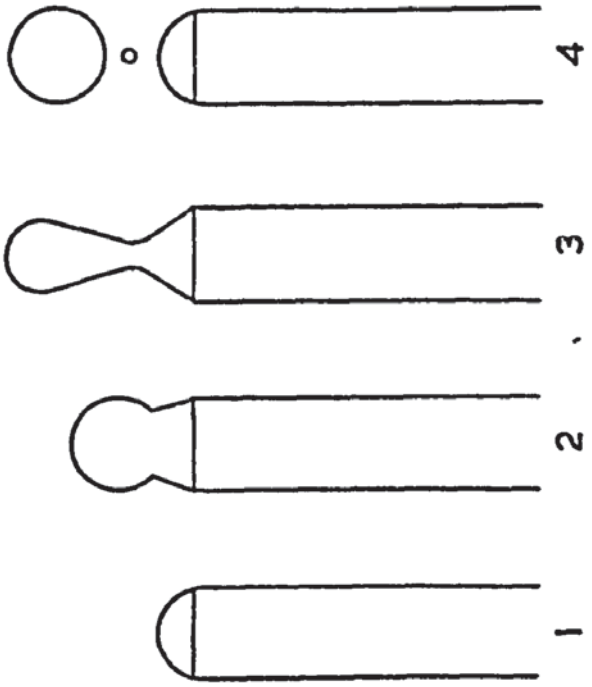

FIG. 3.1. SEVERAL STAGES OF DROP FORMATION

does not wet the surface[55 - 60]. To produce a reasonably uniform drop size under gravity conditions, the following factors are important:

(a) The dispersed phase should not preferentially wet the surface[61,62].

(b) The nozzle velocity should be < 0.5 ft/s[63].

(c) The orifice should have a sharp chamferred end[2].

Obviously for centrifugal contactors the condition (b) seems to be inapplicable since the velocities will have to be considerably higher to allow the flow into the contactor.

3.2.2 Mathematical Models at $U < U_J$.

The Hayworth-Treybal model[64] is based on the assumption that drop detachment does not occur until,

(i) The velocity of the droplet is larger than the velocity of the dispersed phase in the nozzle, and

(ii) The buoyancy force exceeds the force due to interfacial tension.

In addition, the force due to kinetic energy of the dispersed phase is considered to be significant and incorporated in the correlation. The latter along with other principal models are shown in Table 3.1.

Null and Johnson[65] report a correlation based on the two groups,

$$\left(\frac{D^2 \Delta\rho}{8\gamma}\right)^{\frac{1}{2}} \text{ and } \left(\frac{8 v_c'^2 \rho_d}{Dg \ \Delta\rho}\right)^{\frac{1}{2}} \qquad (3.2)$$

This model is derived from a consideration of the geometry of the forming droplets. Two stages have been identified, i.e. the growth at the tip and the detachment stage. Before leaving the orifice the

TABLE 3.1 DROP FORMATION MODELS FOR $U_T > U$

AUTHOR(S)	EQUATIONS	Eqn. No.	REMARKS
Heyworth and Treybal[64]	$(V_F + 4.11\times10^{-4} V_F^{2/3}(\frac{\rho d v_c'^{12}}{\Delta\rho}) = 21\times10^{-4}\frac{\gamma D_N}{\Delta\rho}) + 1.069\times10^{-2}(\frac{D_N^{.747}.v_c'^{1.365}\mu_c^{.186}}{\Delta\rho})^{3/2}$	3.3	Originally given in chart form to enable direct estimation of drop diameter.
Harkins and Brown[66]	$V_o = \frac{\pi D_N \gamma}{\Delta\rho g}.F$	3.4	The factor F introduced to allow for the fraction of drop remaining at nozzle.
Ryan[67]	$V_F = V_o\left(1 + \frac{1.38g\Delta\rho D}{\gamma F}\cdot\frac{D_N U_N}{2U_T} - \frac{2.3\rho_d D_N U_N^2}{2F\gamma}\right)$	3.5	This requires knowledge of U_T which has to be calculated from the Kintner equation.
Rao et al[69]	$V_F = \frac{C}{A} + B(t/A - \frac{1}{A^2}) + (\frac{B}{A^2} - \frac{C}{A})Ce^{-At}$	3.6	For low viscosity liquids.
	$V_F = V_S + Q(\frac{2AD_S}{B})^{\frac{1}{2}}$	3.7	For highly viscous liquids.
Hertjes et al[70]	$V_F = V_{eq} + V_{rl}$ where $V_{rl} = 2T\,t_{rl}$ where $T_2 t_{rl}^2 + (T_8 - T_9)t_{rl} - T_7 = 0$	3.8	This model requires evaluation of terms T_2, T_7, T_8 and T_9 which in turn require complex calculations. The method is therefore, rather cumbersome.

TABLE 3.1 (contd...)

AUTHOR(S)	EQUATION	Eqn. No.	REMARKS
Izard[71]	$F_{Net} = \Delta\rho V_i g + 4/3 \left(1-\frac{\rho d}{2\rho_d+\rho_c}\right)\left(\frac{m^2}{\rho_d \pi R_N^2}\right) - 2\pi\gamma X_i \sin\phi_i - \frac{2M\mu_c}{\rho_d X_{max}}\left(\frac{\mu_c + 1.5\,\mu_d}{\mu_c + \mu_d}\right)$	3.9	
Harris[110]	$V_F = bU_N^2 V_F^{2/3} = QFD_N + b_6 D_N^{1.2} U_N^{0.57} - 0.03\, D_N$	3.10	A modification of the Hayworth-Treybal model
Scheele and Meister[72]	$V_F = F \left[\frac{\pi\sigma D_N}{g} + \frac{20\mu Q D_N}{D_e^2 g} - \frac{4\rho_d Q U_N}{3 g} + 4.5(Q^2 D_N^2 \rho_d / (\Delta\rho g)^2)^{1/3}\right]$	3.11	The model is based on resolution of forces acting on the drop and accounts for fractional volume increase during the necking stage of drop formation.
Vashist[73]	$V_F = F \left[\frac{\pi D_N \sigma}{g\Delta\rho} + \frac{0.2\mu_c Q D_N}{D_e^2 g\ \Delta\rho} - \frac{V_F \rho_d U_N^{2.2}}{2D_e g\Delta\rho} + 4.5\left(\frac{Q^2 D_N 2\rho\ \sigma}{(g\Delta\rho)^2}\right)^{1/3}\right]$	3.12	Based on the above model, it is modified from the kinetic energy term.

drop is considered as a sphere at top and tangent to a right truncated cone passing through the circumference of the nozzle.

Harkins and Brown[66] give an expression for the prediction of drop volume from a consideration of buoyancy and interfacial forces. A factor, F, is introduced to allow for the fraction of the pendant drop remaining at the nozzle when the drop detaches. This is neglected in both the above models.

A semi-empirical equation, equation 3.5, is presented by Ryan[67]. The constants in this equation are evaluated from the Hu-Kintner[68] correlation.

Rao et al[69] report two models, one of which is applicable to a highly viscous continuous phase. Both models, again consider droplet formation to be a two stage process,

(i) The expansion stage when the drop inflates at the nozzle tip, and
(ii) The detachment stage when the drop rises, forms a neck and finally detaches from the nozzle.

The first stage is assumed to end when the buoyancy force equals the interfacial force; the second stage is assumed to terminate when the former exceeds the latter force. The final volume is, therefore, the summation of static drop volume and of the volume during the detachment stage.

Izard's[71] model is based on the calculation of the shape of a droplet forming at the nozzle tip by means of a pressure balance over the drop interface and the use of a force balance to determine if any portion of the forming droplet could break away. The

expression for the net force thus obtained is integrated at the profile as volume of revolution and as surface of revolution about the vertical axis of symmetry between the origin and a horizontal section of the drop. The resulting expressions give the volume and the surface area above that section.

A more sophisticated and practical model is reported by Scheele and Meister[72]. This is based on the resolution of all the forces acting on the drop. An important advance on other models is the inclusion of the accurate means of evaluating the volume during the necking stage of the droplet formation. It is also claimed[72] to work for a large number of systems.

Vashist[73] presents a modified form of the Scheele and Meister model; the difference is in the kinetic force term where allowance is made for the effect of induced continuous phase motion by increasing the coefficient on the velocity term from 2.0 to 2.2.

The model of Hayworth and Treybal[64] is considered to be of a limited value because deviations greater than 300% from the experimental values are reported[65,69,74]. The inadequacies in this model arise because it is based on a force balance made by expressing the various constituent forces acting on the drop as fraction of total drop volume. This cannot be wholly justified since the instant at which forces act is not known and the volume is continually changing. The model also neglects the influence of viscosity of the continuous phase which is known to be important[75].

Rao et al's model[69], though more accurate than both the Hayworth-Treybal[64] and Null and Johnson[65] models, is considered to have

inherent deficiencies. The influence of dispersed phase viscosity is not considered and the maximum size of drop is limited to static size, which is only true for low flow rates.

The semi-empirical correlation due to Ryan[67] has only specific applicability and generalisation to systems other than those investigated is not recommended. Heertjes et al's model[70] is impractical for two or more systems since it involves repetitive calculations for each system. Similarly the Izard model[71] has limitations in that the drop profile has to be known before the volume can be evaluated. The model is, however, reported[71] to give better results than other models. This is shown in Figs. 3.2(a) and (b).

The Scheele and Meister[72] model is derived by the resolution of forces acting on the drop. The significant contribution of this approach is the inclusion of a volume term to account for the fractional increase during the necking stage of the drop formation. Further discussion of this model and its application to drop formation in a centrifugal field is presented in Chapter 6.

3.2.3 Drop Formation at $U \geq U_J$

The correlations discussed in 3.2.2 are limited to conditions when the velocity is below jetting velocity. At higher values of velocity, the mechanism of inflation of the drop until the buoyancy force overcomes the interfacial tension and the drop detaches, no longer holds.

Although original studies[77 - 80] associated with the jet formation employed gaseous jets, models are also available for liquid-

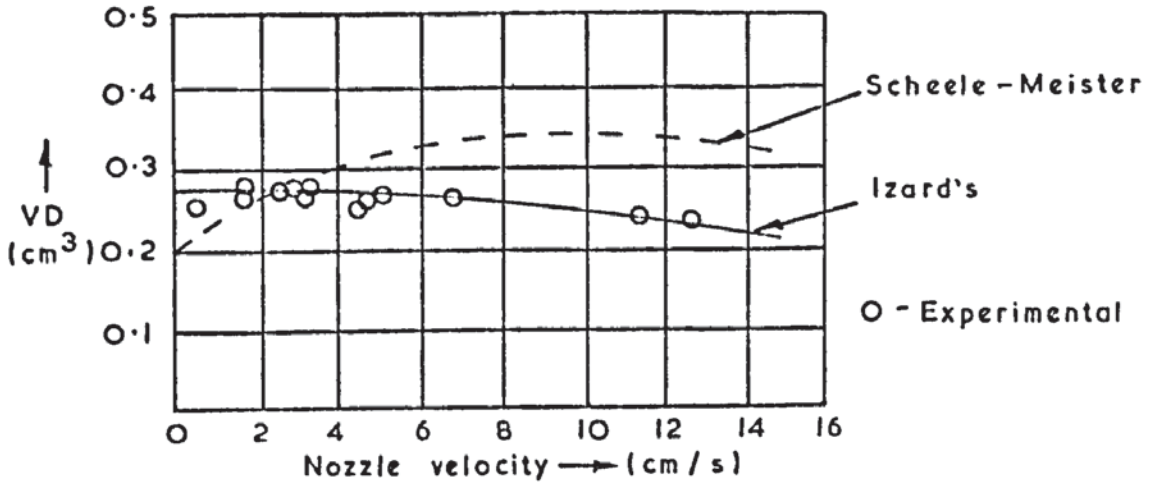

FIG. 3.2.a. Drop volume nozzle velocity dependence for benzene dispersed into water
Nozzle dia. = 0·325cm

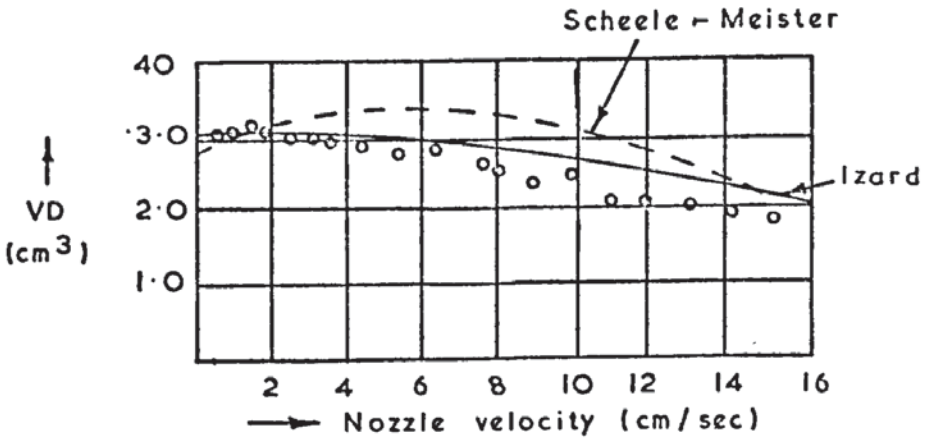

FIG. 3.2.b. VD (Drop volume) - nozzle velocity dependence for 55% cc/u and 45% C_5H_{12} in water
Nozzle dia. = 0·254cm

liquid systems. Funijawa et al[81] report that the jetting velocity can be correlated by,

$$U_J = 4.4\ \sigma^{0.2}\ \phi^{-\frac{1}{2}} \qquad (3.3)$$

Ryan [67] has proposed an equation,

$$U_J = 1.16\ \frac{\sigma}{\Delta\rho\, g\, \phi^2}^{0.95} \left(\frac{\Delta\rho}{\rho_d}\right) (\phi g)^{\frac{1}{2}} \qquad (3.4)$$

Christiansen and Nixon[82] following the earlier work of Rayleigh[83,84] on the instability of jets, proposed a graphical solution for the drop size,

$$\left(\frac{D}{\phi}\right) = 2.07\ \left(\frac{1}{0.485E_o+1}\right) \quad \text{for } E_o < 0.615 \qquad (3.5)$$

and

$$\left(\frac{D}{\phi}\right) = 2.07\ \left(\frac{1}{1.51E_o+0.12}\right) \text{ for } E_o > 0.615 \qquad (3.5a)$$

where E_o is the Eötvös number and is defined as $\left(\frac{g\Delta\rho\phi^2}{\sigma}\right)$.

Perrut and Loutaty[85] propose a similar correlation in that the significance of the Eötvös number is emphasized.

$$\left(\frac{D}{\phi}\right) = 2.07\ (1 - 0.193\ E_o) \text{ for } E_o = 0.011 \text{ to } 1.70 \qquad (3.6)$$

Scheele and Meister[86] report a correlation for the prediction of drop volume from a cylindrical jet, i.e.

$$V = F\ \left(\frac{2\pi\sigma a}{g\Delta\rho}\right) - \left(\frac{4\rho' Q U_N}{3\left(\frac{a}{a_n}\right)^2 g\rho}\right)\ -\left(\frac{4_o \pi Q a}{D_F^2 g\Delta\rho}\right)$$

$$+ 7.15\left(\frac{Q^2 a^2 \rho' \sigma}{(g\Delta\rho)^2}\right)^{1/3} \qquad (3.7)$$

where a, the jet radius one drop diameter from the end of the jet,

can be predicted from Shifflers[87] equation.

Comparison of these correlations, strictly speaking, is difficult since each is derived for special conditions. However, a comparison made by Scheele and Meister[86] is reproduced in Fig.3.3. Allak[88] has adopted the Scheele and Meister's equation since,

(a) The correlation is derived from a sound analysis of the earlier work of Raleigh[83,84].

(b) The correlation has greater applicability than the other equations as the whole range of conditions from infinitely slow drop formation to jet condition are covered. This is probably the most significant reason because the other correlations are restricted, e.g. Perrut et al's[85] correlation is only valid for Eötvös numbers $1.70 < E_o > 0.011$, and

(c) Experimental values closely agree with those predicted by equations 3.3a, 3.3b.

3.3 DROP VELOCITIES

Once a drop is formed and its size established, its subsequent motion through the continuous phase determines to a great extent the degree of effectiveness of the liquid-liquid extractor. The drop velocities determine the residence time available for the drop to exchange mass with the continuous phase. The latter is a function of the degree of turbulence at the interface which is influenced substantially by the drop velocities.

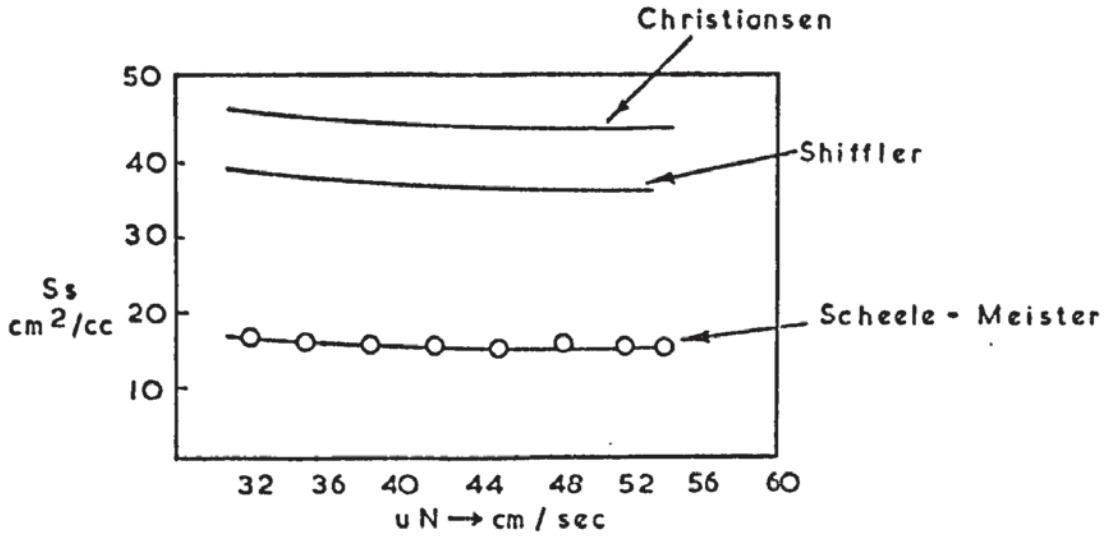

FIG. 3.3.a. Prediction of specific surface in fitting region as a function of nozzle velocity for Neptane / glycerine system
Nozzle dia. = 0 · 0813 μ = 515 cp

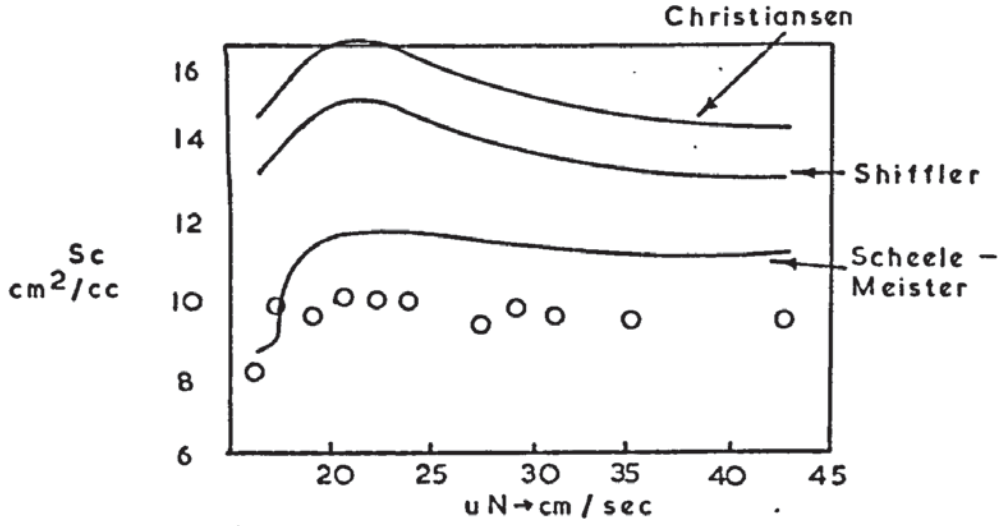

A

FIG. 3.3. b. Prediction of specific surface in fitting region as a function of nozzle velocity for Paraffin oil / water system
Nozzle dia. = 0 254 cm μ = 121 cp

The term velocity can refer to:

(i) True vectorial velocities. These are point velocities and are impossible to measure exactly but an approximation can be obtained from streamline plots by a process of graphical differentiation.

(ii) Semi-vectorial velocities, which generally are estimated by trace photographic methods[89], and

(iii) Terminal velocity. Due to easier determination, the terminal velocity is the most widely used.

However, the term velocity will, henceforth, be defined as the axial vertical distance of travel per unit time. For most columns, this effectively means the terminal velocity since it is attained very rapidly.

The drop terminal velocities in a centrifugal contactor have not been studied previously and as a consequence correlations are not available. It is also not known what influence, if any, the terminal velocity has on the performance of the centrifugal contactor. In view of the lack of direct knowledge, basic literature relating to drops falling under the action of gravity is reviewed here. The correlations presented her are further discussed in chapters 6 and 9, with reference to droplet velocity in centrifugal conditions.

3.3.1 Single Drop Velocity Correlations

The velocity of single drops varies with drop size and other factors. Fig.3.4 shows a generalised plot of terminal velocity against drop sixe for low viscosity systems of high purity and for

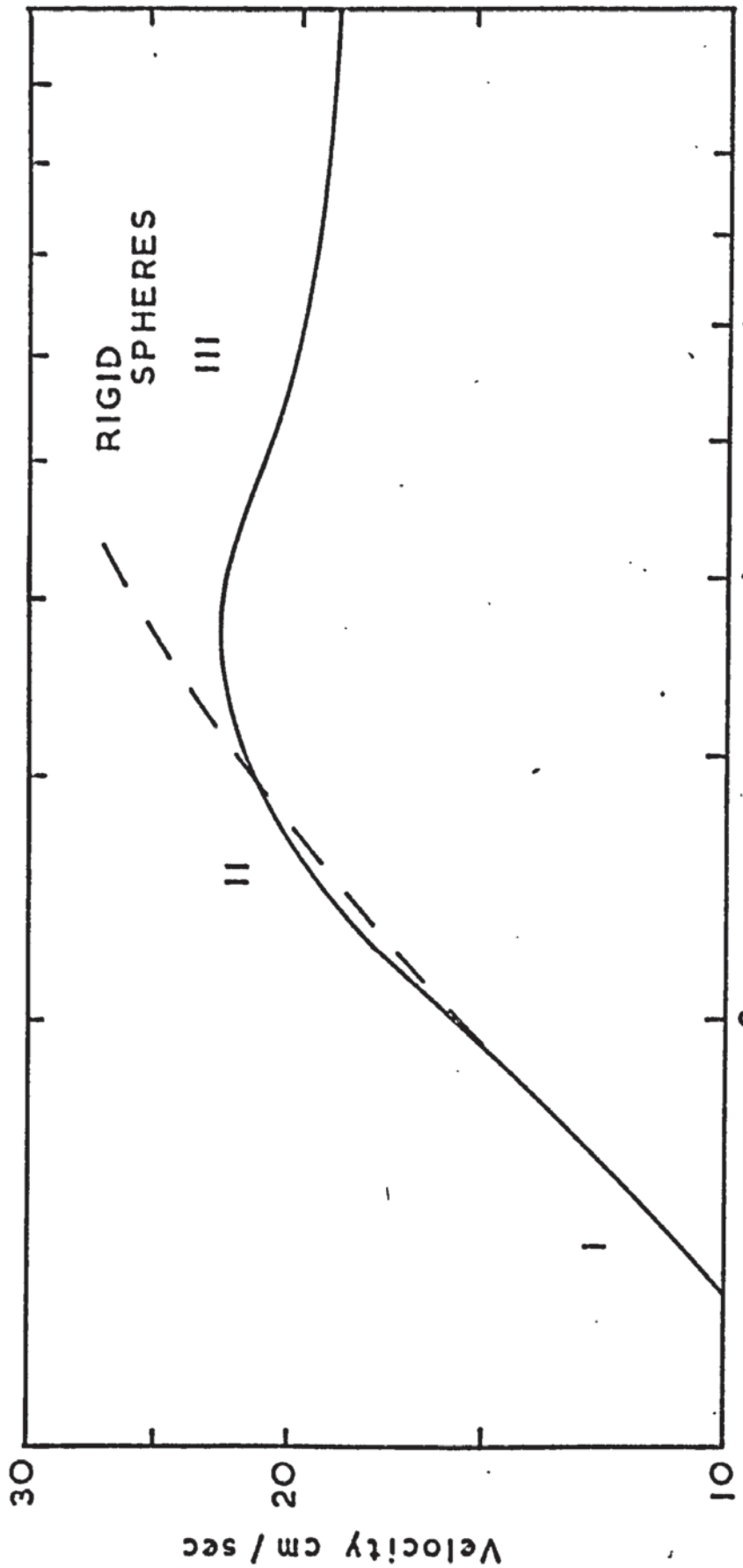

FIG. 3.4. GENERALISED TERMINAL - VELOCITY CURVE

gravity conditions.

Small drops in region I are spherical in shape and behave like rigid spheres, i.e. there is no internal circulation. Their ultimate velocity will generally be that of a rigid sphere of equal density moving in the same continuous phase. In region II the drops are increasingly distorted into a elipsoidal shape with the minor axis orientated along the direction of bulk flow. Horizontal planar symmetry is lost and oscillations set in where the drop size exceeds the peak diameter range. In region III the velocity is almost independent of size and at some critical diameter the oscillations become more violent leading to division into two or more smaller entities.

The studies of drop velocities can be broadly classified in three categories:-

(a) Those in which the drops are assumed to be rigid spheres.

(b) Drops in low viscosity continuous phase.

(c) Drops in high viscosity continuous phase.

This is a convenient classification for the purpose of this review.

(a) Assuming Drops to be Rigid Spheres

Probably the earliest work on drop velocities is due to Hadmard[90], and quite independently, to Rybczinski[91]. Subsequent models attach varying degrees of importance to the different factors. Thus Bond[92] and Bond and Newton[93] account for the influence of interfacial tension at the drop-medium interface. One observation from these studies is that a drop travelling in a continuous phase

behaves differently from a rigid sphere under identical conditions. They report a critical drop size at which this deviation from the rigid sphere behaviour occurs.

Other studies[94-96] have also been made on the rigid drops and the correlations given in Table 3.2.

(b) Drops in Low Viscosity Continuous Phase

Licht and Narasimhamurty[97] report that with any given system, as the drop size is increased, the terminal velocities of the drops increase gradually, reach a maxima and then decrease asymptotically. They also infer that maxima velocity values decrease with lower interfacial tension.

Klee and Treybal[98] give two correlations of velocity with drop diameter and physical properties; one applicable to $D < D_{out}$ and one for $D > D_{out}$. Strom and Kintner [99] report that the terminal velocities of the drops delivered by pouring and nozzle are identical and that Newton's equation for the wall proximity effects predicts values greater than observed. Krishna et al[100] have evaluated typical drag coefficients for organic drops falling in water. Elzinga and Banchero[101] have investigated the effect of surface active materials on the drag coefficients and possibly on the mechanism of drop formation. As for example, drops of very pure systems attain terminal velocities excessively greater than those predicted by Hu-Kintner [102] and Klee and Treybal[98], but the addition of surface active materials results in closer agreement between observed and predicted values from these correlations.

Similar observations are reported by other workers[103-105].

Acrivos and Taylor[106], and Brenner[107] report a theoretical calculation of low Reynolds number resistance of a rigid sphere which is arbitarily or slightly deformed. Hendrix et al[108] report that for non-oscillating drops the drag coefficient versus Reynolds number plot agrees well with that for rigid spheres.

Some of the more important correlations are given in Tables 3.2 and 3.3.

(c) Drops in a High Viscosity Continuous Phase

Johnson and Braiada[96], Harris[110] and Warshay et al[109] have derived correlations for drop velocities in a highly viscous continuous phase. However, since such systems are rarely encountered in centrifugal contactors further discussion is not proposed.

3.3.2 Multiple Drop Velocities

The definitions and significance of drop velocities for single drops are also applicable to multiple droplet situations. However, the presence of surrounding drops and their interaction affects both the individual and collective drop velocities. The situation is thus more complex and the literature concerning the dynamics of multiple drop swarms is sparse.

Raghavendra and Rao[111] investigated the multiple drops of nitrobenzene in a stagnant column of water and report two equations:

$$(N_{cd}N_{we}(N_{sd})^{\frac{1}{2}}) = 0.11\ (\frac{N_{Re}}{N_{sd}})^{1.57} \quad \text{for } (\frac{N_{Re}}{(N_{sd})^{\frac{1}{2}}} < 15 \qquad (3.33)$$

and

$$\left(\frac{N_{cd} N_{we} (N_{sd})^{\frac{1}{2}}}{I_Y}\right) = 0.078 \left(\frac{N_{Re}}{(N_{sd})^{\frac{1}{2}}}\right) \quad \text{for} \left(\frac{N_{Re}}{(N_{sd})^{\frac{1}{2}}}\right) < 25 \qquad (3.34)$$

Gal-Or and Waslo[112] using a free surface model, derive and solve equations of viscous fluid motion and continuity simultaneously with a conservation equation for diffusing surfactants. An equation of terminal velocity for multiple drops falling in the continuous phase, both with and without surfactants is reported, viz:

$$U = \frac{3}{9}\left(\frac{\rho_d - \rho_c}{\mu_c} gr^2\right). \frac{3\,\mu_c(1-\phi^{1/3})(1-\phi^{5/3})}{2\mu_c}$$

$$+ \frac{(3-9/2\,\phi^{1/3}+ 9/2\,\phi^{5/3}- 3\phi^2)(\mu_d+\gamma)}{(1-\phi^{5/3})+(3+2\,\phi^{5/3})(\mu_d +\gamma)} \qquad (3.35)$$

Harris[110] observes that for the streaming drop Raghavendra and Rao's[111] equation is only applicable in certain range of (N_{cd} N_{we} $N_e^{1.5}$) group. He proposes equations that modify the latter. However, even this model is claimed only to work for the acetone-glycerol system and for columns having diameter greater than 10 cm.

Mhatre and Kintener[113] present a model for the droplets in a non-Newtonian continuous phase of very high viscosity.

3.4 DROPLET OSCILLATIONS

Kintner [114] made a photographic study of the effect of oscillation on the internal circulation of droplets. Schroeder and Kintner[115] and Kintner[116] have characterised the type of oscillation by means of Reynoldsnumber. Above a Reynoldsnumber of 200, the oscillations are maintained by vortex discharge behind the

moving drops. Circulation is Hadamard-like movement of liquid within the drop in a manner that is almost laminar.

The frequency of oscillation[114] may be predicted by the Schroeder-Kintner modification of Lambs[117] equation,

$$\omega^2 = \left(\frac{\sigma b}{a^3}\right) \quad \frac{n(n+1)(n-1)(n+2)}{(n+1)\rho_d + n\rho_c} \tag{3.36}$$

in which the empirical amplitude coefficient (b) is best estimated by:

$$b = \frac{D_e^{0.225}}{1.242} \tag{3.36a}$$

The estimation of drop oscillation frequency is from analysis of cinefilms of falling drops. By plotting maximum axis length A_{max} and the equivalent sphere diameter, D_e, the amplitude of oscillation, a_p, can be estimated since

$$a_p = \frac{A_{max}}{2} - a_o \tag{3.36b}$$

Rose[118] has tabulated major and minor axis length from photographs and shows that:

$$\frac{A_{max}}{D} = \text{constant} \tag{3.37}$$

Brunson[119] using this observation and assuming that oscillation is from spherical to oblate ellipsoidal, gives the amplitude of oscillation can be written as a function of $\left(\frac{A_{max}}{D}\right)$,

$$A_p = \frac{1}{2}\left(\frac{A_{max}}{D}\right)^2 + \frac{1}{4G}\left(\frac{D}{A}\right)^4 \ln\left(\frac{1+G}{1-G}\right) - 1 \tag{3.38}$$

TABLE 3.2 CORRELATIONS FOR VELOCITIES OF DROPS (IN GRAVITY COLUMNS)

AUTHOR(S)	EQUATION	Eqn. Number	REMARKS
Hadamard[90] Rybcsinski[91]	$U_T = \frac{F}{6\pi\mu_c r} \left(\frac{3\mu_d + 3\mu_c}{3\mu_d + 2\mu_c}\right)$	3.18	Stoke's law modification for liquid spheres in an infinite mass of liquid for Re up to 4.0 but preferably 1.0.
Johnson and Braida[96]	$N_{cd} N_{we} N_p^{0.15} (\mu_d/\mu_c)^{0.14} \alpha N_{Re} N_p^{-0.15}$	3.19	The droplets of organic liquid falling through a liquid phase over a range of physical properties.
Licht and Narasimhamurty[97]	$N_{cd} = 1.87 \left(\frac{gD^2 \Delta\rho}{4}\right) + 0.425$	3.20	In a stationary medium for $\frac{g D^2}{4}$ 0.4
Klee and Treybal[98]	Below max. diameter. $U_T = 38.3 \rho_c^{-0.45} \cdot \Delta\rho^{0.58} \cdot (0.01\mu_c)^{-0.11} \cdot (D^{0.7})$	3.21	
	Above max. diameter $U_T = 17.6(\rho_c^{-0.55})(\Delta\rho)^{0.28}(0.01\mu_c)^{0.1}(\sigma^{0.18})$	3.22	
Strom Ankintner[99]	$\frac{U_T}{U} = \frac{1}{K} = \left(1 - \left(\frac{D}{d}\right)^2\right)^{1.43}$	3.23	The wall effect for fall of single drops.

TABLE 3.2 (Contd....)

AUTHOR(S)	EQUATION	Eqn. No.	REMARKS
Krishna et al[100]	For $\left(\frac{N_{Re}}{N_{sd}^{0.5}}\right) < 12$, $(N_{cd})(N_{we})(N_{sd})^{0.5} = 5\left(\frac{N_{Re}}{N_{sd}^{0.5}}\right)^{1.05}$	3.24	Dynamic of organic drop in water.
	For $\left(\frac{N_{Re}}{N_{sd}^{0.5}}\right) > 20$ $(N_{cd})(N_{we})(N_{sd})^{0.5} = 0.32\left(\frac{N_{Re}}{N_{sd}}\right)^{2.16}$	3.25	
	For $12 < \frac{N_{Re}}{N_{sd}} < 20$ $U_m = 1.545 \frac{\sigma}{\mu_c (N_{sd})^{0.0767}}$	3.26	
Hendrix, Dave and Johnson[108]	$N_{cd} = 8.70(N_{Re})^{-0.435}\left(\frac{\mu_c}{\mu_d}\right)^{0.184}\left(\frac{\Delta\rho}{\rho_c}\right)^{0.06}$	3.27	Non oscillating single drops.
	$N_{cd} = 8.50\ (N_{Re})^{-0.435}$	3.28	
	$U = 10.0(D)^{0.917}.(\mu_c)^{0.395}(\Delta\rho)^{0.601}$	3.29	

TABLE 3.2 (Contd...)

AUTHOR(S)	EQUATION	Eqn. No.	REMARKS
Harris [110]	$N_{cd}.N_{we}(N_p)^{0.15} = \phi \left(\frac{\mu_c}{\mu_w}\right)\left(\frac{N_{Re}}{(N_p)^{0.15}}\right)^{0.694}$	3.30	Single drops in a highly viscous continuous phase.
	$N_{cd}.N_{we}(N_p)^{0.15} = 2.25\ I_\gamma^{-1}(N_{Re}/(N_p)^{0.15})^{1.37}$	3.31	Streaming drops in highly viscous phase for $2 \quad N_{cd}.N_{we}.N_p^{0.15} \quad 10$
	$(N_{cd}.N_{we}(N_p)^{0.15}) = (N_{Re}/(N_p)^{0.15})^{0.898} \left(\frac{(N_p)^{.29}}{0.0955}\right) I_\gamma^{-0.42}$	3.32	

where the constant G is

$$= 1 - \left(\frac{D}{A}\right)^{6\ \frac{1}{2}} \qquad (3.38a)$$

Brunson also concluded that amplitude of oscillating drop is independent of:

(i) Viscosity of both continuous and dispersed phases, and

(ii) of droplet diameter.

The equations given above for the evaluation of frequency and amplitude of droplet oscillation are applicable only for drops travelling under the action of gravity. Since these parameters have not been investigated in centrifugal contactors, it is not known if the above equations work or not. This is the subject of further discussion in Chapter 9.

4. DROPLET BREAK-UP AND COALESCENCE

4.1 HYDRODYNAMICS OF DROPLET BREAK UP

4.1.1 Hinze[120] Theory

The theory of Hinze, which is generally accepted, postulates that droplets break-up in turbulent conditions due to shear forces in a manner dependent upon the general flow pattern around the droplets. Three basic types of deformation have been identified, i.e.

(a) Lenticular deformation, in which the globule is flattened, forming an oblate ellipsoid in the initial stages. Subsequent deformation leading to eventual break-up depends upon the magnitude of the external sources responsible for the deformation.

(b) Cigar shaped deformation, which entails the gradual elongation of the globule, forming a prolate ellipsoid in the initial stages and then break-up into small droplets.

(c) Irregular deformation. This involves the local deformation of the globule surface resulting in bulges and protuberances. On separation these bulges and protuberances result in small droplets.

The patterns of flow are recognised as being an important factor, and are differentiated by use of dynamic pressure (p) or the viscous stress. Table 4.1 shows the patterns to be expected from various types of deformation and dynamic forces.

Break-up will occur if there is a sufficient degree of

deformation, that is, if the region of the flow pattern causing a specific deformation is sufficiently large to contain the deformed globule and if the flow pattern persists long enough. Dependency on the physical properties, e.g. interfacial tension, viscosity and density is assumed.

For any isolated globule the deforming forces, i.e. the pressure (p) or viscous stress (τ), will be counteracted by a surface force arising from the interfacial tension (σ). Hinze concludes, therefore, that the controlling forces in droplet break-up are,

(i) The dynamic pressure (p).

(ii) Viscous stress (τ) $=(\frac{\mu_d}{D})\ (p/\rho_d)^{\frac{1}{2}}$ and

(iii) Surface force $= (\frac{\sigma}{D})$

From these Hinze selected two dimensionless groups as defining the deformation leading to break-up, i.e.

$$N_{Vi} = \frac{\mu_d}{\sqrt{\rho_d}\ D}\ ,\ \text{a viscosity group}$$

and

$$N_{We} = \frac{\tau}{(\sigma/D)},\ \text{a modified Weber group.}$$

The latter may be compared with the standard definition of Weber group$(\frac{\rho V^2}{\sigma/D})$ where ρU^2 is the dynamic pressure of fluid flow.

The modified Weber group is a simple ratio of the shear stress to the counteracting surface force; large values therefore imply greater deformation and at a certain critical value $(N_{We})_{crit}$ break-up of droplet will occur. The critical value is known to depend on the type of deformation and on the flow pattern around the droplet.

TABLE 5.1 CONDITIONS FOR GLOBULE BREAK-UP[120]

In cases of similar flow pattern persisting throughout the flow regime, all globules larger than the critical size break-up in a similar manner at the same $(N_{We})_{crit}$ value. In more complicated fields, in which different flow patterns are present, $(N_{We})_{crit}$ is known to vary from globule to globule and statistical means are often employed.

4.1.2 Local Isotropic Turbulence Theory

In cases where the system is well agitated Kolmogoroff[121][122] enunciates the concept of 'local isotropy' to describe the behaviour of dispersions. This postulates that instability of the main flow exaggerates the existing disturbances and produces primary eddies. The latter have a wavelength or scale similar to that of the main flow and disintegrate successively into smaller eddies until the energy is dissipated by viscous flow. At greater turbulence, characterised by a high Reynolds number, most of the kinetic energy is present in the large eddies.

If the scale of the main flow is large compared to that of the energy-dissipating eddies, a wide range of intermediate eddies will exist which possess little energy, and, therefore, dissipate little of the total energy. They do, however, transfer as opposed to dissipating, the kinetic energy from large to small eddies. Kolomogoroff concludes from a statistical analysis that the smaller eddies are virtually independent of the primary eddies. If the main flow is time independent, the statistical properties of any eddy smaller than the main flow may be determined by the local energy dissipation rate per unit volume, ε.

If $\overline{U^2}$, $\overline{v^2}$ and $\overline{z^2}$ are root mean square velocities describing the velocity vector at a point, then the condition

$$\overline{U^2} = \overline{v^2} = \overline{z^2}$$

defines ISOTROPIC TURBULENCE. As most practical cases are unisotropic Kolmogoroff assumed isotropy to exist if the volume under consideration is small enough in comparison with the scale of main flow, L. If r is the radius vector $r_1 r_2$ describing two points in this volume, then a velocity vector $\overline{U}(r)$ can be defined by,

$$\overline{U^2(r)} = \overline{U(r_1) - U(r_2)^2} \qquad (4.1)$$

where $\overline{U^2(r)}$ is mainly dependent upon eddies smaller than r, and which are statistically independent of the main flow. Hence for r L, $\overline{U^2(r)}$ is a function of ε, of the dissipation rate and the viscosity of the fluid, v.

$\overline{U^2(r)}$ is also independent of the direction of radius vector r, for small values of r only. Hence the name Local Isotropy. Kolomogoroff defined a parameter η as the scale of eddies of Reynolds number,Re, equal to one and possessing maximum energy dissipation properties. One further assumption made is that if r is much larger than η of the energy dissipating eddies but smaller than the main flow, $\overline{U^2(r)}$ is a function of ε only. By analysis Kolmogoroff shows that

$$\text{for } L >> r >> \eta \quad \overline{U^2(r)} = C_1 \varepsilon^{2/3} r^{2/3} \qquad (4.2)$$

$$\text{for } r << \eta \quad \overline{U^2(r)} = C_2 (\frac{\varepsilon}{v}) r^2 \qquad (4.3)$$

where C_1, C_2 are universal constants and which may be measured. It has also been shown that

$$\eta = v^{\frac{3}{4}} . \varepsilon^{-\frac{1}{4}} \qquad (4.4)$$

Kolmogoroff states that following proviso should be observed,

(a) That the Reynolds number of the main flow is very high, i.e. Re > 50,000, and

(b) The characteristic length, L, of the agitated system for instance the width of agitator blades, is greater than η i.e. L >>η.

4.1.3 Application to Centrifugal Extractors

As there is no literature relating to the droplet break-up in centrifugal contactors, a very concise account of basic equations is presented. On the assumption that Kolmogoroff's distribution law is valid, Hinze[120] demonstrated that,

$$D_{max} \left(\frac{\rho_c}{\sigma}\right)^{3/5} . \varepsilon^{2/5} = C \qquad (4.5)$$

For an arrangement consisting of the co-axial cylinders the constant C has a value of 0.725[125]. Shinnar and Church[125] considered droplet break-up by viscous shear, the magnitude of which at the critical point is given by,

$$\mu_c \left(\frac{\partial u}{\partial x}\right)_{crit} = \frac{D}{\sigma} = C\phi\left(\frac{\mu_d}{\mu_c}\right) \qquad (4.6)$$

where (μ_d/μ_c) is a hyperbolic function describing the stability of a liquid cylinder in viscous fluid[126]. The droplet is assumed

to oscillate for phases having nearly equal densities and viscosities and become unstable if the kinetic energy is sufficient to make up for the difference in the surface energy between the single drop and its daughter drops. This leads to

$$\frac{E_k}{D^2} = \text{constant} \approx 0.26 \qquad (4.7)$$

As E_k is $\propto U^2(D).D^3$ for the case of local isotropy, thus

$$\rho U^2(D)(D)^3 \simeq 0.26$$

$$\text{i.e.} \quad W_e \simeq 0.26 \qquad (4.8)$$

4.2 COALESCENCE

4.2.1 Introduction

Coalescence is known to occur in the centrifugal extractors, butits mechanism and the significance it plays in the extractor's performance have not been ascertained. As a result only the basic fundamentals of coalescence are reviewed here.

Coalescence occurs in the following modes:

(a) drop-interface,

(b) drop-drop, and

(c) in closely packed dispersions.

The essential mechanism in the first two is similar but in the third the situation becomes more complex. In the case of (a) and (b) when a droplet arrives at the interface, or another drop, a film of the continuous phase is trapped between the incoming drop and the interface. By the action of buoyancy force the film is squeezed out and

at a critical thickness it ruptures to allow the contents into the dispersed phase. In the case of (c) the continuous phase is trapped between many drops and it must drain from in between them for the drops to coalesce. This drainage is inhibited by the presence of the surrounding drops near the coalescing pair.

4.2.2 Drop-Interface Coalescence

This type of coalescence will be less significant in a centrifugal extractor than the drop-drop coalescence and will not be discussed in great detail. This may be inferred from the observation of a centrifugal extractor's mechanism of operation.

Table 4.2 shows some of the basic equations for the prediction of mean rest time and mean half-life rest time of droplets coalescing at an interface. The latter parameter is considered to be better since the mean rest time is known to vary in Gaussian-like distribution. Hitit [133], however, reports that there is no significant difference between the mean and half-life coalescence times. Moreover, the applicability of data derived from single drop-interface coalescence to the behaviour of swarms of drops, as for example found in industrial units, is concluded to be questionable.

4.2.3 Drop-Drop Coalescence

Unlike the drop-interface coalescence there are relatively few studies on drop-drop coalescence. This accrues from the inherent difficulties in the case of the latter. However, as stated previously, the mechanism in both cases is similar. In the drop-drop coalescence, two drops approach each other, squeezing out the continuous phase film, separating them, and the rupturing of the film by a disturbance

TABLE 4.2 DROP-INTERFACE COALESCENCE EQUATIONS

AUTHOR(S)	EQUATION	EQN. NO.	REMARKS
Cockbain and Roberts[127]	$\ln N = - kt + C$	4.9	This equation used mean rest time, whereas others prefer to use half-life rest time.
Gillepsi and Rideal[128]	$\ln(\frac{N}{N_o}) = -k(t-t_o)^{1.5} . f\, C_o A_o (\frac{6}{D\mu})^{\frac{1}{2}}$	4.10	In this equation the terms C_o and A_o characterise the disturbance which influences the coalescence.
Elton and Picknett[129]	$\log(\frac{N}{N_o}) = Ct^n$	4.11	This equation is proposed for electrolytes. The exponent varies from n=2 n=3 depending upon system's concentration.
Jeffreys and Hawksely[130]	$t_{\frac{1}{2}} = 4.53 \times 10^5 \left(\frac{\mu_c^{\frac{1}{2}} \cdot \rho^{1.2}}{\sigma^2}\right).\left(\frac{T}{2\sigma}\right)^{-0.7\mu^{\frac{1}{2}}} \cdot D^{0.02}\left(\frac{\sigma^2}{\mu_c^{\frac{1}{2}}}\right)^{0.55} \cdot L^{0.001}\left(\frac{\sigma^2}{\mu_c^{\frac{1}{2}}}\right)$	4.12	This is a very general equation describing the half-life relationship with the physical properties of the system.
Jeffreys and Lawson[131]	$\left(\frac{\sigma t_{\frac{1}{2}}}{\mu_c D}\right) = 1.32 \times 10^5 \left(\frac{L}{D}\right)^{0.18} \left(\frac{D^2 \Delta\rho\, g}{\sigma}\right)^{0.32}$	4.13	This is specific case of 4.12 and assumes negligible temperature dependence

TABLE 4.2 (Contd....)

AUTHOR(S)	EQUATION	EQN. NO.	REMARKS
Davies [132]	$\left(\frac{t_{\frac{1}{2}}}{\mu_c D}\right) \quad \left(\frac{D^2 \Delta\rho\, g}{\sigma}\right)^{\frac{1}{4}}$	4.14	Reported deviation from experimental values if $\pm$ 20%

when the film has been thinned sufficiently.

Theoretical models presented here are arrived at by assuming the said mechanism. The principal ones are tabulated in Table 4.3. Mc Avoy and Kintner's[134] model is derived by assuming that the initial and final film thickness h_1, h_2 respectively, are negligible in comparison with the drop diameter (d). According to Jeffreys and Davies[135] the previous model is a modification of the MacKay and Mason[136] solution for the case of rigid drop approaching a rigid plane interface. Moreover, these workers argue that the previous models are of limited applicability since the process of deformation that occurs in large drops is not considered in their derivations. They therefore report a model for such a case as well as for two unequal spherical drops.

Princen[137] proposed correlations for a non-uniform film and equations are reported for the maximum and minimum thickness of the film. Murdoch and Leng[138] state that all other models apply only to immobile films and report a model for the mobile films. Scheele and Leng[139] have concurred with the accuracy of this model. The model, however, must be treated with caution since a number of assumptions are made which do not seem to be justified, viz:

(a) Assumption is made that the collision between the drops are symmetrical and the thinning film was bound by two flat disc-like expanding interfaces.

(b) That the term in equation (4.2o) has to be

$$\int_o^t \frac{F}{R^4}\, dt$$

TABLE 4.3 THEORETICAL MODELS OF DROP-DROP COALESCENCE

AUTHOR	EQUATION	EQN. NO.	REMARKS
Mc Avoy and Kintner[134]	Rate of film thinning $t = \frac{3\pi\mu_c}{F}\left(\frac{d^2}{4}\right)\ln\frac{h_1}{h_2}$	4.15	When two equal size spherical drops approach and where the finitial and final film thickness n_1, n_2, respectively, are negligible compared to (d).
Jeffreys and Davies[135]	$\frac{dh}{dt} = \frac{Fh}{6\pi\mu_c}\left(\frac{2}{d_1}+\frac{2}{d_2}\right)^2$	4.16	An extension of Mackay/Mason model for the drop-interface coalescence.
	$\frac{dh}{dt} = \frac{-32\pi^2}{3\pi\mu_c d^2 F}\cdot h^3$	4.17	Large drops which deform.
Princen[136]	$\left(\frac{dh}{dt}\right)_{min} = \frac{2.78\pi\sigma^2}{(d^2/4)\mu_c F}\cdot h^3_{min}$	4.18	Formation of a dimple in drop surface resulting in a non unform film between the drops
	$\left(\frac{dh}{dt}\right)_{max} = \frac{13.0\ \pi 3\sigma^4}{\mu_c (d^2/4)F^3}\cdot h^5_{max}$	4.19	
Murdoch and Leng[137]	$h = \frac{h_o}{1+\left(\frac{8R_d}{\pi\mu_d}\right)h_o\int_o^t \frac{F}{R^4}dt}$	4.20	This model is derived for the case of a mobile film and where the drops are of equal size.

evaluated from photographic techniques.

Scheele and Leng[139] report that drops are oscillating, the frequency of which is given by Kintner's equation, and have impact velocities in the range 1.9 to 11.2 cm/sec. Their main conclusions can be summarised as:-

(i) that probability of coalescence is independent of the impact velocity of the two drops.

(ii) that oscillation phase is important in determining the coalescence between two drops.

(iii) that the classical parallel disc immobile interface model describing film thinning is highly inaccurate, and

(iv) the dependence of the rate of expansion of the radius of contact on the oscillation phase at the moment of contact, explains the dependence of coalescence on the drop oscillation behaviour.

Robinson and Hartland[140] have studied the cases where two or more drops are approaching an interface and each other in a two dimensional bed. Sivokova and Eichler[141] in a recent work have investigated the coalescence time between two liquid drops: one drop being vertically above the other, and measuring the time between drops touching and rising in a specially designed section.

5. FUNDAMENTALS OF MASS TRANSFER

5.1 INTRODUCTION

The hydrodynamics of droplets, and the manner in which these affect the volumetric aspects of a centrifugal extractor, have been reviewed in Chapters 3 and 4. The size and velocity of droplets though the continuous phase flow have a significant effect upon mechanisms and efficiency of solute transfer. Relevant data on these phenomena is reviewed in this chapter.

In practical contactors the mass transfer rate is often defined as in equation (3.1), viz:

$$N = K.A.\Delta c \tag{5.1}$$

The overall mass transfer coefficient K is defined so that the characteristics of all flow regimes are included. It is related to the individual transfer coefficients by,

$$\frac{1}{K} = \frac{1}{K_d} + \frac{1}{mK_c} \tag{5.2}$$

The mass transfer rate can be increased by either,

(a) changing the concentration or activity gradient, Δc, or

(b) increasing the interfacial area, A.

(c) mass transfer coefficient K.

In practice the interfacial area is increased by the dispersion of one phase in the form of droplets in the continuous phase. The mass transfer is known to occur in the following stages of the droplet:

(i) During formation of the discrete droplet while still resident on the nozzle or orifice.

(ii) During the acceleration period immediately the droplet leaves the nozzle or orifice.

(iii) During free rise or fall of the droplet at steady state velocity, and

(iv) During flocculation and coalescence at the end of droplets travelling through the continuous phase.

Although studies on the basis of single drop behaviour are often idealised in comparison with droplet behaviour in an actual contactor, it allows a simpler evaluation of mass transfer rates. However, even the single drop analysis is difficult for a centrifugal contactor, since the drops size are not known.

5.2 MASS TRANSFER DURING DROP FORMATION

5.2.1 For Formation Time > 1.5 to 4.0 sec.

The importance of stages (i) to (iv) described above, to the mass transfer is subject to contrary claims. Whilst Sherwood[142] reports that 40% of mass transfer occurs during drop formation, West[143] and others[144,145,146] report it to be 14% and 10%, respectively, Licht and Pansing[147] report that the amount of mass transfer during this stage is insignificant. It is, however, generally agreed that mass transfer does take place during drop formation and models have been proposed to quantify the amount. Although all the models listed in Table 5.1 assume that mass transfer is affected by diffusion, the actual mechanisms are different. However, all the correlations use one of the following in their derivation:

(i) The model of an ageing, rigid boundary layer which increases in surface area.

(ii) In the ageing boundary layer, the concentration gradient increases due to increase in surface area as a result of 'stretching' effect. Correlations using this are often termed 'stretch model'.

(iii) The boundary layer ages as with rigid layer but due to fresh surface element arriving the old surface is increased. Hence the term 'fresh surface model', and

(iv) For the boundary layer a flow pattern has been developed in which varying rate of stretching occurs.

The model due to Pansing[147] has been recommended by some workers,[76] whereas others view it with scepticism. Ilkovic's model[148] has been extensively studied and deviation from the actual value of less than 20% are reported[146]. The models of Coulson and Skinner[149], Heertjis et al[123], Groothius and Kramer[150] and Angelo et al[144] have been reported as having mixed success. Skelland and Muihas[151] having conducted investigation with different models report large deviations of models from the experimental values. This is concluded to be due to the exclusion from these models of:

(a) internal circulation caused by the impinging jet while the drop grows;

(b) the effect of interfacial tension;

(c) influence of the rest drop remaining after detachment; and

(d) disturbances associated with such attachment.

TABLE 5.1

MODELS FOR DROP FORMATION MASS TRANSFER

AUTHORS	MODEL	Equation No.
Licht-Pansing (147)	$K_{df}=6/7\left(\frac{D_d t_f}{\pi}\right)^{\frac{1}{2}}$	5.3
Groothius-Kramer (150)	$K_{df}=4/3\left(\frac{D_d t_f}{\pi}\right)^{\frac{1}{2}}$	5.4
Heertjes et al (124)	$K_{df}=24/7\left(\frac{D_d t_f}{\pi}\right)^{\frac{1}{2}}$	5.5
Coulson-Skinner (149)	$K_{df}=2.(3/5)^{\frac{1}{2}}\left(\frac{D_d t_f}{\pi}\right)^{\frac{1}{2}}$	5.6
Heertjes-De Nie (145)	$K_{df}=2\left(\frac{a_o}{a_r}+\frac{2}{3}\right)\left(\frac{D_d t_f}{\pi}\right)^{\frac{1}{2}}$	5.7
Heertjes- De Nie (145)	$K_{df}=2.(7/3)^{\frac{1}{2}}\left(\frac{a_o}{a_r}+\frac{1}{3}\right)\left(\frac{D_d t_f}{\pi}\right)^{\frac{1}{2}}$	5.8
Ilkovic (148)	$K_{df}=1.31\left(\frac{D_d t_f}{\pi}\right)^{\frac{1}{2}}$	5.9
Angelo et al (144)	$K_{df}=\frac{2}{7}\sqrt{T}\left(\frac{D_d}{\pi t_f}\right)^{\frac{1}{2}}$	5.10

Whereas all these models have the forms,

$$K_{df} = F(D_d/\pi t_f)^{\frac{1}{2}}$$

(151)

Skelland Mirihas Model does not,

$$\left(\frac{K_{df}}{d} \cdot t_f\right) = 0.0432\left(\frac{v_m^2}{dg}\right)^{0.089}\left(\frac{d^2}{t_f . D_d}\right)^{-0.334}\left(\frac{\mu_d}{\sqrt{\rho_d . d . \sigma}}\right)^{-0.601} \qquad 5.11$$

According to these workers, a more realistic model should account for these parameters as well as others, viz:

$$K_{df} = \psi \{t_f, d, d_n, v_n, D_d, \sigma, \rho_c, \rho_d, \Delta\rho, \mu_c \mu_d \}$$

which leads by dimensional analysis to the equation 5.11. The latter is reported to deviate from experimental values by $\pm$ 25 %, for the following range of variables,

$$0.521 \times 10^{-2} \leq \{\frac{K_{df} \cdot t_f}{d}\} \leq 8.140 \times 10^{-2} \qquad 5.12$$

$$1.886 \times 10^{4} \leq \{\frac{d^2}{t_f D}\} \leq 12.31 \times 10^{-4} \qquad 5.12a$$

$$0.165 \times 10^{-2} \leq \{\frac{\mu_d}{(\rho_d . d . \sigma)^{\frac{1}{2}}}\} \leq 0.961 \times 10^{-2} \qquad 5.13$$

$$0.163 \times 10^{-2} \leq \{\frac{v_m^2}{dg}\} \leq 0.3955 \qquad 5.13a$$

This model, however, differs from others in that it covers the mass transfer not during drop formation alone, but also during the detachment stage. It also takes into account the influence of rest drop on the nozzle when the main drop has detached.

5.2.2 At Low Drop Formation Times

Models discussed above were recognised to be invalid[152] for drop formation times of less than 1.5 sec. Coulson and Skinner[149] found that for drop formation times of less than 4.0 sec, the relationship is no longer square root dependant, and, in fact, the exponent was 0.7. Rajan et al[153] also report dependence to be invalid and that the exponent is always greater than 0.5, and generally greater than 0.9.

The reasons underlying the deviation from the square root dependence have been given in terms of internal circulation within the drop and the free convection from the drop. The latter has been shown to be true for high Schmidt number systems. Popovich et al[154] proposed models of the form,

$$N_A = \text{Const.}(C_s - C_o)\left(\frac{D}{\pi}\right) t^{\frac{2n-1}{2}} \qquad 5.14$$

where the initial constant assumes different value for the different models. Furthermore, the time dependence of surface area is assumed to be of the form,

$$A = kt^n \qquad 5.15$$

which for a spherical drop growing at uniform rate can be written as

$$A = \pi d_f^{\,2}\, t_f^{\,-2/3} t^{2/3} \qquad 5.16$$

Rajan et al[154] found that the surface area variation is well represented by equation 5.16 except for an initial period.

Hertjes and De-Nie[155] have presented a correlation modified to take into account the drop formation

$$E_f = 1.32\ \ 2\,\frac{A_{rd}}{V_{dr}} + \frac{4}{3}B(t/t_c)^{-\frac{1}{2}}\,\frac{D_{cst}}{\pi}^{\frac{1}{2}} \qquad 5.17$$

which reduces to

$$E_f = C_D\left(\frac{2A_{rd}}{V_{dr}} + \frac{4}{3}B\right)\left(\frac{Dt_{eq}}{\pi}\right)^{\frac{1}{2}} \qquad 5.18$$

if the expansion of surface is assumed to occur by elements having an initial concentration rather than by really fresh elements.

At high speed formation, which results in a high degree of

TABLE 5.2

MASS TRANSFER CORRELATIONS FOR TO-AND-FROM DROPS IN DISPERSED PHASE

TYPE OF DROP		AUTHOR(S)	CORRELATION	REMARKS	EQN. NO.
RIGID DROP		NEWMAN[158]	$E = \frac{C_o - C_f}{C_o - C^*} = 1 - \frac{6}{\pi^2} \sum_{n=1}^{\infty} \exp(-n^2 \pi^2 \frac{D_D t}{a^2})$	Non-stationary diffusion is assumed to take place.	5.20
		SKELLAND and MINHAS[151]	$K_{d_r} = \frac{S_{drc}}{tc_r A_r (\frac{1}{2}(C_{ai} + C_{af}) - C_a^*)}$	Validity remains to be proven	5.21
NON-RIGID DROP	LAMINAR CIRCULATION	KROING and BRINK[159]	$E = 1 - 3/8 \sum_{n=1}^{\infty} A_n^2 \exp(-\lambda_m . \frac{16 . D_D t}{a^2})$	Developed for Re<1, this is known to work for Re>1 (26)	5.22
	TURBULENT CIRCULATION	HANDLOS and BARON[160]	$E = 1 - 2 \sum_{n=1}^{\infty} A_n^2 \exp(\frac{-\lambda_n U_t}{128(1+\frac{\mu_D}{\mu_c})d})$		5.23
NON RIGID DROP	OSCILLATION	ROSE and KINTNER[161]	$E = 1 - \exp(-\frac{2\pi D_E}{V} \int_{t_o}^{t_f} \frac{1}{f_1(t)} ((\frac{3V}{4\pi(a_o + a_p \lvert \sin\omega' t \rvert^2)})^2 . \frac{1}{2\alpha} \ln\frac{1+\alpha}{1-\alpha} + (a_o + a_p \lvert \sin\omega' t \rvert^2)) dt)$		

circulation, Johnson[156] has proposed,

$$E_f = \frac{20.6}{d}\left(\frac{\pi}{Dt_f}\right)^{\frac{1}{2}} \qquad 5.19$$

Groothuis and Kramer[150] observed a jet action in the drop at Reynolds number, Re > 40-50 and reported deviations from the diffusion models in this range.

5.2.3 Relevance to Centrifugal Contactors

From the general observation of geometry and working of centrifugal contactor, it is known that the drop formation times are likely to be extremely small compared with gravity towers. In view of this it is probably true to say that the equations 5.14 to 5.19 have a greater chance of being successful than equations 5.3 to 5.13. In any case, of the total mass transfer that occurs during drop formation is likely to be very small in comparison with that during other stages of the droplet life in the centrifugal contactor developed here.

5.3 MASS TRANSFER DURING DROP RELEASE

The amount of mass transfer which occurs during the drop release is a matter of controversy. Popovich et al[154] conclude that no significant mass transfer takes place during drop release contrary to the findings of Licht and Conway[89]. Studies made by Marsh et al[157] and by Heertjes-De-Nie[155], however, tend to support the latter observation.

If, as is reported, the mass transfer in a gravity contactor during the drop release is insignificant, that occurring in a centrifugal contactor is likely to be even less significant.

5.4 MASS TRANSFER TO AND FROM DROPS

5.4.1 In Dispersed Phase

Drops are of three types, i.e. rigid spherical, circulating and oscillating. The former are small and the process of mass transfer is one of non-stationary diffusion. Conversely, non-rigid drops are generally large and either oscillate or exhibit internal circulation.

Models proposed for both types of drops are tabulated in Table 5.2. One of these, due to Newman[158], is valid for a rigid drop possessing no internal circulation. The Skelland and Muihas[151] model also assumes a rigid drop but the validity remains to be experimentally verified. Models applicable to non-rigid drop vary according to the ambient conditions. Thus Kroing and Brink[159] proposed a model for the non-rigid drop in lammar regime and Handlos and Baron[160] for the turbulent zone. For oscillating drops however, significant deviation from the Handlos and Baron[160] are known to occur. Rose et al[164] therefore proposed a model, equation 5.24, to account for such drops. According to these authors, the oscillations occur at Re = 200, and are maintained by vortex discharge behind the moving drops. The model, however, cannot be evaluated analytically and requires digital computation. Deviation of $\pm$ 15% from the experimental values are claimed.

Since in a centrifugal contactor the type of drop i.e. rigid, non-rigid or oscillating, is not known the validity of any model for such contactors has not been ascertained.

5.4.2 Mass Transfer in a Continuous Phase

A number of correlations are reported in literature, Table 5.3, for both rigid and non-rigid drops. Difficulties are encountered in estimation of rate of mass transfer in the continuous phase, because of inadequate knowledge of the role of the wake behind the drop. The coefficient of mass transfer K, is, therefore, related to Sherwood number.

The model that accounts for the influence of wake, equation 5.27, is reported to predict with no greater accuracy than the others. Oscillating drops have been reported[158,159] as being 45% more efficient in mass transfer than drops without oscillations. Garner et al[170] report a correlation for such drops and which has been recommended for its accuracy[145]. A more empirical equation has been reported by Hughmark[169], but its general applicability remains to be proven.

Although some authors[165] attach importance to the influence of the wake behind the drop, this may not be so important for practical contactors. In the latter, drops occur in swarms which probably destroy the wakes by mutual interaction and by turbulence. Even in the case of single drop studies, it has been shown that the wake diminishes rapidly with the distance travelled by the drop[170].

5.5 MASS TRANSFER DURING COALESCENCE

Mass transfer can occur during coalescence at the phase boundary or between pair of drops. The fraction of mass transfer

TABLE 5.3

CORRELATIONS FOR CONTINUOUS PHASE MASS TRANSFER COEFFICIENT

TYPE OF DROP	AUTHORS	CORRELATION	REMARKS	EQN. NO.
RIGID DROPS	Linton et al[163]	$Sh=0.582(Re)^{\frac{1}{2}}(Sc)^{1/3}$	Does not account for wake or diffusion mechanism	5.25
	Rowe et al[164]	$Sh=2+0.76(Re)^{\frac{1}{2}}(Sc)^{1/3}$	This model accounts for diffusion by inclusion of 2.0	5.26
	Kinard et al[165]	$Sh=2+(Sh)_n+0.45(Re)^{\frac{1}{2}}(Sc)^{1/3}+0.484(Re)(Sc)^{1/3}$	Transfer occurs by diffusion, conversion	5.27
NONRIGID DROPS	Boussiness[166]	$Sh = 1.13(Re)^{\frac{1}{2}}(Sc)^{\frac{1}{2}}$	Non-rigid drops not showing oscillations	5.28
	Garner, Tayeban et al[167]	$Sh=0.6(Re)^{\frac{1}{2}}(Sc)^{\frac{1}{2}}$	Non-rigid drops not showing oscillations	5.29
	Garner et al[168]	$Sh=50+0.0085(Re)(Sc)^{0.7}$	Oscillating drop	5.30
	Hughmark[169]	$Sh=2+0.084(Re^{0.484}.Sc^{0.0339}\left(\frac{dg}{D^{2/3}}\right)^{1/3}\ 0.072)^{3/2}$	Oscillating drop	5.31

by coalescence is a subject of debate: whereas Licht and Conway[89], Coulson and Skinner[149] submit that it is the same order of magnitude as that during drop formation, Skelland and Muihas[157] observe otherwise. Angelo and Lightfoot[172] corroborate the latter conclusion, but Heertjes and De-Nie[152] report that the mass transfer in the coalescence stage may be ignored.

Johnson and Hamielec[162] propose that the efficiency of transfer can be expressed as,

$$E = \frac{2Ai}{v}\left(\frac{D\theta}{\pi}\right)^{\frac{1}{2}} \qquad 5.32$$

The assumptions made in this model are that as each drop settles it spreads as a layer of initial uniform concentration across the previously settled phase and that the transient mass transfer occurs until the next drop arrives to cover the surface.

Jeffreys and Lawson[124], however, report that with concentration of acetone less than 5% coalescence was stepwise, and both first step and overall times were influenced by the initial concentration of diffusing component.

Muirhas and Skelland[151] have developed two models, the more fundamental of which can be written as,

$$\frac{K_{dc}t_f}{d} = 0.1727\left(\frac{\mu_d}{\rho_d D_d}\right)^{-1.15}\left(\frac{\Delta\rho g d}{\sigma}\right)^{1.302}\left(\frac{v_t^2 t_f}{D_d}\right)^{0.146} \qquad 5.33$$

Deviation of $\pm$ 25 % from the experimental values has been claimed for this equation.

Mass transfer by coalescence of pair of drops has been shown

to be potentially more significant than drop-phase boundary coalescence . Boyens and Lawrence[173] and El-Defrawi et al[174] report the strong presence of circulation induced by agitation and shear and its effect upon the mass transfer rate.

Coalescence in centrifugal contactors has not been studied and no firm conclusion on equation 5.32 and 5.33 can be made.

6. CENTRIFUGAL EXTRACTOR FUNDAMENTALS

6.1 GENERAL

The importance of droplet phenomena in extraction equipment has been discussed generally in previous chapters. Means of producing droplets and predicting their size and velocities have also been reviewed. The purpose of the chapter is to correlate published work on droplet phenomena and mass transfer operations for a centrifugal extractor.

6.2 OPERATIONS OF CENTRIFUGAL EXTRACTOR

6.2.1 Mechanisms of Operation

The flow patterns in a centrifugal extractor are largely determined by the internals, and as these are not visible, the information available is conjectural. Furthermore the two basic types of centrifugal extractor, the continuous differential and the stagewise continuous, will each have different mechanisms. However, a review of literature gives no information on the latter class of centrifugal extractor.

Most continuous differential centrifugal extractors have a number, e.g. 10 to 18, concentric annuli which are interconnected by slots. The heavy liquid enters the extractor through the rotary seals and passes into the rotor, the actual extraction chamber, near the axis. The light liquid is similarly fed to the extractor and passes to the periphery of the extraction chamber. Centripetal force causes the heavy liquid to flow outwards towards the periphery, therby displacing the light liquid inwards. In the zone where the

heavy liquid predominates, a layer of light liquid accumulates and on reaching a certain head it flows through the slots. Similarly, in the zone near the centre of the rotor, which is dominated by light liquid, the heavy liquid forms a layer on the inner side of each ring.

The perforations allow two way flow of the two liquids. For instance, as the heavy liquid passes outwards through a slot it forms doplets of dispersed phase in the continuous light liquid layer on the outer side of the metal partition. The droplets travel radially until they coalesce with the heavy liquid layer on the inner side of the next ring. Similarly, at the other end, the droplets formed from the light-liquid through slots travel in the heavy liquid zone which near the periphery is the continuous phase. The effect is the creation of an interfacial area through which mass transfer takes place. The principle is that of repeatedly mixing and settling the two liquids, and this is accentuated by the centrifugal force which also makes the two layers flow past each other until they pass into the adjacent annulus.

The conditions existing in the rotor are often visualised as comprising a 'principal interface' and series of 'minor interfaces'. The heavy phase predominates from the principal interface outwards. Between the principal interface and axis, the light phase predominates. In each clearance between the concentric cylinder accumulated dispersed phase develops sufficient head so as to pass through the slots. Hence, even in the region where light liquid predominates, some heavy phase is present passing outwards. The position of the principal interface has considerable effect on the performance of the centrifugal

extractor: thus, if it is caused to move out of the contacting chamber by one or the other liquid, flooding will occur. In commercial extractors, the principal interface is often controlled by a back pressure regulator in the light-liquid-out stream. At a fixed setting of the back pressure regulator, an increase in flowrate will increase the light-liquid-out pressure.

6.2.2 Pressure Characteristic of a Centrifugal Extractor

From the paragraph above it is obvious that pressure balances play a significant part in the performance inside a centrifugal extractor. Todd[175] studied this in some detail and the salient features are reviewed here. This treatment is explained by reference to Figs.6.1.(a), (b), which represent side and front view of a cross-section of a Podbielniak extractor, and to Figs.6.2(a),(b) where analogies are drawn with legs of manometers. According to Todd[175] the principal interface is controlled by imposing a back pressure on the light-liquid-out, LLO, stream and the pressure at the heavy-liquid-out point, R_{HLO}, is given by:

$$P_H = 0.513 \times 10^{-6} \; R^2 N^2 \; G_H \qquad (6.1)$$

where G_H is the specific gravity of the heavy phase. This equation according to Todd[175] represents one leg of the imaginary manometer in Fig.6.1

The pressure at the rim outboard of R_{LLO} must also be equal to pressure given by equation 6.1. This can be considered as the second leg of the imaginary manometer: both legs are equal as far back as the principal interface. Inboard of that level in 'B' leg an

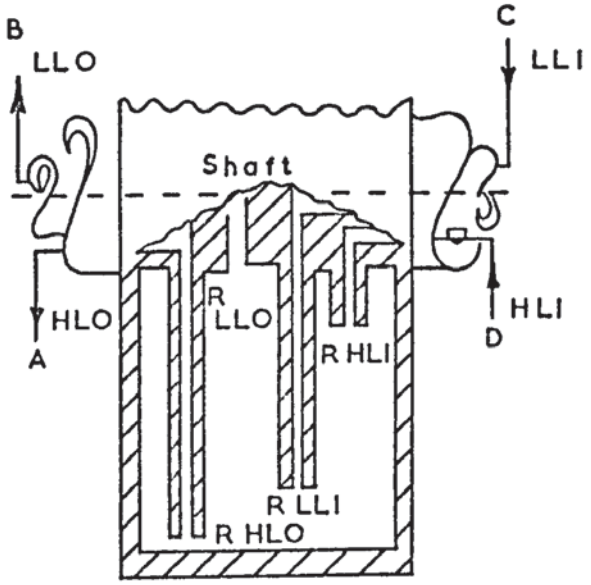

FIG. I. A. SIDE VIEW CROSS SECTION OF A PODBIELNIAK EXTRACTOR. ROTOR.

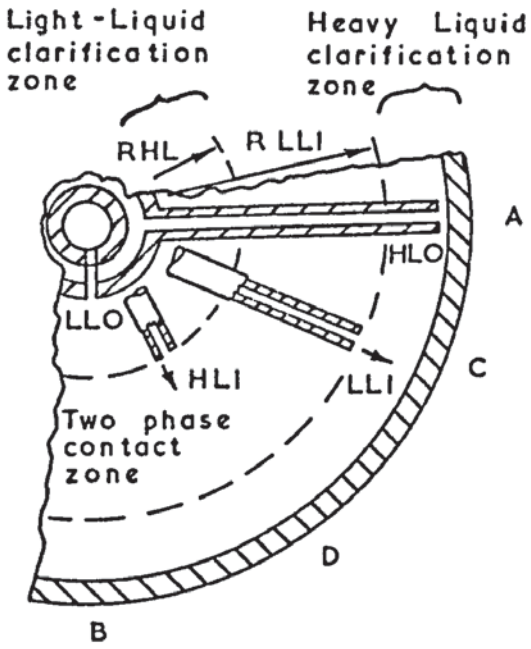

FIG. 6.1.B. FRONT VIEW OF THE ROTOR

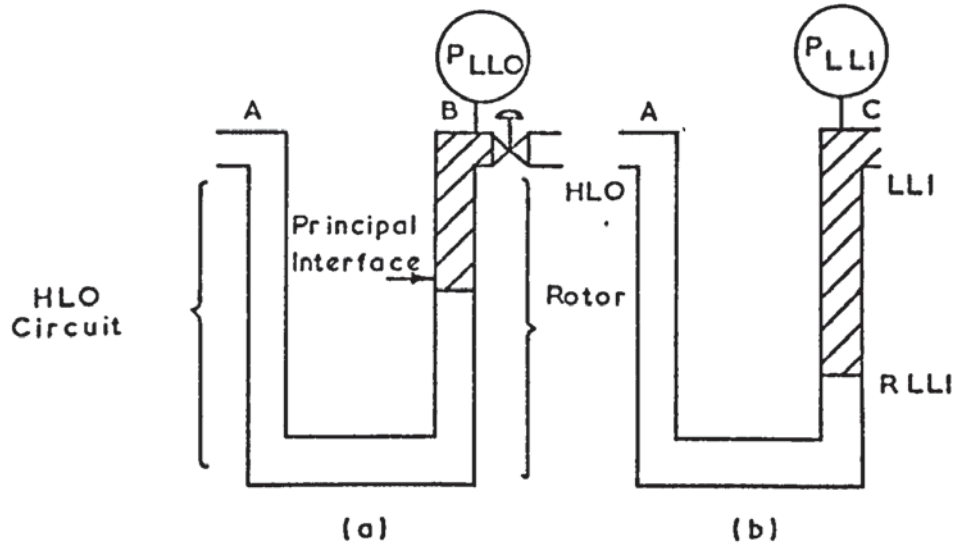

FIG. 6.2. MANOMETER ANALOGIES FOR DETERMINING (a) THE INTERFACE LOCATION AND (b) PRESSURE REQUIRED TO PUMP LIGHT LIQUID INTO THE ROTOR

additional pressure has to be imposed at P_{LLo}. Imposition of larger or smaller pressure can cause the rotor to fill with light phase and heavy phase respectively.

By using a similar analogy, Todd[175] presents an equation for the prediction of inlet pressure required to pump the liquid-liquid into the rotor P_{LLi},

$$P_{LLi} = P_{HLo} = 0.513 \times 10^{-6}(R_{LLi})^2 N^2 G \qquad (6.2)$$

where G is the difference in specific gravities ($G_{HLo} = G_{LLi}$). The light-liquid-in pressure, P_{LLi}, is insensitive to the location of the principle interface as long as this is inboard of R_{LLi}. As the interface is moved outwards by imposing larger P_{LLo}, the light-liquid-in pressure, P_{LLi}, increases exactly as P_{LLo} increases.

Similarly, Todd[175] used the manometer analogies to calculate the pressure required to pump the heavy liquid into the rotor, P_{HLi}. If the principal interface is outside R_{HLi}, pressure P_{HLi} equals P_{LLo}, and if it is inboard of R_{HLi} the pressure P_{HLi} is no longer sensitive to the location of interface.

To summarise, therefore, it can be shown that these pressure balances influence the flooding limits and hence the operating range of a centrifugal extractor.

There are, however, pressure losses across the centrifugal extractor, which are incurred at entry, exit and through the contacting zone. The pressure drop at $\omega = 0$, P_0, is dependent only upon the geometry and flowrate, Q, and can be predicted from the equation,[176]

$$\Delta P_0 = 0.034\ Q^{1.6} \qquad (6.3)$$

For $\omega > 0$, an additive term is included to account for the rotation i.e.

$$\Delta P_N = \Delta P_O + 5.7 \times 10^{-5} QN \qquad (6.4)$$

6.3 HYDRODYNAMIC STUDIES

6.3.1 Hold Up

Few attempts have been made to quantify and predict the hold-up in a centrifugal extractor because of the difficulty in applying normal gravity tower hold up measurement techniques.

The hold up in a centrifugal extractor is contained in two functional units. One is the rotor or the contacing zone, and the other comprises the seals and feed and product lines. If V_E is the total extractor volume and V_C is the rotor or contacting volume, the seal volume V_S is :-

$$V_S = V_E - V_C \qquad (6.5)$$

Previous workers[177,44] obtained results on a Podbielniak model 5000 (the 'Pup') which show that values of both V_E and V_C were different in each case. Barson and Beyer[175] found V_E to be 600 cc and V_C to be 65 cc, but Jacobsen and Beyer[44] report the values to be 638 cc and 529 cc respectively. Morgenthaler et al[178] reports values of V_E and V_C that are in closer agreement with the former. Clearly the procedures of measuring the hold up and the factors affecting hold up require further elucidation.

Basrsèn and Beyer[177] and Morgenthaler et al[178] measured the hold up by valving off both the feed and effluent streams, stopping the rotor, and draining. Jacobsen and Beyer[44] consider this

technique to be of limited value since the liquid streams leaving the rotor follow an extremely tortuous path. They employed another approach: displacement of one phase in the extractor by another. If subscripts L and H denote light-liquid and heavy liquid respectively then:

$$V_E = V_H + V_L \tag{6.6}$$

$$V_C = V_{CH} + V_{CL} \tag{6.7}$$

$$V_S = V_{SH} + V_{SL} \tag{6.8}$$

$$V_L = V_{CL} + V_{SL} \tag{6.9}$$

$$V_H = V_{CH} + V_{SH} \tag{6.10}$$

In these equations V_E, V_C, V_S, V_{SH} and V_{SL} are constants, whereas V_L, V_H, V_{CL} and V_{CH} are variables dependent upon experimental conditions. Jacobsen and Beyer using the earlier work[177,178] obtained a relationship between the light-liquid-out pressure (P_{Lo}) and the heavy phase volume of the contacting section, V_{CH}; viz

$$V_{CH} = \pi b \left(r^2 - \frac{2g.P_{Lo}}{\Delta\rho_\omega^2}\right) \tag{6.11}$$

which when substituted into Equation (6.7) yields :

$$V_{CL} = (V_C - \pi br^2) + \left(\frac{2\pi bg}{\Delta\rho_\omega^2}\right). P_{Lo} \tag{6.12}$$

Since πbr^2 is volume of contacting section,

$$V_C = \pi br^2$$

$$\text{i.e. } V_{CL} = \left(\frac{2\pi bg}{\Delta\rho\omega^2}\right) . P_{Lo} \tag{6.13}$$

Substitution into (6.9) and (6.10) yields

$$V_H = (\pi br^2 + V_{SH}) - \left(\frac{2\pi bg}{\Delta\rho_\omega^2}\right) . P_{Lo} \tag{6.14}$$

$$\text{and } V_L = V_{SL} + \left(\frac{2\pi bg}{\Delta\rho\omega^2}\right) P_{Lo} \qquad (6.15)$$

Jacobsen and Beyer experimentally determined that the volumes V_L and V_H are dependent upon the range of light-liquid-out pressure P_{Lo}. (Fig. 6.7). Thus,

For $P_{Lo} < 96$ lb/in^2 $\quad V_H = 663.14 - 5.03\ P_{Lo}$ (6.14a)

$$V_L = 84.38 + 5.04\ P_{Lo} \qquad (6.15a)$$

For $P_{Lo} > 96$ lb/in^2 $\quad V_H = 314.53 - 1.41\ P_{Lo}$ (6.14b)

$$V_L = 417.83 + 1.57\ P_{Lo} \qquad (6.15b)$$

The extractor hold up V_E is obtained from the substitution of equations (6.14a) and (6.15a) and equations (6.14b) and (6.15b) into equation (6.6) yield,

$$V_E = 7.47.52 + 0.01\ P_{Lo} \qquad (6.6a)$$

$$V_E = 732.36 + 0.016\ P_{Lo} \qquad (6.6b)$$

respectively. Predicted values for V_E and V_C show good agreement with experimental values for the particular system, i.e. Podbielniak Model 5000, 'pup'. General applicability for other models is not claimed, although it is suggested that the relationship should be linear, i.e.

$$V_E = (\text{constant } C_1) + (\text{constant } C_2)\ P_{Lo}.$$

Jacobsen and Beyer use an extension of these equations to define operating limits of the extractor, which will be discussed in Section 6.3.2.

No other work exists which shows the hold-up relationships. Data from manufacturers is also not available on request.

6.3.2 Flooding Phenomena

Todd[176] reports the flooding of the Podbianiak extractor to be similar to columns in that three types can occur, viz:

(a) Shaft flooding - or the light liquid flooding.

(b) Rim flooding - or the heavy liquid flooding.

(c) Capacity flooding.

Shaft flooding is observed by the entrainment of heavy liquid into the ligh liquid effluent and may occur, even at low capacities, by shifting the major interface through the light liquid clarifying zone. The latter is shown by Fig. 6.1b. At higher capacities shaft flooding can occur, even with the major interface positioned in the contacing section, when the clarifying section residence time and settling forces are insufficient to achieve coalescence and disengagement of droplets generated in the contacting zone.

Rim flooding or heavy-liquid flooding is observed by the entrainment of light-liquid into the heavy liquid effluent, and can occur in analogous manner at the extreme end of the centrifugal contactor. Capacity flooding is observed by simultaneous flooding or entrainment at both ends of the unit. It is initiated in the contacting zone and occurs when an excessive head (h) of coalesced dispersed phase is required to generate the pressure drop for flow of liquids through the orifices.

Jacobsen and Beyer[44] report only two types of flooding to occur in centrifugal extractors. However, the types are the same as those reported by Todd[176], but these workers classify (a) (b)

as one and (c) as another type of flooding.

Since the flooding of any type can cause destabilisation of the system, the prediction of operating limits are necessary. Jacobsen and Beyer[44] used equations (6.11) viz (rearranged),

$$P_{Lo} = \frac{\Delta\rho\omega^2}{2g_e} \left(r^2 \frac{V_{CH}}{\pi b}\right)^1 \qquad (6.16)$$

The values of r, b and $\Delta\rho$ are known but the value of V_{CH} has to be determined. Since at flooding point the liquids spill over into the effluent when the major interface is forced out of the contacting zone, the value of $(V_{CH})_F$ can be determined. Jacobsen and Beyer [44] were able to enunciate the operating limits, viz:

$$(P_{Lo})_{FH} = (4.86 \times 10^{-6})\ \omega^2 \qquad (6.17)$$

at flooding in the heavy liquid. For flooding of light liquid,

$$(P_{Lo})_{FL} = (0.477 \times 10^{-6})\ \omega^2 \qquad (6.18)$$

As the agreement between predicted and experimental values is claimed to be good, equation (6.16) is concluded to predict the operating limits satisfactorily as shown by Figs. 6.4, 6.5.

Whereas Jacobsen and Beyer used light-liquid-out pressure (P_{Lo}) with the speed of rotation (ω) as means of defining operating limits, Barson and Beyer used P_{Lo} and the light-liquid-rate of flow (R_L) and the maximum back pressure. At fixed heavy liquid flow rate, various light liquid rates are set and for each setting the light-liquid-out pressure measured at incipient flooding. This provides one limiting curve. The other being from the regulation of back pressure to set the desired light liquid rate and measuring light-

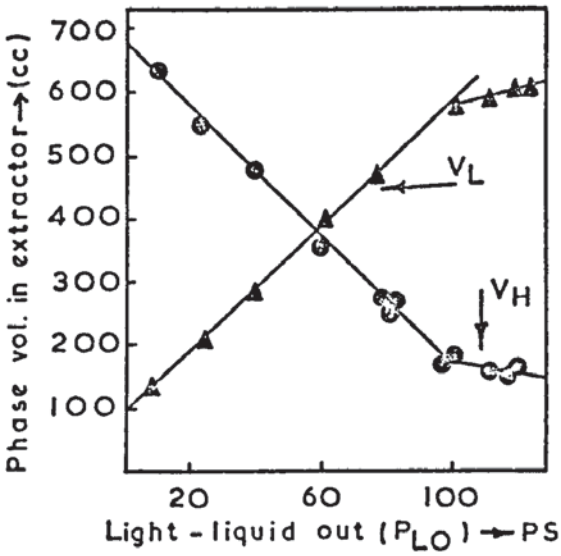

FIG. 6.3. Isoamyalcohol - water system
Rotor speed 5000 R.P.M.
Variation of Rotor volume with
Light - liquid out. Pressure (P_{LO})

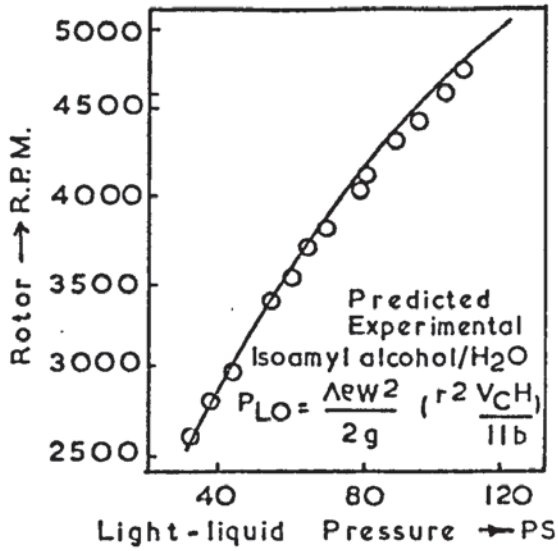

FIG. 6.4. Relationship between
Rotor speed and Light - liquid -
out. Pressure at flooding in
Heavy liquid out

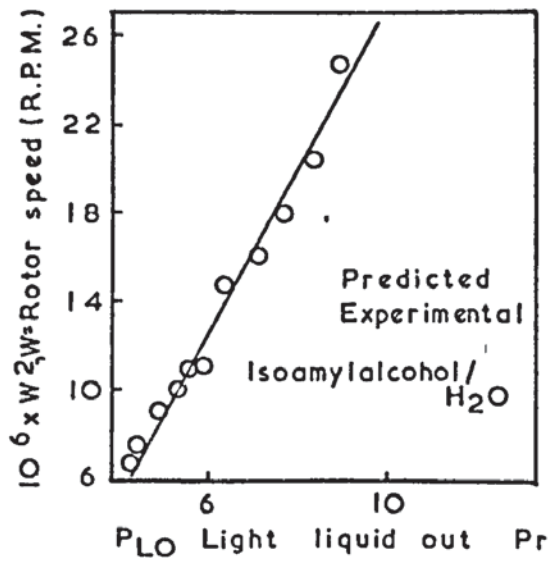

$$P_{LO} = \frac{\Delta \rho W^2}{2g} \left(12^2 \frac{V_C H}{11 b}\right)$$

FIG. 6.5. Relation between Rotor speed and
Light - liquid - out Pressure at flooding the
Light liquid

liquid-out pressure. As can be seen from the Figs.6.6 and 6.7, the first operating curve shows linear relationship and that at maximum back-pressure setting it is curve. The operating range is said to lie between the two lines. The maximum total capacity reported for the extractor (Pup model of Podbielniak) was 425 and 450 cc/min, for boric acid-isoamly alcohol-water system. If this combined flow capacity is exceeded simultaneous flooding occurs in both the streams. Also, capacity is reported to decrease at lower rotor rotational speeds. Todd also used the latter approach in defining the flooding curves, i.e. the ordinate represents the range of back pressues on the light-liquid leaving, for which the extractor can be operated. As can be seen from Fig.6.8 the capacity flooding occurs very rapidly and the definition of exact pointsfor the rim and shaft flooding is difficult.

By making a mass balance over the orifice, Todd et al[176] arrived at a very simplified equation, i.e.

$$2\ (\rho_H - \rho_L)\ R\omega^2 h = \rho_C \left(\frac{Q_C}{A_C}\right)^2 + \rho_D \left(\frac{Q_D}{A_D}\right)^2 \qquad (6.19)$$

From their data on a pilot scale extractor they conclude that the combined flow is proportional to the first power of speed, which is similar to the equation (6.19). The total capacity is reported to be higher when the ratio of the light liquid to heavy liquid is increased.

In the case of a commercial extractor, similar results to the pilot scale are reported. However, in some cases deviations are reported. This is especially so in systems that very readily emulsify and the simple linear relationship between the rotor speed and the combined flow does not hold. In these cases, the pressure differential

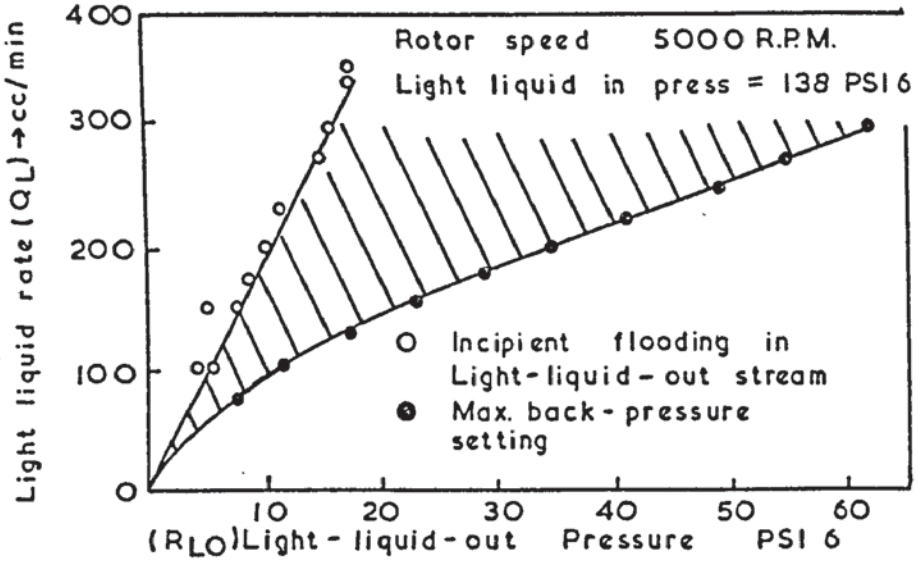

FIG. 6.6. Operating range for clear effluent streams at heavy-liquid flow rate Q H = 100cc/min

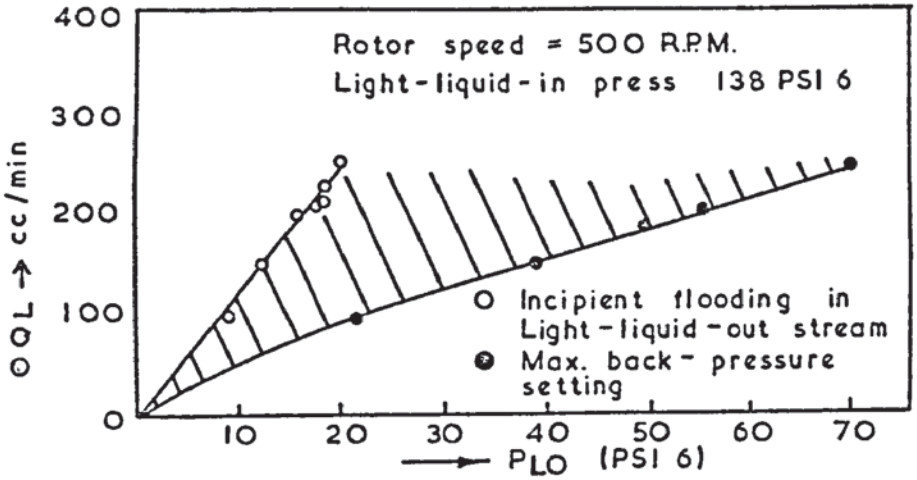

FIG. 6.7. QH = 150

FIG. 6.8. Flooding envelopes at QK ½QW (Kerosene/system)

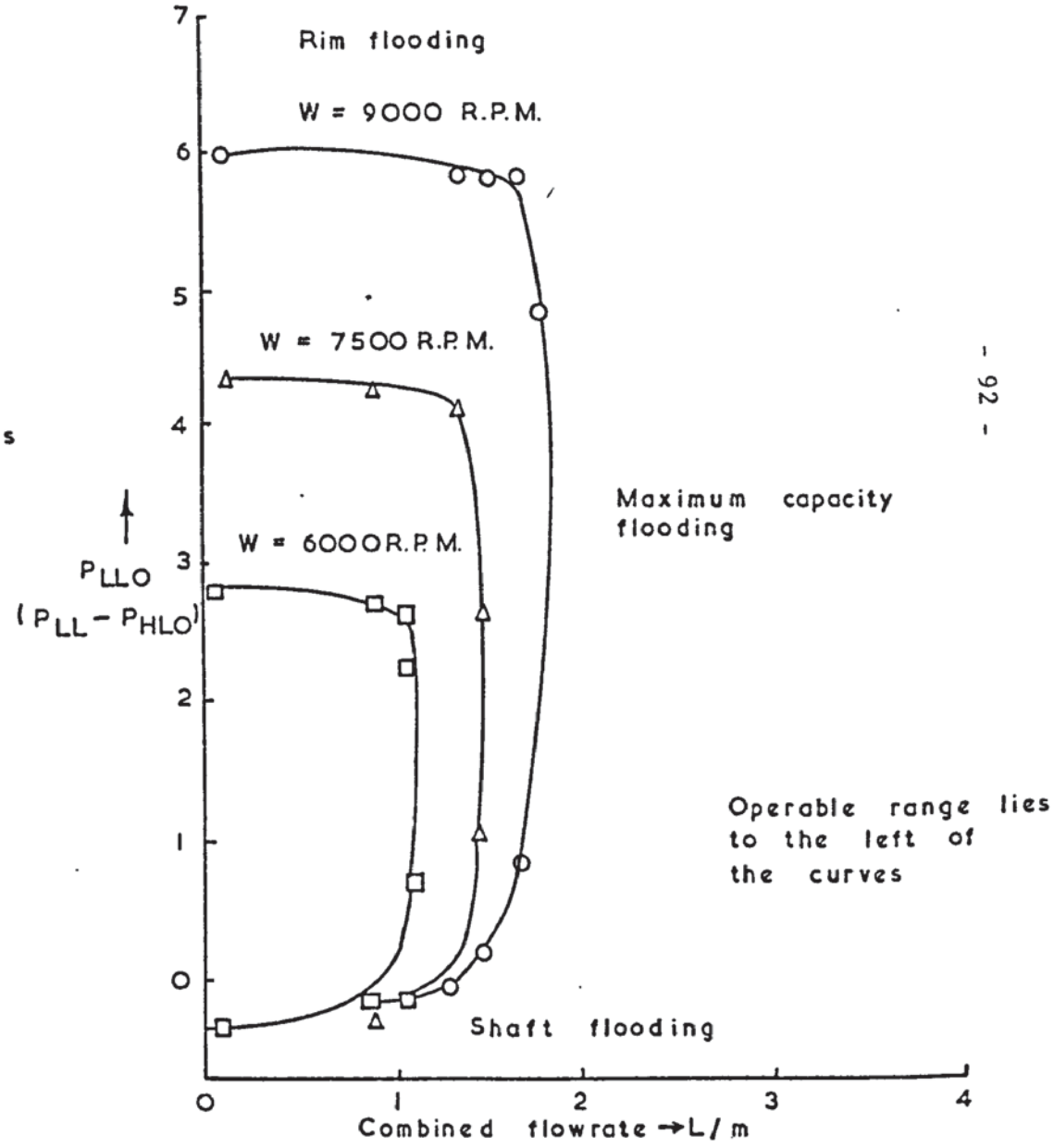

over which a centrifugal extractor may be operated is expanded as the rotor speed is increased, but the capacity flood point is not increased proportionately.

6.3.4 Flow in Centrifugal Fields

6.3.4.1 Discharge from Orifices

Unlike the other extraction equipment, flow dynamics of centrifugal extractors are not fully available in literature or understood. However, some Japanese work[179,180] has been devoted to the study of the flow of liquids in air from openings in a side wall of a revolving cylinder. But the study of flow out of orifices in centrifugal fields applicable to liquid extraction has been done by Russian workers[42,43,18].

The process of flow of liquids in a centrifugal field is made more complex than in a gravitational field by the occurrence of Corolois force acting on small parts of the liquid moving about the revolving rotor. The direction and size of this force changes according to the direction of movement of the part of the liquid and the speed of relative movement. This force breaks the symmetry of the lines of flow of flowing liquid and will affect the dynamics of flow in a centrifugal field in a manner dissimilar to that in the case of gravitational flow.

By means of partial visual observations, Ponikarov[43] et al report that five characteristic states of discharge of liquid exist viz:

(i) drop state with an uneven separation of drops;

(ii) drop state with an even separation of drops;

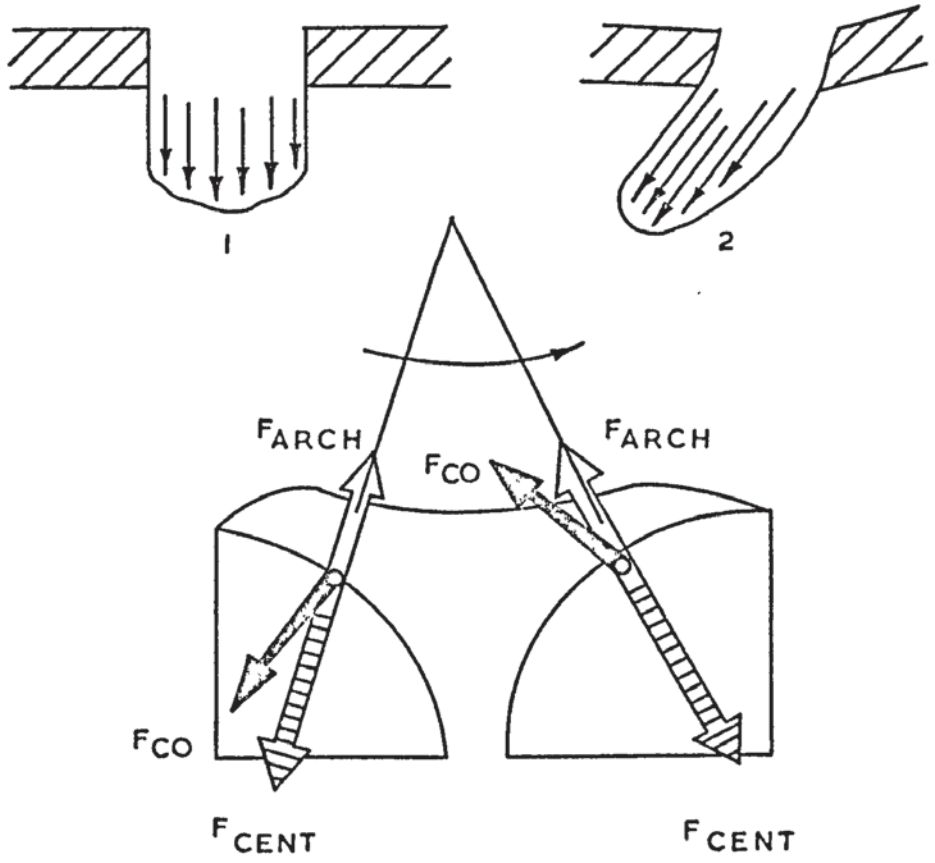

FIG. 6.9. 1,2 LINES OF FLOW FOR A CENTRIFUGAL FIELD
3 SCHEME OF FORCES ACTING
F_{CO} COROLOIS FORCE
F_{CENT} CENTRIFUGAL FORCE
F_{ARCH} ARCHIMEDIAN FORCE

(iii) jet spray state;

(iv) pulse jet state; and

(v) flare state.

Bochkarev et al[42], however, report that only three conditions persist, i.e. drop, jet and spray. The transition from one state is dependent upon the pressure of discharge: the factors influencing the latter are reported as:

(a) angular velocity of rotation of the drum;

(b) the thickness of the layer of the discharging liquid;

(c) the radius of perforated cylinder; and

(d) physical properties of the continuous and the dispersed phase.

Ponikarov et al[43] defined a coefficient of discharge by the relationship,

$$Q = Cod \quad Q_T \tag{6.20}$$

The theoretical flow rate Q_T was obtained from application of Bernouillis equation and after simplifying assumptions,

$$Q_T = A_o \, \omega \left(\frac{\Delta\rho}{\rho_c} (r_c^2 - r_i^2)\right)^{\frac{1}{2}} \tag{6.21}$$

Thus the coefficient μ_{dis} is

$$Cod = \frac{Q}{\omega A_o \left(\frac{\Delta\rho}{\rho_c} (r_c^2 - r_i^2)\right)^{\frac{1}{2}}} \tag{6.22}$$

The data obtained for the coefficient of discharge was correlated by two dimensionless numbers: the first being defined as ratio of Corolois force and the difference of centrifugal and Archimedian forces, i.e.

$$\text{1st dimensionless No} = \left(\frac{\rho dQ}{A \rho \omega r}\right)$$

The second number was defined so as to take into account the size of orifice and the size of contact cylinders, i.e.

$$\text{2nd Dimensionless No} = (A_o/A_c)$$

It was found that there were separate relationships depending upon the state of fluid issuing from the orifice.

For drop condition,

$$C_{od} = 0.75 \left(\frac{\rho dQ}{\Delta\rho \omega r}\right)^{0.9} \cdot (A_o/A_c)^{-0.07} \qquad (6.23)$$

For jet condition

$$C_{od} = 0.3\left(\frac{\rho dQ}{\Delta\rho \omega r}\right)^{0.12} (A_o/A_c)^{-0.07} \qquad (6.24)$$

It is also reported by Ponikarov et al[43] that transition from drop to jet condition can be characterised by the first dimensionless number.

Thus the criterion is,

$$N_1 = \left(\frac{\rho dQ}{\Delta\rho \omega r}\right) < 0.36 \quad \text{drop condition}$$

$$N_2 = \left(\frac{\rho dQ}{\Delta\rho \omega r}\right) \geq 0.36 \quad \text{jet condition}$$

Bochkarev et al[42], however, report that this number is a modification of the Froude number (F_r). Also the value of this number (N_1) that characterises the change from drop to jet condition is reported to be 0.48 as shown by Fig. 6.10. As is clear from this in the case of the jet flow there are two different cases. In the first case of flow, Bochkarev et al infer an even jet comes out of the orifice which then falls into drops of almost equal size. This field is

FIG. 6.10 THE DEPENDENCE OF COEFFICIENT OF DISCHARGE C_d ON THE DIMENSIONLESS NUMBER $(\rho Q/\Delta P W R)^{(42)}$

defined by $(F_r)_{mod} = N_1 \simeq 0.48$. In the second case separation of the small drops occurs from the side of the jet and when $(F_r)_{mod} = 1$ a clear dispersion of emerging jet into many small drops was observed.

Thus for two cases there are different correlations.

(i) when $(F_r)_{mod} = 0.48$, the coefficient of discharge C_{od} is

$$C_{od} = 1.25 \ (F_r)_{mod}^{0.9} \qquad (6.25)$$

(ii) when $(F_r)_{mod} = 1$, the coefficient C_{od} is,

$$C_{od} = 0.63 \ (F_r)_{mod}^{0.12} \qquad (6.26)$$

However, unlike Ponikarov's criterion these two equations do not show the significant influence of dimension of opening and the contact cylinder. As with equations (6.23), (6.24), the influence of physical properties on C_{od} are also not shown.

6.3.4.2 Flow Over a Weir

As was discussed in Chapter 2, there are some types of centrifugal extractor, classified as stagewise countercurrent, which employ annular weirs. Efficient operation of such extractors requires that the two discharging weirs should match, which in practical terms is achieved by physically changing one or both of the weirs to correspond to the densities of specific liquids. Jenning[12] considers this to be impractical and means of fixing the interface by theoretical calculations are required.

Jenning[12] reports that flow over a circular weir in a centrifugal field is given as:

$$Q_\omega = Kf\pi\omega r_*^3 \ (1-F)^{3/2} \qquad (6.27)$$

It is attributed by Jennings to Webster[53,54] but cannot be authenticated since the work is only available for the official use of American Atomic Energy Commission.

By means of a pressure balance for a centrifugal field, Jenning[12] obtains

$$\rho_c(r_i^2 - r_c^2) = \rho_d(r_i^2 - r_d^2)$$

which was then substituted into equation (6.27),

$$r_i = \left(\frac{r_c^2 - r_d^2(\rho_d/\rho_c)}{1-(\rho_d/\rho_c)} \right)^{\frac{1}{2}}$$

since $r_c^2 = r_{*c}^2 F$ and $r_d^2 = r_{*d}^2 F$, then

$$r_i = \left(\frac{r_{c*}F - r^2_{d*F}(\rho_d/\rho_c)}{1-(\rho_d/\rho_c)} \right) \qquad (6.28)$$

6.3.5 Drop Size in Centrifugal Extractors

Fox[18] reports a very approximate method of predicting drop sizes in centrifugal extractors. It is more of an estimate rather than a means of predicting. Starting with the assumption that the Stokes Law is approximately valid, the settling velocity of a drop can be written as:

$$V_d = \frac{2gr^2}{9\mu_c} \qquad (6.29)$$

In this equation r, the mean droplet radius, is related to the interfacial tension for packed columns, and assumed to hold for centrifugal extractors, by

$$r^2 = \frac{5\sigma}{16\Delta\rho\omega^2 R} \qquad (6.30)$$

Hu and Knitner[68] have actually questioned the validity of this relationship even for packed columns; Fox[18], nevertheless assumes its validity for centrifugal extractors which is highly questionable. Since the $(\omega^2 R)$, the centrifugal force, is of the order 1500-5000 g's, Fox states that the droplet radi will be 40 to 70 times smaller in the centrifugal extractor than in a gravitational tower.

In his work, Fox[18] compares the performance of a centrifugal extractor and a gravity tower and observes 45 fold increase in extraction rate. This is attributed to the increase in interfacial area available for mass transfer: the interfacial area being measured by the surface area/volume ratio of a spherical drop, i.e.

$$A = 3/r = 3\left(\frac{16\Delta\rho g}{5\sigma}\right)^{\frac{1}{2}} \qquad (6.31)$$

This equation, according to Fox[18], predicts interfacial area per unit volume to be 40 to 70 times greater than in the equivalent gravity columns.

In Chapter 3 many correlations are discussed for predicting the size of droplets in conventional columns, but there is none available for centrifugal extractors. This, however, does not preclude the modification of some of these correlations, since most are derived from the same basic principle, i.e. the droplet in the first stage 'necks' and then breaks away when the buoyancy force overcomes the interfacial tension,(at low velocities). At jetting velocity or above, the mechanism is no longer the same. Since both states are known to exist in centrifugal extractors, drop size correlations for both the droplet and jet conditions are necessary.

In the aforementioned chapter, it is concluded that Scheel-Meister correlations are probably the most useful, from the view point of reliability and being more simple to use, viz:

At low velocities (i.e. below jetting),

$$V_F = F\left(\frac{\pi D_N}{\Delta\rho g}\right) + \frac{20\mu Q D_N}{D_F^2 \Delta\rho g} - \frac{\Delta\rho_d Q U}{3\Delta\rho g} + \left(\frac{Q^2 D_N^2 \rho_d \sigma}{(g\Delta\rho)^2}\right)^{1/3} 4.5) \qquad (4.12)$$

And from cylindrical jets

$$V_F = F\left(\left(\frac{2\pi a}{g\Delta\rho}\right) - \left(\frac{4\rho' Q U_N}{3\left(\frac{a}{an}\right)^2 g\Delta\rho}\right) - \left(\frac{40\mu Q a}{D_F^2 g\Delta\rho}\right) + 7.15(Q^2 A^2 \rho' \sigma/g\Delta\rho)^2)^{1/3}\right) \qquad (4.19)$$

which reduces for long jets, to

$$V_F = \frac{2\pi^2 (a^3)\ /2}{N(ka)_{max}(U_1/U_A)\ \ /2} \qquad (6.32)$$

The principal difference between the mechanism of drop formation under gravity conditions and in centrifugal fields is that in the latter the controlling force is the centrifugal and not the inter-facial tension.

Hydrodynamics of droplet break-up in centrifugal fields is also completely unknown and it is open to question whether the Hinze[120] fundamental theory is observed or not. Moreover, the local isotropic theory of Kolmogoroff[121,122] cannot be verified since no data exists. However,

it is felt that this concept may hold since the theory is a statistical hypothesis.

As the drop size is not known, that a particular type of size distribution exists for centrifugal extractors cannot be ascertained.

6.3.6 Drop Velocities in Centrifugal Field

No literature pertaining to droplet behaviour in a centrifugal field exists but one research paper on behaviour of bubbles exists. It is therefore presented here as being an analogy and which can be extended to actual drops.

Safanov and Krylov[181] consider bubble units with a cylindrical liquid layer rotating with a drum with a perforated lateral surface. According to these authors the dynamics of formation and subsequent motion of bubbles through a liquid layer in a field of high centripetal forces has a number of specific features. For example, the values of resistance coefficients for single spherical bubbles found in such fields are significantly greater than the corresponding motion in gravity fields.

Using the work of Kochin et al[182] and Hayes et al[183], Safanov and Krylov[181] given an equation for a single bubble which moves in a cylindrical liquid layer rotating at a constant angular velocity (ω), viz:

$$(\rho_g + X\rho_l)\frac{dU}{dR} - \left(\frac{\pi r^2 \rho_e}{V}\right) U^2 + 2(\rho_l - \rho_g)\omega^2 R = 0 \qquad (6.33)$$

where X is a coefficient characterising the effect of 'added mass'. Safonov and Krylov[181], in an earlier work, had derived an expression for the coefficient of 'added mass' (X) for bubbles, viz:

$$X = \left(\ln \frac{p + \sqrt{p^2-1}}{p - \sqrt{p^2-1}} - \frac{2\sqrt{p^2-1}}{p}\right)\cdot\left(2p\sqrt{p^2-1} - \ln \frac{p+\sqrt{p^2-1}}{p - \sqrt{p^2-1}}\right)^{-1} \tag{6.34}$$

where p = a/b and a and b are the major and minor semi-axes of the ellipsoid (the shape of the bubble). P = 1 and x = 0.5 for a spherical bubble. For a system characterised by very high Reynolds number, i.e. a highly turbulent flow, Safonov and Krylov assume that the resistant coefficient ξ does not depend on rate of motion. Thus for the trajectory segment which is unaffected by feed opening, the solution of equation 6.33 is given as,

$$U = \frac{2\omega^2 V}{\xi_{\pi r^2}} \left(R + \frac{XV}{\xi_{\pi r^2}}\right)^{\frac{1}{2}} \tag{6.35}$$

The authors also conclude that the effect of boundary conditions on the rate of motion of a bubble disappears at distances from the feed opening which are greater than $(\frac{2r}{3})$. Furthermore, since R is very much greater than the bubbles characteristic dimension, the term $(\frac{XV}{\xi \pi r^2})$ is ignored, i.e.

$$U = \left(\frac{2\omega^2 VR}{\xi \pi r^2}\right)^{\frac{1}{2}} \tag{6.36}$$

If the bubbles equivalent radius (req) is set, i.e.

$$(req(n) = r \text{ then,}$$

$$U = \gamma \sqrt{j\ req} \tag{6.37}$$

where $j = \omega^2 R$ is the centripetal force and γ is a numerical coefficient defined by the correlation,

$$\gamma = (3\xi n^2/8)^{\frac{1}{2}} \qquad (6.38)$$

Good experimental agreement with equation 6.37 is reported within the constraints assumed in deriving this equation. This is evident from Fig.6.11, which shows that the bubble's rate of motion is proportional to the square roots of the products (jreq). Experimental values of (ξ) of (n) are reported as 1.5 and 2 respectively in Re range 10 to 3×10^4.

This treatment of bubble's motion in a centrifugal field may be further extended to take into account other forces which have been omitted in derivation of the equation 6.33. Further discussion and detailed analysis follows in Chapter .

As mentioned in 6.3.5, Fox[18] assuming Stokes Law to hold, derives

$$Vd = \frac{2gr^2\Delta\rho}{9\mu_c} \qquad (6.29)$$

and

$$r^2 = \frac{5\sigma}{16\Delta\rho\omega^2 R} \qquad (6.30)$$

Substituting equation 6.26 into 6.25 yields an equation for settling velocity in terms of interfacial tension and viscosity, viz:

$$Vd = \frac{5\sigma}{72\mu_c} \qquad (6.39)$$

According to Fox[18] this equation is not intended to show a precise relationship but to indicate that, under conditions where Stokes Law is valid, the settling velocity is primarily determined by the physical properties of the liquids. Fox[18] points to the vertical

FIG. 6.11 RATES OF MOTION OF SINGLE BUBBLES IN A FIELD OF THE CENTRIPETAL $j = w^2R$ (181)

component of drop velocities in various types of extractor as being similar and of the same order as predicted by the equation 6.35. For centrifugal extractors and a 20 tray-tower the velocities are quoted as 0.127 cm/s and 0.285 cm/s respectively, as compared with 0.30 cm/s predicted by the above equation. However, no mention is made of how the value for the centrifugal extractor is arrived at. Since the extractor described had no transparent rotor or portholes for observing the drops, the results are of a doubtful nature.

Fox[18], furthermore, concludes that the settling rate is not substantially accentuated by the presence of the centripetal force in the centrifugal extractor. This is inferred from the absence of $(\omega^2 R)$ term in the equation 6.35, the validity of which is justified from the settling velocity values. It is a surprising conclusion inferred from an equation which is not a 'precise relationship'.

6.3.7 Residence Time

One advantage of centrifugal extractors is that the hold-up or residence times are extremely short. For example, Jenning[12] has designed an extractor for uranium enrichment having residence time of 2 seconds per stage. The larger commercial extractors, however, have residence times of about 6 seconds per stage[12], and 24 seconds per stage[179]. This compares very favourably with towers where residence times of 1080 seconds per stage for a tray tower, and 180 seconds per stage for a packed tower are reported by Fox[18].

Todd[176] has constructed a distribution of residence times from which observations are made about back-mixing. The distributions were determined by injection of a pulse of concentrated NaNo3 solution

FIG. 6.12 RESIDENCE TIME DISTRIBUTION FOR CENTRIFUGAL EXTRACTOR (176)

and measuring the cumulative amount collected in the effluent as a function of time. Fig. 6. 12 shows a comparison of accumulative distribution with the theoretical curve for 13 well mixed stages in series. Todd[176] concludes from this that each compartment in the extractor is well mixed and that essentially there is no back-mixing.

The residence times of actual drops inside the rotor have not been determined so far. Although this will bear relationship to the residence time per stage, it will not be the same.

6.4 MASS TRANSFER STUDIES

In comparison with the hydrodynamics, some data on the mass transfer operations of centrifugal extractors are available in the literature. However, in most cases this is limited to the performance of particular models which renders direct comparison difficult. Fundamental concepts are not expounded except in one case which is discussed below.

6.4.1 Concept of Stages and Efficiency

In literature associated with mass transfer studies in centrifugal extractors an analogy is made with gravity towers, by which it is meant extraction equipment that operate under gravitational fields, as opposed to centripetal, and the theoretical stages calculated in similar fashion. Whereas the former have discrete physical stages, the differential centrifugal extractor, strictly speaking, does not. It does possess internals of various designs but they are all exclusively derivatives of perforated cylinders arranged so that spacing increases towards the periphery.

Whether one can term these as 'stages' is debatable.

It is reported that theoretical stages of any centrifugal extractor are dependent upon the following parameters;

(i) Speed of rotation (ω). Barson and Beyer[177]. This is shown by Fig. 6.13.

(ii) Flow ratio of the two liquid streams. Barson and Beyer[177] and Jacobsen and Beyer[44]. Figs. 6.14, 6.15 show this dependence.

(iii) Light-liquid-out pressure P_{LLo}. Barson[184] reports the effect of low values of P_{LLo}, whereas Jacobsen[185] reports at higher values of P_{LLo}. Fig.6.16 illustrates this.

(iv) System used. Barson and Beyer[177] report different numbers of theoretical stages even with identical speed of rotation and the flow ratio. Furthermore, varying numbers of stages were obtained depending on whether the extraction is from isoamyl alcohol into water, or from water into alcohol. The system used was isoamyl alcohol-water and boric acid.

If these factors, that affect the number of theoretical stages, are kept constant and the internals changed, the number of stages will be different. Doyle et al[186] report that the number of theoretical stages varies in a linear fashion with the diameter of the rotor, as shown by Fig.6.17. The slope of this line is reported to be 1.12.

The factors listed above affect the number of stages in an extractor, having the same internals, in different ways. From Fig.6.13, it is apparent that not only the number of stages increases

TEXT CUT OFF IN ORIGINAL

FIG. 6.13 Effect of speed on Theoretical stages [177]

FIG. 6.14 Stages with various flow ratios [177]

FIG. 6.15 Stages with flow ratio [44]

FIG. 6.16 Variation of number of stages with light liquid pressure at different flow ratios [44]

FIG. 6.17 Stages variation with Rotor diameter [184]

VARIATION OF THEORETICAL STAGES OF CENTRIFUGAL CONTACTOR WITH VARIOUS FACTORS

with speed of rotation but also the number is greater at higher flow rate of the light liquid. There seems to be a contradiction between the reports of Barson and Beyer[177] and Jacobsen and Beyer[44], as observed from Figs. 6.14 and 6.15. However, both indicate that by increasing flow ratio the number of theoretical stages also increases. The dependency of the theoretical stages upon the light-liquid-out pressure at low flow ratios is reported to be insignificant. At high flow ratios, this assumes greater significance, as can be seen from Fig.6.16.

Even though application of the theoretical stages concept to centrifugal extractors has very significant shortcomings, it is persistently found in the literature where it is often calculated from Mc Cable Thiele plots. Jacobsen and Beyer[44], Barson and Beyer[177] use the following expression due to Colburn and Pigford , viz:

$$N = \frac{(\ln(1-J)(Q+J)\ )}{(\ln\ 1/J)} \qquad (6.40)$$

which for liquid-liquid extractors becomes,

for above equilibrium line,

$$N = \frac{\log(1-\frac{(y_1-y_2)(m-a)}{a(y_2-mx_2)})}{\log\ (a/m)} \qquad (6.41)$$

and for below equilibrium line,

$$N = \frac{\log(1\ -\ \frac{(x_1-x_2)(a-m)}{(mx_2\ -\ y_2)})}{\log\ (m/a)} \qquad (6.42)$$

Doyle et al[186] introduce a new concept - the Radial Distance Equivalent to a theoretical stage, (R.D.E.T.S.). By analogy with a

gravity this is illustrated in Fig. 6.18. The authors report that R.D.E.T.S. decreases in length as the radius of the rotor increases, i.e. as periphery is approached the length decreases. The concept of R.D.E.T.S. is used to define the theoretical stage efficiency of a centrifugal extractor. However, other authors define the latter in other ways. Fox[18] defines it in terms of the viscosity index (VI), but without giving details. The value quoted for overall efficiency is 30%. The Murphee-efficiency is also calculated by Fox[18], viz:

$$\eta_{MURPHEE} = \frac{\text{(Actual change in extract gravity in a stage)}}{\text{(Change which would have occurred if equilibrium had been achieved}}$$

Reported value of Murphee-efficiency is 27.8%.

Jenning[12] calculates overall efficiency of up to 87% at extremely high rotational speeds. The extractor, however, is primarily designed for extraction of uranium and is of stagewise countercurrent type. The overall efficiency is calculated from the expression,

$$E_{OV} = \frac{\ln\ 1 + \left(\frac{E_{cc}}{1+(1-E_{cc})}\right)(E_f - 1)}{(\ln E_f)} \qquad (6.43)$$

where E_{cc} is the countercurrent efficiency and E_f is the extraction factor. The extraction factor E_f is kept constant by manipulation of flow conditions, so that E_{OV} could be determined from the above equation. Mini extractors such as this are of only a few inches in diameter and are primarily used in the research into uranium extraction and, therefore, are not representative of commercial extractors.

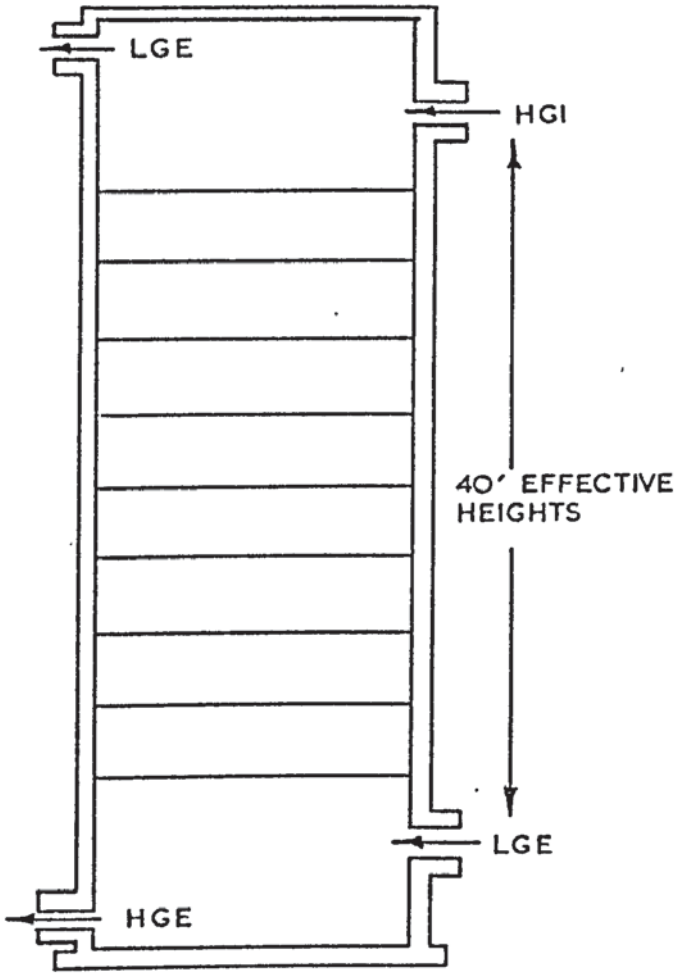

HEIGHT EFFECTIVE FOR A THEORETICAL STAGE H.E.T.S. = 8′

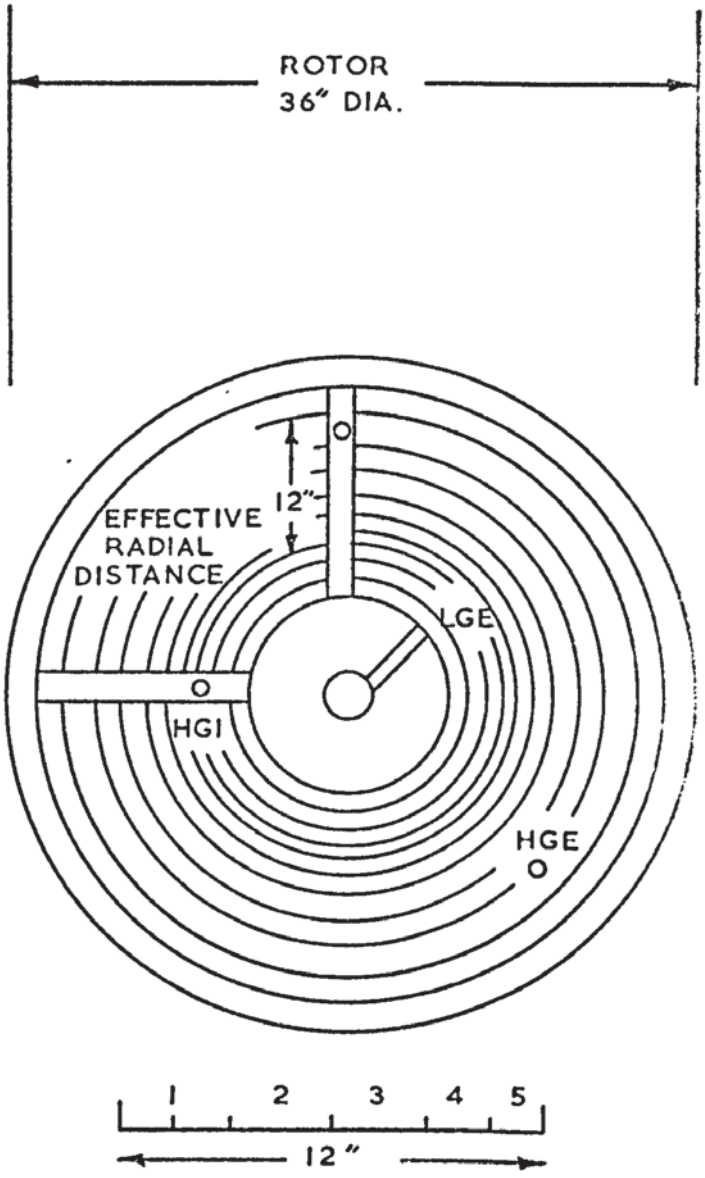

RADIAL DISTANCE EFFECTIVE FOR A THEORETICAL STAGE (R.D.E.T.S.)

FIG. 6.18 THEORETICAL STAGE COMPARISON

To summarise: the concept of a theoretical stage in a centrifugal contactor is questionable; data shows that theoretical stages vary with many factors even in the same extractor; and that overall efficiency is of the order of 30% in commercial centrifugal extractors.

Doyle et al[19] have introduced two new terms which, according to them, are of fundamentally new conception: CONTROLLED GRADIENT MIXING ENERGY AND CONTROLLED GRADIENT SEPARATING FORCE. The reasoning behind the definition is as follows: Any extractor, gravitational or centrifugal, contains solute gradient, increasing from bottom to top or top to bottom depending on whether the selective solvent is heavy phase or light phase. If in the former case emulsification of solute occurs at the bottom, then the energy for mixing also should have gradient: most vigorous at the top and least vigorous at the bottom where both phases are high in solute content. The reverse is true if the selective solvent was light phase: i.e. most vigorous mixing at bottom and least vigorous mixing at top, where both are rich in the solute. The energy necessary to produce this type of mixing is termed, Controlled Gradient Mixing Energy.

Since in any extraction equipment the process of mixing is followed by separation, another term, the controlled gradient separation force, is defined by Doyle et al. This, however, does not exist in gravity columns as the latter are subject to a constant force of 1g. In the centrifugal extractor the controlled gradient separating force is easily obtained by varying the rotational speed.

Doyle et al[19] claim that these new concepts are useful in

determining the optimum conditions of any extractor, especially the centrifugal. Whilst the concepts are easily understood the workers do not make clear, how these help in bringing about the optimum conditions in the operation of a centrifugal extractor.

6.4.2 Mass Transfer Rates

In Chapter 5, the mass transfer associated with the drop formation and during the other stages of its life are discussed. Whereas for other extractors such information is in abundance, that applicable to or derived from the operations of centrifugal extractors is negligible. Furthermore, since this work is primarily directed towards the hydrodynamic studies of centrifugal extractors, the mass transfer studies will only be discussed in brief.

Whereas in gravity columns the drop formation time is much greater than that in centrifugal extractors, the amount of mass transfer will be considerably less in the latter than 10% or 14% (Angel[145] and West[143] respectively) found in the former. What form will the mechanism be ? 'Fresh surface model', or the Stretch model' ?

As during the formation stage, the mass transfer during other stages can only be guessed at. However, taking the geometry of the centrifugal extractors into account it seems clear that the two most important stages of mass transfer are:

(i) Coalescence. This is due to the fact that drops will, as a result of the geometry of the equipment, constantly collide with each other and coalesce with the phase boundary, and

(ii) the time when drops are travelling at settling velocities.

Since these observations are based on the study of the centrifugal contactors reviewed in Chapter 2, supporting evidence from the literature is not available. It is imperative, therefore, that the droplet hydrodynamics in centrifugal contactors be studied.

7. EXPERIMENTAL INVESTIGATIONS

7.1 GENERAL

The scope of this work may be summarised as:

(i) To design and construct a pilot scale centrifugal extractor suitable for visual observation and photography of droplet hydrodynamics.

(ii) To investigate the behaviour of drops forming, travelling and coalescing in a centrifugal field, and

(iii) On the basis of (ii) to deduce the mechanisms of mass transfer within centrifugal extractors and to propose design criteria.

7.2 MATERIAL OF CONSTRUCTION

A flow diagram of the equipment is given in Fig. 7.1. The main feature, the centrifugal contactor, is shown diagrammatically in Fig. 7.2. Fig. 7.3 shows the design of end plates of the contactor. The apparatus comprised the centrifugal contactor and means of supplying to, and receiving liquids from, it. These are described in detail in the following sections.

7.2.1 End Plates of the Contactor

The material of construction for the end plates had to be:

(i) Transparent

(ii) Resistant to solvent attack

(iii) Of sufficient strength to withstand very high centrifugal force.

According to Todd[176] the force can be as much as 10,000 gs. The contactor developed here was capable of producing a centrifugal force of up to 5000 gs. Strengthened glass was considered to be too weak, therefore a polycarbonate, Macralon of 5mm thickness was used.

7.2.2 Other Materials of Construction

Briefly these can be summarised as:

(i) All pipe work was of Q.V.F. industrial glass to allow for observation of flow and ease of cleaning.

(ii) Stainless steel was employed for the extractor rotor rim, storage reservoirs, delivery and exit tubes to the extractor, and pump contact parts.

(iii) Polytetrafluoroethylene , P.T.F.E., was used for pipe connection, gaskets, and as sealing material between the stainless steel rim and transparent end plates. This has been reported[76] to be completely inert to the solvents used.

7.3 SELECTION OF LIQUID-LIQUID SYSTEMS

A major factor affecting the selection of liquid-liquid systems was the need for the polycarbonate end plates to be unaffected by prolonged exposure to such liquids. Several organic liquids, e.g. Toluene, acetone, etc., produced 'fogging' of sample plates and since this would have hindered vision, viz the end plates, other liquid systems were selected. These were:

(a) Kerosene

(b) Paraffin

(c) B.P. lubricant oil CS40

(d) B.P. lubrican oil EM35c.

Distilled water was used as the continuous phase in each case to reduce operating hazards with non-flame proof electrical equipment.

7.4 DESIGN AND DESCRIPTION OF EQUIPMENT

Since the major commercial extractors, viz the Podbielniak and Quadronic extractors, are of the differential continuous type and these are of simpler construction than stagewise designs, a single stage differential type was designed.

7.4.1 Initial Design

The rotor, i.e. the contacting section of the centrifugal extractor, was of 35.84 cm diameter and comprised 0.64 cm thick stainless steel rim to which the transparent end plates were secured by means of four lugs situated at the end of each spoke of a wheel shaped brass support. The tranparent end plates were sealed to the rim by P.T.F.E. gaskets.

The centre of the rotor was of stainless steel and had a complex network of delivery and exit points to the rotary seals at both ends of the contacting section. Protruding from the central rotor were eight channels - four on either side. The channels, of 13.24 cm length, were arranged perpendicularly to each other and had interchangeable nozzles. The latter facility was incorporated to allow various sizes of nozzle on each channel. The first design comprised three orifices of 1.05 mm diameter per channel and was found to give droplets of extremely small size and which could not be measured.

The design and location of orifices is clearly important in centrifugal extractors but there are little data on their effects. Several patents[33] recognise the importance of orifice shape and pattern; the main consideration is to suit combined throughput capacity from maximum to minimum[39].

The rotor, comprising the two transparent end plates held to the stainless steel circular rim and the internals, was provided with two concentric tubes on each side to transfer liquids to and from the rotor. This assembly was held horizontally by two rigid supports and driven by means of an a.c. Voss motor, via a pulley system. To facilitate rotation there were two self aligning bearings, one on each side of the assembly.

The assembly was enclosed in a steel casing as a safety measure; this had two quadrant shaped port holes on opposite sides. To minimise vibration at high speed, the whole apparatus was secured to a strong wooden table, via rubber shock absorbing pads. Liquids were delivered to and removed from the contacting section via mechanical rotary seals on either side of the assembly. The seals manufactured by Filton, Ltd., can operate at maximum pressure of 300 lbs/m^2.

7.4.2 Final Design of the Contactor

A number of modifications were found necessary after commissioning. The end plates were found to crack after two or three runs, as illustrated in Plate 7.2a. Detailed examination revealed that the cracks emanated from sub-microscopic pits made when the end plates were being constructed. To eliminate these

the following heat treatment was enacted:

(i) The plates were finely polished;

(ii) Cleaned with detergent and hot water and rinsed with hot and cold water;

(iii) Heated in oven for 12 hours at 120°C;

(iv) While hot, the edges were heated with even application of gas flame and then lightly glazed in flame;

(v) The surfaces were flamed to remove visible scratches-

(vi) General heating with flame to remove bowing;

(vii) After cooling to 80°C, the surfaces were inspected under polarised light to reveal stress;

(viii) The stress thus revealed was relieved with flame;

(ix) The plates were heated to 150°C for ½ hour on glass plate,

(x) Annealed down to 120°C in ½ hour and then to 80°C for further ½ hour.

Following this treatment the plates were found to crack after 30 -40 runs only, and even then only slightly. This is shown by Plate 7.1.

Another modification was the reduction of leakage from the rotor. This often occurred at full loads and since it was in spray form it was extremely dangerous. By increasing the lugs on the rotor to 24 and employing P.T.F.E. paste instead of the tape, the leakage was considerably reduced.

Since the required speed of rotation was in the range 2000 to 5000 r.p.m., and a.c. 3-phase motor was employed. As a result, however, flexibility was lost, due to the changing of pulley ratio every time a new speed was to be investigated. In

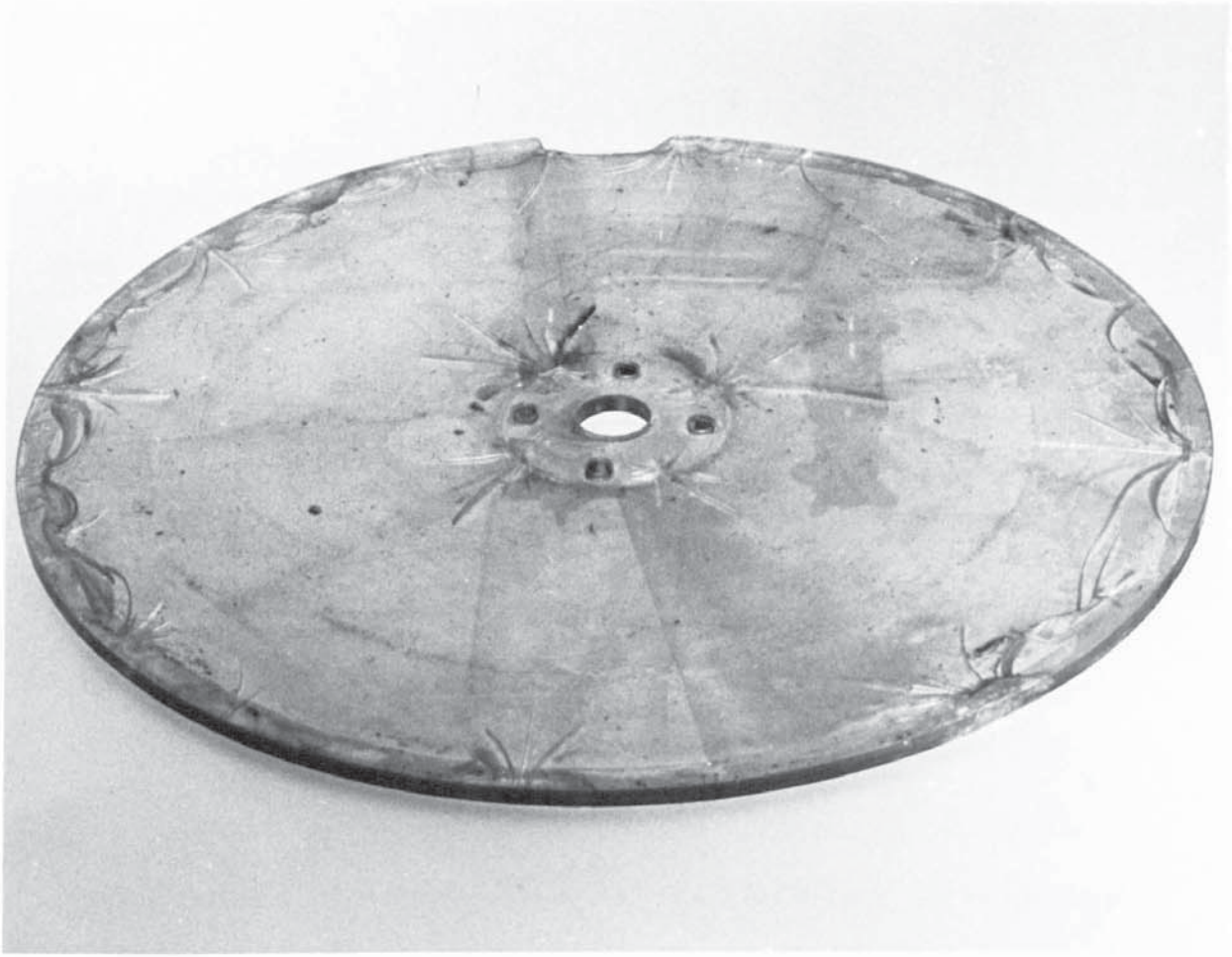

Plate 7.1 UNTREATED CONTACTOR END PLATES

Plate 7.1 TREATED CONTACTOR END PLATES

the previous design the speed could be controlled directly from a crosswall voltage regulator. The speed in all cases was measured by a stroboscope with a range of 0-10,000 r.p.m.

In the initial design no means of comparing the droplet size with known dimensions existed. A 'T' shaped wire of 0·0624 cm dia. was therefore, welded between the channels. The assumption was made that its presence would not substantially affect the size of droplets as they travel towards the central rotor. This 'T' piece is shown in Fig. 7.3. Figs. 7.2 and 7.3 show the final design of the contactor.

Drainage in the initial design was facilitated by suction of liquid by means of a pump. This was unsatisfactory for measuring the volumetric hold-up. A drainage point was, therefore, drilled into the rotor and liquid entrained by the pressure difference existing between the inside and outside of the rotor.

7.4.3 Design of Other Sections

The system, excluding the contactor, comprised conventional reservoirs and means of delivering liquids of measured pressure and rates of flow. Four 10 litres stainless steel cylindrical vessels and two 10 litres glass vessels were used as storage reservoirs. The transfer of liquids was effected by means of two Stuart-Turner, No.10 pumps, capable of delivering 0.1515 litres per sec. against 0.52 metres of water. The pumps were of stainless steel, and equipped with glands adapted for use with corrosive liquids. The throughput through the pump was controlled by a Cresswall voltage regulator, which like all the electrical wiring, was protected against fire hazard by enclosing in a metal box.

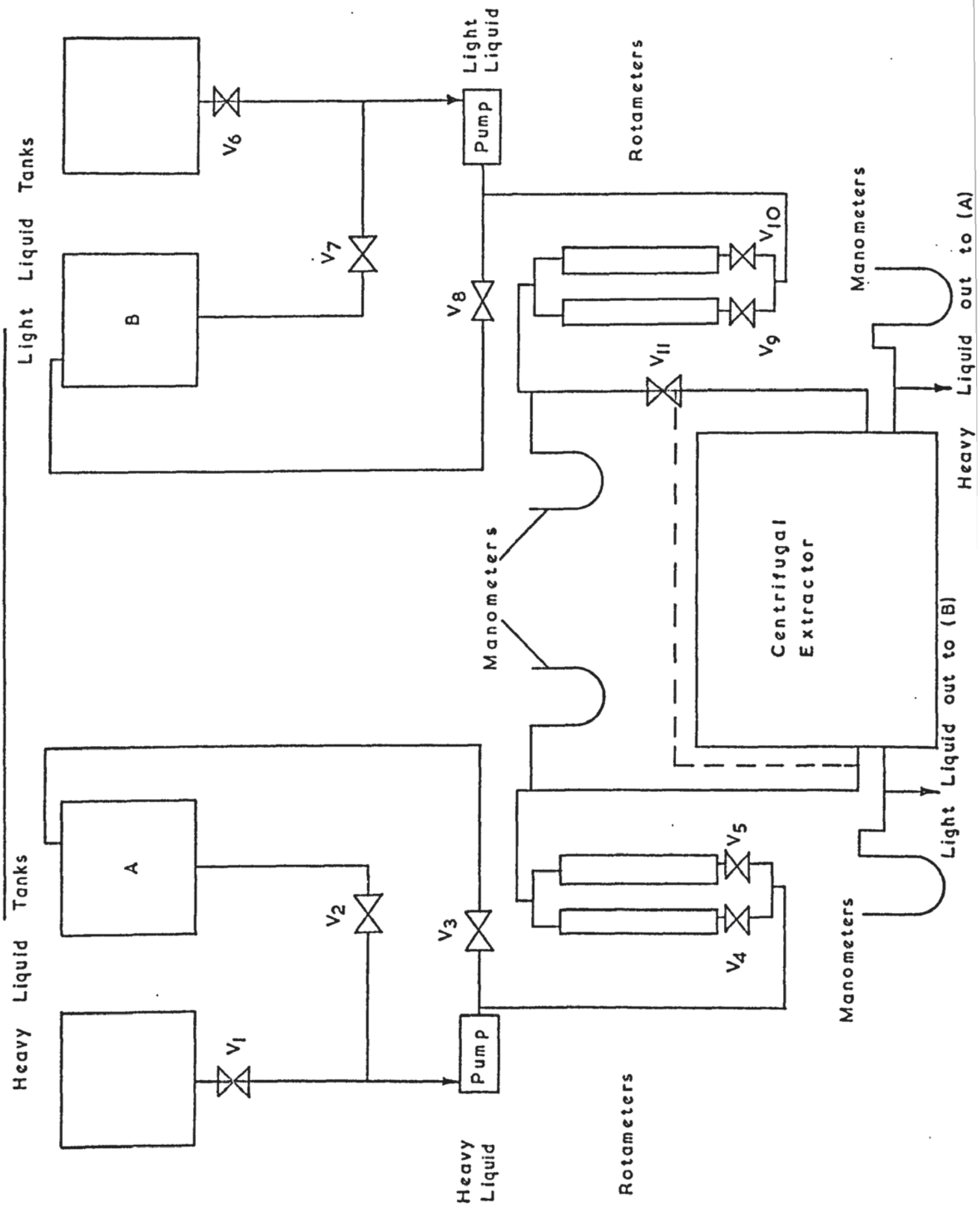

FIG. 7.1 ARRANGEMENT OF THE APPARATUS

FIG. 7·2. CROSSECTIONAL VIEW OF CENTRIFUGAL EXTRACTOR

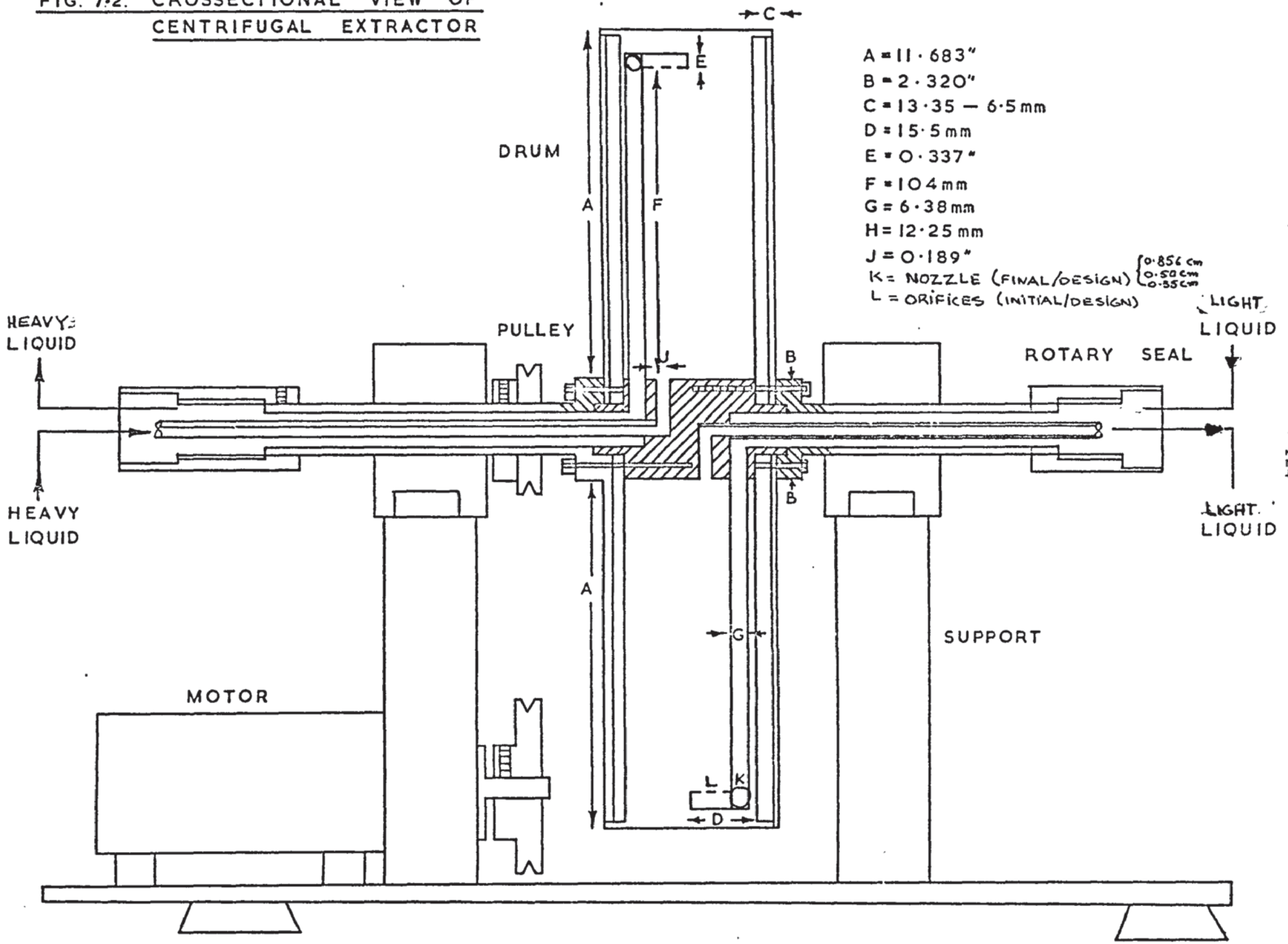

Flow rates were measured by independently calibrated rotameters with stainless steel floats. So as to cover a range of flow rates two rotameters, Nos. 10F to 16F were employed for each delivery line. To ensure minimisation of float fluctuations and hence the pressure fluctuations, a by-pass was made for each of the liquid streams.

Since the inlet and outlet pressures are important factors, governing the flooding of centrifugal contactors, accurate measurements are necessary. Initially vacuum pressure guages, 0 - 100, psi were employed, but due to their slow response to minute pressure fluctuations, mercury manometers were used in the final design. Since the back pressure in centrifugal extractors is high and can cause the expulsion of mercury from the manometers, glass reservoirs were fitted on each manometer.

The complete system is shown diagramatically by Fig. 7.4, and illustrated by Plates 7.2 and 7.3

7.5 PHOTOGRAPHIC APPARATUS

The first method of recording the droplets inside the contactor was still photography. The camera used was a Pentax Ashai, but this produced inconclusive results. The failure was not of the camera, rather that of the still photographic technique as a means of observing both extremely fast and small objects. The lighting was provided by two 500W photo-flood lamps.

The second method was the use of moderately high speed cine cameras. The camera, a Millikan DBM3, fitted with required

lenses was used at different speeds, viz, ranging from 50 to 500 frames per second. The film used in each case was a Kodak Tri-X which was subsequently checked to confirm the speed of the camera from spark traces on the edges of the film. The lighting was provided by two 500W photo flood lamps placed near the opposite window. To diffuse the light from the lamps, tracing paper was attached to the window opposite to that from which photographs were being taken.

The third photographic technique was the usage of a higher speed camera, viz, a Wollensak Fastax, type WF14, with range of 500 f.p.s.to 6000 f.p.s. and fitted with a Fastax-Raptor 50 mm or 152 mm, f2 lens, as required. Unlike Millikan, the speed of the film in this case was determined by selecting the applied voltage and checking against manufacturer's calibration chart. The lighting was provided by two 750W photo flood lamps and was diffused by tracing paper attached on the window of the contactor.

The fourth camera employed was a Hyspeed model, 1420/16, manufactured by John Hartland, with 750 mm lens. The camera had 20 - 20,000 f.p.s. range, but was operated only up to 10,000 f.p.s. Lighting was provided by a single 1,000 watt Quartz-iodine lamp.

7.6 EXPERIMENTAL PROCEDURES

7.6.1 General

Since the speed of the contactor could not be changed quickly, it required dismantling of pulleys, all the studies were carried out at one speed before changing the speed. For example, at 2750 r.p.m, the operational characteristics, the droplet phenomena and flow from nozzles into centrifugal fields, were all studied. Furthermore, the nozzle diameters were altered at the same speed. The speed of the contactor was altered by changing the diameter of the adjustable pulley and hence changing the ratio of pulley diameters. The speed of the contactor was measured with a stroboscope, the accuracy of which was $\pm$ 25 r.p.m.

7.6.2 Hold-up Studies

Two techniques were used in the determination of hold-up of a centrifugal contactor, viz:

(a) Direct Method

This involved the isolation of liquid streams in the contactor and the direct measurement after draining. Before isolating the contactor it was ensured that stable conditions existed, i.e. that the pressure manometers and the rotameter readings were steady with maximum fluctuations of $\pm$ 0.5 scale reading. By closing valves V_4, V_5, V_9, and V_{10}, as shown in Fig. 7.1, the flow of heavy and light phases to the contactor was stopped. Similarly, the flow out of the contactor was shut off by closing the valves on the out-lines. The extractor was then switched off

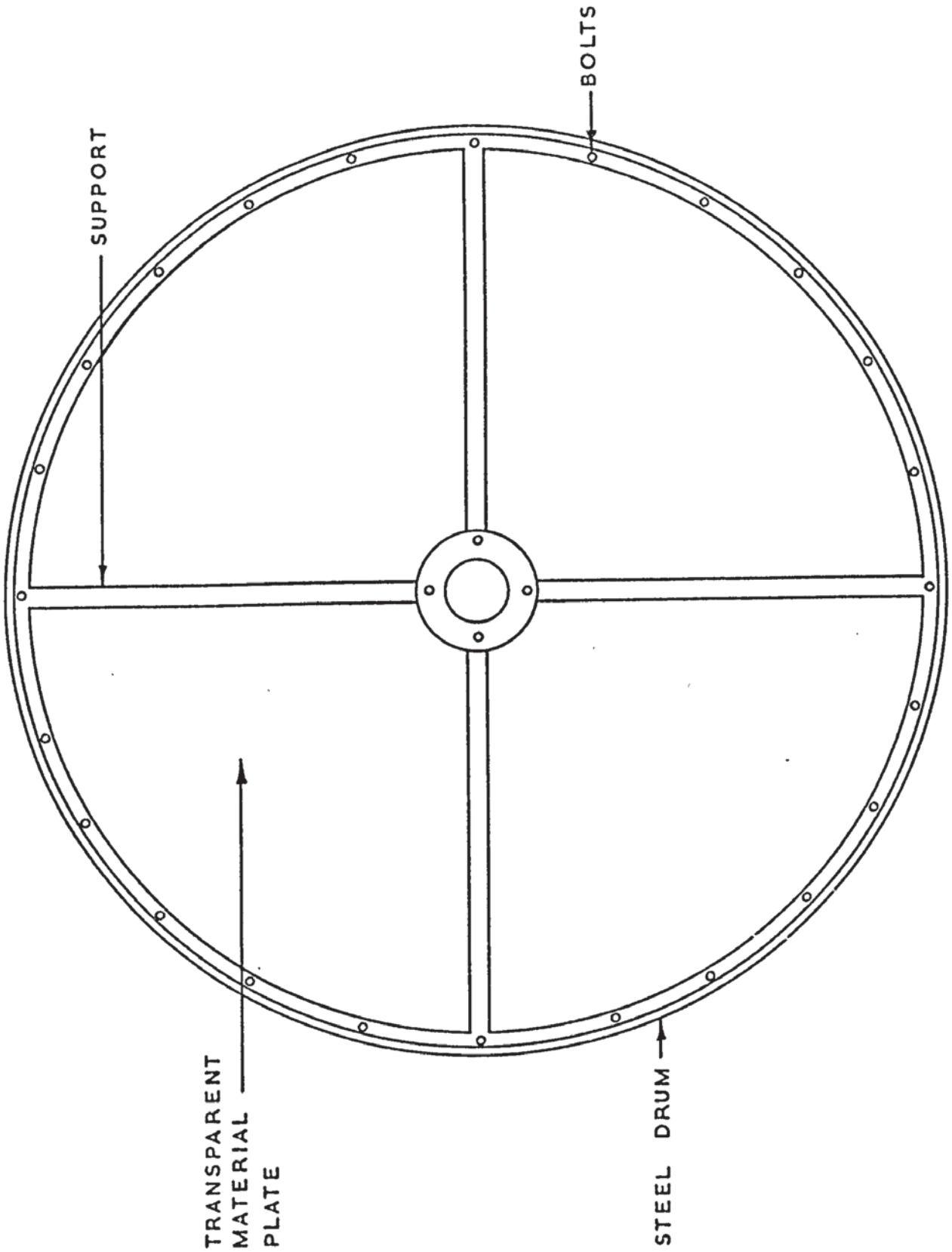

FIG. 7.3 SIDE VIEW OF DRUM

and drained through the draining plug in the contactor. After separation of the two phases each was weighed to determine the volume.

The determinations were carried out at two speeds of rotation, i.e. 1750 and 4600 r.p.m. At each speed the systems used were Kerosene/water and paraffin/water. Furthermore, each time a number of runs were made to check the reproducibility of results.

(b) The Displacement Method

This method entailed the displacement of one phase in the contactor by another, and measuring its volume. At stable conditions the heavy phase flow into the contactor was stopped by closing valves V_4 and V_5 shown in Fig.7.1. The light liquid was then introduced to the heavy phase in the tube by opening the 3-way valve V_{11}. By closing the light liquid out tube, the total input to the contactor was forced through the heavy liquid out line, thereby displacing the heavy phase. The rotor speed was not reduced while the displacement of the heavy phase was occurring. The mixture of the two phase was collected, separated and the heavy phase weighed to determine the volume. The rotor was then stopped to allow for any remaining heavy phase to be flushed out. The fraction of the heavy phase collected this way was separated and weighed to determine the volume. The combination of the values gives V_H.

To determine the light-liquid volume in the contactor and seals V_L, the procedure above was reversed, i.e. the light liquid was displaced by the heavy phase. This was carried out at the same flow rates and pressure readings as in the determination of V_H

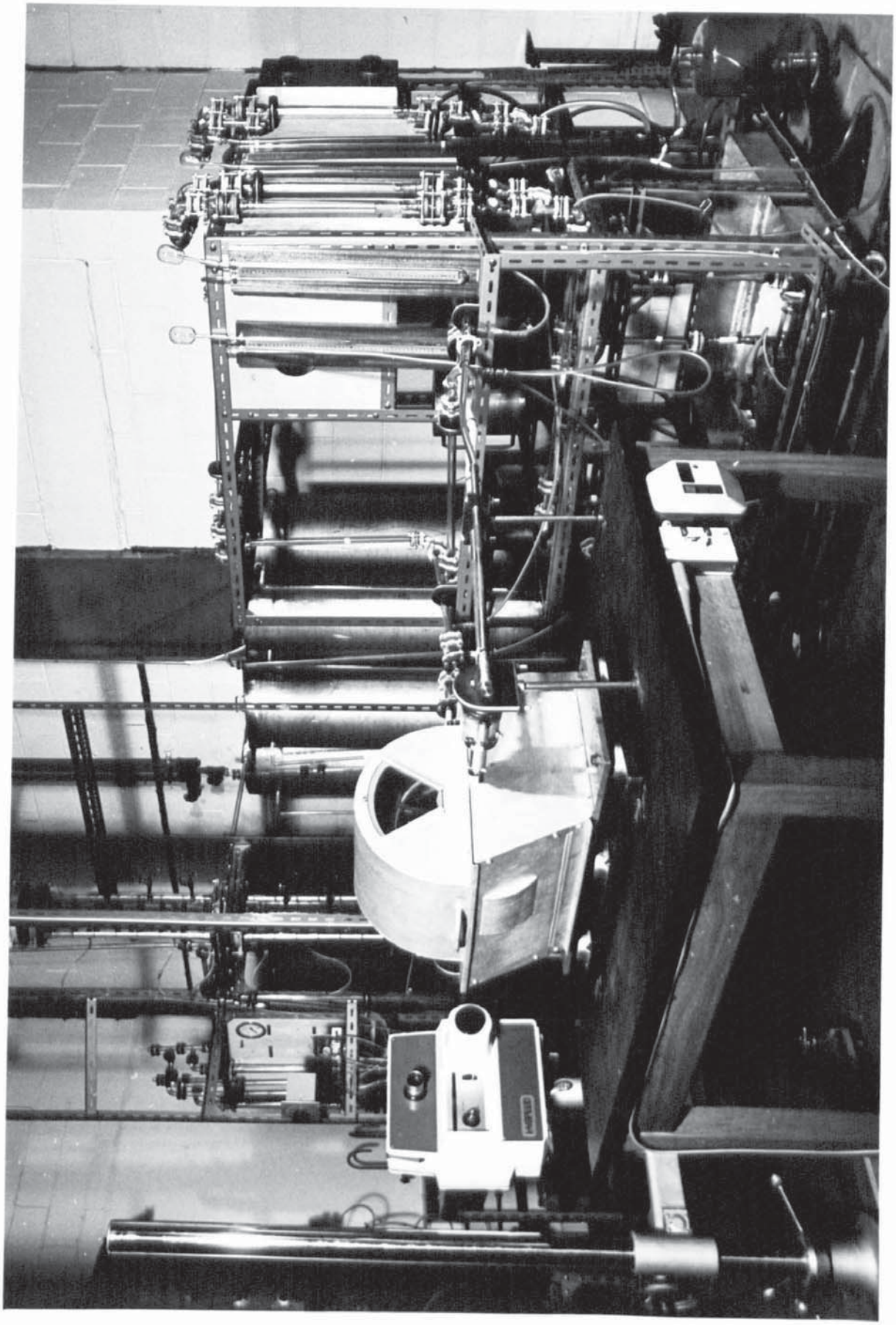

PLATE 7.2 COMPLETE APPARATUS WITH CAMERA IN POSITION

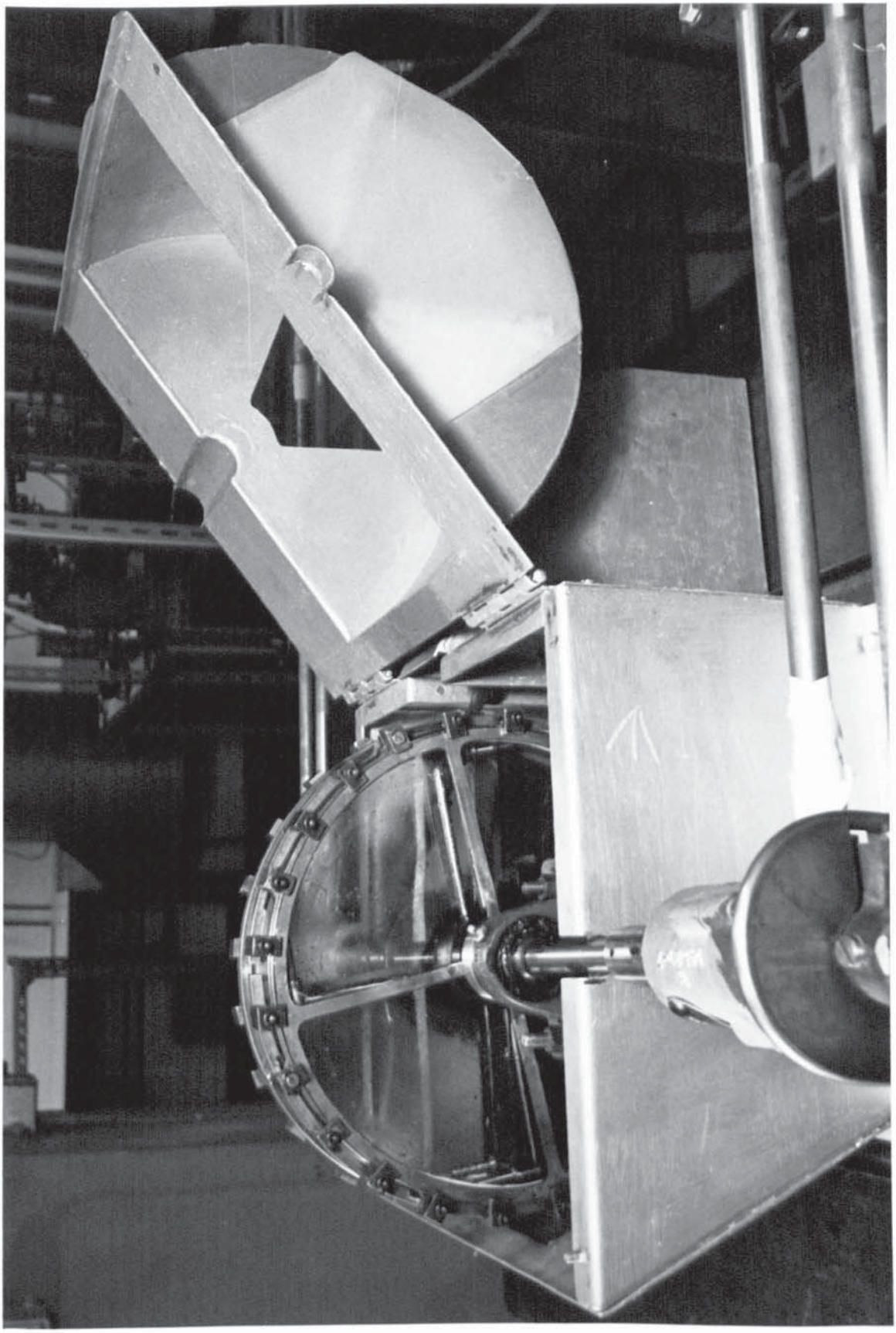

PLATE 7.3 CENTRIFUGAL CONTACTOR

above. To ensure the exact conditions the height of the principal interface was ascertained to be as in the determination of V_H.

The determinations were carried at the same two speeds as in (a) i.e. 1750 and 4600 r.p.m.

7.6.3 Flooding Studies

Flooding characteristics of a centrifugal contactor can be presented in two ways, viz:

(a) The combined flow rate, Q, versus light-liquid-out pressure P_{LLO}, and

(b) The combined flow rate, Q, versus the back pressure $\overline{P}_{LLO}$ which is equal to $P_{LLO} - P_{HLO}$.

The investigations were carried out for two phase ratios, viz $Q_L = 0.5\ Q_H$ and $Q_L = 2.0\ Q_H$, at each of the four contactor speeds. The procedure in each case is illustrated with reference to Fig.7.1.

By manipulating valves V_1 to V_5 and V_6 to V_{10} the flow rates of both phases to the contactor were controlled so that $Q_L = 0.5\ Q_H$. At stable conditions the light-liquid-out pressure, P_{LLO}, and heavy-liquid-out pressure P_{HLO} were recorded. At increased flow rates but at the same phase ratio the two pressures were observed and recorded at stable conditions. Three types of flooding was observed - shaft, followed by flooding, and then the capacity flooding.

A number of runs were made for the same phase ratio to establish the reliability of the first set of results. At the higher speeds, this was particularly necessary since the pressure and rotometer readings fluctuated considerably.

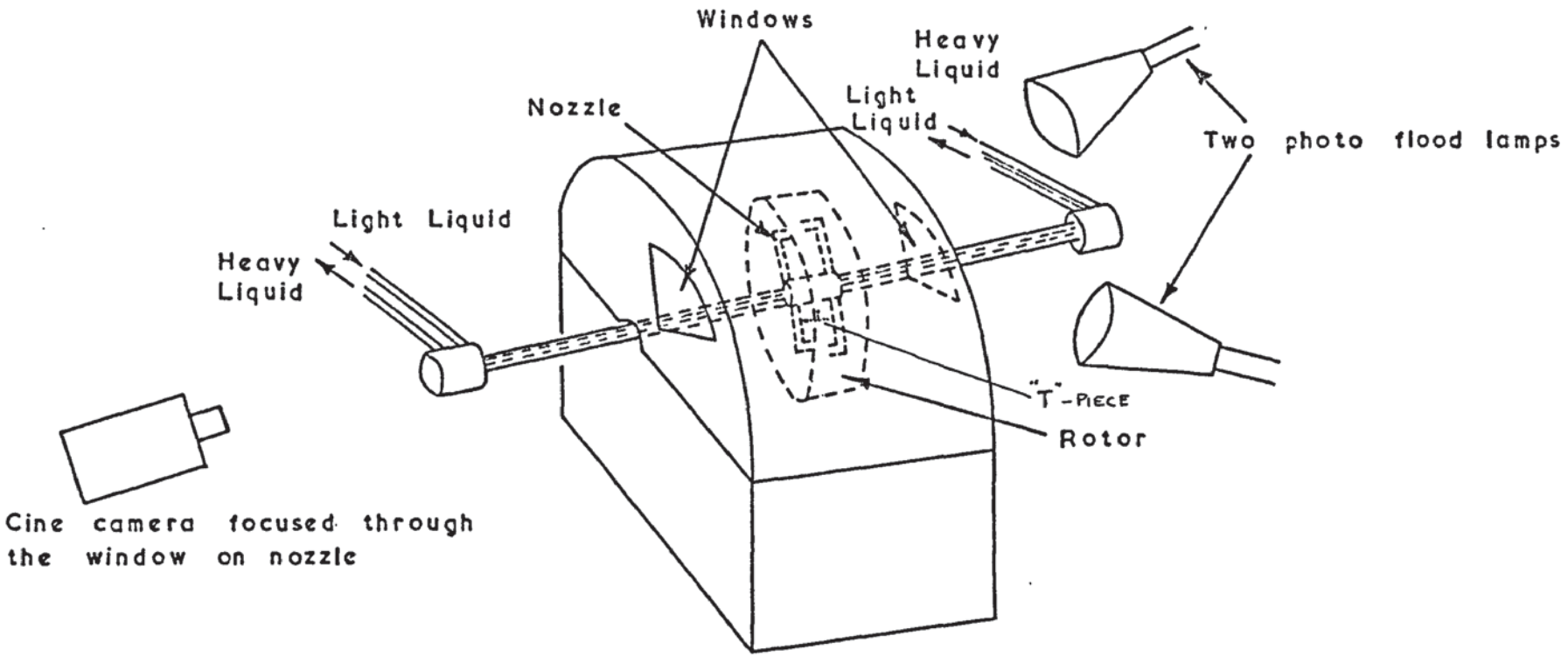

FIG. 7.4. ARRANGEMENT FOR PHOTOGRAPHY OF DROPS IN CENTRIFUGAL CONTACTORS

7.6.4 Studies of Flow from Nozzles into Centrifugal Fields

To illustrate this the procedure for kerosene-water system at a rotation speed of 2750 r.p.m. and nozzle diameter 0.856 cm. is given with reference to Fig. 7.1. Initially the reservoirs were filled with the appropriate phase and pumped through the by-pass system. This is important for kerosene since it allowed thorough mixing of the red oil soluble dye to produce uniform colour. The contactor was switched on and the photographic equipment set up, as shown in Fig. 7.5.1. If the kerosene was from a new batch, the equipment was allowed to run for 30 minutes so that the streams were mutually saturated.

The flow rates of kerosene and water were controlled by valves V_4, V_5 and V_9 and V_{10} respectively and measured by the calibrated rotameters. The water flow rate was kept constant while the kerosene flow rate was altered by valves V_9 and V_{10}. At each setting of V_9 and V_{10} and stable conditions, the Fastax camera was switched on for fraction of a second. The film was changed when necessary - generally after about four seconds, i.e. film changed every few rotation speed settings. The camera setting was: f = 11 and voltage = 60V 1750 f.p.s. and it was focussed on the 'T' piece in the middle of the rotor.

The effect of the following parameters on the flow from nozzles was investigated;

(a) Speed of rotation, ω. At ω = 1750, 2750, 3460 and 4600 r.p.m.

(b) Nozzle diameter, D_N. At D_N = 0.856 cm, 0.5 cm.

(c) Viscosity, μ,of the light phase. At μ = 1.5572 cp, 34.3875 cp.

7.6.5 Drop Size/Velocity Studies

These were almost entirely conducted with the Wollensak Fastax, type Wf14 high speed camera. The arrangement of the apparatus is shown in Fig. 7.4. The camera was focussed on the nozzle near the end plate nearest to the camera and loaded with high speed Kodak Tri-X film. The procedure adopted can be illustrated with ω = 4600 r.p.m., D_N = 0.856 and paraffin/water system.

Before each run, it was always ensured that both phases were mutually saturated and that the instrument readings were stable. It was recognised early in the experiments that often the liquid issued from the nozzle when these were at the bottom of revolution and thus hidden from view. To overcome this, use was made of the fluctuation in the paraffin-in-pressure. This was recognised as being due to the liquid jetting out into the contactor. Thus whenever pressure fluctuated, the camera was switched on. The film was only partially used for a given flowrate so that 4 to 5 flowrates could be photographed on one film. Having studied at 4600 r.p.m., the speed ω was altered by changing pulley diameter ratio. Hence a new speed could be investigated. In most cases up to three speeds were studied on one film.

7.6.6. Cleaning Procedure

After completion of each study the whole apparatus was cleaned. The apparatus was first thoroughly flushed out with distilled water and then completely filled up with 10% solution of Decon 10.

It was left for approximately twelve hours and then washed with about 100 litres of fresh distilled water. It was found that if the contactor was left with the detergent solution for more than 12 hours, the end plates became hazy.

The dye used, oil soluble, was first studied for its negative effect on the end plates of the contactor. This was done by soaking 10 x 10 Makralon samples in paraffin, kerosene and glycerol with dye dissolved for 2, 4, 8 and 12 hours.

MATHEMATICAL MODELS OF DROPLETS IN CENTRIFUGAL CONTACTOR

8.1 MODEL OF DROP FORMATION BELOW JETTING VELOCITY

The principal forces acting on a drop during the process of formation at an orifice/nozzle in a centrifugal field are:-

(i) The buoyancy force due to the density difference between the two liquids, F_B.

(ii) The interfacial tension force F_S.

(iii) The drag force exerted by the continuous phase to keep the drop in the nozzle, F_D.

(iv) The centrifugal force, F_{CE}, due to rotation of the system at speed of ω.

(v) The kinetic force associated with fluid flowing out of the nozzle, F_K.

(vi) The Coriol is force F_{CO}. This can be ignored for Re < 1.0, and will therefore not play an important role in drop formation

The mechanism of formation is assumed to be similar to that under gravity conditions, i.e.

(a) The growth of the drop

(b) 'Necking' of the drop, and

(c) Rupture when the opposing forces are equal.

However, the 'necking' stage of drop formation under centrifugal condition is, unlike under gravity, of extremely small duration, and its significance in terms of volume flowing into the drops will be small.

At point of rupture from the nozzle, the forces acting on the drop can be equated, viz:

$$F_B + F_K + F_{CE} = F_S + F_D + F_{CO} \tag{8.1}$$

However, the Corolois force is negligible compared to F_{CE} when the drop formation occurs below the jetting velocity[72], and can be ignored.

The buoyancy force F_B is given by the expression,

$$F_B = V_{FS}\Delta\rho g \tag{8.2}$$

where V_{FS} is the drop volume when 'necking' starts.

The interfacial tension force F_S can be expressed in terms of nozzle inside diameter, D_N, and the interfacial tension σ;

$$F_S = \pi\sigma D_N \tag{8.3}$$

The centrifugal force F_{CE} by definition is,

$$= \Delta\rho\omega^2 R \tag{8.4}$$

where ω is the speed of rotation and R is the radius from the centre of the rotor.

The formulation of the drag force F_D in a centrifugal field is made by analogy with the Scheele and Meister [72] and Vashist[73] treatment. F_D by definition is,

$$= \frac{C_D \pi \rho}{8} U_F^2 (D_{FS})^2 \tag{8.5}$$

By assuming a solid spherical drop the coefficient of drag C_D is given by,

$$C_D = \frac{24\mu}{D_{FS} U_F \rho} \tag{8.6}$$

Substitution of 8.6 into 8.5 yields,

$$F_D = \frac{3\pi\mu D_{FS} U_F}{F^{1/3}} \tag{8.7}$$

However, U_F can be written as[72],

$$U_F = \frac{2QF^{2/3}}{\pi D_F^2} \tag{8.8}$$

where F is the Harkin-Brown factor. Substituting 8.8 into 8.7,

$$F_D = \frac{6\pi QF^{1/3}}{D_F} \tag{8.9}$$

However, in derivation of 8.8 spherical growth was assumed, which is now always the case. Furthermore, in the same derivation it was recognised that the nozzle diameter to drop diameter ratio was critical. Since Harkin-Brown factor F is also dependant upon this ratio, it is probably better to express the equation 8.10 in general terms, viz:

$$F_D = K_D \frac{\mu Q}{D_F}\left(\frac{D_N}{D_F}\right)^n \tag{8.10}$$

The kinetic force F_K may be evaluated if assumption is made that all the energy in the issuing liquid will be transmitted to the drop in the process of being formed. The incremental force is then given by

$$dF_K = {}_d U_z^2 dA \tag{8.11}$$

If assumption is made that the velocity profile within the nozzle is parabolic, then

$$U_Z = 2U_N \left[1-\left(\frac{R}{R_N}\right)^2\right] \tag{8.12}$$

Substituting (8.12) into (8.11), integrating and simplifying

yields,

$$F_K = 4/3\ \rho_d\ QU_N \tag{8.13}$$

However, the assumption above is only justified when the straight section of the nozzle is greater than 100 pipe diameters. It is therefore, better to write 8.13 in general terms, i.e.

$$F_K = K_f \rho_d . QU_N \tag{8.14}$$

Substituting 8.14, 8.10, 8.4, 8.3, and 8.2 into 8.1,

$$V_{FS}\ \Delta\rho g\ + K_f \rho_d QU_N + \Delta\rho\omega^2 R = \frac{K_D\ \mu Q}{D_F}\left(\frac{D_N}{D_F}\right)^n + \pi\ D_N\ \sigma$$

by $g\Delta\rho$ on both side, and re-arranging,

$$V_{FS} = \frac{K_D\ \mu Q}{\Delta\rho D_F\ g}\left(\frac{D_N}{D_F}\right) + \frac{\pi\ D_N \sigma}{g\Delta\rho} - \frac{\omega^2 R}{g} - \frac{K_f \rho_d QU_N}{g\Delta\rho} \tag{8.15}$$

The final drop volume can be expressed as

$$V_F = F(V_{FS} + V_{FN}) \tag{8.16}$$

where V_{FN} is the volume of liquid which flows into the drop during the 'necking' part of drop formation. Under gravity conditions Rao[69] shows that,

$$V_{FN} = Qt_B \tag{8.17}$$

where t_B is of the order of 0.05 seconds. In centrifugal fields t_B is several orders of magnitude smaller and the term Qt_B becomes extremely small. It is therefore ignored as being negligible. Thus,

$$V_F = FV_{FS} \tag{8.18}$$

Substituting into 8.15 and putting $n = 1$[72].

$$V_F = F\left\{\frac{\pi\sigma D_N}{g\Delta\rho} + \frac{K_D \mu Q D_N}{D_F^2 g\Delta\rho} - \frac{\omega^2 R}{g} - \frac{K_f \rho_d Q U_N}{\Delta\rho g}\right\} \qquad (8.19)$$

The constants K_D and K_f will have to be determined experimentally.

8.2 VELOCITY OF DROPS IN A CENTRIFUGAL FIELD

Consider a drop, of diameter d, in a rotating drum at a distance R from the centre.

Let ρ_d = be the density of the medium.

v_d = be kinematic viscosity of medium.

ω = angular speed of drum.

μ = viscosity (dynamic).

d = diameter of drop.

$U_r U_\psi$ = velocity components

The forces acting on the drop are as in 8.1, i.e.

(i) Centrifugal force F_{CE}

(ii) Coriol is force F_{CO}

(iii) Archimedes force F_B

(iv) Drag or resistance to flow, F_D.

Assumptions made are that:

(a) Velocity component in the Z direction is negligible. This is largely borne out by visual observation of drop trajectory.

(b) That collisions between particles are negligible, i.e. its path is not hindered. This assumption is not altogether incorrect since drop collisions were observed very infrequently in the middle of their trajectories. Collisions

were observed to occur when extremely near the central rotor.

(c) That the Reynolds number is $\gg 1$. Under such condition the Coriol is forces are very important.

Applying Newton's law of motion, i.e.

$$\text{Forces} = (\text{mass}) \times (\text{acceleration}) \tag{8.20}$$

Resolving forces in radial direction

$$V_{FS}\rho_d\left(\frac{dU_r}{dt}\right) = -V_{FS}\left(\frac{\rho_d U_r^2}{R}\right) + V_{FS}\left(2\rho_d U_\psi \omega\right) + V_{FS}\left(\frac{U_\psi^2 \rho_d}{R}\right) + \Delta\rho g V_{FS} - F_D \tag{8.21}$$

The drag force F_D can be evaluated from its definition, i.e.

$$F_D = 3\pi\mu d(U_r/\omega R) \quad \text{where radial velocity} = \left(\frac{U_r}{\omega R}\right)$$

÷ 8.21 by V_{FS} and evaluating F_D/V_{FS}

$$= \frac{3\pi\mu d(U_r/\omega R)}{\text{Volume } V_{FS}} = \frac{3\pi\mu d(U_r/\omega R)}{(4/3)\pi(d^3/8)}$$

i.e. $$\therefore \quad F_D/V_{FS} = \frac{18\ U_r}{\pi d^2 . \omega R}$$

$\therefore$ 8.21 becomes

$$\rho_d\left(\frac{dU_r}{dt}\right) = \left(2\rho_d U_\psi \omega\right) + \left(\frac{U_\psi^2 \rho_d}{R}\right) + \Delta\rho g - \left(\frac{\rho_d U_r^2}{R}\right) - \left(\frac{18\mu\ U_r}{\pi\ d^2 \omega R}\right) \tag{8.22}$$

x equation 8.22 by $\left(\frac{1}{\rho_d \omega R}\right)$ to simpify,

$$\frac{1}{\omega R}\left(\frac{dU_r}{dt}\right) = \left(\frac{2U_\psi}{R}\right) + \left(\frac{U_\psi^2}{R^2\omega}\right) + \left(\frac{\Delta\rho 1}{\rho_d g \omega R}\right) - \left(\frac{U_r^2}{R^2\omega}\right) - \frac{1}{\omega R}\frac{18\mu}{\rho_d \pi d^2}\left(\frac{U_r}{\omega R}\right) \tag{8.23}$$

Now $\frac{d(U_r/\omega_R)}{dt} = \frac{1}{\omega_R} \frac{dU_r}{dt} + U_r$

$= \frac{1}{\omega_R}(\frac{dU_r}{dt})$ if ω is constant.

if $(\frac{U_r}{\omega_R})$ is defined as a dimensionless velocity X then further simplifications can be made i.e. Equation (8.23) becomes

$$(\frac{dx}{dt}) = \frac{(2\omega U_r)}{\omega R} + \omega(\frac{U_\psi^2}{R^2\omega^2}) + (\frac{\Delta\rho}{g\rho_d\omega R}) - (\omega X^2) - (\frac{18vm}{\pi d^2\omega R} \cdot X)$$

8.24

The term $2\omega \frac{U_\psi}{\omega R} + \omega\frac{U_\psi^2}{R^2\omega^2}$ can be simplified because

$$\omega\ (\frac{2U_\psi}{\omega R} + \frac{U_\psi^2}{\omega^2 R^2}) = \omega\ \ (1 + \frac{U_\psi}{\omega R})^2 - 1$$

$$(\frac{dx}{dt}) = \omega\ (1 + \frac{U_\psi}{\omega R})^2 - 1 \quad - (\omega X^2) + (\frac{\Delta\rho}{g\rho_d\omega R}) - (\frac{18vm}{\pi d^2\omega R} \cdot X)$$

8.25

If $(1 + \frac{U_\psi}{\omega R})$ is defined as another dimensionless velocity, Y, then

$$(\frac{dx}{dt}) = (\omega Y^2 - \omega X^2) + (\frac{\Delta\rho}{g\rho_d\omega R} - \omega) - \frac{18v_m}{\pi d^2\omega R} \cdot X$$

$$(\frac{dx}{dt}) - \omega(Y^2 - X^2) + (\omega - \frac{\Delta\rho}{g\rho_d\omega R}) + \frac{18v_m}{\pi d^2\omega R} \cdot X = 0$$

i.e. $\frac{dx}{dt} - \omega(Y^2 - X^2) + K_1X + K_2 = 0$ 8.26

where X, Y are dimensionless velocities,

$$1 = \frac{18v_m}{\pi d^2\omega R}, \quad K_2 = (\omega - \frac{\Delta\rho}{g\rho_d\omega R})$$

Resolving in the ψ direction

In the other direction, the centrifugal force becomes insignificant and can be ignored, thus the controlling forces are:

(i) Corolois force

(ii) Drag force

i.e.

$$\rho \frac{dU_\psi}{dt} - \frac{18\mu}{\pi d^2} \left(\frac{U_\psi}{\omega R}\right) - \left(2\rho U_\psi \frac{U_r}{R}\right) \qquad 8.27$$

as before i.e

$\div$ by ρ and ωR to give

$$\frac{1}{\omega R} \frac{dU_\psi}{dt} = \frac{-18\mu}{\omega R \rho \pi d^2} \left(\frac{U_\psi}{\omega R}\right) - \frac{2U_\psi}{R} \frac{U_r}{\omega R} \qquad 8.28$$

Now $$\frac{1}{\omega R} \frac{dU_\psi}{dt} = \frac{d(U_\psi/\omega R)}{dt} = \frac{d}{dt}\left(\frac{U_\psi}{\omega R} + 1\right)$$

$$\frac{dY}{dt} = \frac{-18\mu}{\omega R \rho \pi d^2} \left(\frac{U_\psi}{\omega R}\right) - \frac{2U_\psi}{R}(X) \qquad 8.29$$

Now $$\frac{U_\psi}{\omega R} = Y - 1 \quad \text{Since } Y = \frac{U_\psi}{\omega R} + 1$$

$\therefore$ 8.29 becomes

$$\frac{dy}{dt} = {}_1(Y-1) - 2X\omega(Y-1) \qquad 8.30$$

$\therefore$ Combining 8.26 and 8.30,

$$\frac{dx}{dt} = \omega(Y^2 - X^2) + K_1X + K_2 = 0$$

$$\frac{dy}{dt} + K_1(Y - 1) + 2X(Y - 1)\omega = 0$$

where $k_1 = \dfrac{18v_m}{\pi d^2 \omega R}$

$$k_2 = \left(\omega - \frac{\Delta\rho}{dg\rho\omega R}\right)$$

9. RESULTS AND DISCUSSION

9.1 OPERATIONAL CHARACTERISTICS OF THE CONTACTOR

9.1.1 Hold-up Studies

Study of the hold-up in the contactor was carried out the two methods explained in Chapter 7. Although these methods have been previously employed[44],[177], the results obtained varied considerably. The hold-up of the contactor is in two functional sections: one is the rotor and the other comprises the seals and feed and exit lines. The direct method was used for Kerosene-water and Paraffin-water systems at rotor speeds of 2750 r.p.m. and 4600 r.p.m. respectively. The mean hold-up for Kerosene-water system at 2750 r.p.m. is V_E = 5043 cc and for Paraffin-water at 4600 r.p.m. is V_E = 5114cc, as tabulated in Appendix B.1.1.

The indirect method is more complex but yields not only the volume of the rotor V_c but also the total extractor volume VE. The results are tabulated in Appendix B.1.2. The values of V_E obtained by both methods are compared in Tables 9.1. and 9.2.

TABLE 9.1

METHOD	SYSTEM	FLOW RATES QH	QL	SPEED OF ROTATION ω r.p.m.	CONTACTOR VOLUME V_E cc
DIRECT	Kerosene	4	5	2750	5043 ± 60
	Paraffin	3	5	4600	5114 ± 38
INDIRECT	Kerosene	3	6	2750	4932 ± 47
	Paraffin	4	6	2750	4926 ± 24
	Kerosene	6	6	4600	4931 ± 16
	Paraffin	4	3	4600	4928 ± 21

As can be seen from Table 9.1 the values for V_ϵ obtained are very similar, the difference being 5%. However, the inference that the direct method is equally as accurate as the indirect method for determining the hold-up of commercial centrifugal extractors is not justified. Whereas the commercial extractors have extremely intricate internal packings, i.e. concentric cylinders with different sized orifices to present a tortuous path for the liquids, this contactor by virtue of simpler internals, allowed an easier path for the liquids. The liquids were, therefore, easily withdrawn. Furthermore, the direct method allows only for an approximate volume of the hold-up in the seals, which can contain a significant amount, e.g. 11%, of the total extractor volume. The displacement method is more accurate and has general applicability: it can also provide parameters that can be used for defining operating limits of centrifugal contactors.

Equations shown in Chapter 6 can be verified from the hold-up studies. Earlier work of Morgenthaler et al[178] and Barson and Beyer[177] showed that the heavy-liquid volume in the contactor, V_{CH} is given by,

$$V_{CH} = \pi b(r^2 - \frac{2gP_{LO}}{\omega^2}) \qquad (6.11)$$

Using this equation, it is shown in Chapter 6 that the total extractor volume VE should have a linear relationship with the light-liquid-out pressure P_{LO}, since

$$VE = V_H + V_L \qquad (9.1)$$

and $$V_H = (\pi br^2 + V_{SH}) - \frac{2\pi bg}{\Delta\rho\omega^2} \cdot P_{LO} \qquad (6.14)$$

$$V_L = V_{SL} + \frac{2\pi bg}{\Delta\rho_\omega 2} \cdot P_{LO} \qquad (9.2)$$

To test the validity of these equations, the values of V_H and V_L are plotted against the light-liquid-out pressure P_{LO}, in Figures 9.1 and 9.2. These show that the relationships are linear, as predicted, and that the heavy phase volume in the contactor decreases linearly. Furthermore, there is general agreement with the results obtained previously[44] shown in Figure 6.3. However, unlike Fig. 6.3, the Figures 9.1 and 9.3 do not show the 'straightening-out' of the lines at high values of P_{LO}. This can be explained since in the extractor studied by these workers[44]. A residual amount of heavy or light liquid remained in the rotor, depending on the type of flooding occurring; this required disproportionate amount of inlet pressure to displace. In this contactor the design of internals enabled the liquids at the centre or the periphery to flow out of the rotor more readily.

The hold-up data is correlated in similar method to equations 9.1, 9.2 and 6.14, viz, the phase volumes in the contactor vary according to,

$$VH = a_1 + m_1 P_{LO} \qquad (9.2)$$

$$VL = a_2 + m_2 P_{LO}$$

The constants are a function of (ω) and are given in Table 9.2.

Equations 6.14 and 9.2 can be used to define an 'effective width' of the contactor for hold-up studies, since

$$\text{gradient of these equations} = \frac{2\pi bg}{\Delta\rho_\omega 2}$$

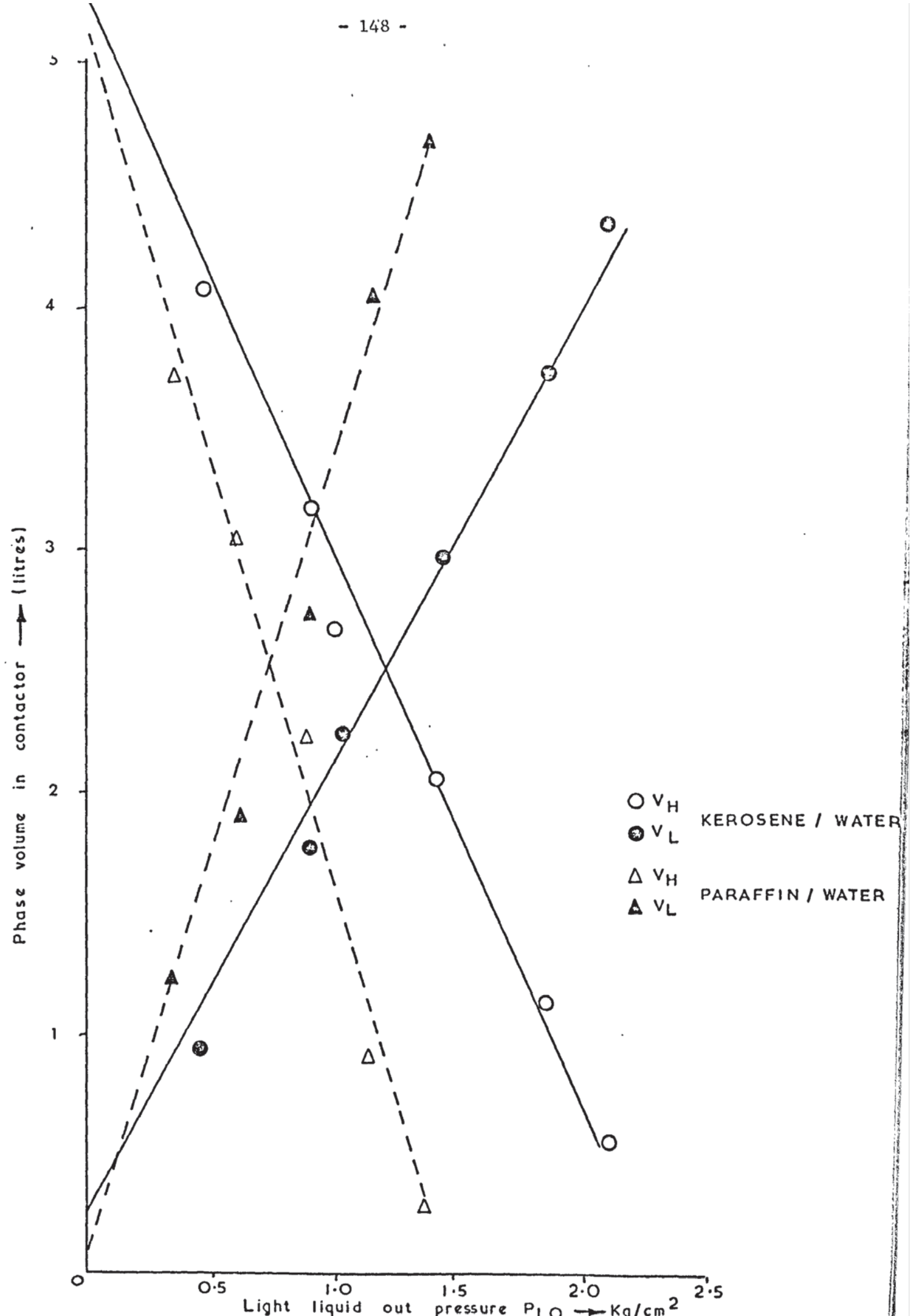

FIG. 9·1 VARIATION IN PHASE VOLUME IN THE CONTACTOR (V_E) WITH LIGHT-LIQUID-OUT PRESSURE P_{LO} AT ω = 2750 R.P.M. $V_E = V_H + V_L$

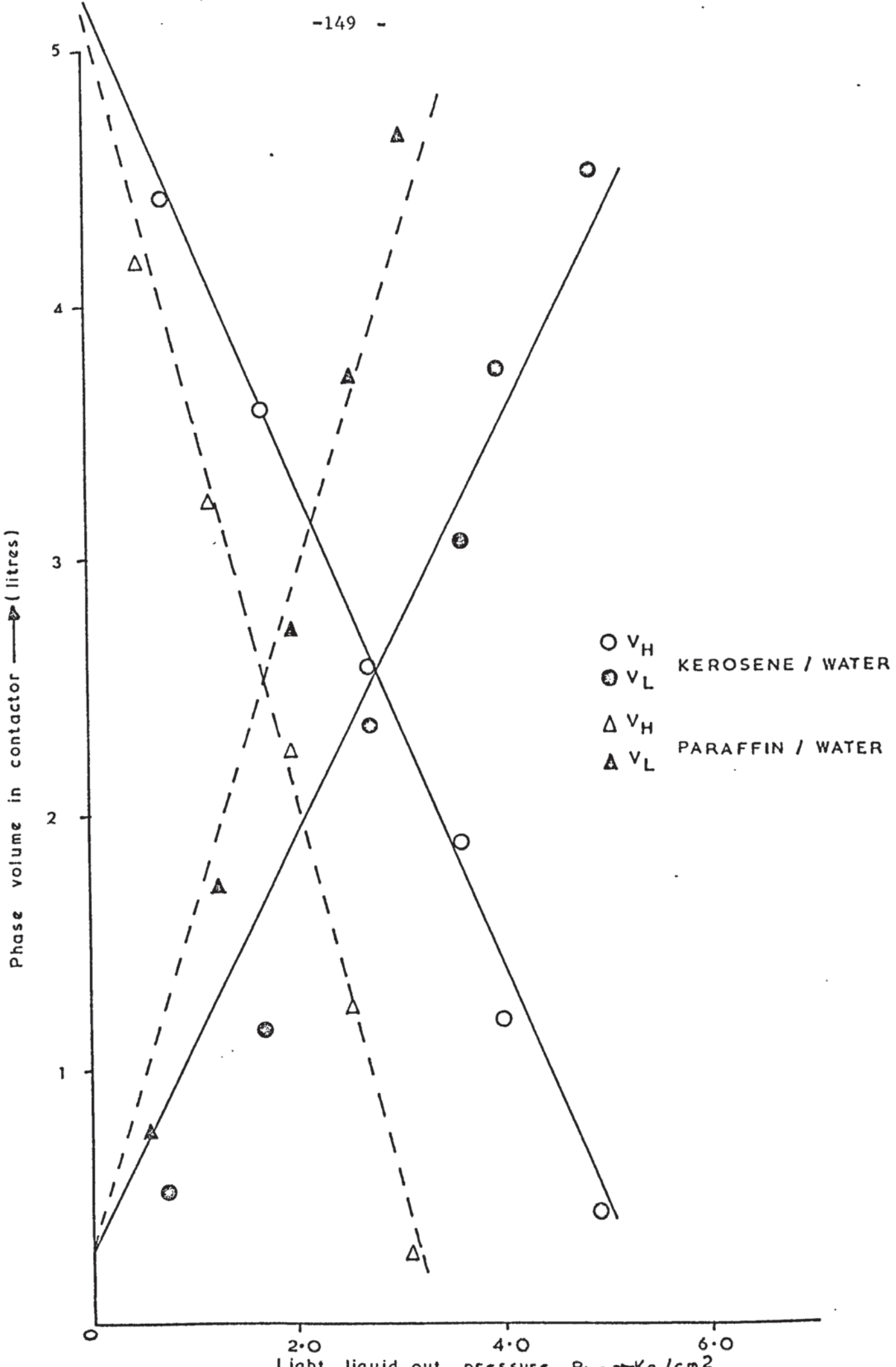

FIG. 9-2 VARIATION OF PHASE VOLUME IN CONTACTOR (V_E) WITH LIGHT - LIQUID - OUT PRESSURE P_{LO} AT ω=4600 R.P.M. $V_E = V_H + V_L$

$$\text{i.e. } b = \frac{\text{gradient}.\Delta\rho\omega^2}{2\pi}$$

TABLE 9.2

ω	a_1	a_2	a_3	m_1	m_2
1750	5.25	0.235	5.49	2.86	2.55
4600	5.12	0.140	5.26	1.05	1.06

However, ω must be defined correctly. In the earlier work[44] this was wrongly used as r.p.m. because this must be defined in radians. The concept of 'effective width', b, is quite useful since it enables the prediction of pressure requirements of any given centrifugal contactor from hold-up studies. Table 9.3 shows the values of b calculated for this work.

TABLE 9.3

ω R.P.M.	$\Delta\rho$ kg/cm^2	Effective width b m x 10^{-2}	Actual width of contactor m x 10^{-2}
2750	0.2555×10^{-3}	7.318	6.35
	0.1279×10^{-3}	6.952	6.35
4600	0.2555×10^{-3}	7.095	6.35
	0.1279×10^{-3}	7.197	6.35
Mean effective width 'b' = .07141 m			

Although the effective and actual width are of the same order, this is not always the case. The explanation for it here is associated with the internals of the contactor in that the path of the

liquid path is of primary importance.

9.1.2 Flooding Phenemona

Study of flooding phenemona in the centrifugal contactor enabled the definition of its operational limits. As explained in Section 6.3.2 three types of flooding are possible, viz:

(a) shaft flooding - or the light liquid flooding

(b) rim flooding - or the heavy liquid flooding, and

(c) the capacity flooding.

Although all three types were observed, capacity flooding was too difficult to accurately study for this contactor, because its internals allow easier path for the liquid and the onset of such flooding occurs very rapidly.

When the centrifugal contactor is operating there are distinct zones of liquids in the rotor: the light clarifying zone near the centre, the heavy clarifying zone near the periphery of the rotor and a less distinct zone where the two phases are in contact. Shaft flooding occurs when the interface is moved through the light clarifying zone until it reaches the shaft. This type of flooding can occur at different flow ratios. Rim flooding occurs when the interface is moved through the heavy clarifying zone near the periphery of the rotor. Capacity flooding occurs when entrainment of both heavy and light liquids occurs at both ends of the contacting rotor. The latter is initiated in the two phase zone, and was less easily observed in this contactor since this zone was very small $\simeq$ 0.01 m.

In common with other solvent extraction equipment, the prediction of the operational limits are extremely important. In the literature cited in Section 6.3.2, two methods are given for representing the flooding in centrifugal contactors. Whereas Jacobsen and Beyer[44] used light liquid pressure P_{LO} against flow rate, Todd[176] and Barsen and Beyer[177] preferred to use the back pressure $\overline{P_{LLO}}$ where,

$$\overline{P}_{LLO} = P_{LO} - P_{HO}.$$

The latter method is better since the envelopes obtained show clearly the onset of capacity flooding which the former method does not. Both methods of representing the flooding limits are shown in Figures 6.6, 6.7, and 6.8. The results obtained are shown overleaf by Figures 9.3, 9.4 and 9.5.

Two flow ratios were used in the study, i.e. $Q_K = 0.5\ Q_w$ and $Q_K = 2.0\ Q_w$. Figures 9.3 to 9.4 show that the onset of shaft, rim and capacity flooding are clearly defined. The maximum obcissa lines represent inoperable capacity flooding for the respective conditions, whereas the plotted points represent a full range of operable major interface positions from light liquid flooding to heavy liquid flooding. Furthermore, it appears that the total capacity of the contactor is higher when the ratio of light-to-heavy liquids is increased. This accords with equation 6.19, viz

$$2(\rho_4 - \rho_L)R\omega^2 h = \rho_c\left(\frac{Qc}{Ac}\right)^2 + \rho_D\left(\frac{Q_D}{A_D}\right)^2 \qquad (6.19)$$

which also shows that the combined flow is proportional to the first power of speed.

Although the effect of increasing the perforations/orifices was not investigated it appears from equation 6.19 that the capacity will increase proportionately.

9.1.3 Pressure Characteristics

The correct interpretations of pressure readings of a centrifugal contactor are necessary for its operation. In chapter 6 the pressure characteristics were described in terms of 'legs' of manometers, viz Fig. 6.2.

The location of the principal interface, controlled by imposing a back pressure on the light-liquid-out stream, dictates the operational limits of a contactor since moving it through the various phase zones can cause shaft or rim flooding. Similarly, it is necessary to know the pressure required to pump both the heavy and the light phases through the contactor at any given rotor speed. Equations 6.1 and 6.2 in Section 6.2 are claimed[44] to predict these pressures. Although these equations were not fully investigated, observation of Figs. 9.6, 9.7 and 9.8 indicates that the pressures are in fact a function of second power of ω, as predicted.

Pressure losses also occur across the contactor. These can be divided into entry and exit losses. This is important, since there is a significant contribution of rotation above that at zero ω, and that this additional energy dissipation is one of the factors controlling droplet size. An equation of the form has been proposed viz:

$$\Delta P_{\omega} = \Delta P_{o} + 5.7 \times 10^{-5} Q\omega \qquad (6.4)$$

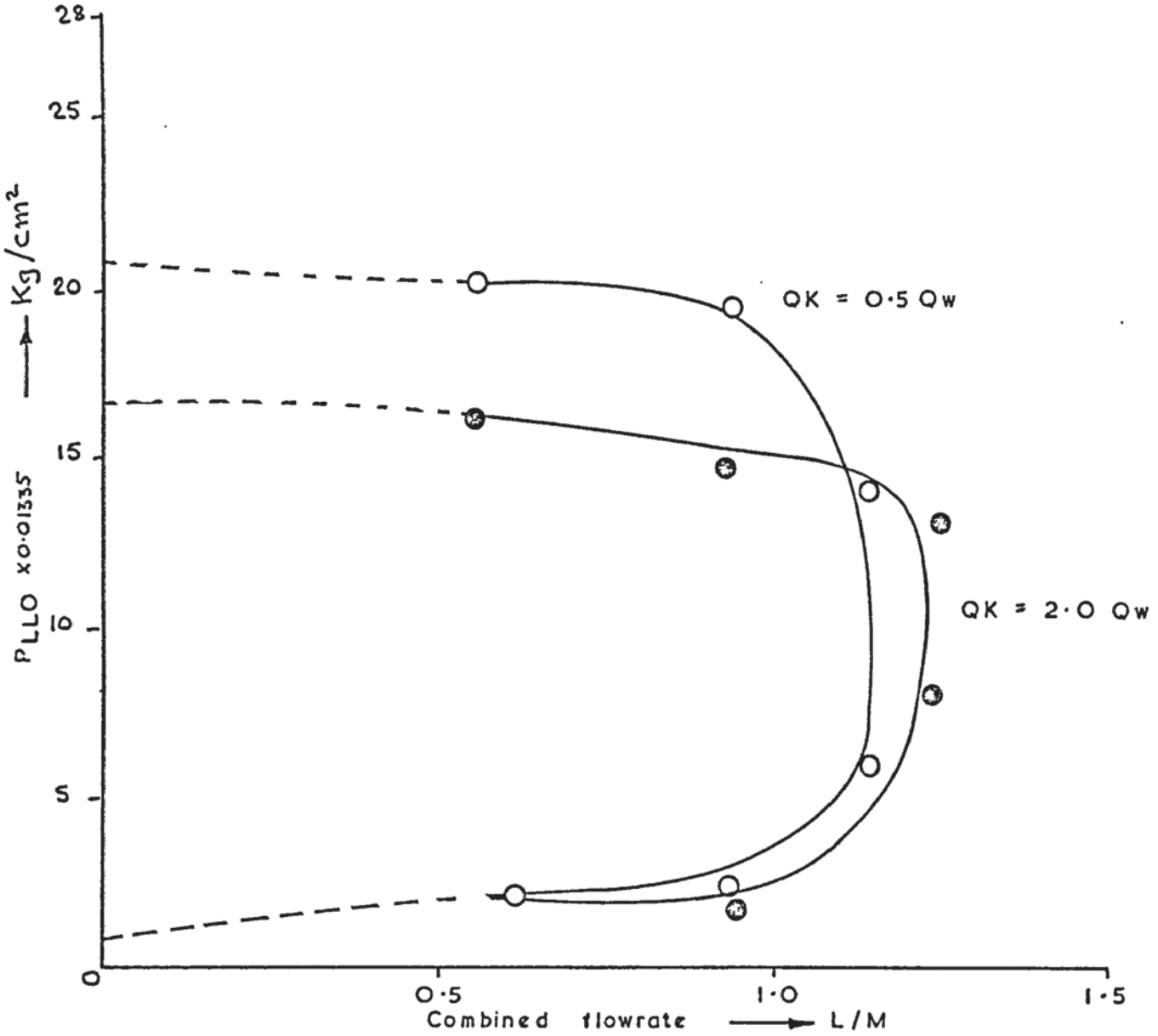

FIG. 9-3 FLOODING ENVELOPES FOR KEROSENE / WATER SYSTEM
ω = 2750 R.P.M.

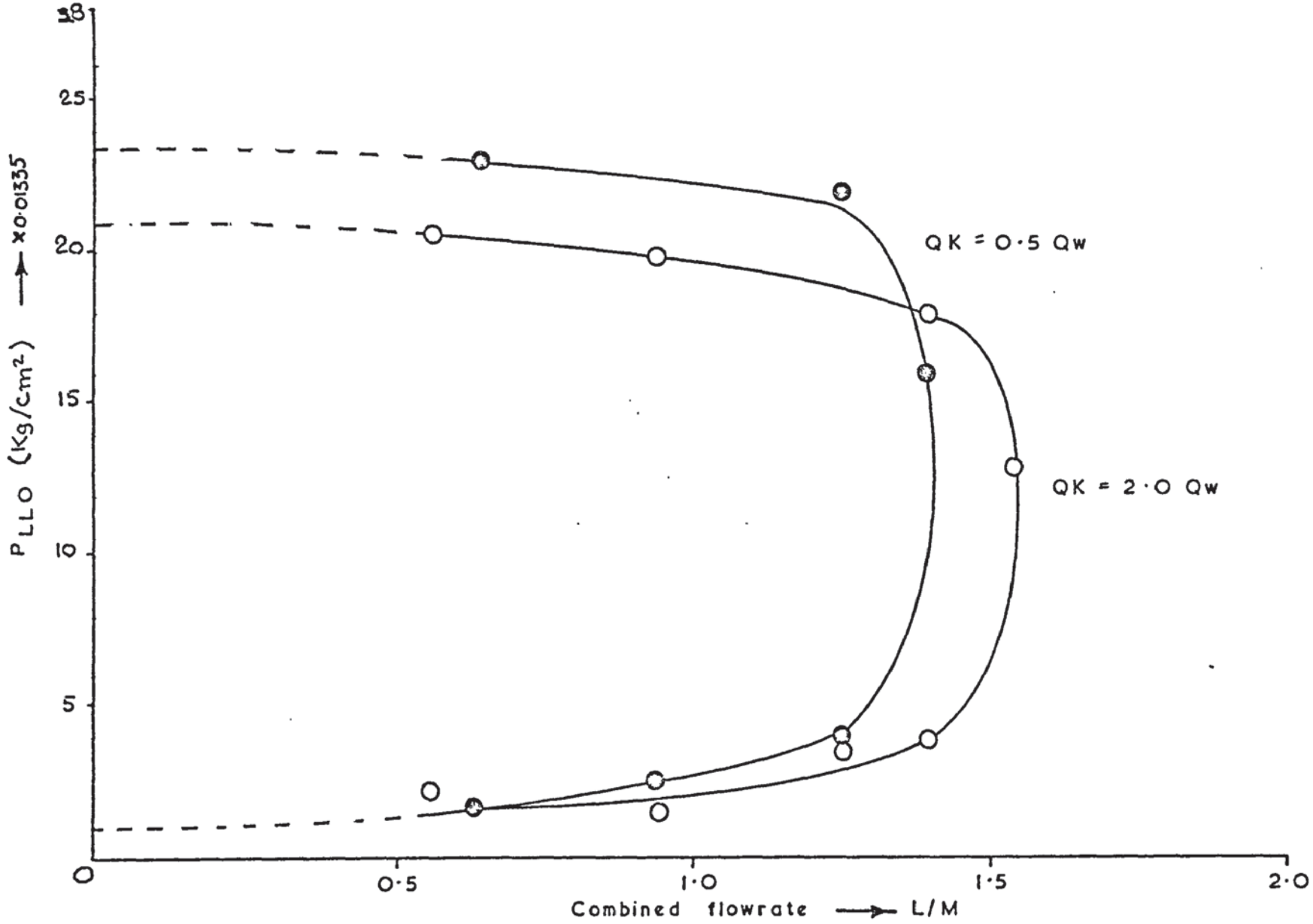

FIG. 9-4 FLOODING ENVELOPES FOR KEROSENE / WATER ω = 3460 R.P.M.

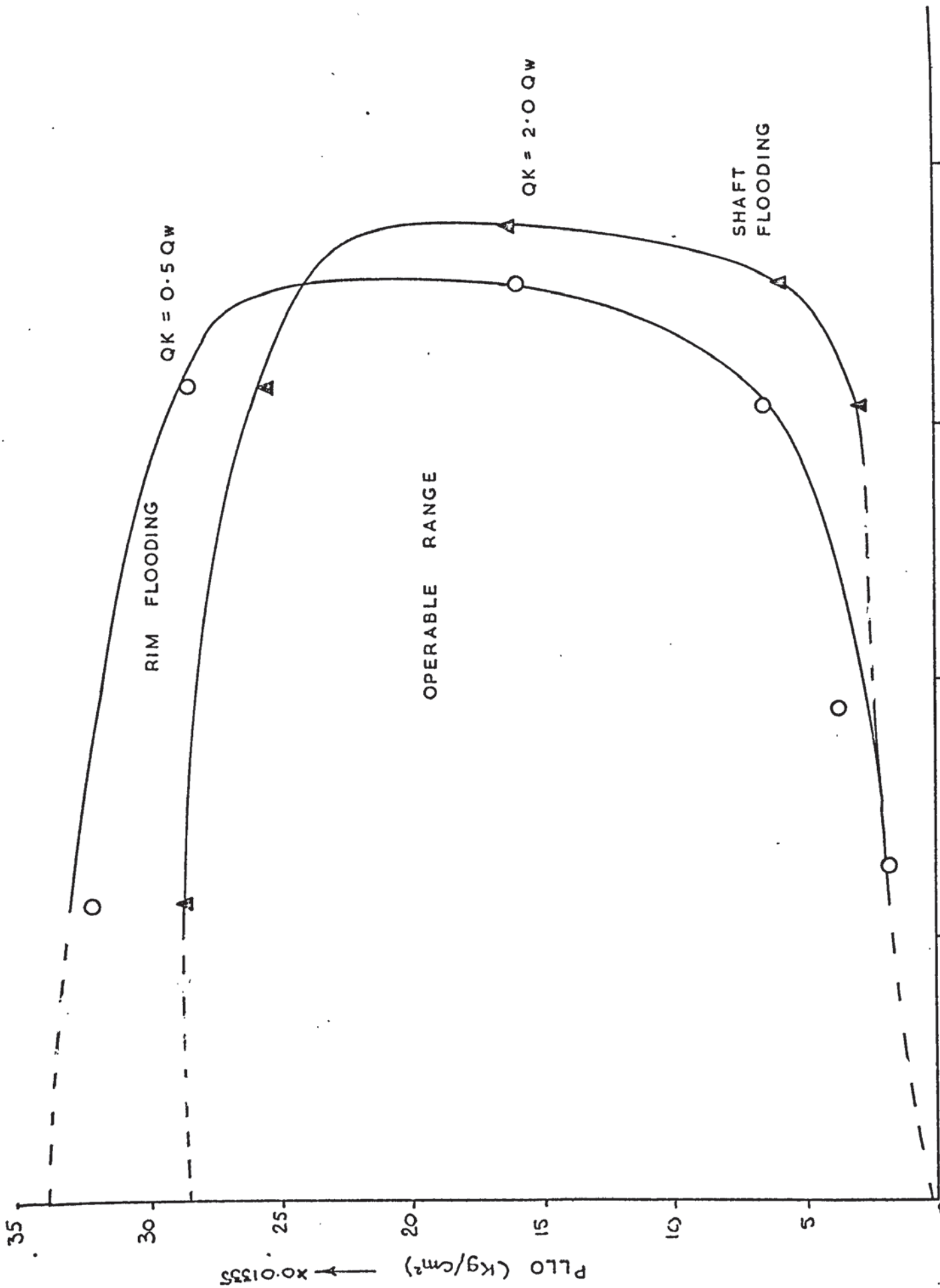

FIG. 9-5 FLOODING ENVELOPES FOR KEROSENE WATER SYSTEM ω = 4600 R.P.M.

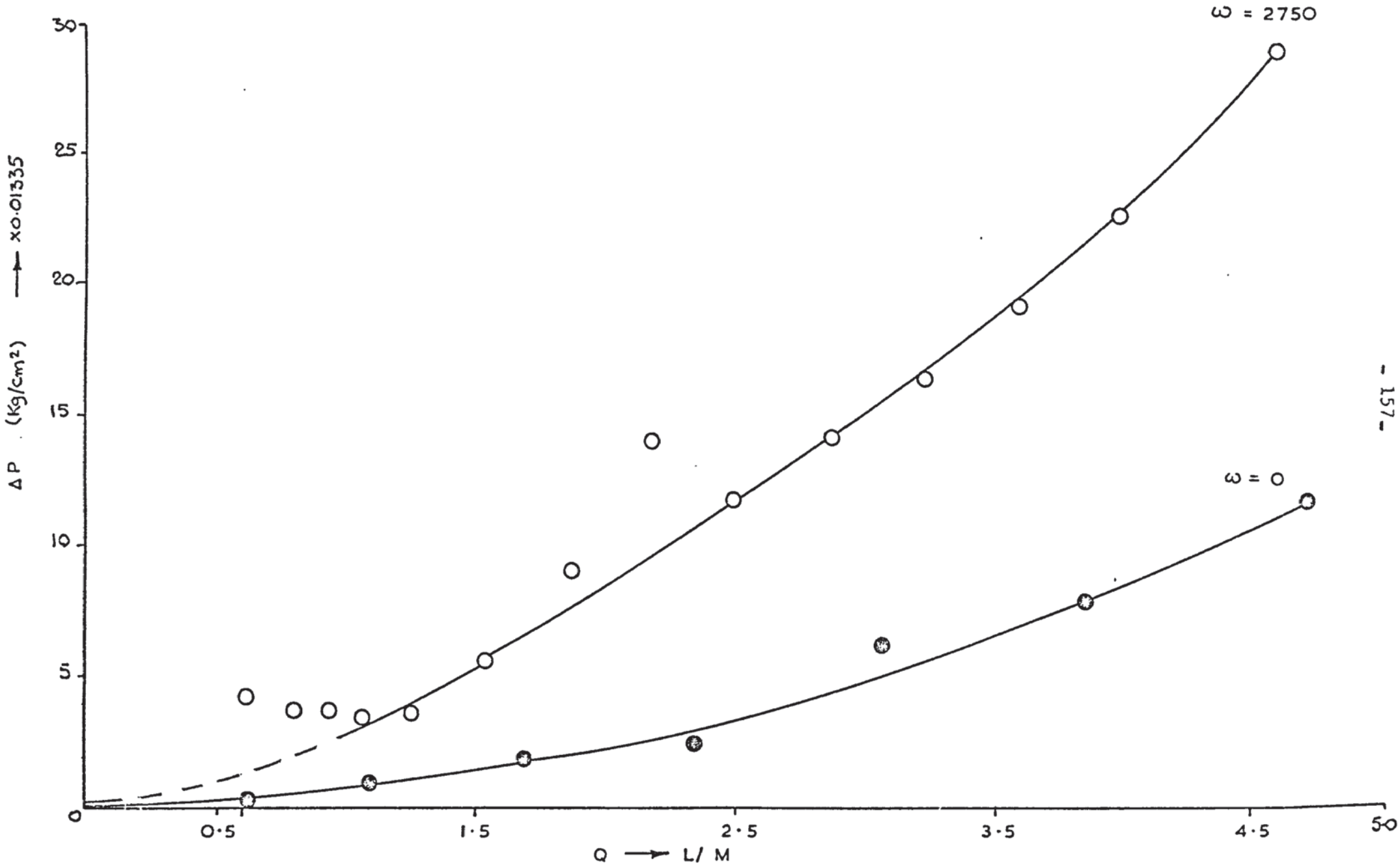

FIG. 9·6 PRESSURE DROP THROUGH CENTRIFUGAL EXTRACTOR FOR WATER PHASE $\omega = 2750$

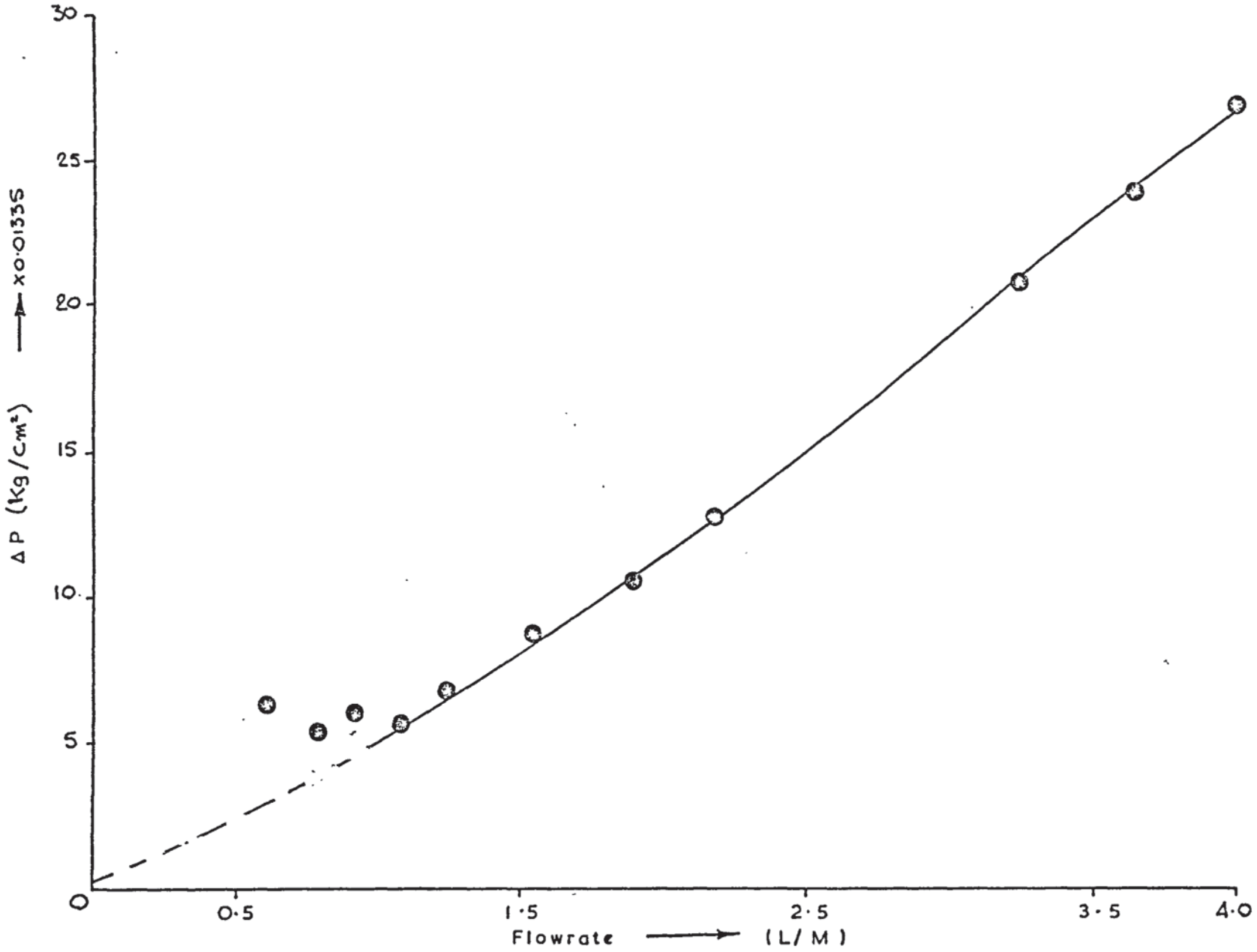

FIG. 9-7 PRESSURE DROP THROUGH CENTRIFUGAL EXTRACTOR FOR WATER PHASE $\omega = 3460$

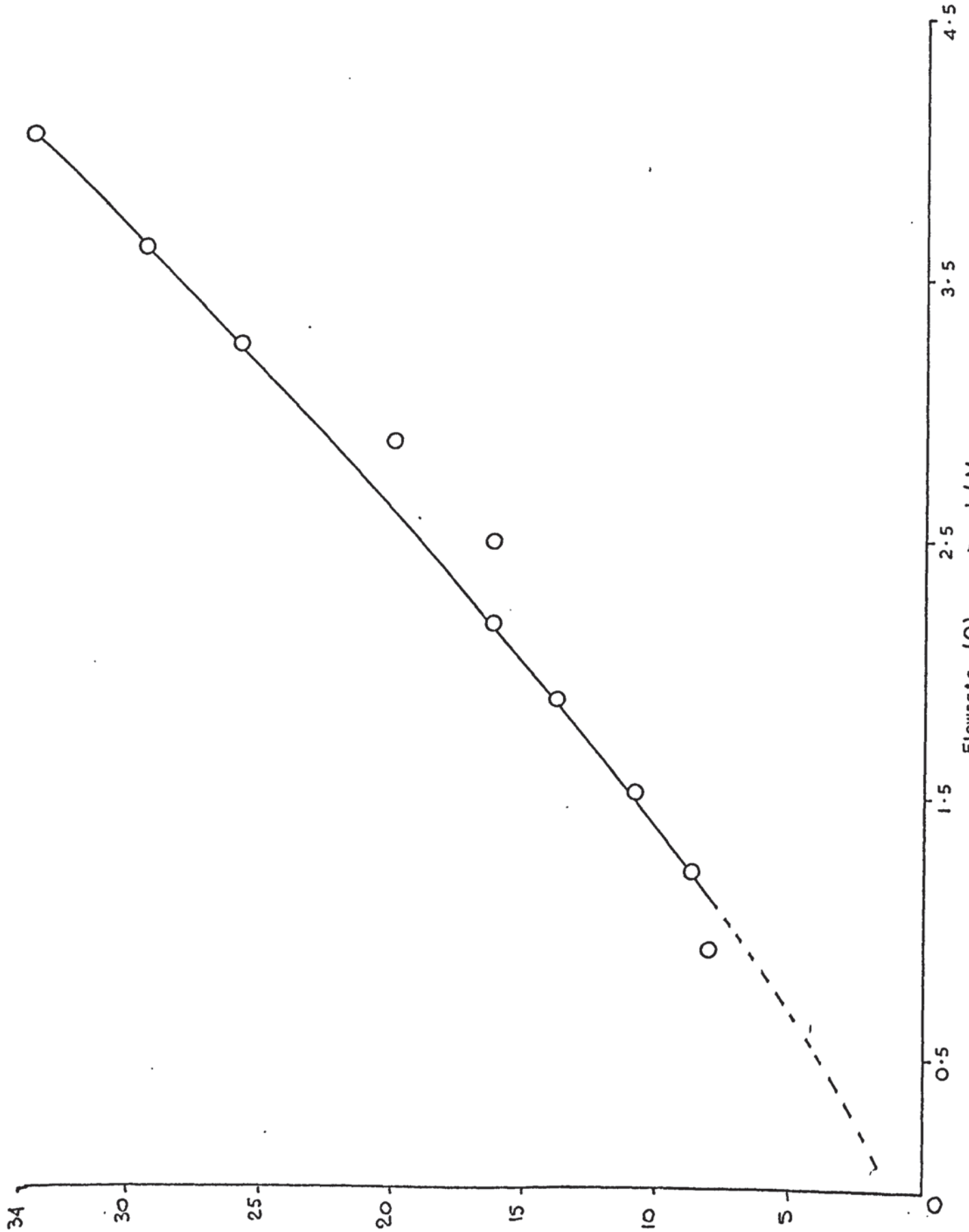

FIG. 9-8 PRESSURE DROP C/E FOR WATER PHASE ω = 4600 R.P.M.

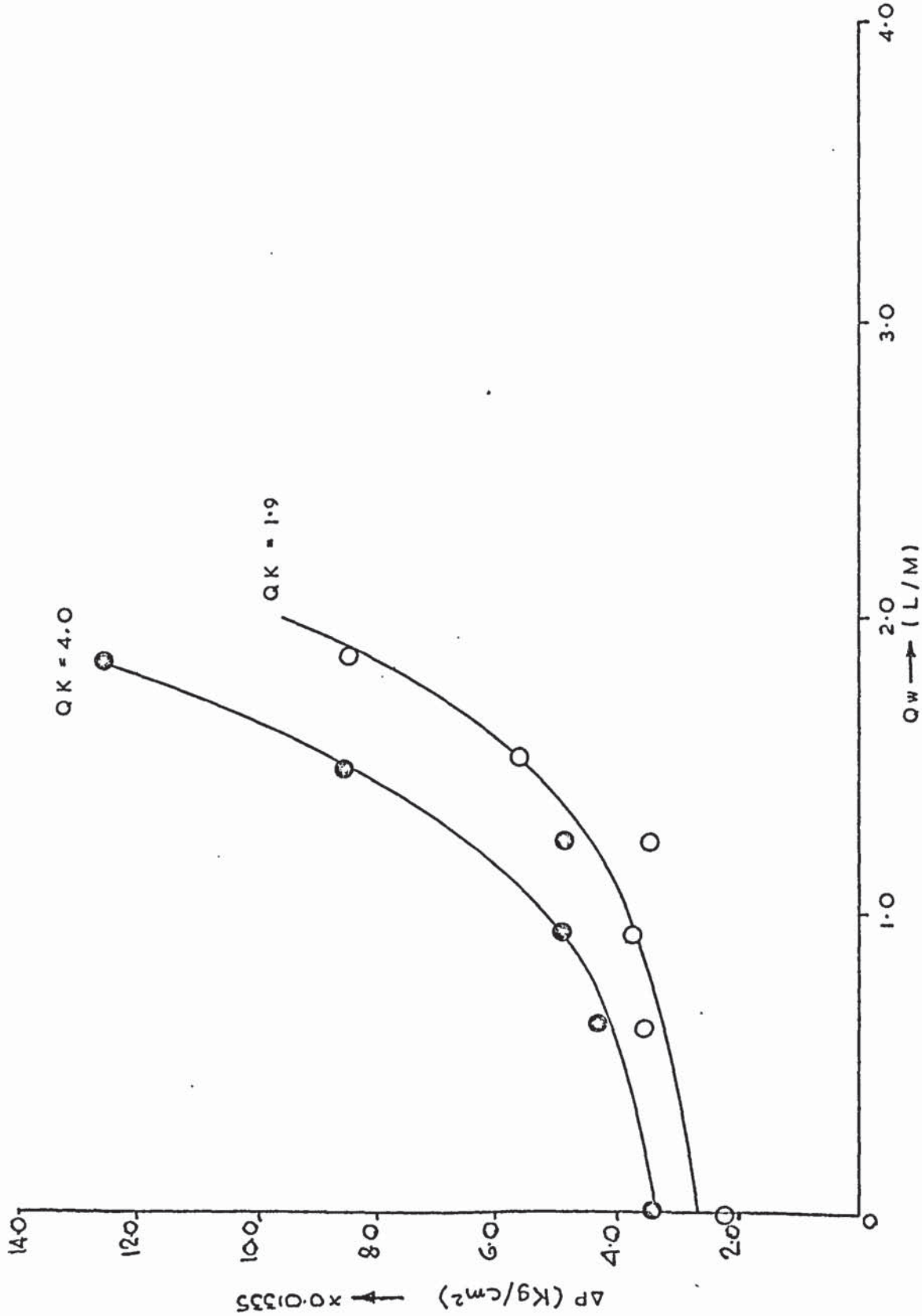

FIG. 9 – 9 EFFECT OF WATER FLOW ON KEROSENE PRESSURE DROP AT 2750 R.P.M.

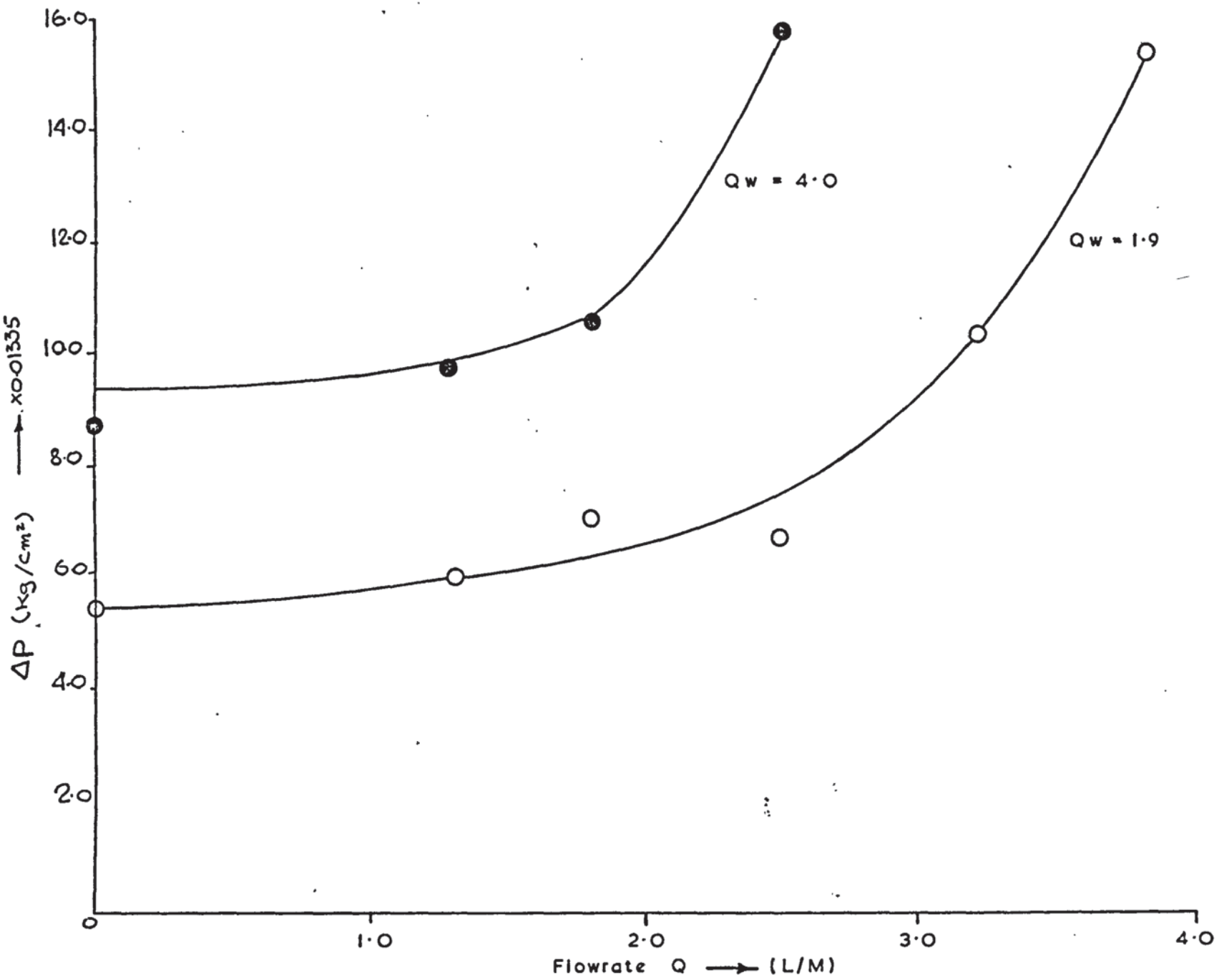

FIG. 9-10 EFFECT OF KEROSENE ON WATER PHASE PRESSURE DROP (2750 R.P.M.)

Experimental data from this work confirms, as shown by Figures 9.6, 9.7 and 9.8, where the pressure loss across the contactor is plotted against combined flow rate. By means of least square method, the data was correlated to give,

$$P_{\omega} = P_{o} + 1.506 \times 10^{-3} Q\omega \qquad (9.4)$$

Some difference in the value of constants in equations 6.4 and 9.4 is to be expected because of the differences in geometry between the contactors. The increased rotor diameter of the contactor developed here (.29 m as opposed to 0.178 m) resulted in the pressure loss being greater, as shown by the greater value of the constant in equation 9.4.

Effect of one phase flow rate on the pressure drop of the other phase was also investigated. The results are shown in Figures 9.9 and 9.10 for the Kerosene-water system. As the flow was increased, the required pressure increased due to both an increased hold-up of the dispersed phase and the competition of both fluids for the available flow passageway within the rotor. Curves similar to Figures 9.9 and 9.10 have been reported[176].

9.2 STUDIES OF DISCHARGE RATES

9.2.1 Types of Flow

The shape, size and velocity of droplets are of primary importance in determining the mass transfer characteristics of the contactor. Initial studies were therefore directed towards the understanding of dynamics of flow in centrifugal fields. The process of flow of liquids under the action of centripetal force is complicated

by the existence of this and the Corolois force. The number and direction of forces acting on an element of liquid just inside and outside the nozzle have been identified previously[42]. Whereas Podbielniak[23] discounts the possibility of 'jetting' of liquid in centrifugal contactors, Ponikarov et al[43] report that it can occur and that five characteristic states of discharge of liquids exist. By techniques described in Chapter 7, data was obtained to account for the influence of various factors on the theoretical flow rate Q_T,

$$Q_T = f\ (\omega, A, R_c, R_i, \Delta\rho, \rho_d) \qquad (9.5)$$

Following Ponikarov et al[43], a coefficient of discharge C_{od} was defined,

$$C_{od} = \frac{Q_T}{Q_a} \qquad (9.6)$$

The following regimes were discernible from the cine films taken of the contactor, viz:

(a) Drop regime. In this regime the liquid issued in discrete droplet form. Projection at slow speeds ranging from 1 to 6 f.p.s. was necessary to observe the discretness of the flow. This regime was observed for both the Kerosene/water and Paraffin/water systems at all speeds, from 1750 r.p.m. to 4600 r.p.m.

(b) Jet regime. This describes the issuing of a jet from the nozzle and its subsequent break up into discrete drops. Unlike (a) above, jets were not always observed with both

systems; especially at high speeds. For the Kerosene/ water system the jet regime was not observed at 3460 r.p.m. and 4600 r.p.m. This can be explained in terms of the pressure required to pump the light phase into the rotor. Thus equation 6.2 shows that the light-liquid-in pressure P_{LL}, is proportional to ω^2 and $\Delta\rho$. Whereas for Kerosene the density difference is 0.255×10^{-3} kg/m^3, that for Paraffin is 0.1279×10^{-3} kg/m^3. The pressure required for Kerosene was therefore, greater than for paraffin.

9.2.2 Correlation of Results

An attempt was made to correlate the data in terms of the two dimensionless groups; the first number was defined as the ratio of Corolois force and the centrifugal i.e.

$$N_1 = \left(\frac{\rho_d U_N}{\Delta\rho \omega R}\right)$$

The second group accounted for the influence of the surface areas of orifice and the central rotor, i.e.

$$N_2 = \left(\frac{A_o}{A_c}\right)$$

Contrary to the conclusions of Ponikarov[43] it was not possible to correlate the significance of this group on C_{od}. Since the first dimensionless group contains the most important of the forces, graphs of this against the coefficient C_{od} are shown in Figs. 9.11 to 9.19.

Three distinct zones are apparent from these Figures each representing a different regime for liquid issuing from the nozzles.

The graphs accurately predict the range of each regime and confirm that jet regime of discharge was not achieved for Kerosene/water system at high values of ω. However, there is a scatter of points in the range of $N_1 = 0.30$ to $N_1 = 0.51$ on all Figures. Whereas visual observation revealed only two flow regimes, viz: drop and jet, the Figures appear to indicate the existence of a third regime. Since the scatter appears for all the three nozzle diameters, four speeds of rotation and both systems, it is not due to experimental error. The region may therefore be considered as a Transition regime in which both types of flow occur.

Fig. 9.19 summarises the results for all values of D_N and ω for both systems, it defines -

(a) The Transition regime, irrespective of the physical properties of the liquids and the speed of rotation, and

(b) Correlations for the prediction of the onset of the jetting state.

Use of the Least Square Method for fitting the data yielded the correlations,

For $N_1 \leq 0.30$, the drop state exists and

$$C_{od} = 3.73 \left(\frac{\rho_d U_N}{\Delta\rho \omega R}\right)^{1.52} \qquad (9.6)$$

For $0.30 < N_1 < 0.51$, the Transition state exists

For $N_1 > 0.51$, the jet state exists, and

$$C_{od} = 0.63 \left(\frac{\rho_d U_N}{\Delta\rho \omega R}\right)^{0.031} \qquad (9.7)$$

These conclusions are contrary to those reported by the

other workers[42,43] who, as shown in Fig. 6.10, did not recognise the Transition zones. Although both Figures 6.10 and 9.19 are similar in shape, the former shows that the change from the droplet state to jet regime is immediate. The phenomena is unlikely to be a function of the geometry of the contactor. However, there may be a significant influence by another dimensionless group, e.g. one that takes into account the area of nozzle and some other characteristic area, albeit not that which Ponikarov et al[43] define in equations 6.23 and 6.24.

Whereas the change from droplet regime to jet regime under gravity is immediate, under centrifugal conditions the presence of centripetal and Corolois forces appears to cause the transition regime.

From Fig. 9.19 the velocities that characterise the various flow regimes are tabulated as an example for ω = 2750 r.p.m. in Table 9.3.

TABLE 9.3

NOZZLE VELOCITIES IN THE CONTACTOR

FLOW REGIME	NOZZLE VELOCITY U_N cm/s	
	KEROSENE	PARAFFIN
End of Droplet Regime	63.12	26.96
Jet Regime	105.20	44.94
Transition Regime	THIS regime exist between the two values for the respective systems	

These values may be compared with those obtained for gravity

conditions i.e. 15 to 20 cm/s[175].

9.2.3 Significance to Centrifugal Contactor Operations

The study of discharge rates enabled the prediction of:

(i) A droplet regime,

(ii) A Transition regime,

(iii) A jet or spray regime.

This knowledge is important because the prevailing conditions inside the contactor determine the droplet formation mechanism and hence the droplet size. The significance of the droplet size to the performance of the contactor, discussed in detail in 9.3.4, is obvious.

The study has provided two correlations which define the state of the dispersed phase in terms of physical properties, speed of rotation (ω) and radius of the nozzle from the shaft, R. The correlations also provide useful design procedures. This is discussed in 9.5.

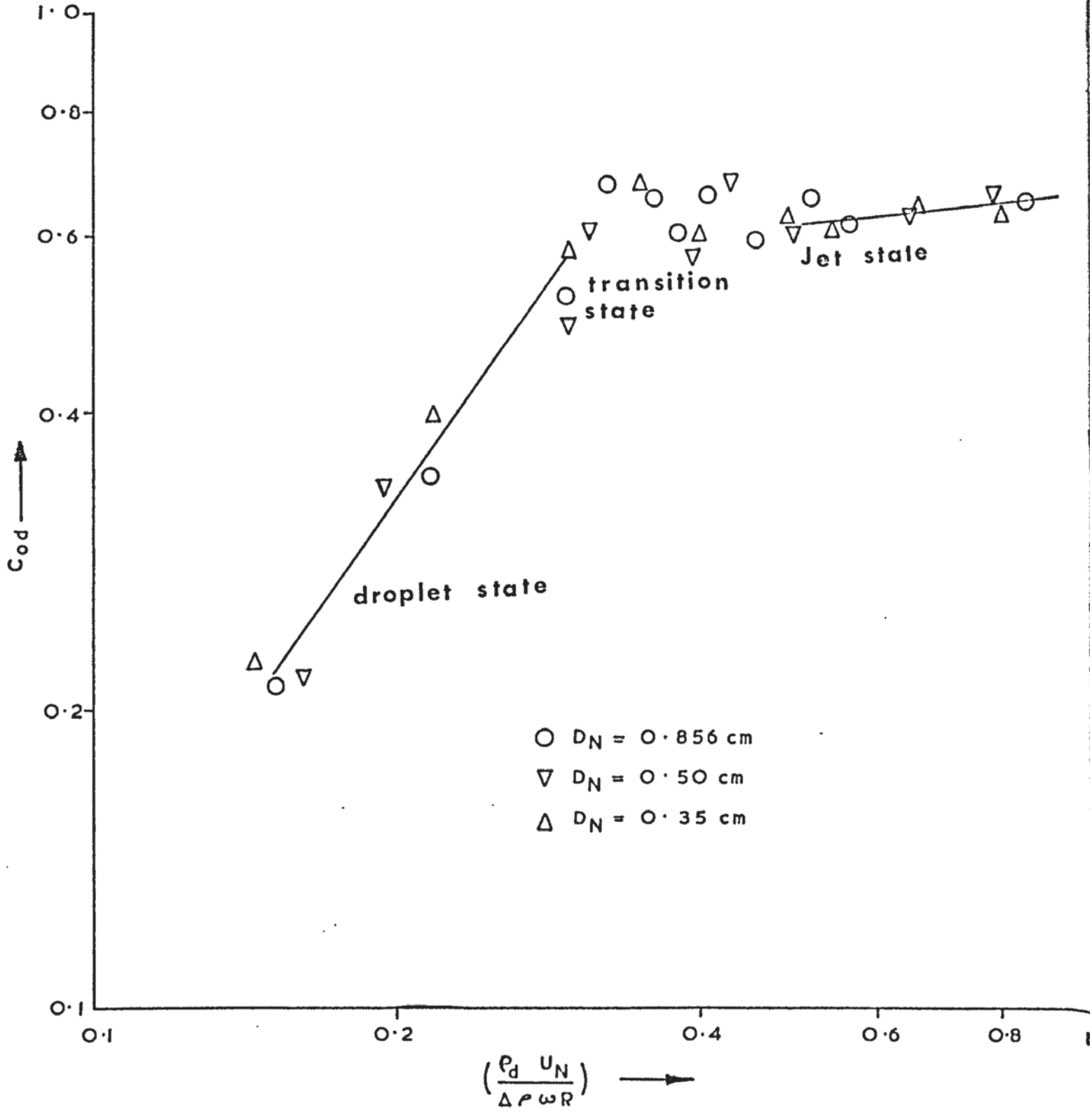

FIG. 9-11 RELATIONSHIP BETWEEN THE COEFFICIENT OF DISCHARGE C_{od} AND THE DIMENSIONLESS GROUP $\left(\frac{\rho_d U_N}{\omega R \Delta\rho}\right)$ AT ω=1750 R.P.M AND KEROSENE / WATER SYSTEM

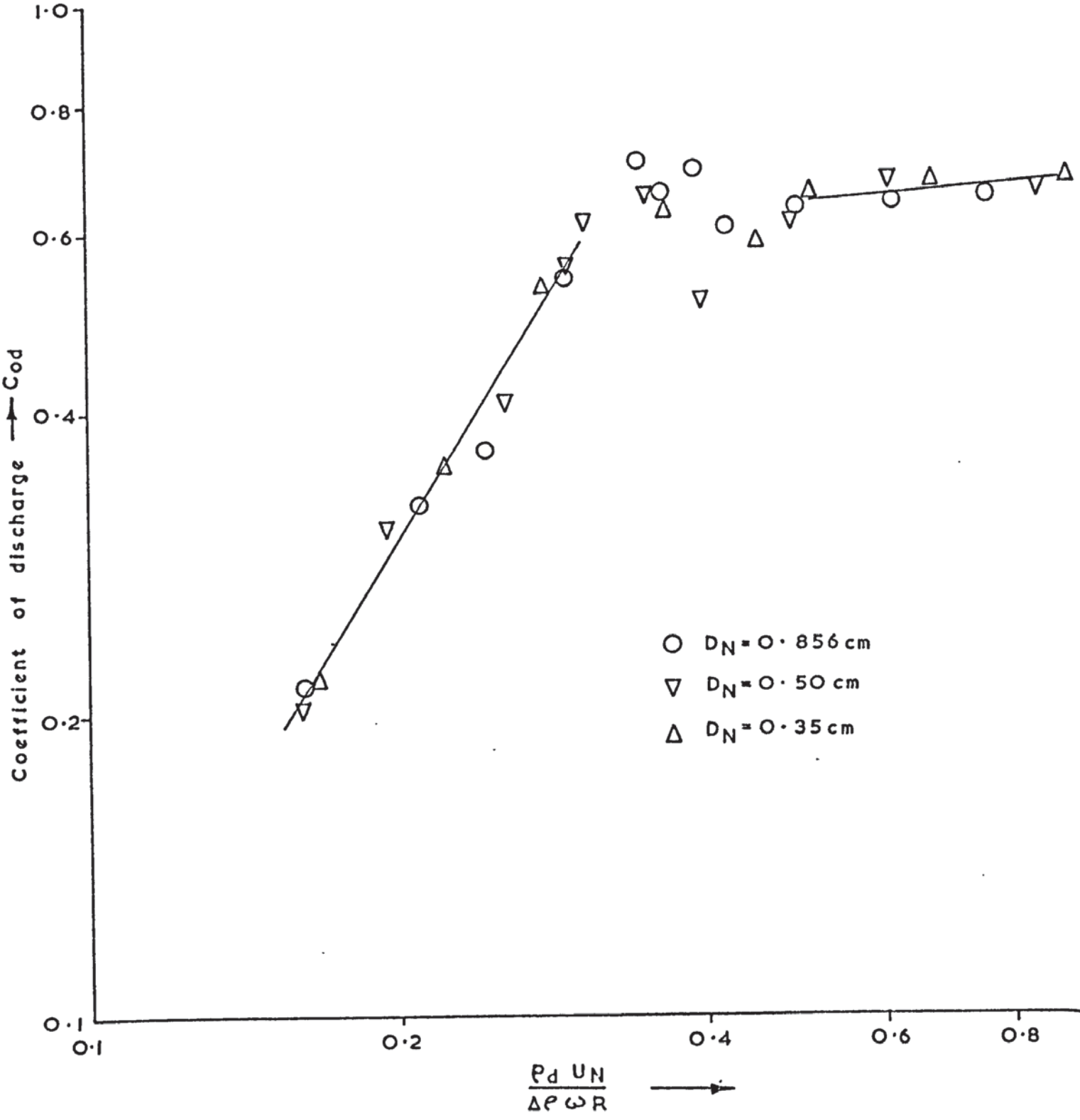

FIG. 9·12 RELATIONSHIP BETWEEN THE COEFFICIENT OF DISCHARGE C_{od} AND THE DIMENSIONLESS GROUP $\left(\frac{\rho_d U_N}{\omega R \Delta\rho}\right)$ AT ω=1750 R.P.M. AND PARAFFIN / WATER SYSTEM

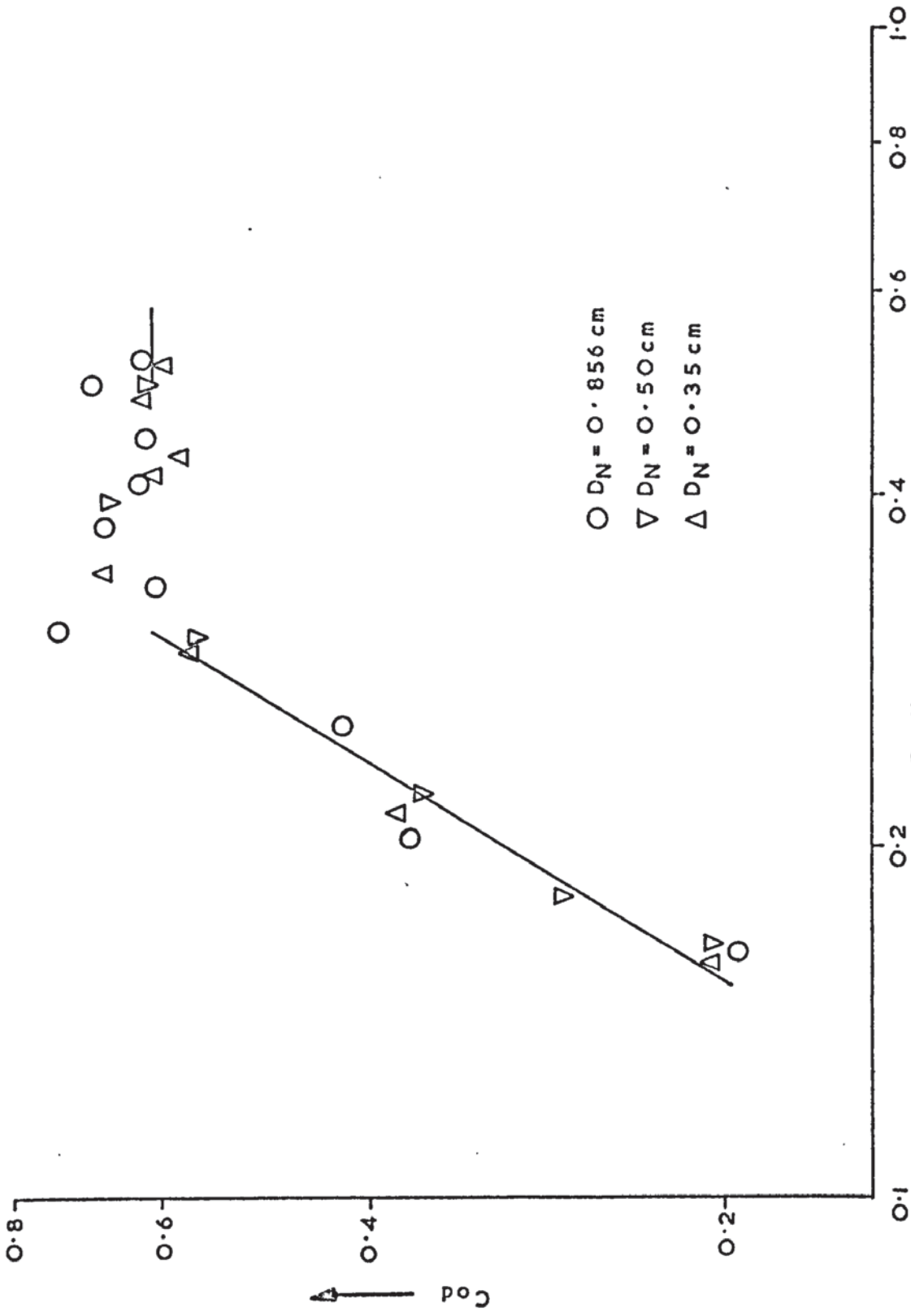

FIG. 9-13 RELATIONSHIP BETWEEN THE COEFFICIENT OF DISCHARGE C_{od} AND THE DIMENSIONLESS NUMBER $\left(\frac{\rho_d U_N}{\Delta \rho \omega R}\right)$ AT ω = 2750 AND KEROSENE / WATER SYSTEM

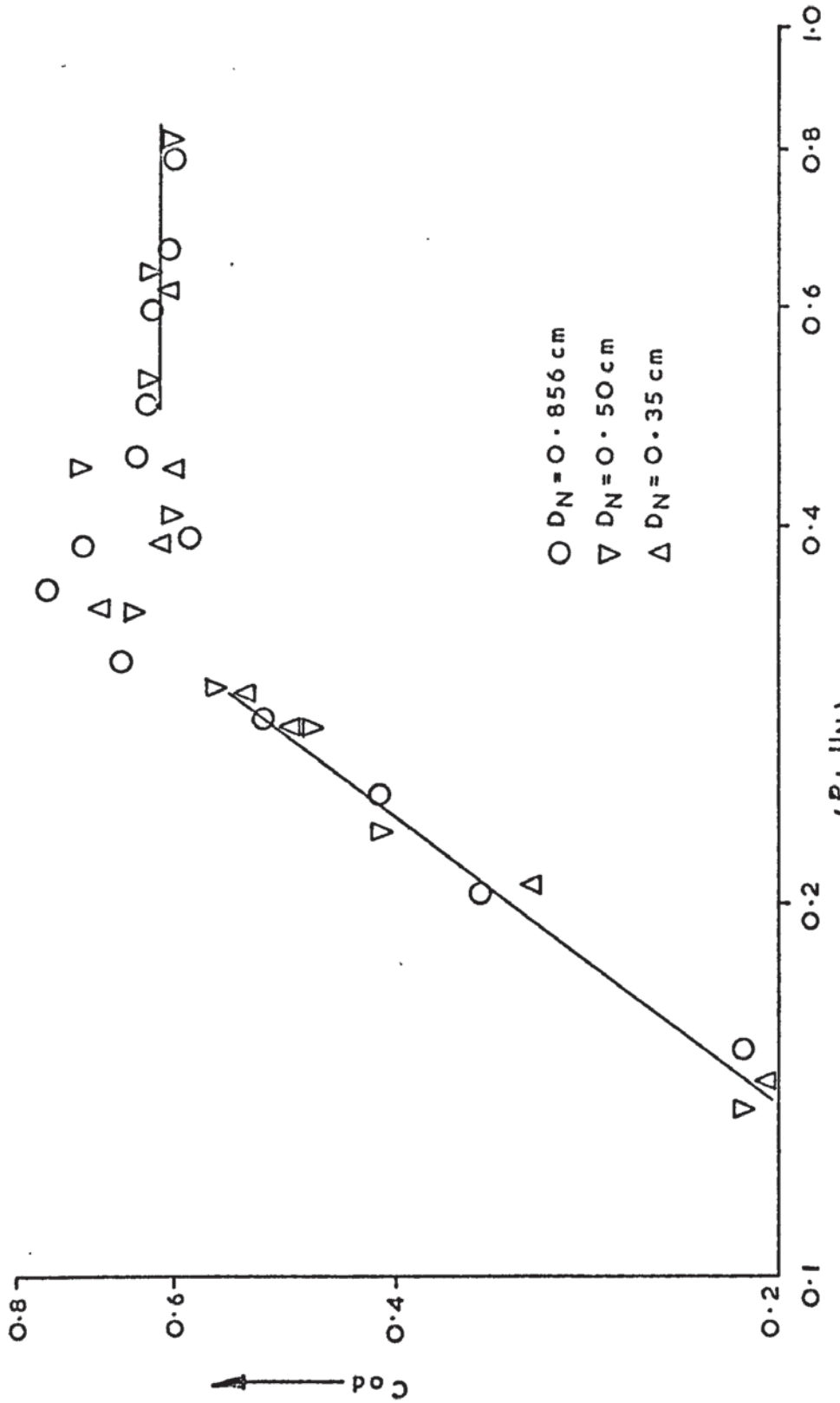

FIG. 9-14 RELATIONSHIP BETWEEN COEFFICIENT OF DISCHARGE C_{od} AND THE DIMENSIONLESS NUMBER $\left(\frac{\rho_d U_N}{\Delta \rho \omega R}\right)$ AT ω = 2750 R.P.M. AND PARAFFIN / WATER SYSTEM

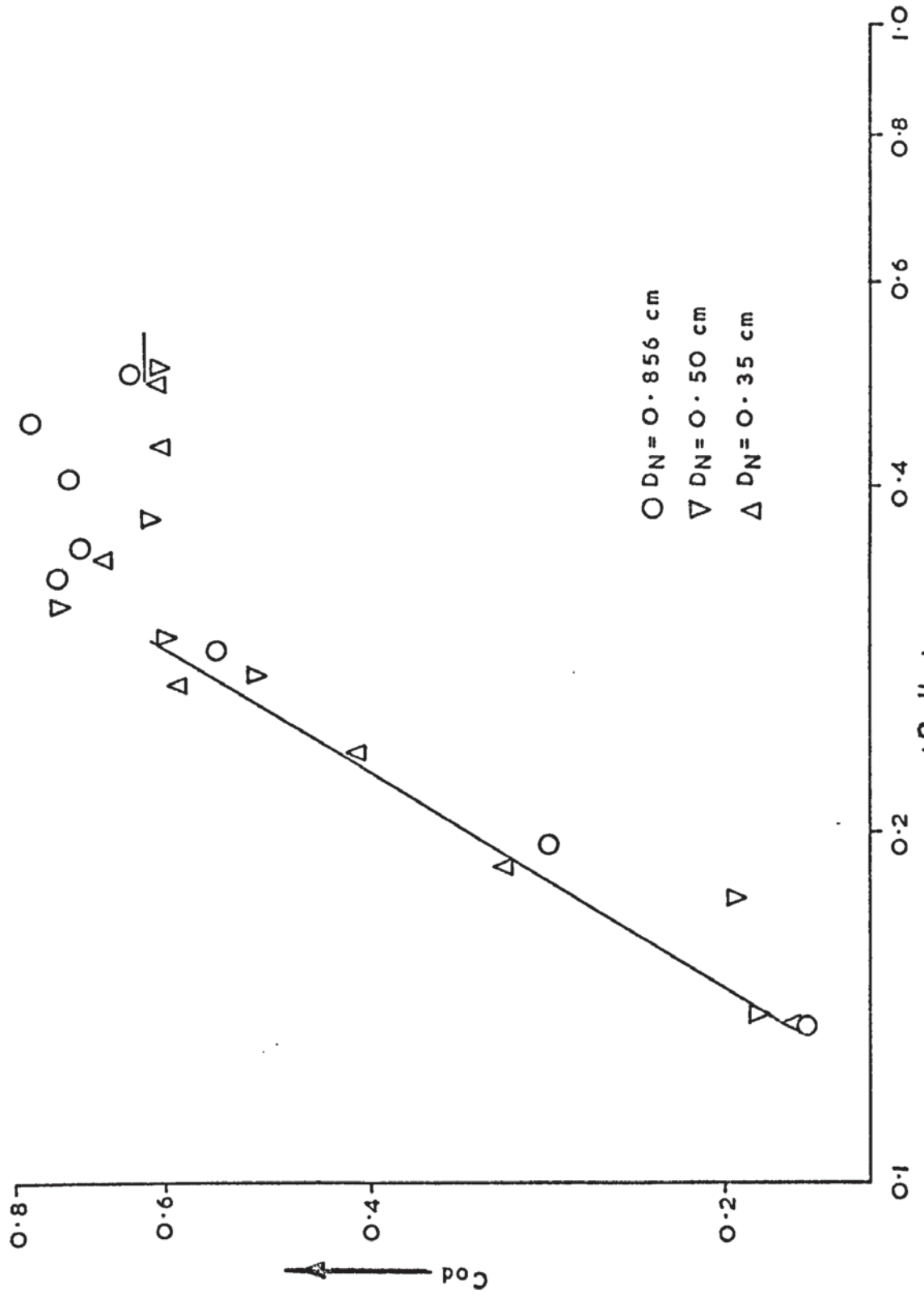

FIG. 9·15 RELATIONSHIP BETWEEN COEFFICIENT OF DISCHARGE C_{od} AND THE DIMENSIONLESS NUMBER $\left(\frac{\rho_d U_N}{\Delta \rho \omega R}\right)$ AT ω = 3460 R.P.M. AND KEROSENE / WATER SYSTEM

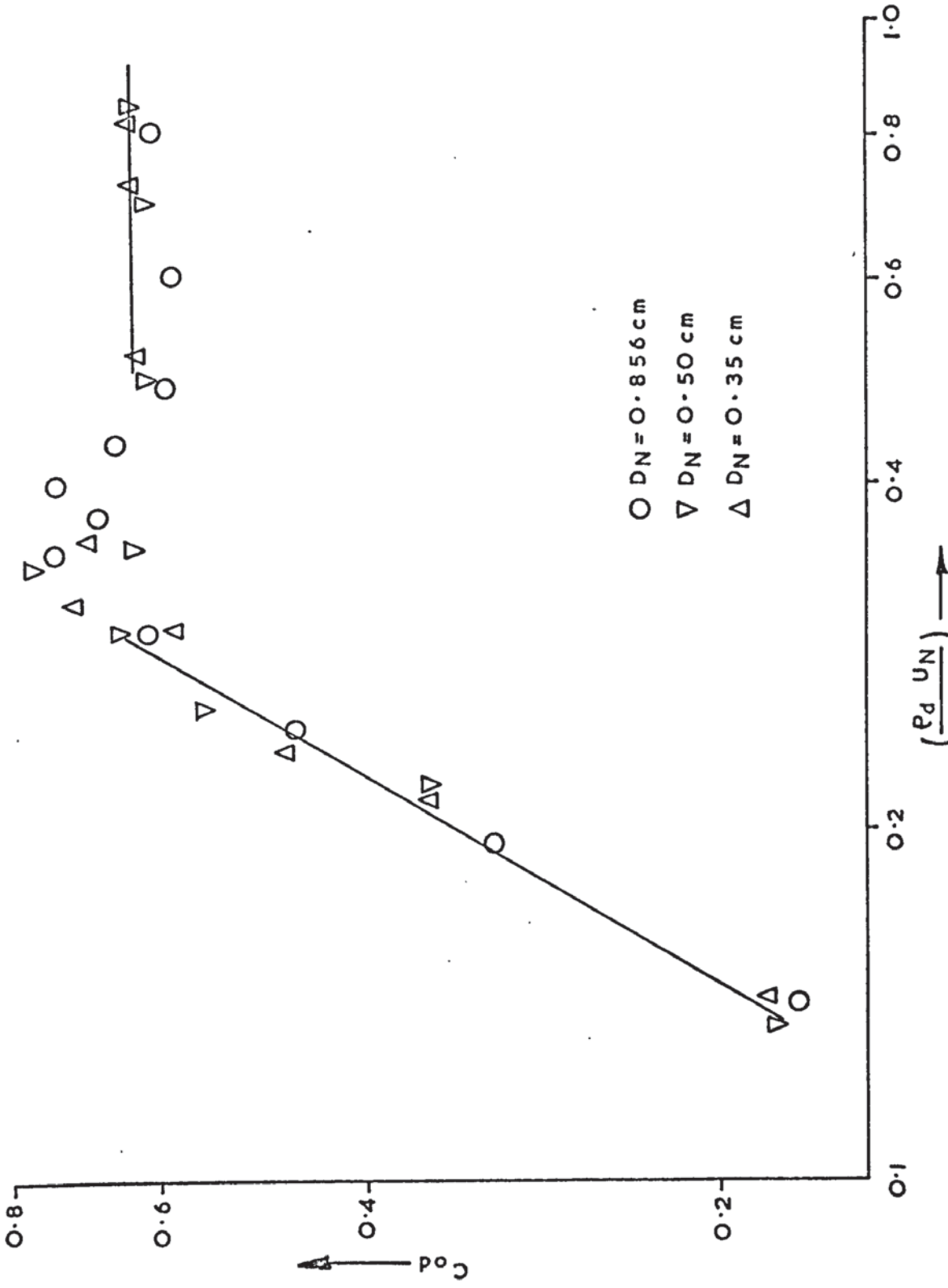

FIG.9-16 RELATIONSHIP BETWEEN COEFFICIENT OF DISCHARGE C_{od} AND THE DIMENSIONLESS NUMBER $\left(\frac{\rho_d U_N}{\Delta \rho \omega R}\right)$ AT ω = 3460 R.P.M. AND PARAFFIN / WATER SYSTEM

TEXT CUT OFF IN ORIGINAL

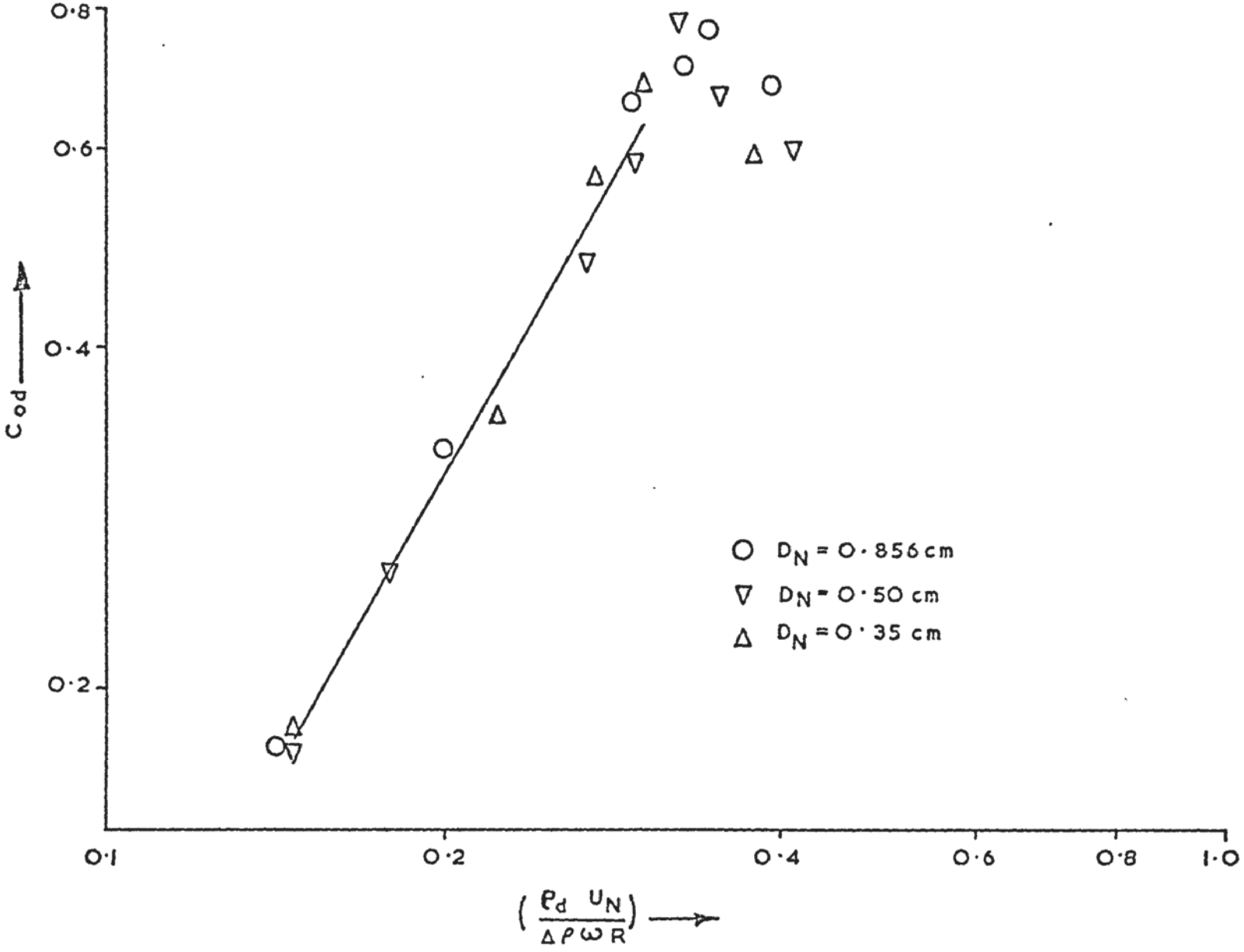

FIG. 9-17 RELATIONSHIP BETWEEN COEFFICIENT OF DISCHARGE C_{od} AND THE DIMENSIONLESS [illegible] AT $\omega = 4600$ R.P.M. AND KEROSENE / WATER SYSTEM

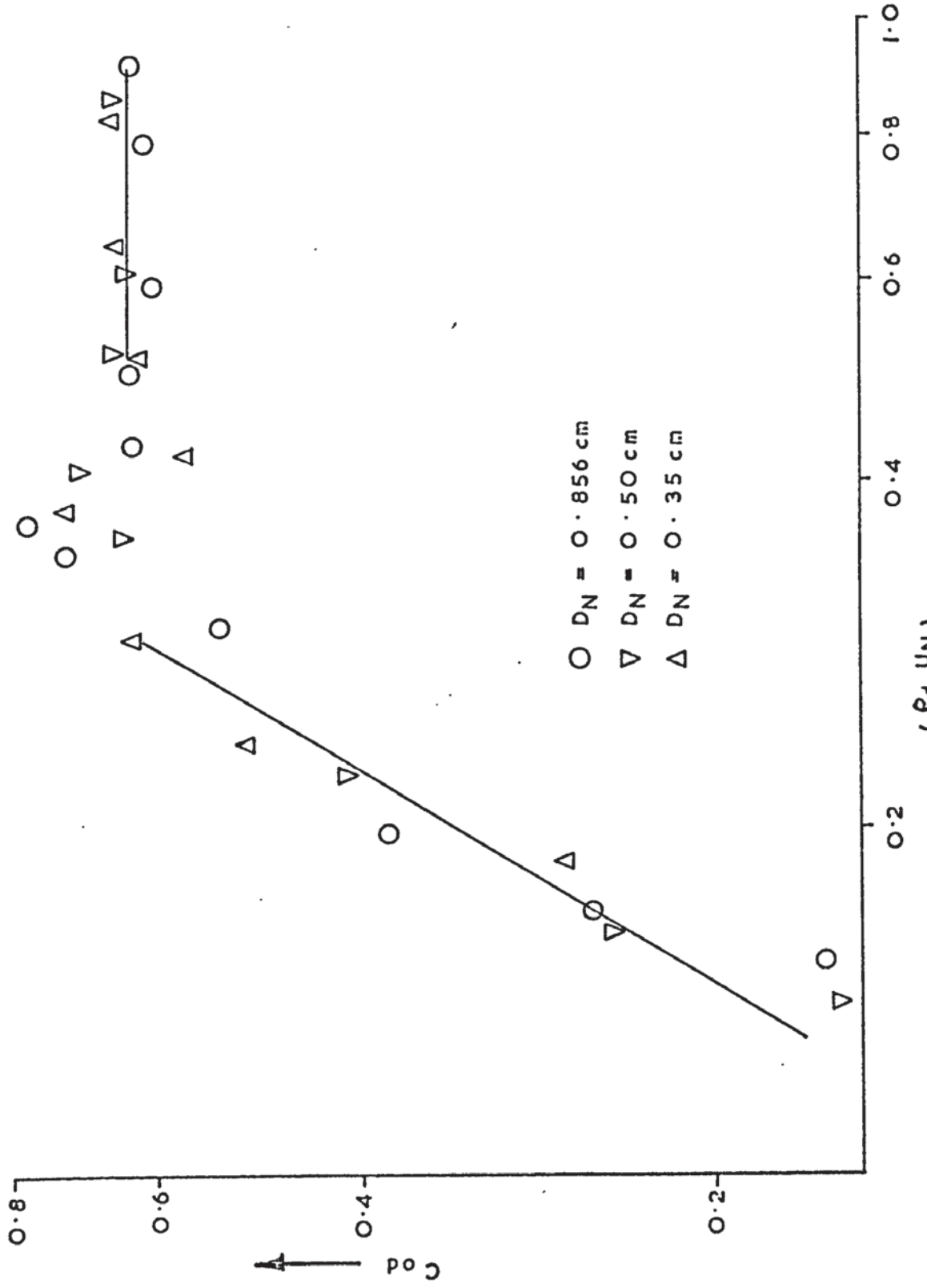

FIG. 9-18 RELATIONSHIP BETWEEN THE COEFFICIENT OF DISCHARGE C_{od} AND THE DIMENSIONLESS NUMBER $\left(\frac{\rho_d U_N}{\Delta \rho \omega R}\right)$ AT ω = 4600 R.P.M. AND PARAFFIN / WATER SYSTEM

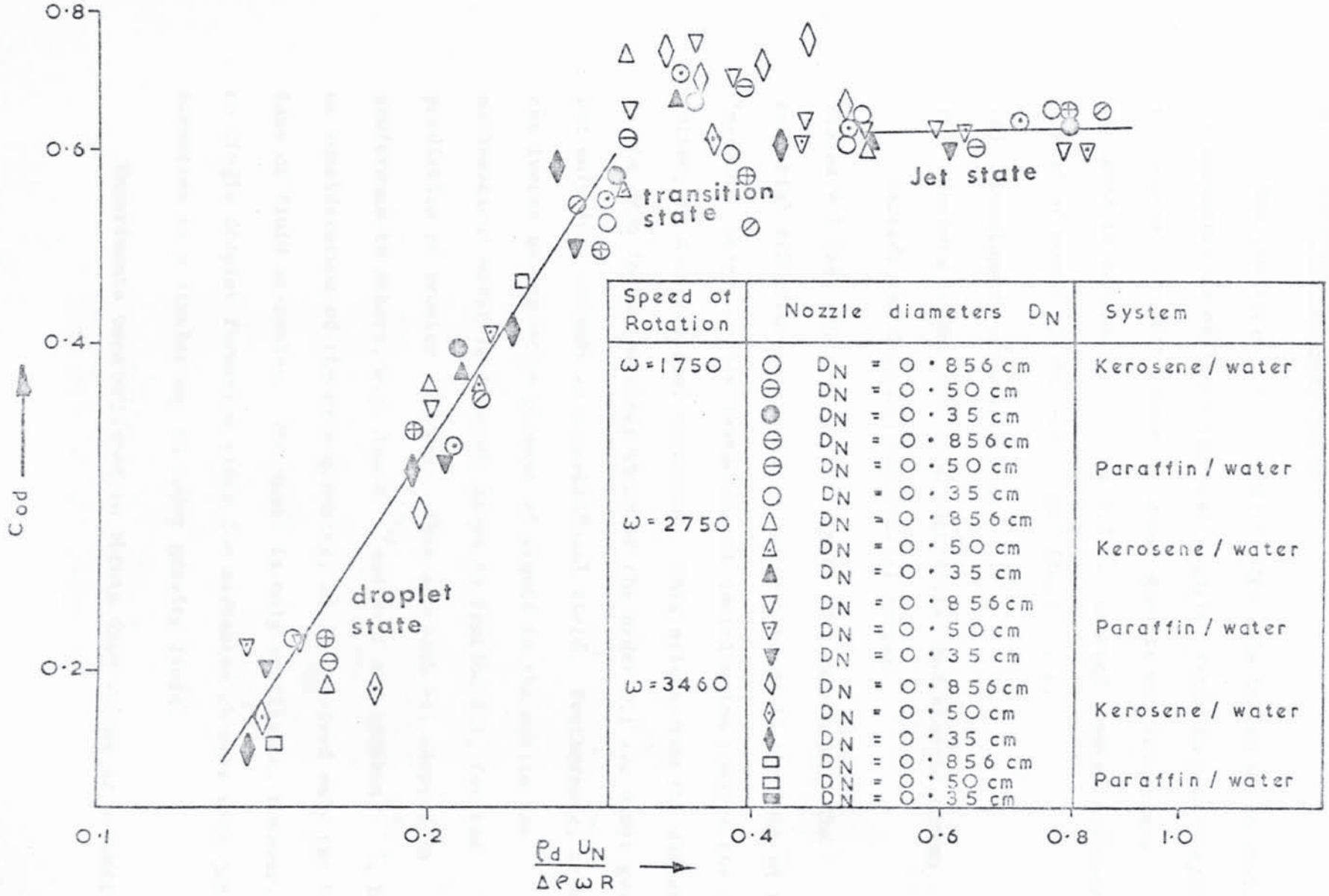

FIG 9-19 combination of FIGS 9-11 to 9-18

9.3 DROPLET FORMATION STUDIES

9.3.1 Experimental Observations

The prediction of size of the droplets formed at an orifice is necessary to evaluate the mass transfer rates in centrifugal contactors. Droplet formation under gravity conditions are reviewed in Sections 3.2.1 and 3.2.2. Initial studies indicated a similar mechanism in centrifugal fields, i.e.

(a) Development of static drop,

(b) Rupture of the drop when centrifugal and kinetic forces exceeds the drag and interfacial forces.

Plates 9.1 (a), (b) and (c) illustrate this mechanism. The essential difference between the two mechanisms is the lack of a 'necking' stage, or its insignificant contribution towards the drop volume, in a centrifugal contactor. This arises from the difference in the drop formation times which of the order 0.1 sec under gravity but only 10^{-4} seconds in a centrifugal field. Furthermore, from the forces acting on an element of liquid in the nozzle the mathematical model is derived, given in Section 8.1, for the prediction of droplet volumes. This approach was adopted in preference to others, e.g. Izard[71] and Null and Johnson[65], based on consideration of the drop geometry, as it involved only the basic laws of fluid mechanics. The model is only applicable, however, to single droplet formation since the mechanism changes with jet formation in a similar way to under gravity field.

Experiments were designed to obtain drop volume as a function

Plates 9.1

DROP FORMATION MECHANISM

Paraffin/Water System

ω = 1750

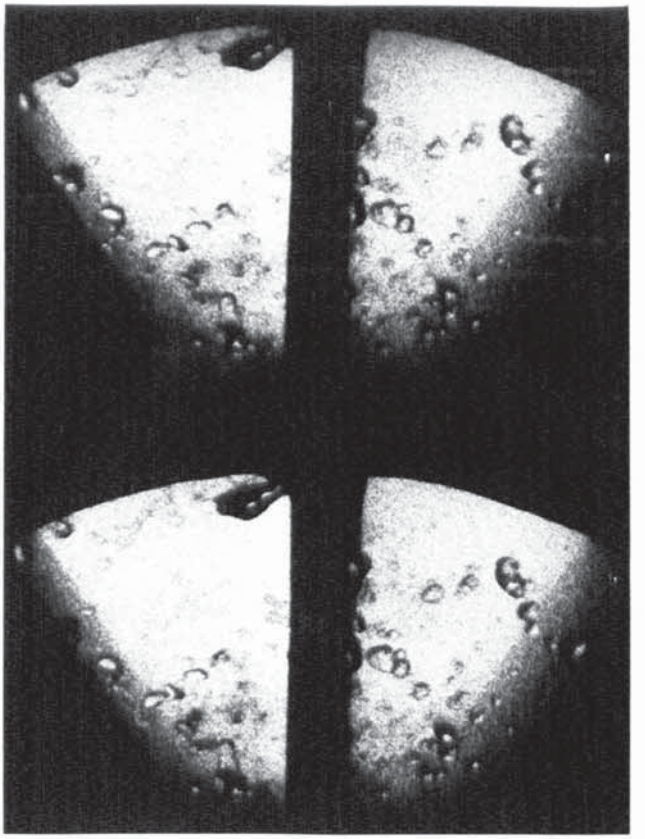

(a)

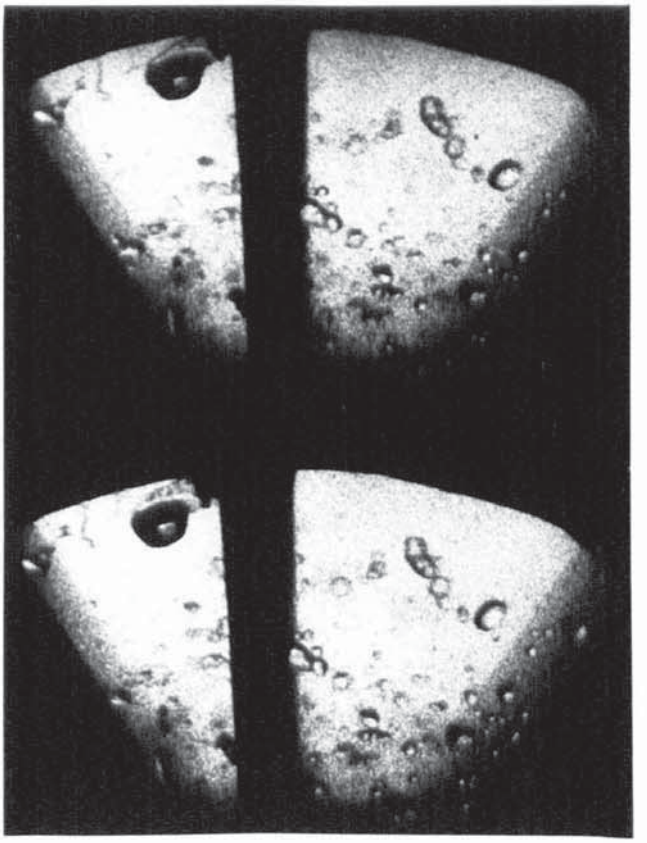

(b)

Plate 9.1

DROP FORMATION MECHANISM

Paraffin/Water System

ω = 1750

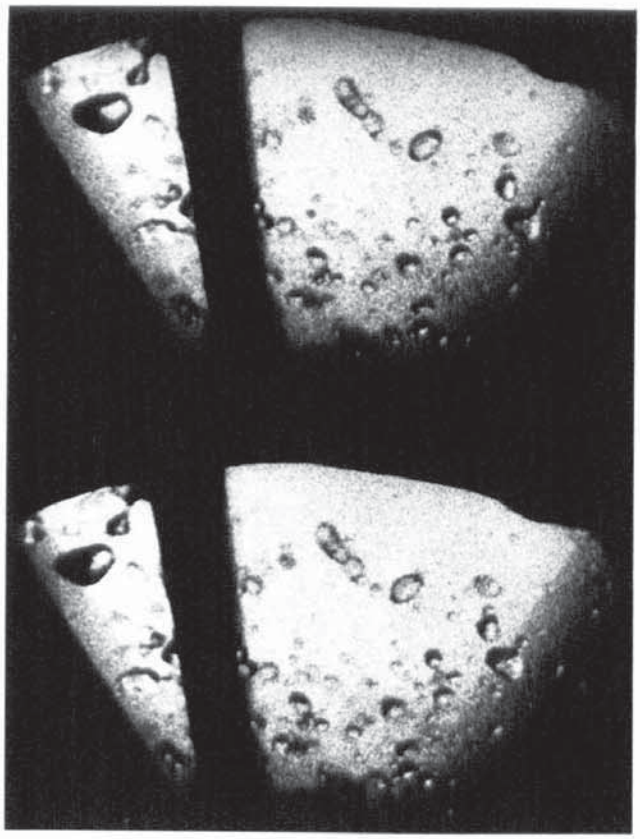

(c)

of nozzle diameter, velocity, and speed of rotation for systems with a wide range of physical properties. With all the systems the dispersed phase was of lower density than the continuous phase, which was distilled water. Drop diameters were measured from the cine film analyser projection on screen. If the drop was deformed from a spherical shape, the drop diameter was recorded as the arithmetic average of the major and minor diameters. Christiansen[82] has shown that this procedure causes less than 5% error in the calculation of drop volume if the ratio of major to minor axis is less than 1.7. In this study the drop diameter ratio was less than 1.5 for most of the drops.

In this study droplet sixe was measured by the following procedure. For a given system each film represented one nozzle diameter D_N and various speeds of rotation. The film was projected onto a paper screen and the droplet traced on the screen so that its two axes could be measured. The exact number of droplets measured for each nozzle velocity U_N depended on the quality of the films. Thus, on the films taken with the Hyperspeed camera enabled as many as 30 to 40 droplets to be measured. Standard deviations for each sample of droplets are calculated and showed that increasing the sample size did not produce a proportional decrease in the standard deviation. The average standard deviations for each of the samples were of the order 20%. The points on Figures 9.20 to 9.40 are therefore drawn to reflect the deviation from the mean droplet size. The droplet size data in Tables D.5 to D.8, and the droplet tracings on paper and the films are deposited with the Department library.

Drops recorded on film showed a considerable degree of variation

in shape and hydrodynamics. For example,

(a) Rigid drops were principally formed at high speeds of rotation, ω = 3460, 4600 r.p.m., and the lower nozzle diameter.

(b) Oscillating droplets were also observed. These were often produced at low values of ω, e.g. 1750 r.p.m. and at D_N = 0.856 cm.

The latter observation was unexpected since the centripetal force near the periphery of the rotor exceeded 1500 G's at all times and a maximum of 5000 G's was achieved.

9.3.2 Evaluation of Constants K_D, K_f of the Model

The model derived in Section 8.1 was used to calculate drop volumes for all the systems listed in Appendix A. Systems were selected to cover a wide range of viscosity values as shown in Table 9.4.

TABLE 9.4

DISPERSED PHASE	VISCOSITY μ_d cp	INTERFACIAL TENSION N/m
Kerosene	1.557	0.0140
EM35C OIL	8.613	0.0045
CS40 OIL	12.012	0.0011
Paraffin	34.387	0.0385

The model droplet volume is given by,

$$V_F = F \quad \frac{\pi\sigma D_N}{g\Delta\rho} + \frac{K_D \mu_d Q D_N}{D_F^2 g\Delta\rho} - \frac{\omega^2 R}{g} - \frac{K_f \mu_d Q U_N}{\Delta\rho g} \qquad (8.17)$$

The value of the two constants included to compensate for assumptions in its derivation need to be determined experimentally. The reason for including empirical constants in an otherwise theoretical analysis are:-

(a) The constant K_D is used in the drag term in place of the value, 6.0, given in equation 8.9, to allow for assumptions made in the derivation, for example that the continuous phase velocity relative to the droplet is negligible. This is, however, not true in practical conditions[72], and

(b) The constant K_f used in the kinetic force term instead of the value 4/3 obtained by theoretical analysis, is again to compensate for certain assumptions in deriving equation 8.14. The assumption that the velocity profile within the nozzle is parabolic, is valid only when the straight section of the nozzle is greater than 100 pipe diameters[72]. This was not the case in this study.

The drag and kinetic terms constant K_D, K_f were evaluated in the following manner:- Equation 8.15 gives the volume of the static drop, i.e.

$$V_F = F\left(\frac{K_D \mu_d Q D_N}{D_F^2 g \Delta\rho} + \frac{\pi\sigma D_N}{\Delta\rho g} - \frac{\omega^2 R}{g} - \frac{K_f \rho_d Q U_N}{g \Delta\rho}\right) \qquad (8.15)$$

In a contactor operating at zero speed, i.e. at $\omega = 0$, the centrifugal force term becomes zero. Furthermore, by using Kerosene as the dispersed phase and operating at small flow rates and nozzle velocities the kinetic term could be neglected compared to the drag term. For example at $Q = 0.005$L/S $U_N = 0.0868$ m/s the kinetic

force term is 0.1287, whereas the drag term is 5.131, i.e. it is almost 40 times greater. Kerosene was chosen because due to its low viscosity, the drag force is much smaller than for paraffin or the oils under the same conditions.

When the terms $(\frac{\omega^2 R}{g})$ and $(\frac{K_f \rho_d Q U_N}{g \Delta\rho})$ become zero and negligible respectively, equation (8.15) yields a value of the constant K_D since,

$$V_F = F(\frac{\pi\sigma D_N}{\Delta\rho g} + \frac{K_D \mu_d Q D_N}{D_F^2 \Delta\rho g})$$

where V_F is known experimentally and the other terms can be calculated from values of D_N, Q, $\Delta\rho$, g and σ. The data is, therefore, presented in terms of D_N, U_N, ω and μ.

Although the constant were obtained from data when the dispersed phase density was less than the continuous phase density, the analysis should be valid in the reverse situation provided injection is in the same plane. The only difference between the two situations is the direction of pressure gradient in the continuous phase relative to the direction of dispersed phase injection.

Before the model could be used, the Harkins-Brown factor F had to be determined. This was computed for each droplet from a plot of F Vs $D_N(F/V_F)^{\frac{1}{2}}$ given by Scheele-Meister[72].

9.3.3 Comparison of Model and Experimental Results

Equation (8.17) was used to calculate drop volumes for comparison with experimental results. Data is presented in terms of parameters that affect droplet size, i.e.

$$V_F = f\ (D_N,\ U_N,\ \omega,\ \mu_d,\ \rho_d,\ \sigma,\ R) \qquad (9.8)$$

The flowrate Q is not included since the nozzle velocity U_N is dependent upon it. The inclusion of the radius of nozzle from the centre of rotor, R, is quite significant, since the centrifugal force $(\frac{\omega^2 R}{g})$ depends upon this radius. Thus a R decreases, as in commercial centrifugal extractors, the force decreases thereby increasing the droplet volume. The most important physical property is the viscosity of the dispersed phase μ_d and is included. The data is, therefore, presented in terms of D_N, U_N, ω and μ_d. Drop volume data are shown in Figures 9.20 to 9.33. These illustrate the variation of drop volume with the nozzle velocity, U_N, for three nozzle diameters, D_N, at given speed of rotation ω. Both the experimental and the model curves are as expected from the equation 8.17, since the latter contains the term,

$$(\frac{3.1\rho_d}{\Delta\rho g}(QU_N)\ )$$

which predicts a relationship of the type $V_F \alpha U_N^2$. Furthermore, there is some similarity with the Izard model for droplet formation under gravity conditions, as shown in Figs. 3.2, 3.3. This is despite the Izard model being derived from analysis of droplet geometry instead of a force balance.

The deviation from the experimental results is relatively small, a maximum of 15%, in the linear region of the curves. However, the deviation increases rapidly in the remaining portion of the curve up to a maximum of 66% at high nozzle velocity U_N.

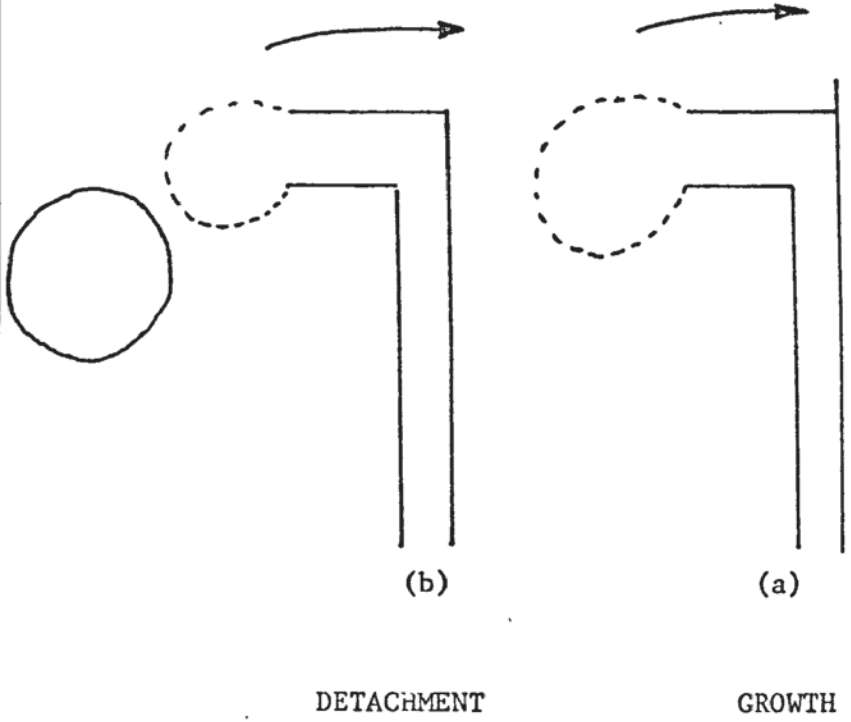

SINGLE DROPLET FORMATION STAGES AT NOZZLE

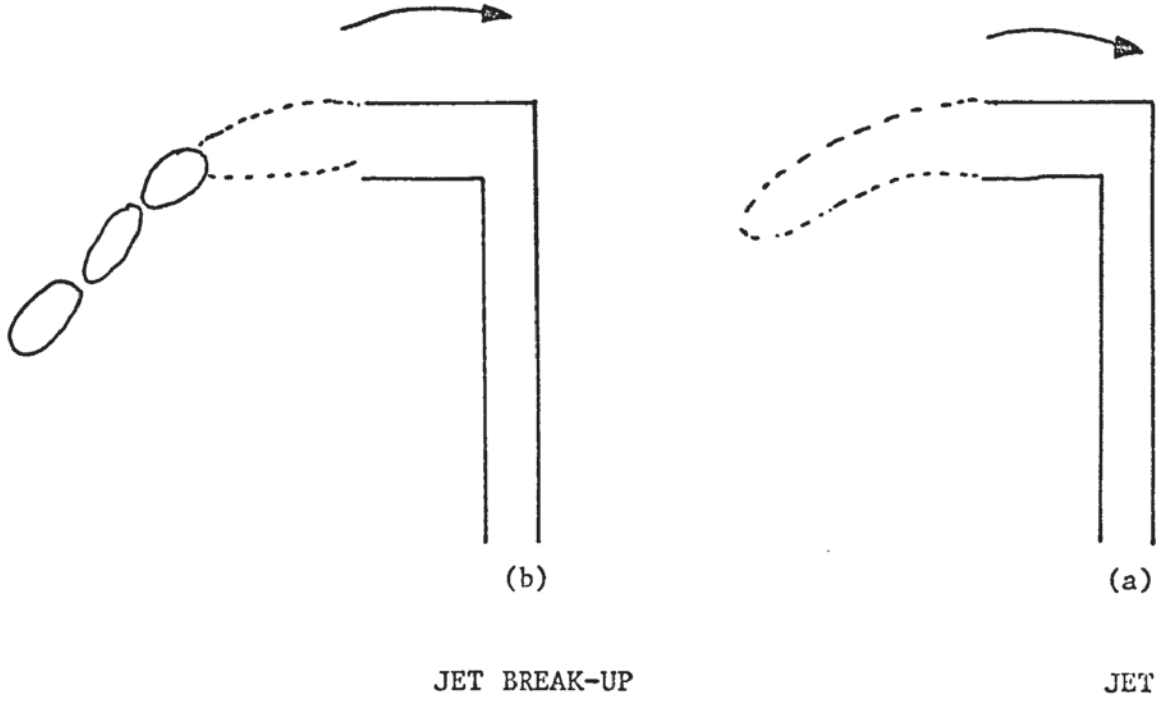

STAGES OF JET FORMATION FROM NOZZLES

PLATE 9.1a MECHANISMS OF DROPLET FORMATIONS IN THE CENTRIFUGAL CONTACTOR

The deviation from the experimental curves also,

(a) increases with decreasing nozzle diameters, D_N;

(b) increases with increasing speed of rotation ω; and

(c) increases with systems of higher viscosity, μ_d.

The model becomes less accurate with these because it was derived assuming single droplet formation. As is evident from Section 9.2, jetting occurred in the contactor. In Fig. 9.20, jetting velocities calculated from Fig.9.19 are plotted to illustrate the droplet and transition states. In the drop state the deviation between the model and experimental data is of the order $\pm$ 8% but in the transition and jet states of dispersed phase flow, the deviation increases considerably. The model, therefore, is accurate for the droplet state for which it was derived.

The deviation is presumed to increase with increasing ω, partly because of the influence of Corolois force which was neglected in the model, and which probably assumes greater influence at high ω. However, the deviation is also due to experimental error arising from the difficulty in measuring small droplets which may be conglomerates of two or more smaller droplets.

However, neither jetting nor the influence of Corolois force can explain the increase in deviation for systems of higher values of viscosity, μ_d. It may be that the constant, $K_2 = 3.1$, which was evaluated by operating contactor at $\omega = 0$ for a low viscosity system varies in value. It was assumed that the kinetic term becomes insignificant, but it may be that at high speed of rotation,

the kinetic force becomes more significant.

The variation of droplet volume with nozzle velocity at constant nozzle diameter D_N = 0.856 cm, and varying rotor speeds ω are illustrated in Figs. 9.34 to 9.37. These are only drawn for Kerosene/water and Paraffin/water, since the other two systems, i.e. EM 356C oil and CS40 oil have viscosities between 1.557 and 34.3875 cp. Figs. 9.34 and 9.35 show the values predicted from the mathematical model, and Figs. 9.36 and 9.37, the experimental values.

The curves show that:

(i) With increasing rotor speed there was decrease in the droplet volume for the systems studied.

(ii) The rate of decrease of the droplet volume with ω is of the same order in each case.

However, this method of presentation does not show the significance of viscosity. This is shown by Fig. 9.38 which is plotted with V_F V_s, the viscosity of the dispersed phases at constant nozzle diameter of 0.856 cm, and nozzle velocity of .49 m/s. It is apparent that with decreasing μ_d, the rate of decrease in droplet volume is linear with constant slope.

To confirm (ii) above, Figs. 9.39 to 9.42 have the speed of rotation ω as the ordinate at constant nozzle velocity U_N = 0.49 m/s and diameter D_N = 0.00856 m. The mathematical model shows close agreement initially but the deviation becomes significant at higher values of ω. Since the nozzle velocity is in the region of the

Transition regime 0.40 to 0.66 m/s, as shown in Fig. 9.33, some deviation would be expected. However, the graphs show 'tailing off' and further increase in ω does not produce a proportionate decrease in drop volume. This would be expected, since it is not possible to obtain droplets of zero volume, no matter how much the rotor speed is increased. This observation is important in the design of centrifugal contactors since it defines the limit of ω beyond which it is not desirable to operate any contactor. For the contactor in this study, this limit was 5000 r.p.m. It also defines a minimum droplet size for each chemical system. This size for the systems studies vary from 0.2 c.c. for Kerosene to 1.2 c.c. for paraffin. It is presumed that the minimum droplet size depends upon the viscosity of the dispersed phase.

9.3.4 Significance to Centrifugal Contactor Operations

For centrifugal contactors the mass transfer rates can be defined in the same way as for gravity equipment, i.e.

$$N = K.A\Delta C \qquad (5.1)$$

and

$$\frac{1}{K} = \frac{1}{K_{d.}} + \frac{1}{mK_c} \qquad (5.2)$$

The interfacial area and therefore, the drop size, is one of the controlling factors which determine the overall mass transfer rate. As explained in Chapter 5, mass transfer can also be evaluated from individual droplet mass transfer analysis.

Mass transfer occurs in four stages of the droplets life, listed in Section 5.1, i.e.

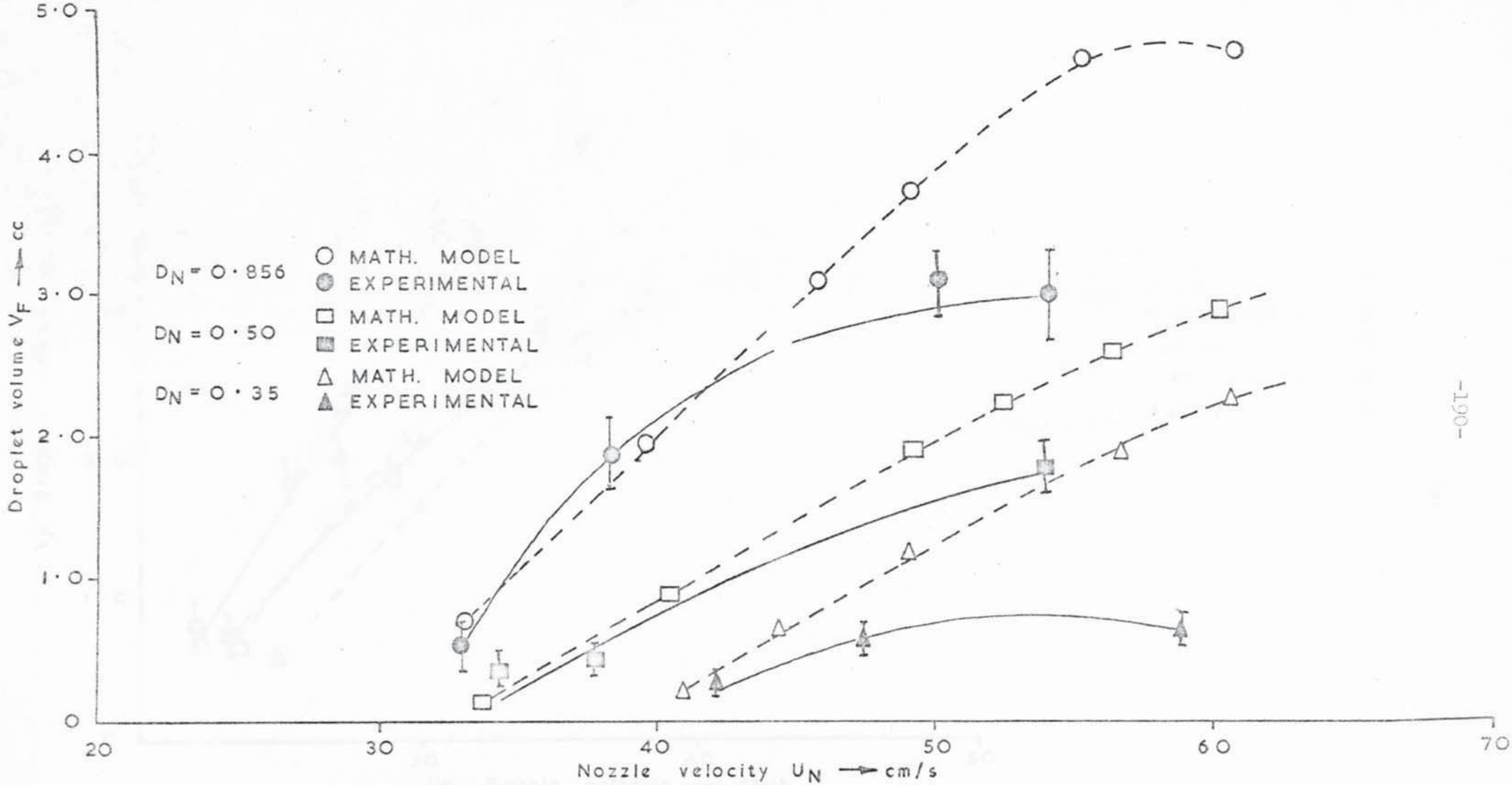

FIG.9·20 DROPLET VOLUME – NOZZLE VELOCITY DEPENDANCE IN THE CENTRIFUGAL CONTACTOR KEROSENE / WATER SYSTEM ω = 1750 R.P.M.

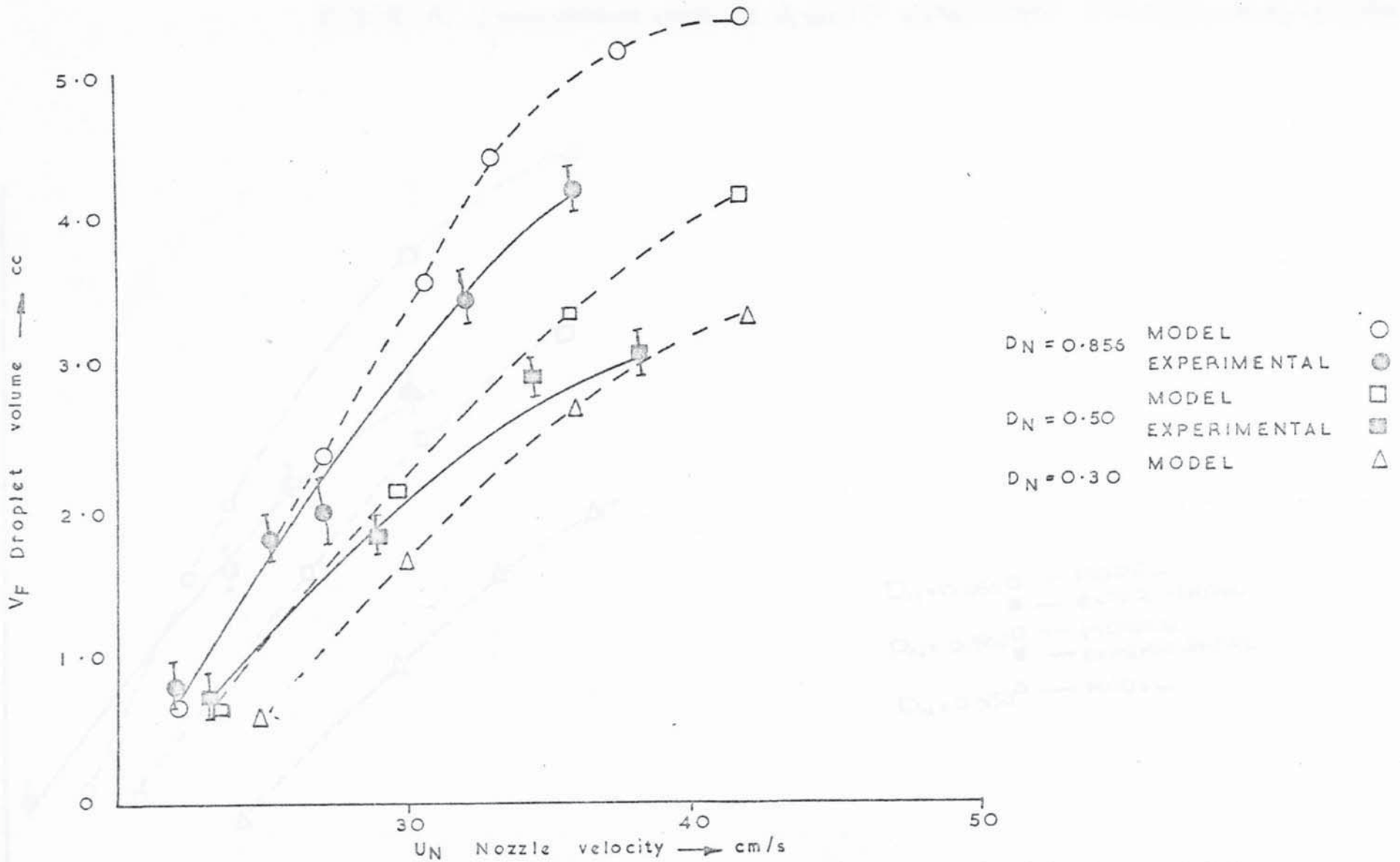

FIG. 9. 21 DROP VOLUME NOZZLE VELOCITY DEPENDANCE EM 35C OIL SYSTEM
ω = 1750 R.P.M.

FIG. 9.22. DROP VOLUME - NOZZLE VELOCITY DEPENDANCE . C·40·OIL/WATER. ω = 1750 R.P.M.

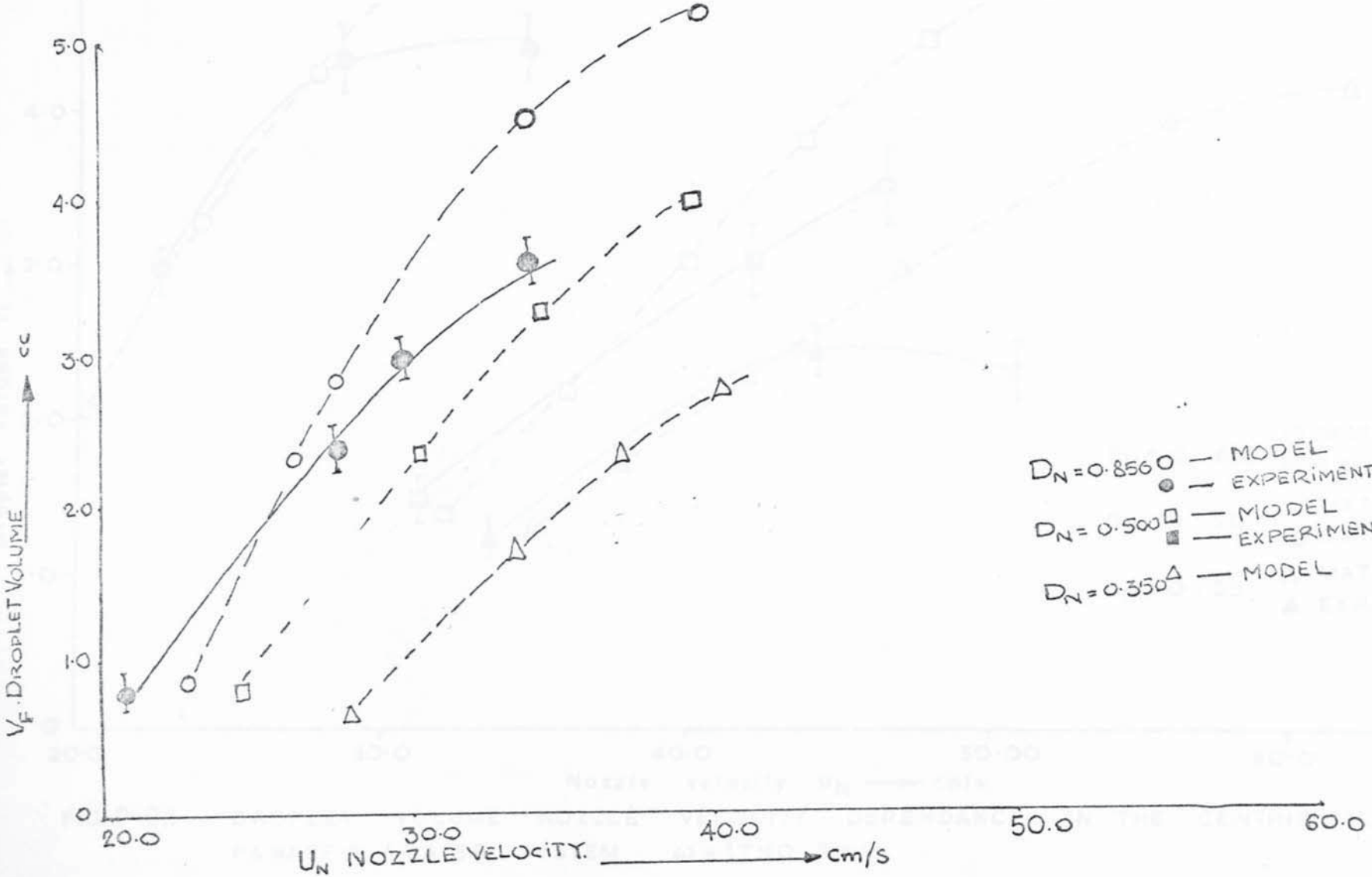

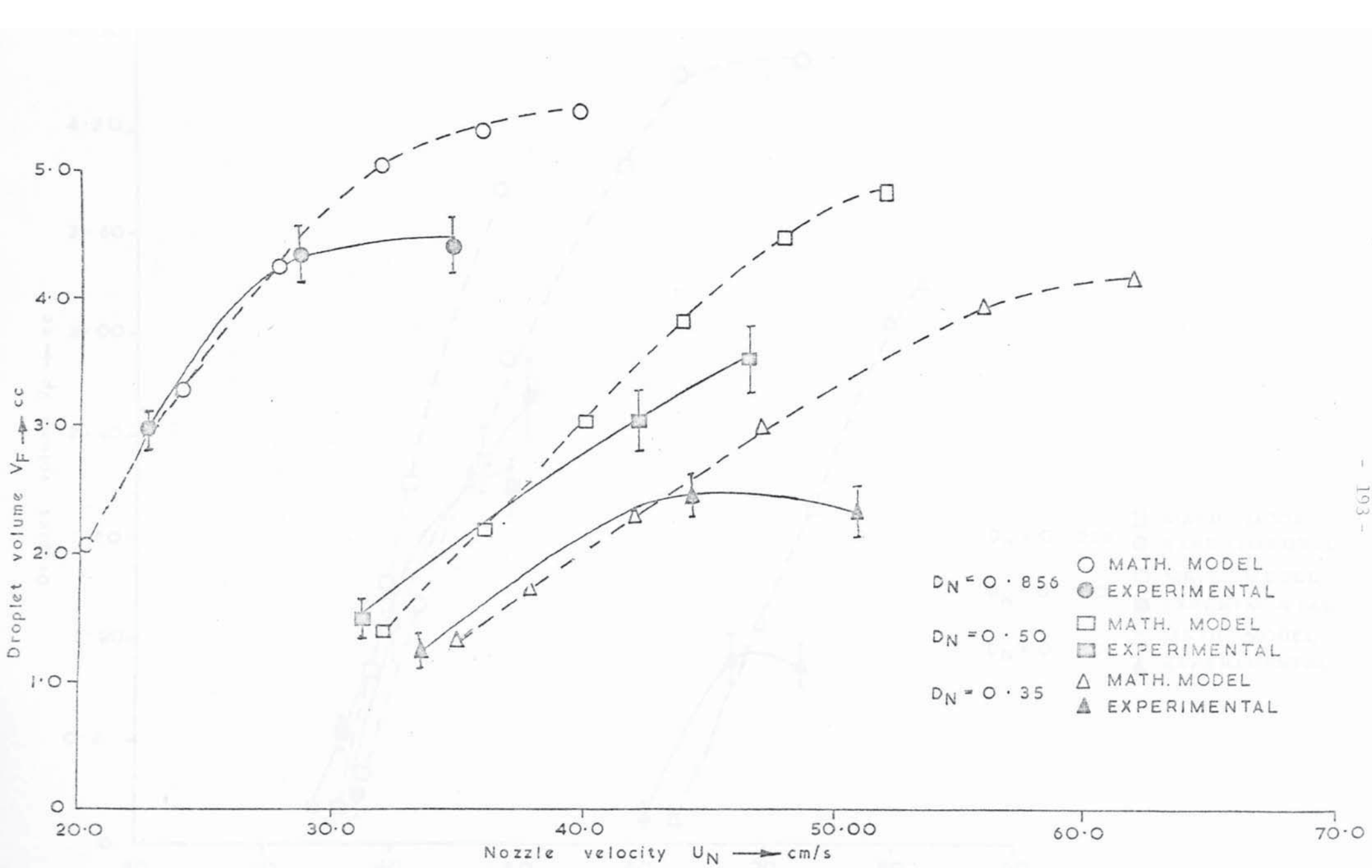

FIG.9-23 DROPLET VOLUME – NOZZLE VELOCITY DEPENDANCE IN THE CENTRIFUGAL CONTACTOR PARAFFIN / WATER SYSTEM ω = 1750 R.P.M.

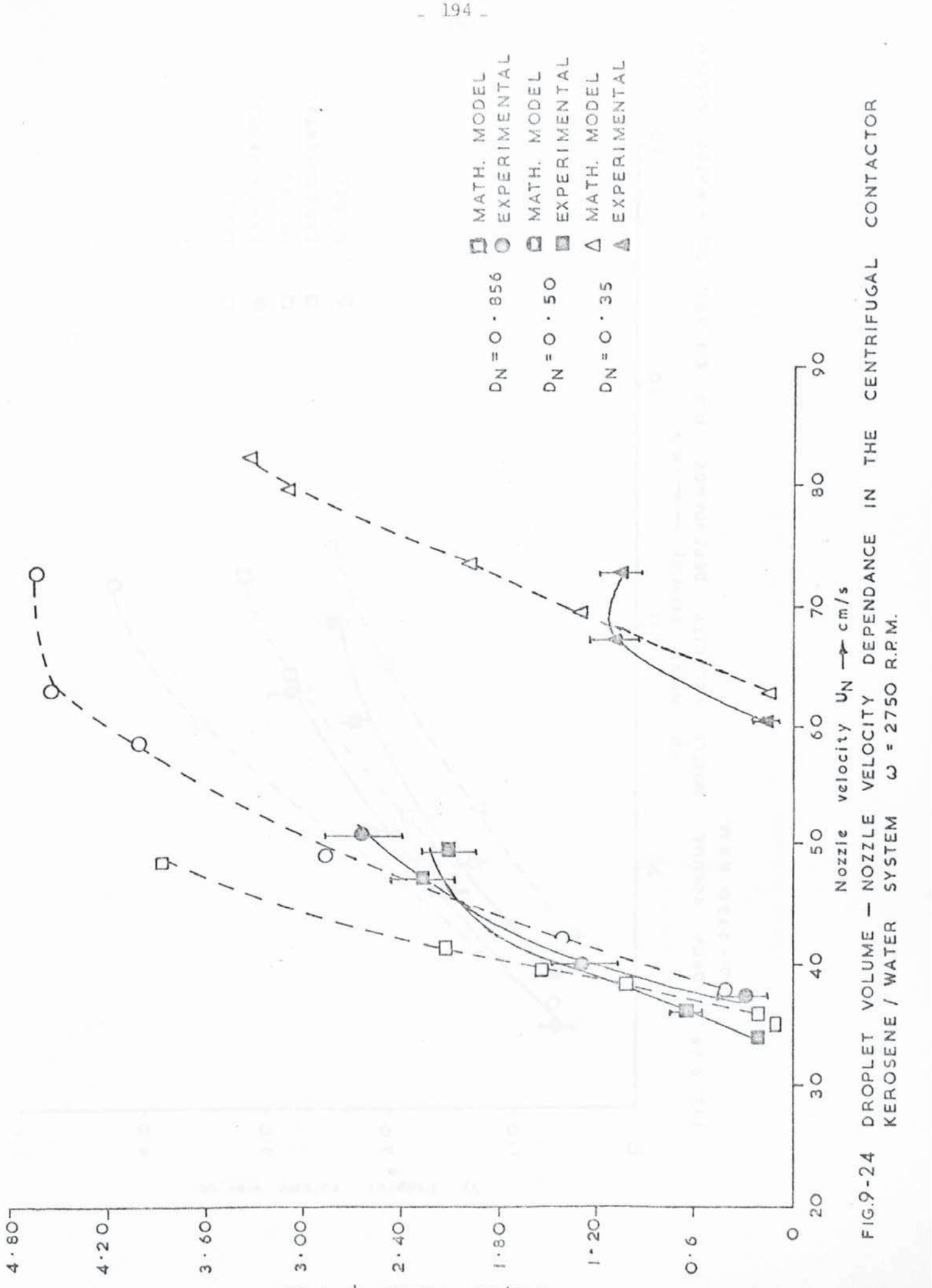

FIG.9-24 DROPLET VOLUME — NOZZLE VELOCITY DEPENDANCE IN THE CENTRIFUGAL CONTACTOR
KEROSENE / WATER SYSTEM ω = 2750 R.P.M.

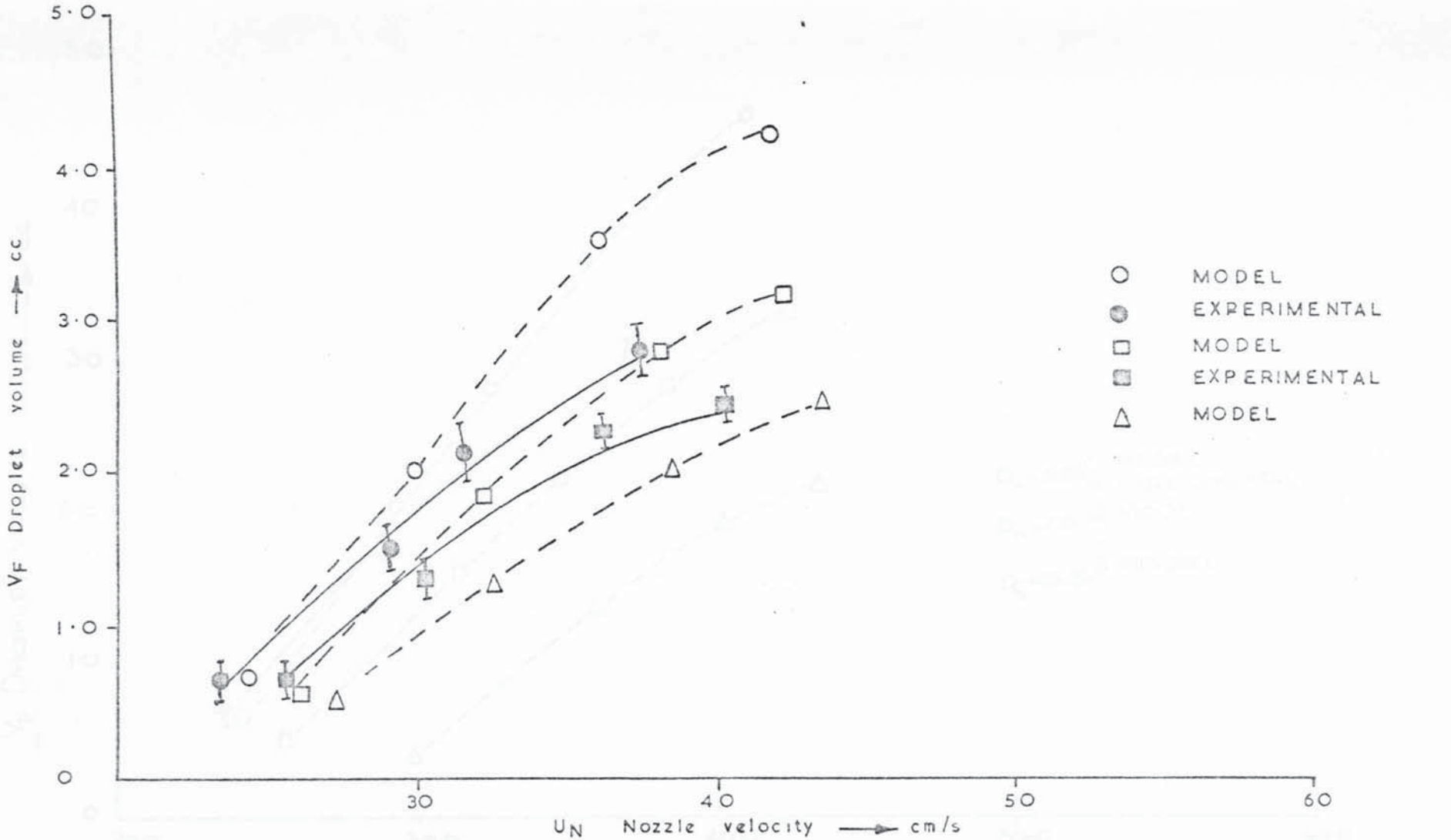

FIG. 9.25 DROP VOLUME NOZZLE VELOCITY DEPENDANCE FOR EM·35C OIL — WATER SYSTEM
ω = 2750 R.P.M.

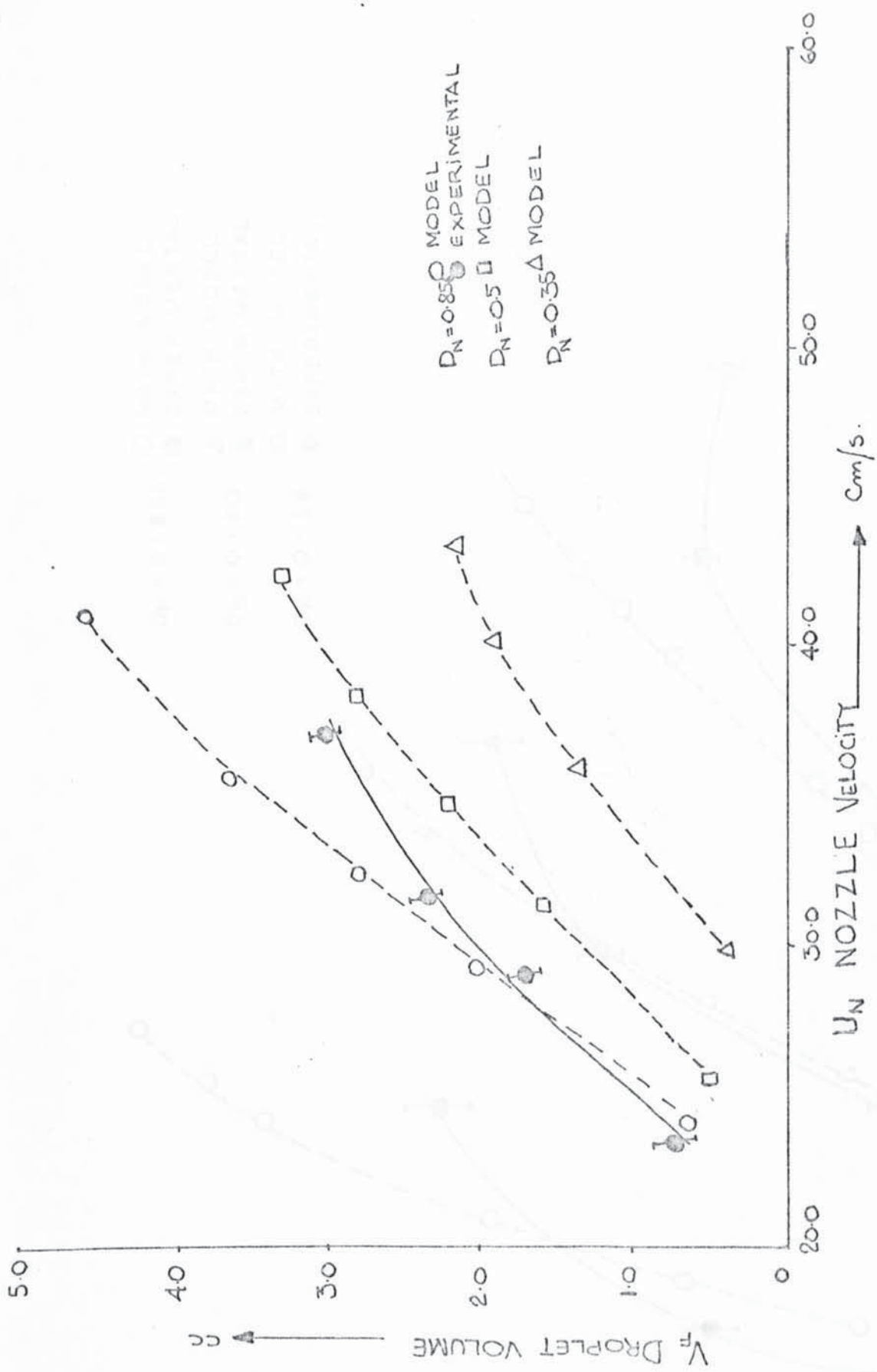

Fig. 9.26. Drop Volume Nozzle Velocity Dependance. C.40.Oil. ω=4750 R.P.M.

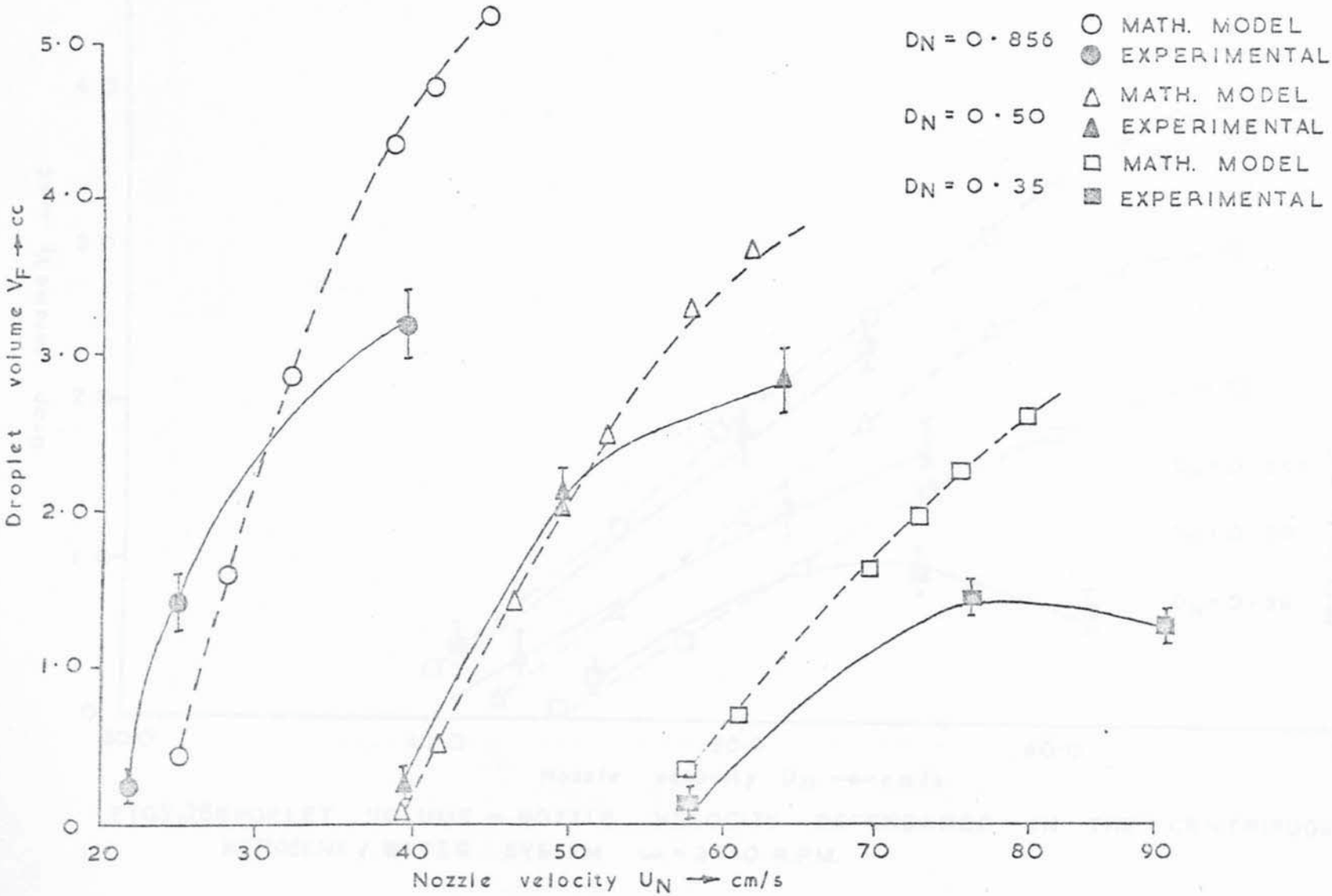

FIG.9-27 DROPLET VOLUME – NOZZLE VELOCITY DEPENDANCE IN THE CENTRIFUGAL CONTACTOR · PARAFFIN / WATER SYSTEM, ω=2750 R.P.M

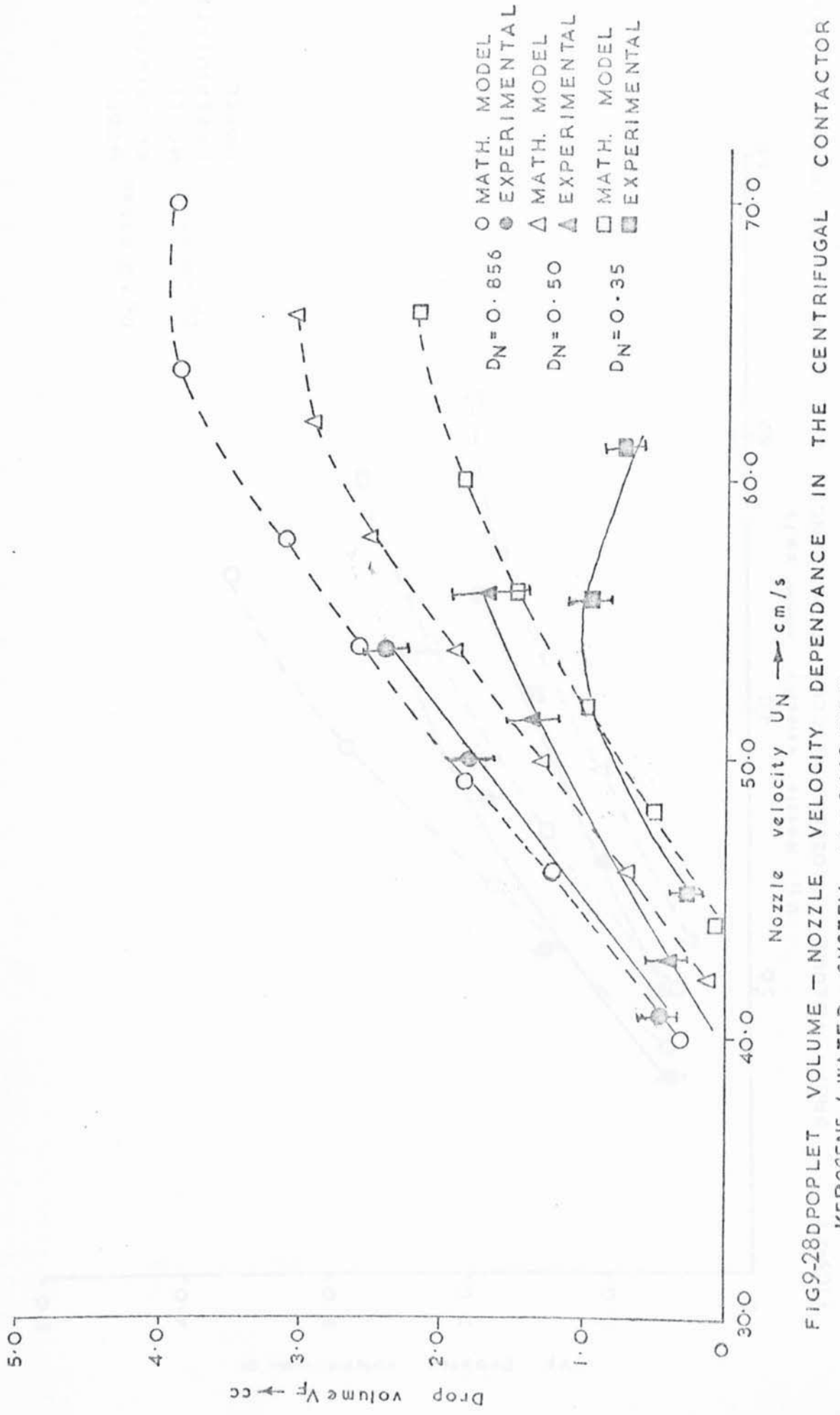

FIG9-28DROPLET VOLUME – NOZZLE VELOCITY DEPENDANCE IN THE CENTRIFUGAL CONTACTOR
KEROSENE / WATER SYSTEM ω = 3460 R.P.M.

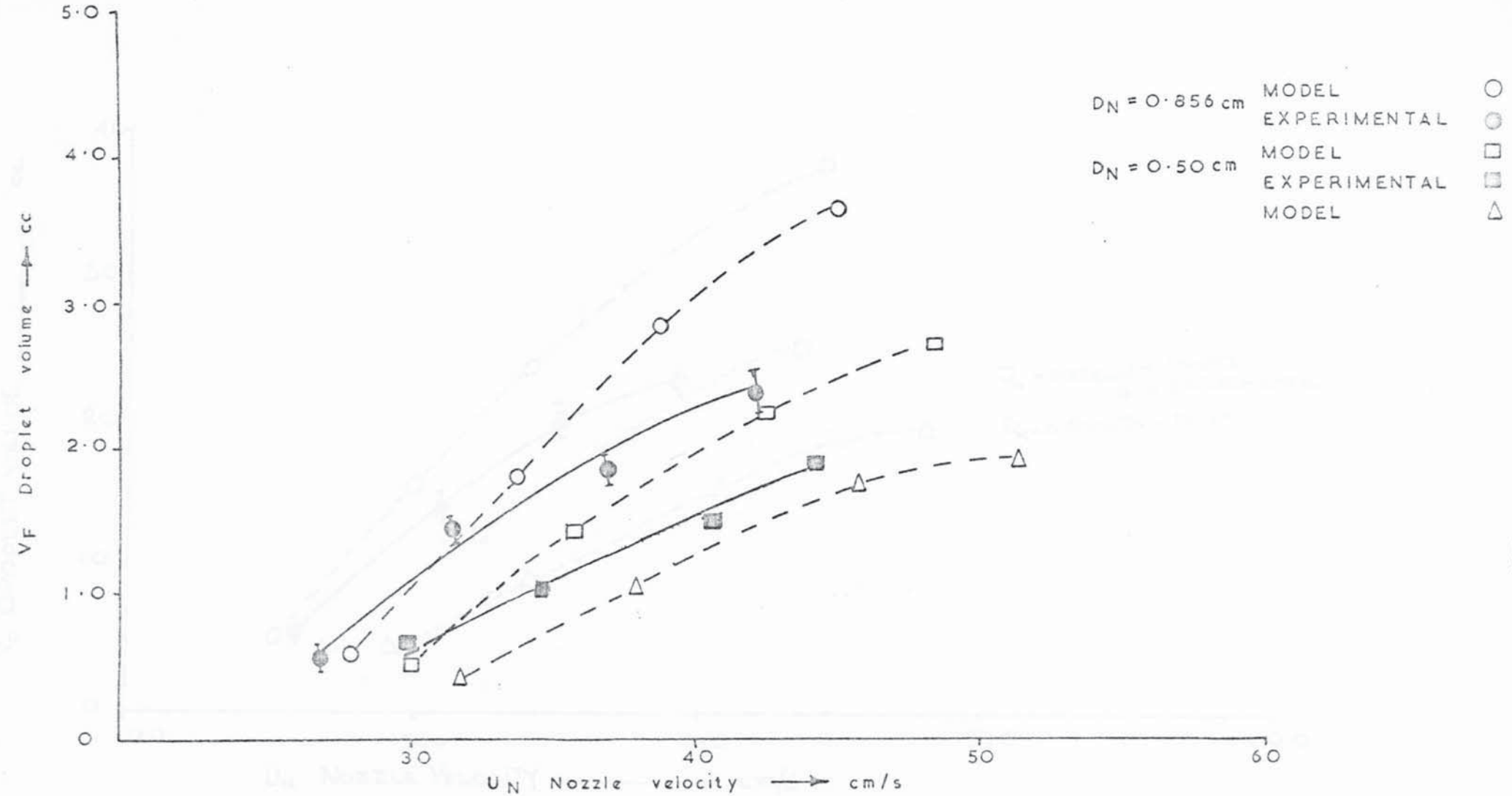

FIG9-29 DROP VOLUME NOZZLE VELOCITY DEPENDANCE FOR EM 35 C OIL – WATER SYSTEM.
ω = 3460 R.P.M.

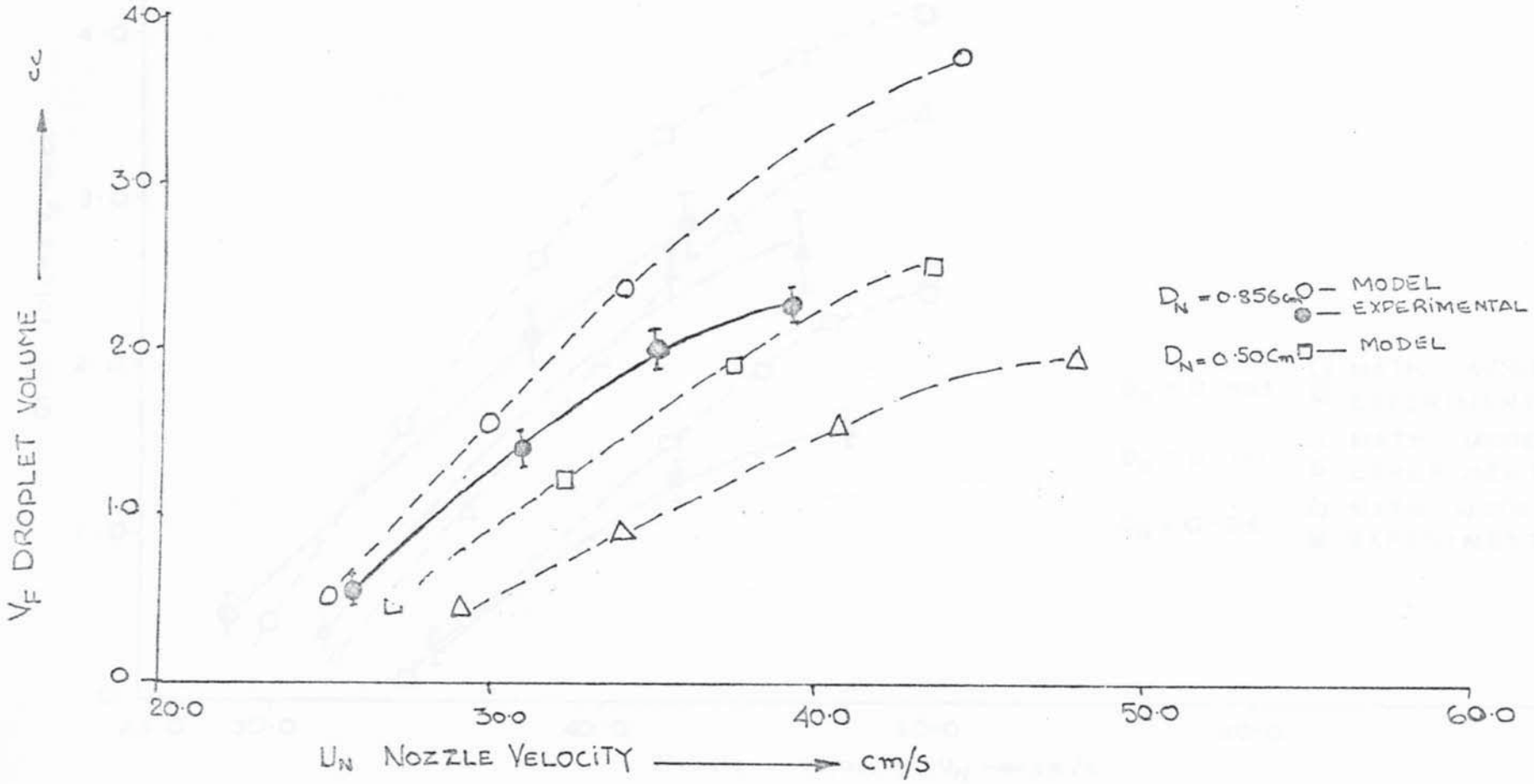

FIG. 9.30. NOZZLE VELOCITY - DROP VOLUME DEPENDANCE. C.40.OIL SYSTEM. ω = 3460 R.P.M.

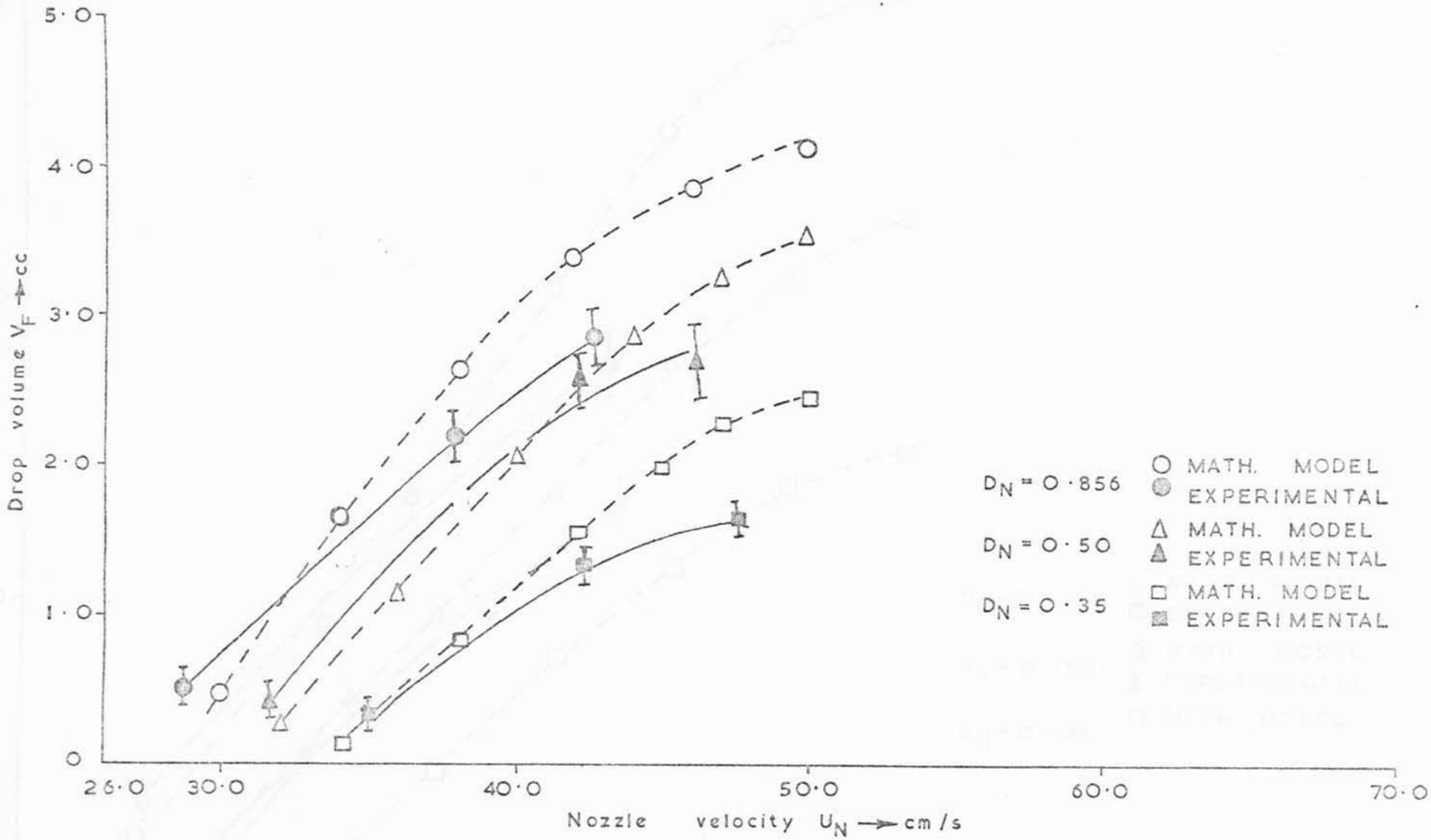

FIG. 9-31 DROPLET VOLUME — NOZZLE VELOCITY DEPENDANCE IN THE CENTRIFUGAL CONTACTOR. PARAFFIN / WATER SYSTEM ω = 3460 r.p.m

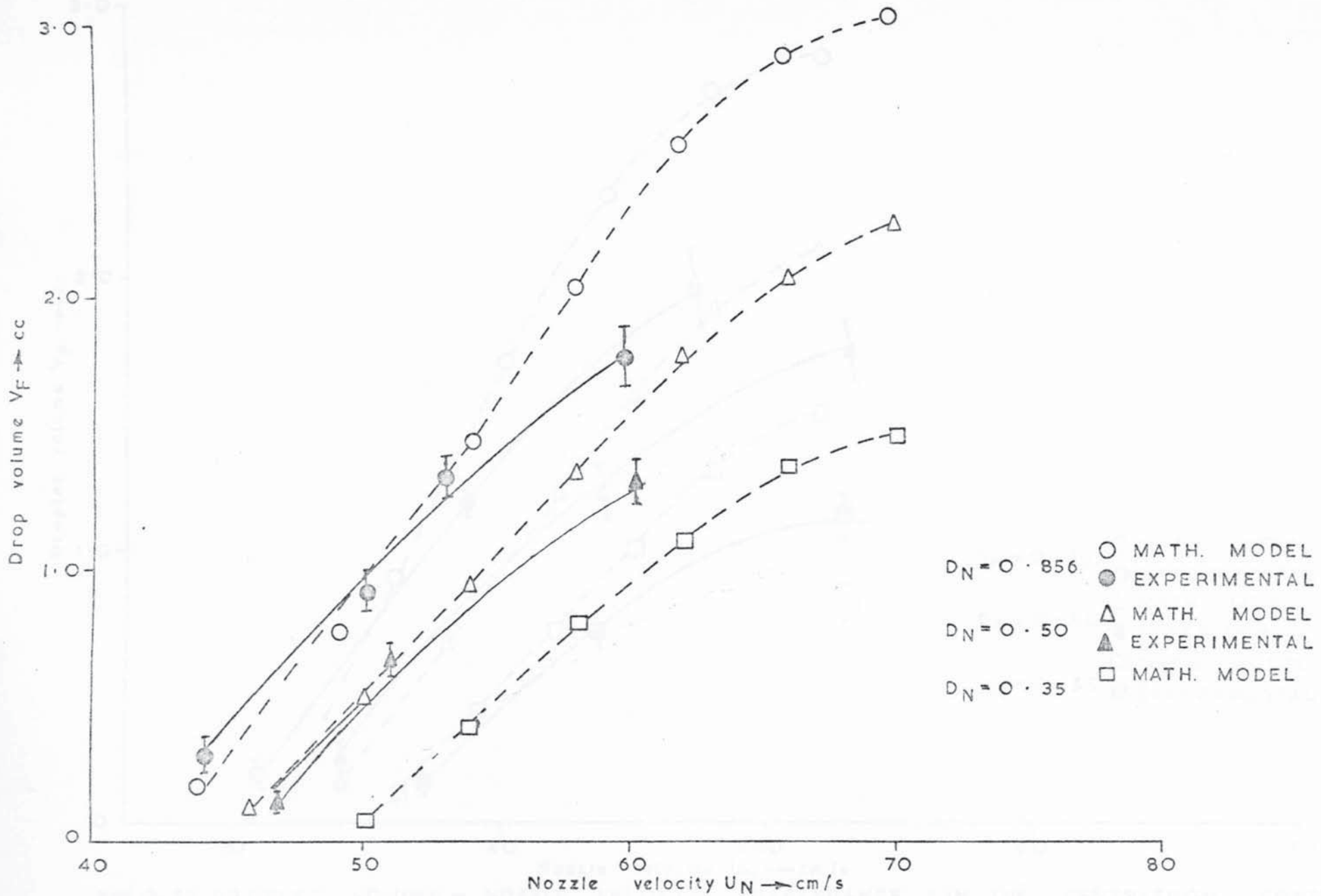

FIG.9-32 DROPLET VOLUME — NOZZLE VELOCITY DEPENDANCE IN THE CENTRIFUGAL CONTACTOR KEROSENE / WATER SYSTEM ω = 4600 R.P.M.

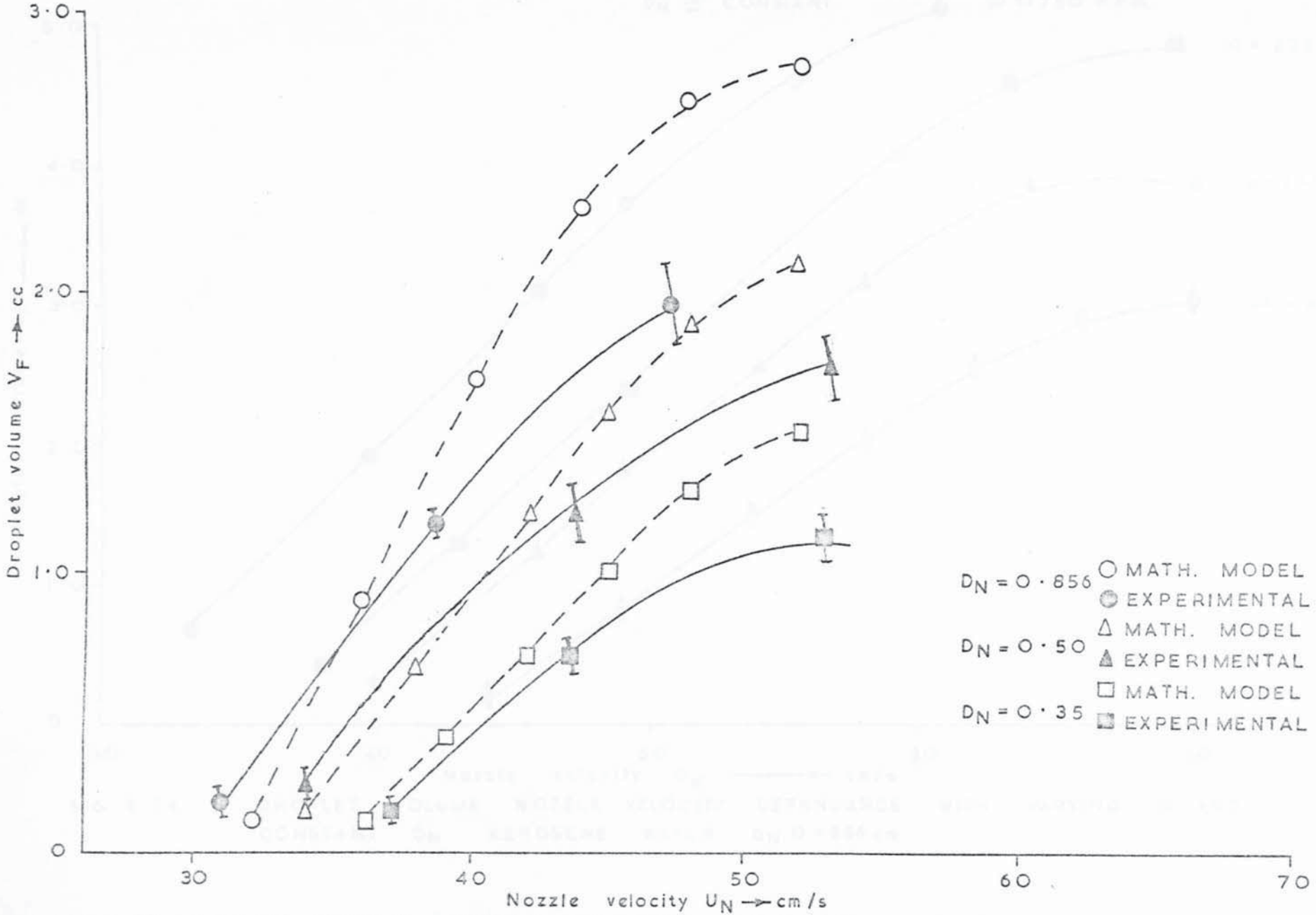

FIG. 9-33 DROPLET VOLUME – NOZZLE VELOCITY DEPENDANCE IN THE CENTRIFUGAL CONTACTOR. PARAFFIN / WATER SYSTEM ω = 4600 R.P.M

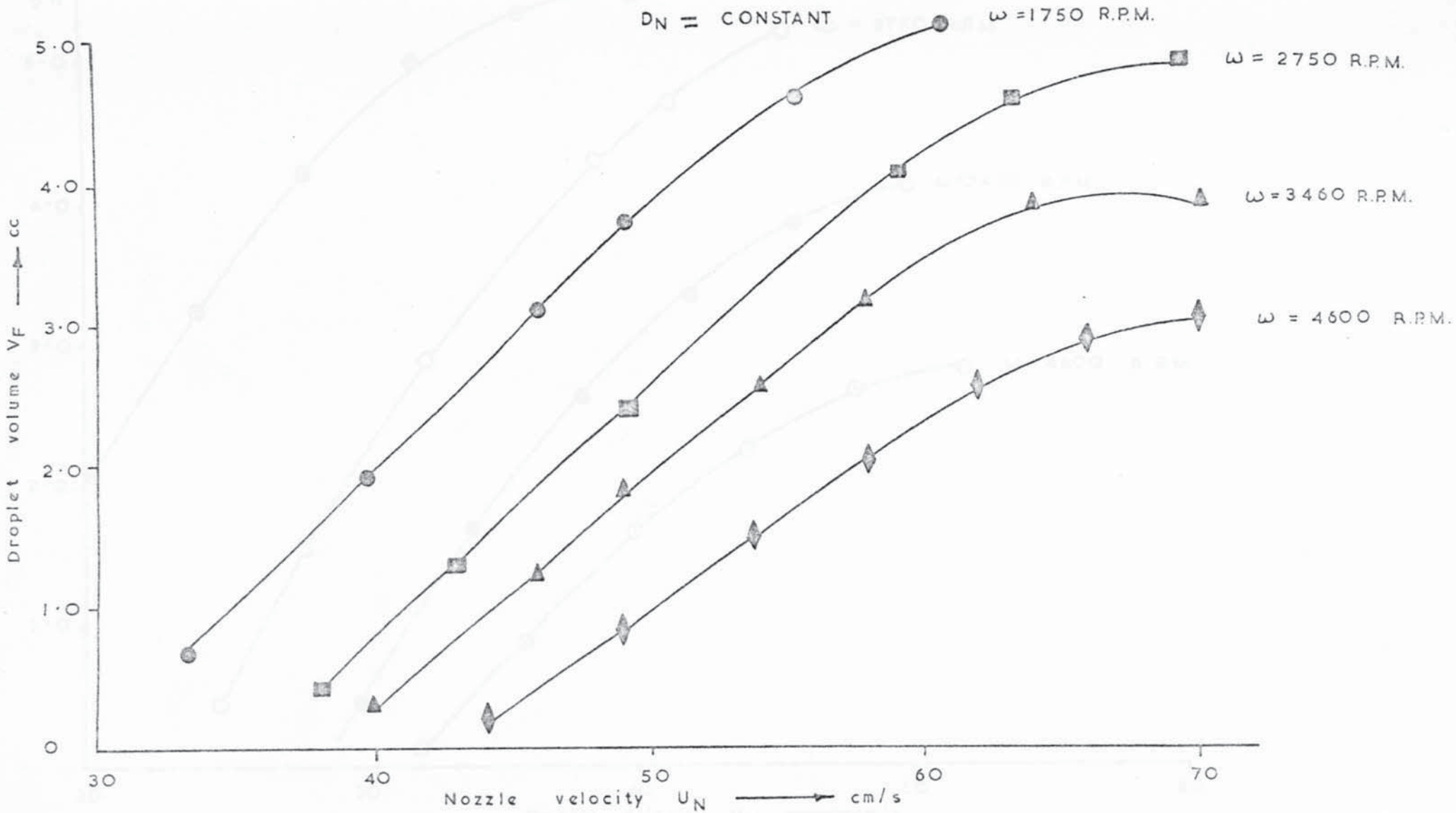

FIG. 9.34 DROPLET VOLUME NOZZLE VELOCITY DEPENDANCE WITH VARYING ω AND CONSTANT D_N KEROSENE WATER D_N O = 856 cm

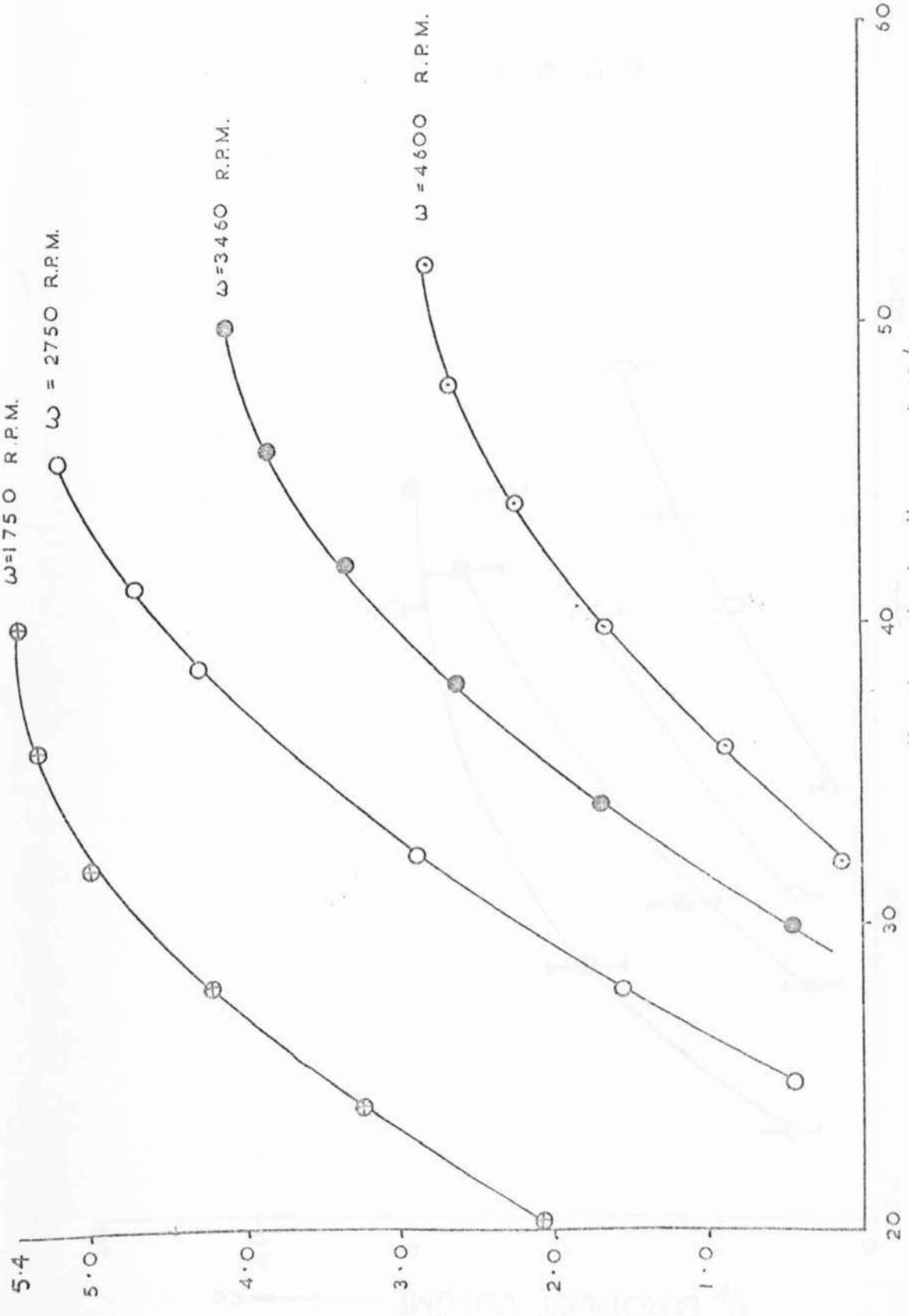

FIG. 9.35 DROPLET VOLUME - NOZZLE VELOCITY DEPENDANCE WITH VARYING ω AND CONSTANT D_N PARAFFIN - WATER $D_N = 0.856$ cm

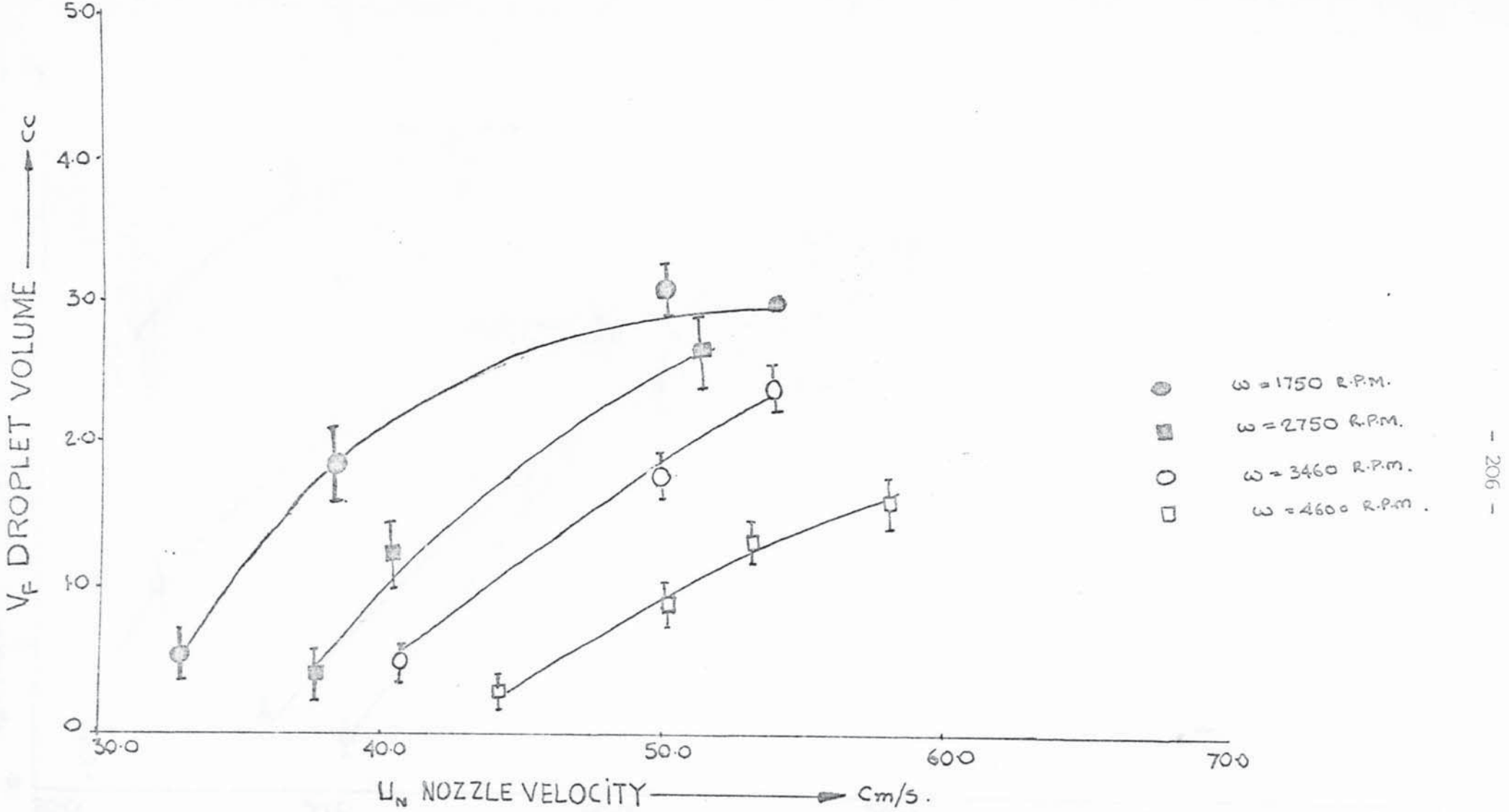

FIG·9·36 DROPLET VOLUME–NOZZLE VELOCITY DEPENDANCE AT CONSTANT D_N FOR KEROSENE-WATER SYSTEM (EXPERIMENTAL VALUES)

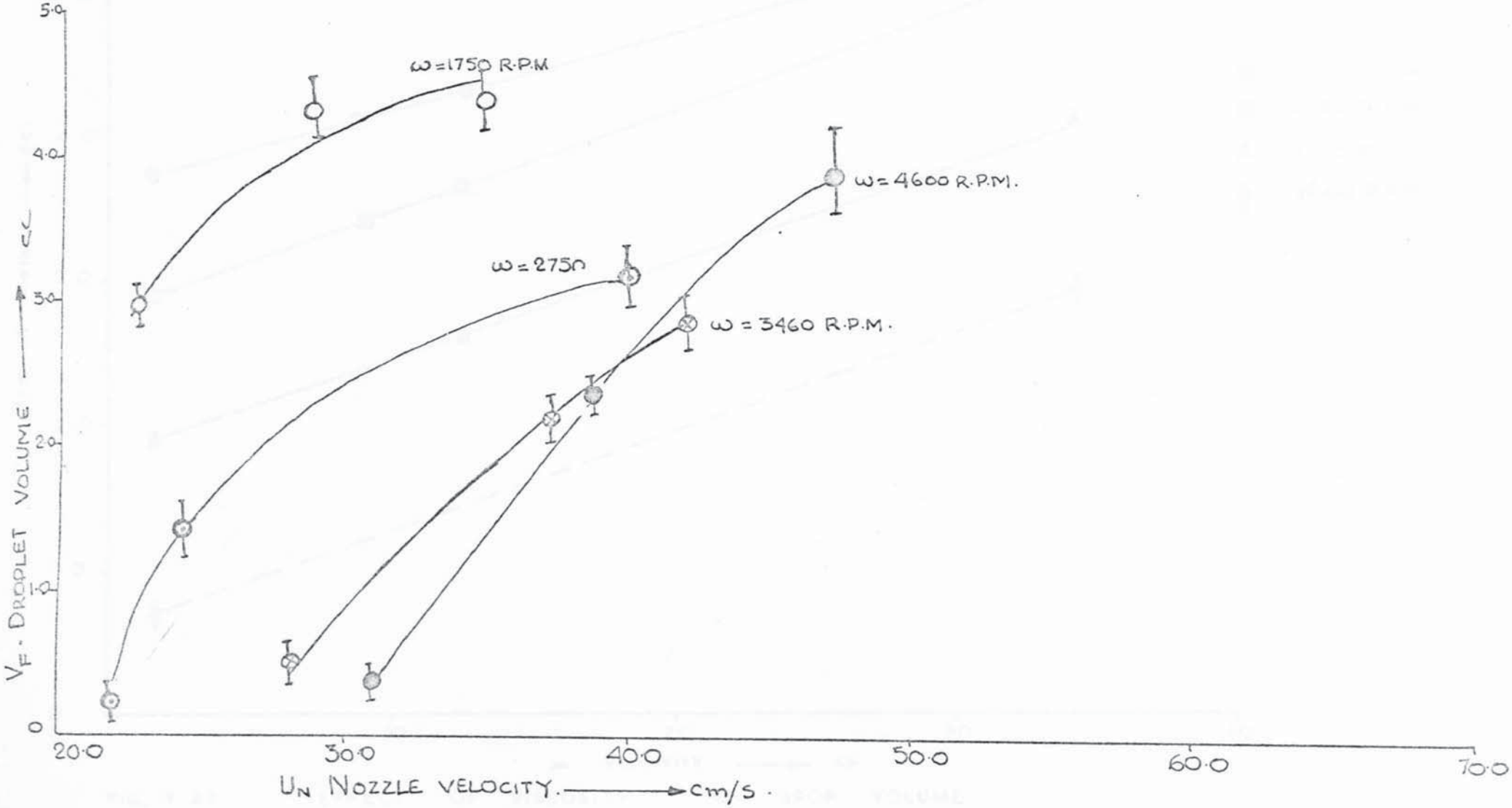

FIG. 9·37. DROPLET VOLUME-NOZZLE VELOCITY DEPENDANCE WITH EXPERIMENTAL VALUES. PARAFFIN-WATER. SYSTEM. D_N=0·856cm.

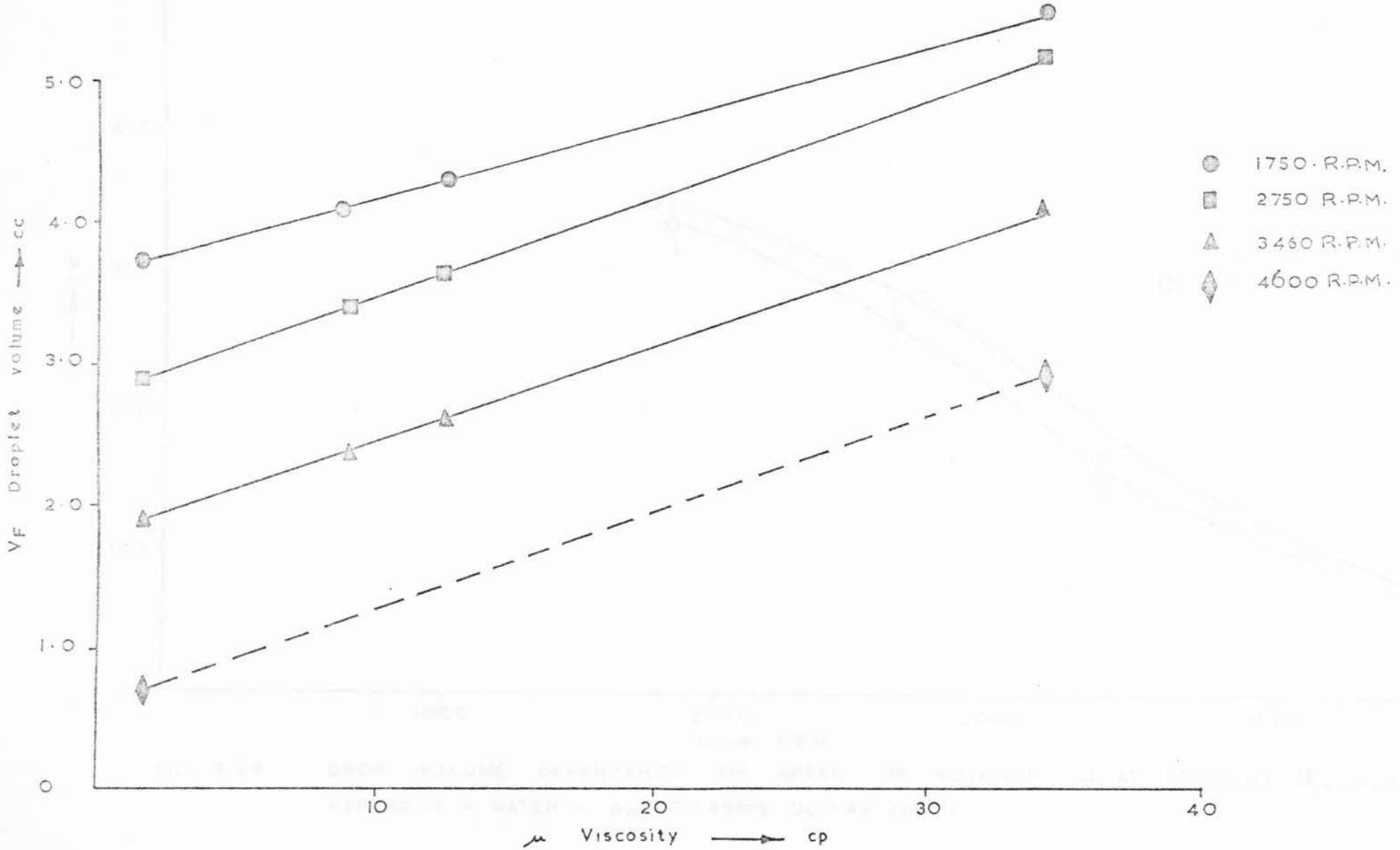

FIG. 9. 38 EFFECT OF VISCOSITY ON DROP VOLUME

D_N = 0 856cm U_N = 39·19 cm/s

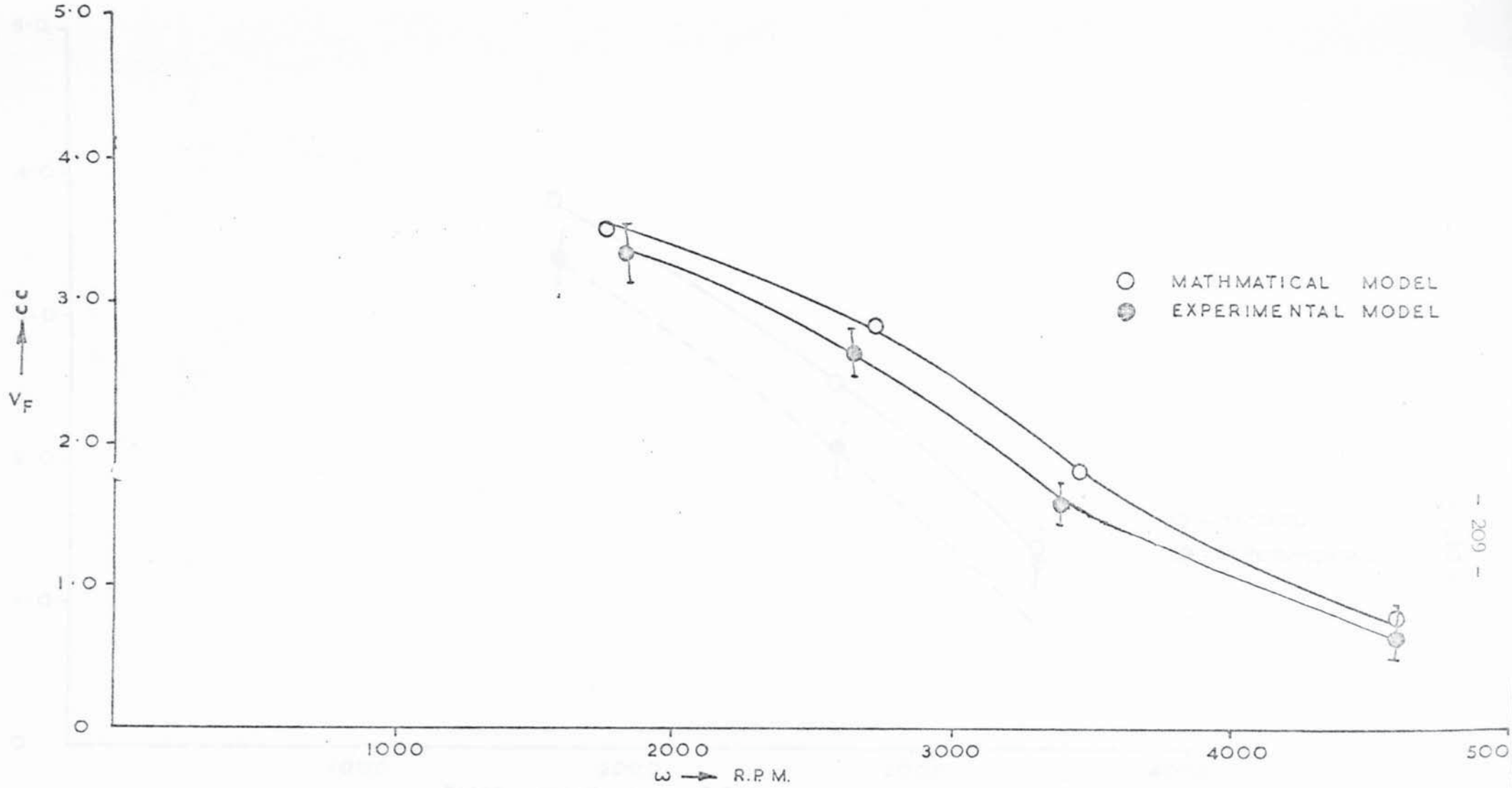

FIG. 9.39 DROP VOLUME DEPENDANCE ON SPEED OF ROTATION ω AT CONSTANT U_{NI}, D_N.
KEROSENE — WATER . D_N = 0 · 856cm U_N = 49 cm/s .

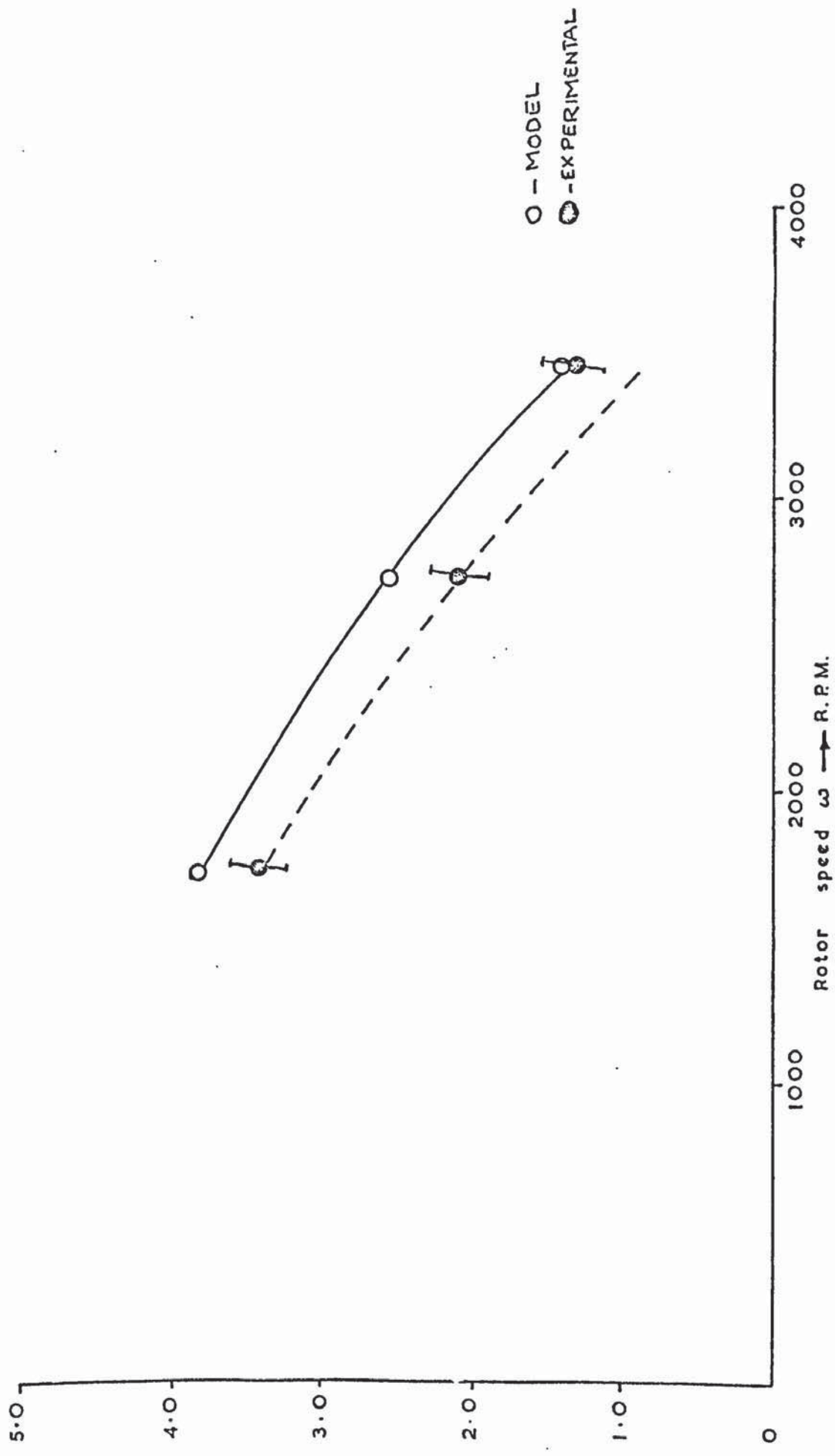

FIG. 9.40 DROP VOLUME DEPENDANCE ON SPEED OF ROTATION ω AT CONSTANT U_{Ni}, D_N. E.M. 35C OIL-WATER SYSTEM, D_N=0·856, U_N=32 cm/s

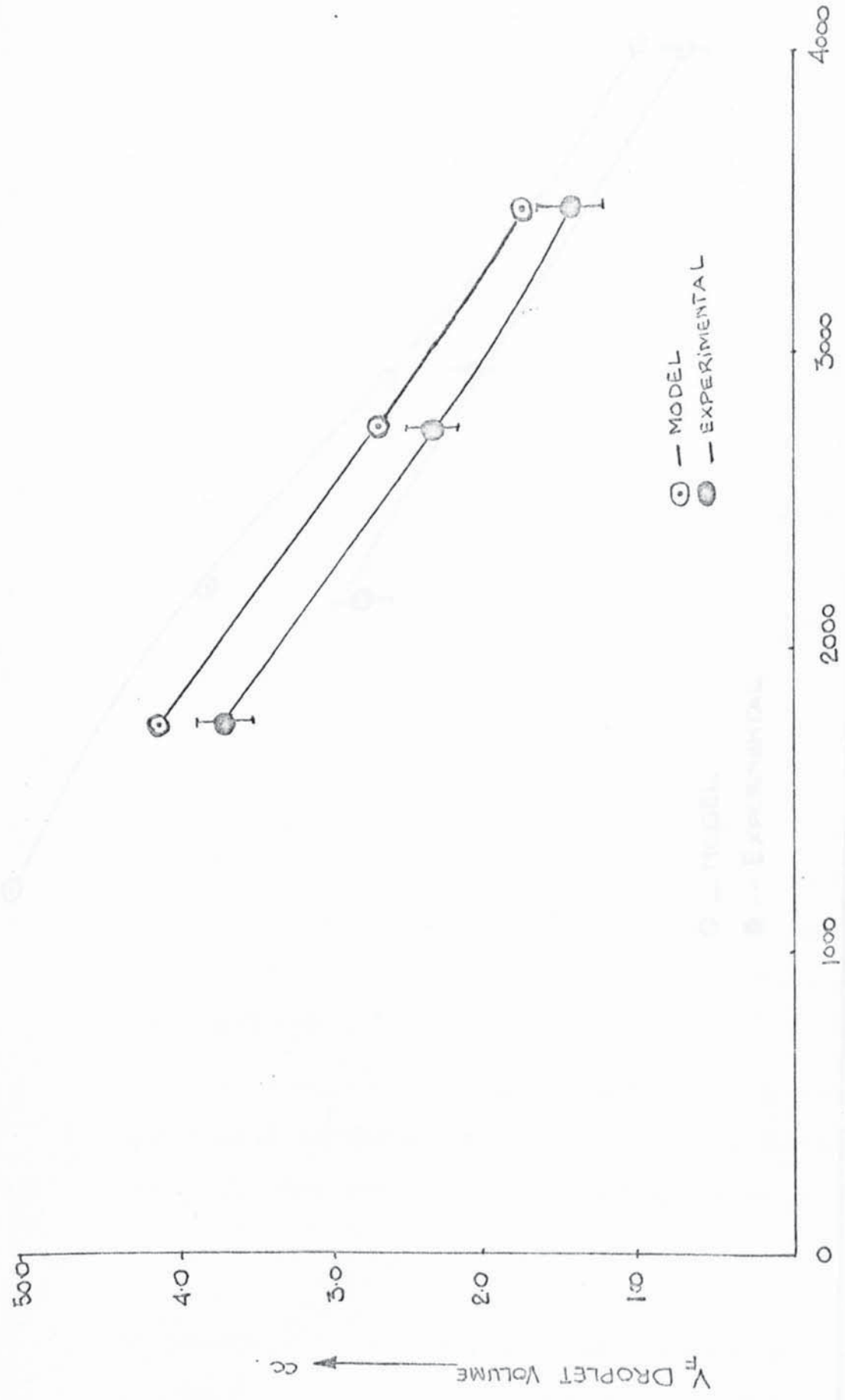

FIG. 9.41. DROPLET VOLUME DEPENDANCE ON SPEED OF ROTATION ω. C.40 OIL SYSTEM. $D_N = 0.856$ cm. $U_N \approx 32$ cm/s.

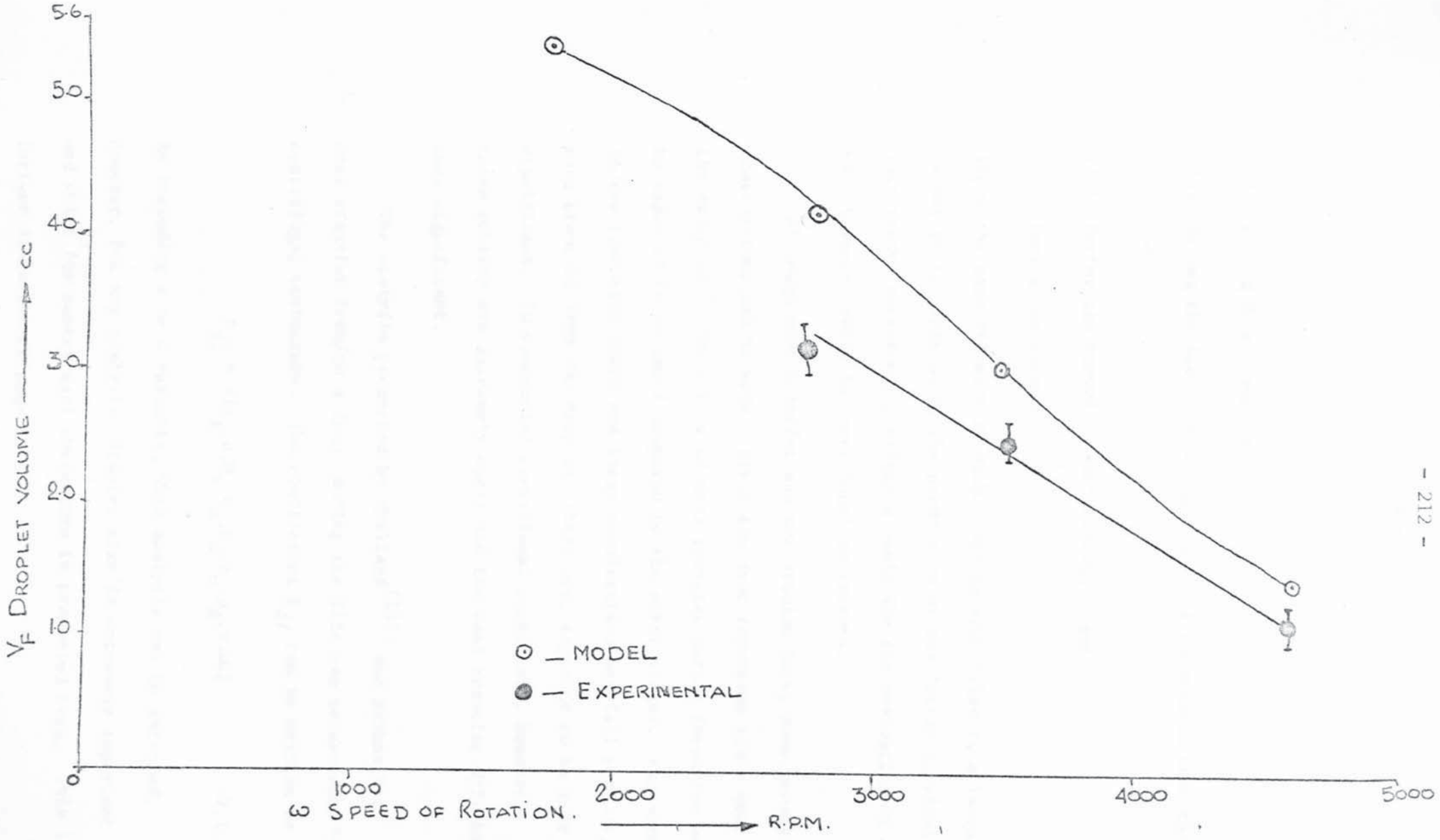

FIG. 9.42. DROPLET VOLUME – SPEED OF ROTATION (ω) DEPENDANCE. PARAFFIN WATER SYSTEM, $D_N = 0.856$ cm, $U_N \approx 40$ cm/s

(i) During drop formation;

(ii) During the acceleration period after detachment from the nozzle;

(iii) During the travel of the droplet; and

(iv) During coalescence.

Since the mass transfer at each stage is controlled to a large extent by the drop size, the prediction of the latter is vital. This study, therefore, provides a basis for the evaluation of mass transfer rates in centrifugal contactors.

Although mass transfer was not studied here, some general observations can be made. Since the drop formation times were of the order 10^{-4}, the extent of mass transfer during formation would be expected to be small compared to the other stages. Furthermore, in the contactor there are large acceleration and fall periods, mass transfer from the drop is, therefore, expected to be more significant. In commercial centrifugal contactors, however, these periods are extremely small and the mass transfer will be less significant.

The analysis presented by Skelland[151] and Minhas for mass transfer from/to a drop during its life can be extended to centrifugal contactors. The coefficient K_{df} can be written as

$$K_{df} = f(t_f, d, D_N, V_n, D_d, \mu_c, \mu_d, \omega, U_r) \qquad (9.10)$$

by including ω as a variable. This analysis can be extended. However, for any analysis, droplet size is extremely important and which for centrifugal contactors is presented here. This is

further discussed on page 230.

9.4 DROPLET VELOCITY STUDIES

9.4.1 General Observations

The motion of droplets through the continuous phase determines not only their hydrodynamics mode but also the residence time. Both factors have a significant effect on the efficiency of the contactor. The motion of droplets under gravity and correlations presented for both single and multiple droplets are reviewed. However, under the action of centrifugal force these models are invalid since the acceleration force on the drops is then many times greater.

Study of the droplets in the contactor showed that once formed they travelled both tangentially and vertically. The majority travelled from the nozzle radially and gradually reached the principal interface near the rotor where they coalesced. However, some were observed to travel almost directly to the centre of the rotor. Plates 9.2 (a), (b), (c), (d), (e), (f), show typical droplets in motion. At velocities greater than the jetting velocity U_J, the jet was observed to bend, disintegrate, and travel in a direction opposite to the direction of rotation. The forces acting on a drop are the centrifugal and Coriol is forces and since the former acts in the direction of rotation, bending of jet must be due to the Coriol is force exceeding the centripetal force. The Coriol is force, therefore, plays an important role in determining the velocity and the path of droplets in centrifugal fields.

9.4.2 Methods of Solution of the Model

The model from Chapter 8 is

$$\frac{dX}{dt} - \omega(Y^2-X^2) + k_1X + k_2 = 0 \qquad (8.26)$$

Plate 9.2

Drops in Motion

C.S.40/water system,

ω = 2750

U_r 40 cm/s

(a)

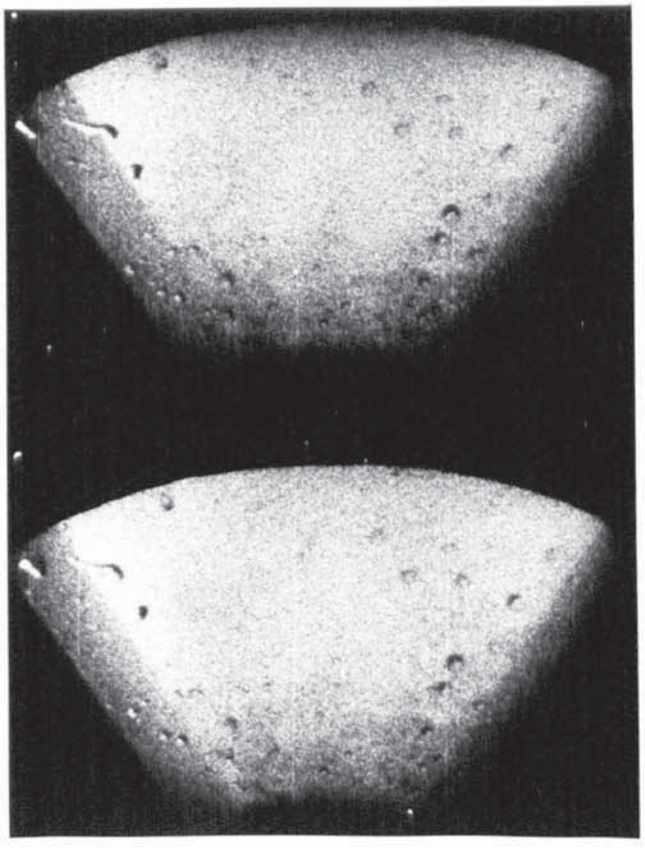

(b)

Plate 9.2

Drops in Motion

C.S.40/water system,

ω = 2750

U_r 40 cm/s

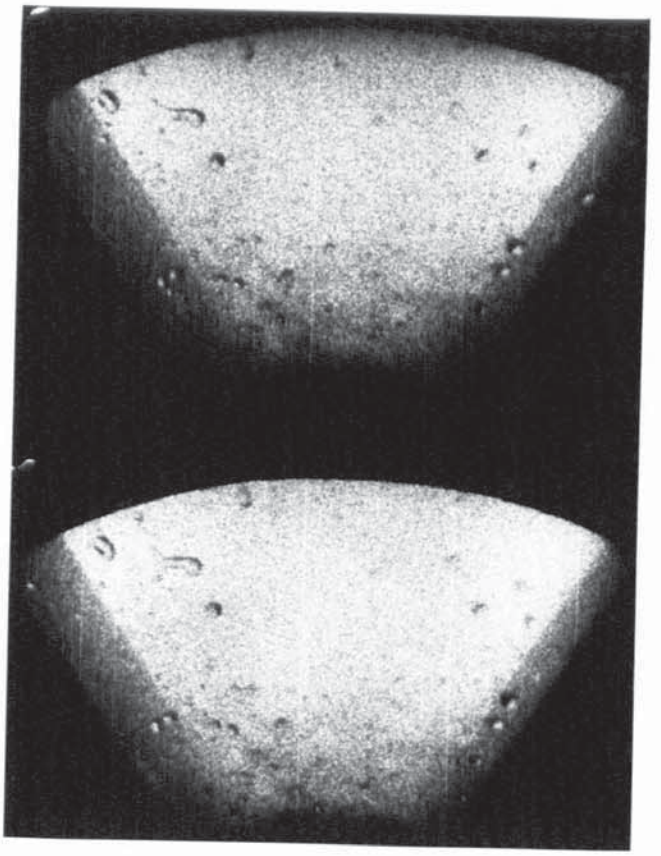

(c)

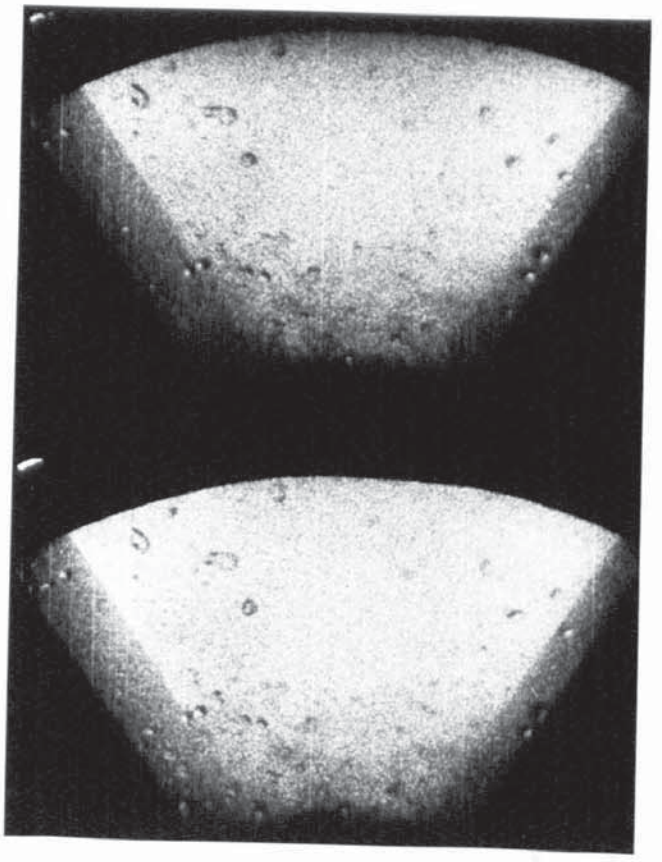

(d)

Plate 9.2

Drops in Motion

C.S.40/water system,

ω = 2750

U_r 40 cm/s

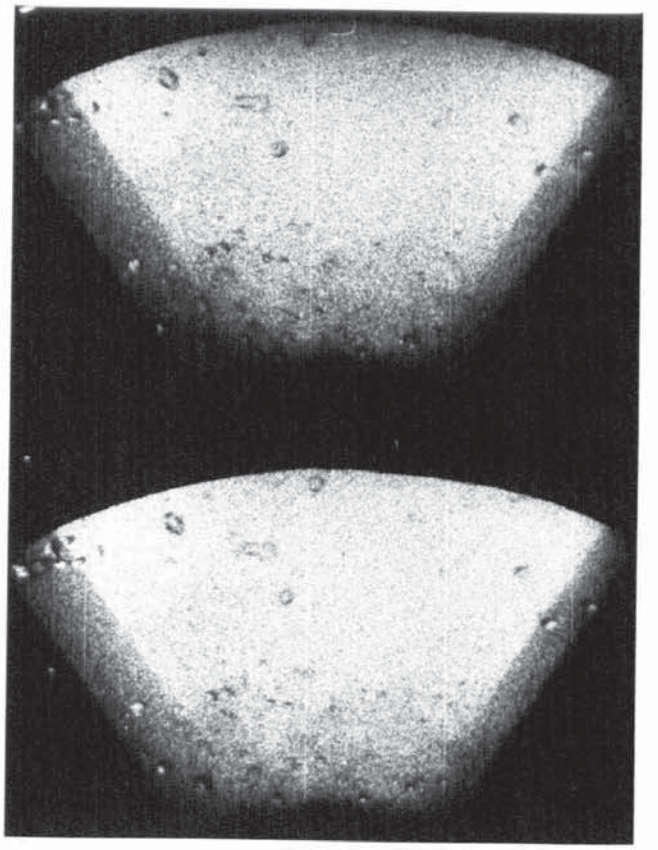

(e)

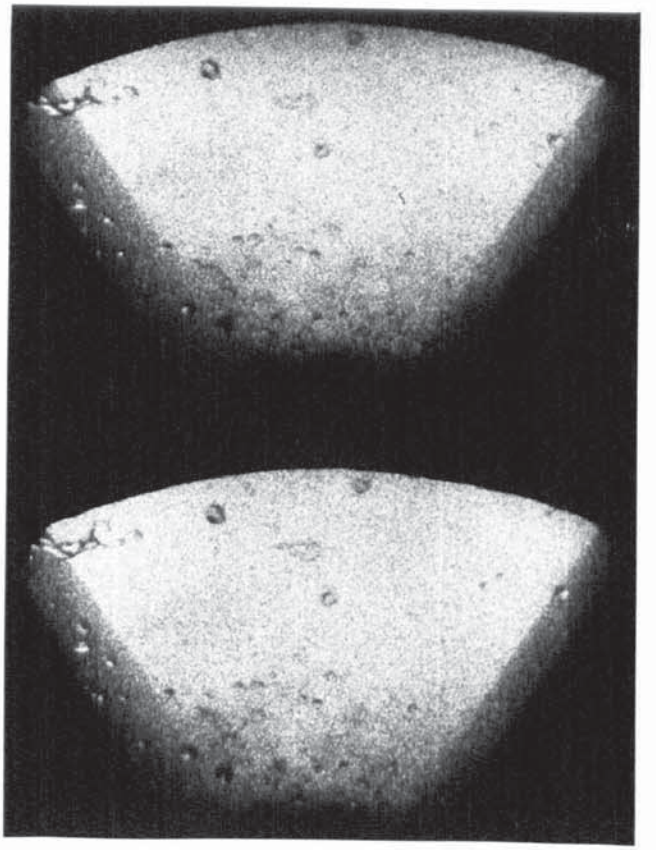

(f)

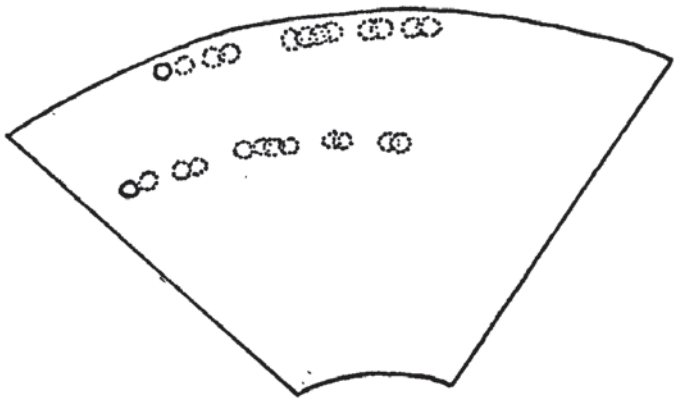

PLATE 9.2A TRACING OF TWO DROPLETS FROM FRAMES (a) to (f) TO SHOW TRAJECTORIES OF DROPLETS

$$\frac{dY}{dt} + k_1(Y-1) + 2 \times (Y-1)\omega = 0 \qquad (8.30)$$

where

$X = \frac{U_f}{\omega R}$, $Y = 1 + \frac{U_x}{\omega R}$ are two dimensionless velocities. Two methods of numerical solutions were studied:-

Method (a) This involved the expression of X and Y as Maclaurin Series in t, i.e.

$$X(t) = X(o) + X^{(1)}(o)t + X^{(2)}(o)\frac{t^2}{2!} + \text{---} X^{(n)}(o)\frac{t^n}{n!} + \text{----} \qquad (9.11)$$

$$Y(t) = Y(o) + Y^{(1)}(o)t + Y^{(2)}(o)\frac{t^2}{2!} + \text{---} Y^{(n)}(o)\frac{t^n}{n!} + \text{----} \qquad (9.12)$$

where $X^n(o)$ denotes $\frac{dX^n}{dt^n}$ evaluated at t = 0.

$X(o) = Y(o) = 0$

From (8.26) $X^{(1)}(o) = -K_2$

(8.30) $Y^{(1)}(o) = K_1$

Differentiate (8.26) with respect to (t),

$$\frac{d^2X}{dt^2} + 2X\omega\frac{dX}{dt} - 2Y\omega\frac{dY}{dt} + K_1\frac{dX}{dt} = 0 \qquad (9.13)$$

Hence at t = 0 $X^{(2)}(o) = -K_1 K_2$

Differentiate (8.30) w.r.t(t)

$$\frac{d^2Y}{dt^2} + \omega 2\frac{dX}{dt}.Y + \omega 2\frac{dY}{dt}X + K_1\frac{dY}{dt} - 2\omega\frac{dx}{dt} = 0 \qquad (9.14)$$

Hence at t = 0 $Y^{(2)}(o) = -K_1^2 - 2\omega K_2$

Now (9.13) simplifies to $\frac{d^2X}{dt^2} + (2\omega x + K_1)\frac{dx}{dt} - 2Y\omega\frac{dY}{dt} = 0$

Differentiate w.r.t(t)

$$\frac{d^3X}{dt^3} + \omega 2(\frac{dX}{dt})(\frac{dX}{dt}) + (2X\omega + K_1)\frac{d^2X}{dt^2}$$

$$-\omega 2(\frac{dY}{dt})(\frac{dY}{dt}) - \omega 2Y\frac{d^2Y}{dt^2} = 0 \qquad (9.15)$$

Hence at t = 0 $X^{(3)}(o) = +2\omega K_1^2 - 2\omega K_2^2 - K_1K_2^2$

Similarly simplifying and differentiating leads to $Y^3(o)$. Thus a Maclaurin series is generated, viz:

$$X(t) = -K_2 + K_1K_2\frac{t^2}{2!} + (2\omega K_1^2 - 2\omega K_2^2 + K_1K_2^2)\frac{t^3}{3!} \qquad (9.16)$$

$$Y(t) = +K_1 - (K_1^2 + 2\omega K_2)\frac{t^2}{2!} \qquad (9.17)$$

Method (b) This is referred to as the Picard's solution and also involves generation of a Series. Thus,

$$\frac{dX_n}{dt} = f(X_{n-1}, Y_{n-1}) \qquad (9.18)$$

$$\frac{dY_n}{dt} = g(X_n, Y_{n-1}) \qquad (9.19)$$

Now

$$X_1 = \int_o^t -K_2\,dt = -K_2t$$

$$Y_1 = \int_o^t K_1\,dt = K_1t \qquad (9.20)$$

$$X_2 = \int_o^t (K_1^2t^2 - K_2^2t^2 + K_1K_2t - K_2)\,dt$$

$$= K_1^2\frac{t^3}{3} - K_2^2\frac{t^3}{3} + K_1K_2\frac{t^2}{2} - K_2t \qquad (9.21)$$

Similarly

$$Y_2 = \int_o^t \left| -2\left(K_1^2 \frac{t^3}{3} - K_2^2 \frac{t^3}{3} + K_1 c_2 \frac{t^2}{2} - K_2 t\right) K_1 t - K_1^2 t + K_1 \right| dt$$

$$= \int_o^t \left(-2K_1^3 \frac{t^4}{3} + \frac{2}{3} K_2^2 K_1 \frac{t^4}{3} - K_1^2 K_2 t^3 + 2K_1 K_2 t^2 - K_1^2 t + K_1\right) dt$$

(9.22)

In this fashion X_3, Y_3, etc. can be obtained to give a series, which can be solved by finite difference approximations.

Visual observation of the droplets showed that the radial velocity and therefore X, was the larger of the two velocities. Therefore the series for X from both the methods was solved. However, as the manual calculations showed that the series converges slowly an alternative solution was sought. Using the S.L.A.M. computer language a solution was obtained. The programme is given in Appendix F.

9.4.3 Comparison of Model and Experimental Results

From equations 9.15 and 9.20, the analytical solution of radial velocity X is of the form,

$$X = f(K_1, K_2) \qquad (9.23)$$

or

$$U_r = \omega R \times f(K_1, K_2) \qquad (9.23)$$

Hence the radial velocity U_r can be presented as a function of the constant $K_1 = \left(\frac{18V_c}{\pi D^2 \omega R}\right)$, $K_2 = \left(\omega \frac{-\Delta\rho}{g\rho_d \omega R}\right)$ and the speed of rotation ω. However, since K_2 is a function of the density, the data is presented in Figs. 9.43, 9.44 and 9.45, with K_1 as the abcissa.

The graphs demonstrate that the agreement between the

experimental and model velocity values is good at all values of the droplet velocity U_r. The discrepancy between the two curves is a minimum, about 8%, at low values of k_1 and maximum, about 15% at k_1 values in the range 4.0 to 7.0. This accuracy of the prediction of radial velocities implies that the assumptions made on deriving the model are largely justified. One assumption was that the droplets are rigid and spherical in shape. This was not always the case since non-spherical and non-rigid drops were also observed.

A study of the graphs shows that:-

(a) At the same value of k_1 at constant ω, the droplet radial velocity decreased with increasing density. This would be expected since $k_2 = \omega(1 - \frac{\Delta\rho}{g\rho_d R})$, contains the term $\frac{1}{\rho_d}$ and as ω, R were constant for each graph, the radial velocity is a function of k_2 and k_1.

(b) At the same value of k_1 for any given system there was an increase in the radial velocity with ω. This can be deduced from equation 9.22 demonstrating a linear relationship between U_R and ω.

(c) The radial velocity tends to decline after a peak value of k_1 and which is approximately 2.5 irrespective of the system. Thus at ω = 1750, $(k_1)_{peak}$ = 3.0, at ω = 2750 $(k_1)_{peak}$ = 2.5 and ω = 3460 $(k_1)_{peak}$ = 2.0.

The model may be compared with a modified Stokes law viz,

$$(U_r) = \frac{\Delta\rho\omega^2 RD}{\mu_c} \qquad (9.25)$$

Simplifying in terms of k_1,

$$= \left(\frac{\pi\omega RD^2}{18v_c}\right) \times \frac{\Delta\rho}{D\pi\rho_d}$$

i.e

$$U_r = k_1 \frac{\Delta\rho}{D\pi\rho_d} \qquad (9.26)$$

Fig. 9.46 illustrates the comparison between equation 9.26 and the mathematical model. The modified Stokes formula, yields only an approximation and is totally invalid under certain conditions. Thus for k_1 in the range 2.5 to 8.0 the deviation between the model and equation 9.25 is approximately 35% and for k_1 less than 1.5, it can be greater than 200%. The reason for such large discrepancies between the two is the importance of Corolois force which is not accounted for in the Stokes formula. Also the ideal conditions assumed in the Stokes Law do not hold in the contactor at these values of k_1.

9.4.4 Significance to Centrifugal Operation

A centrifugal contactor is often selected for a process because the residence time per stage is extremely small compared to gravity towers. This is achieved due to the accelerated settling effect produced by the centrifugal force. Previous work[176] on centrifugal contactor residence time employed a technique of injecting dye into inlet streams and recording the time for the dye to appear in the outlet stream. This method is very approximate because the time recorded includes the residence time in the mechanical seals and pipework in addition to that contactor in itself.

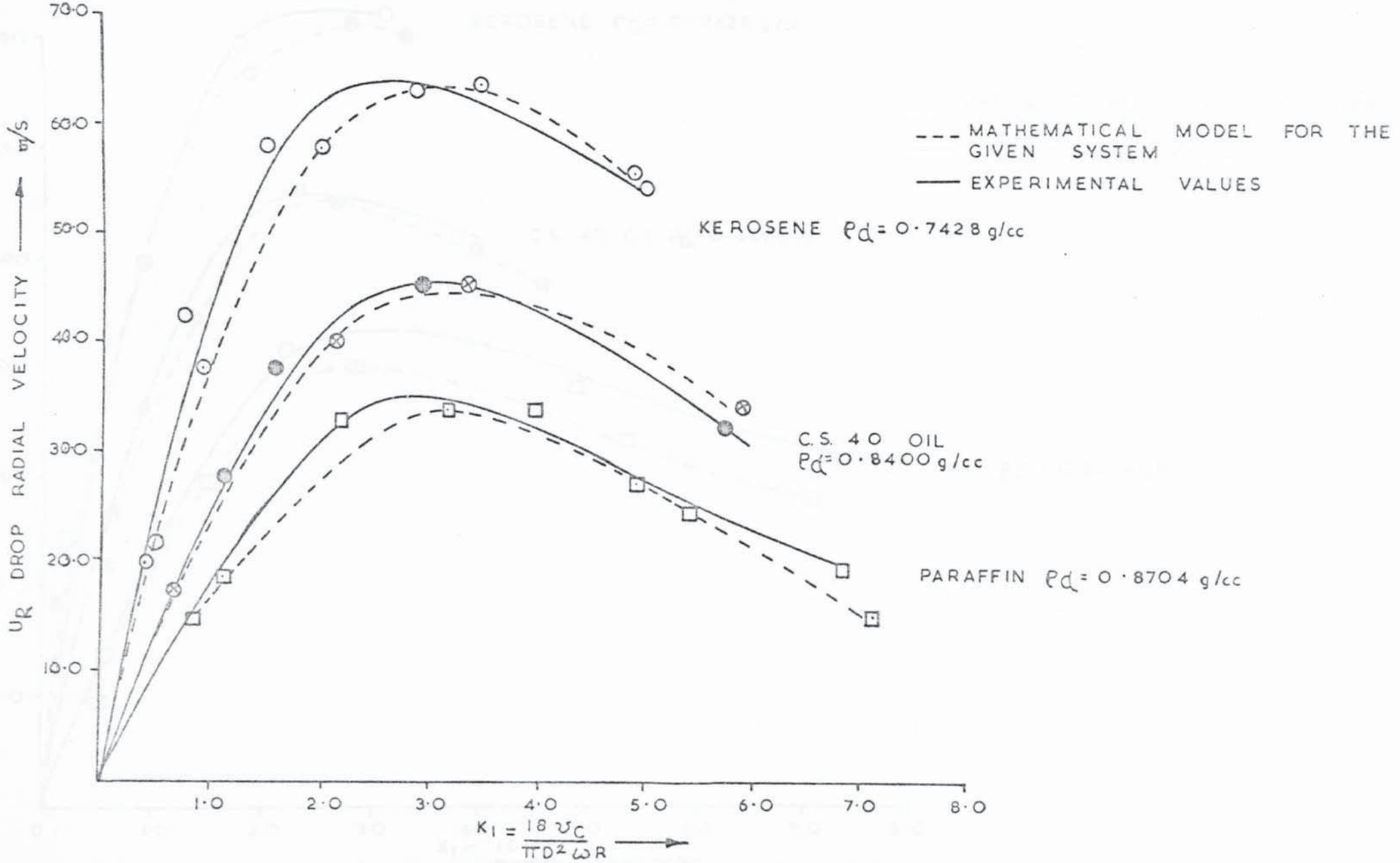

FIG.9-43 VARIATION OF RADIAL VELOCITY U_R FOR DIFFERENT SYSTEMS AT ω = 1750 R.P.M.

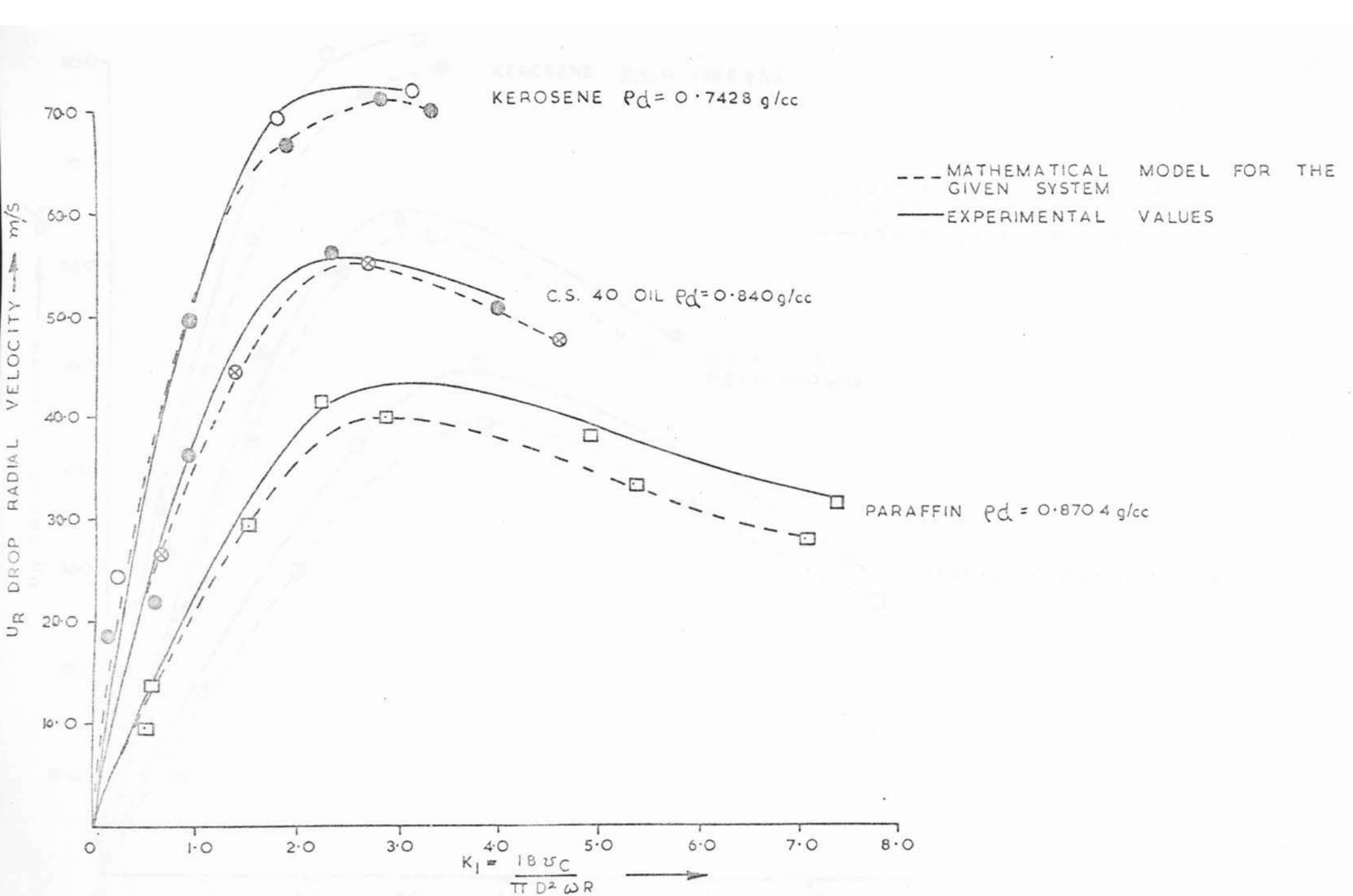

FIG. 9-44 VARIATION OF RADIAL VELOCITY U_R FOR DIFFERENT SYSTEMS AT ω = 2750 R.P.M.

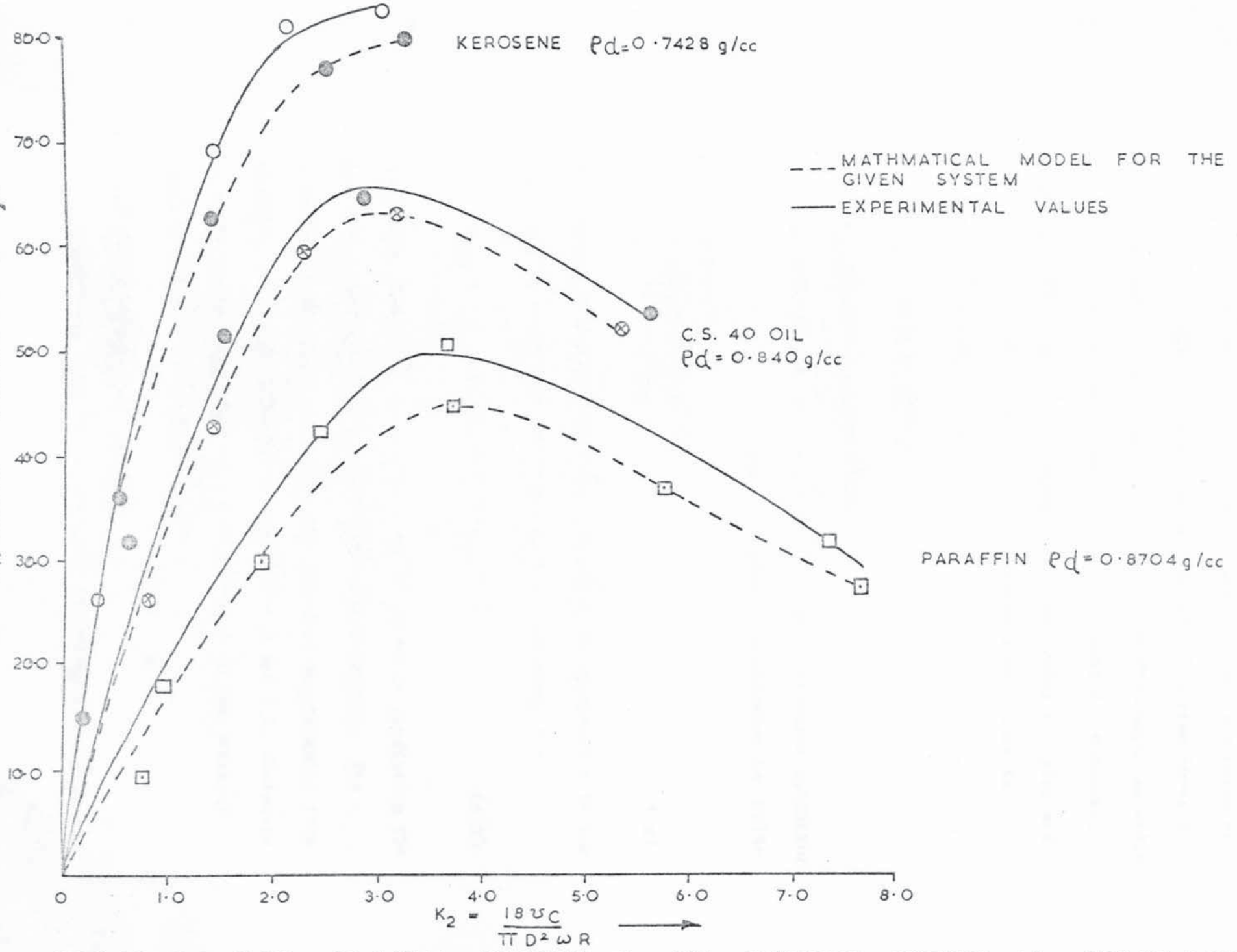

FIG.9-45 VARIATION OF RADIAL VELOCITY U_R FOR DIFFERENT SYSTEMS AT ω=3460 R.P.M.

PAGE NUMBERING AS ORIGINAL

The model derived in this study enables the prediction of droplet radial velocity from a knowledge of the system physical properties and the speed of rotation ω. From the radial velocity value a theoretical residence time can be computed. Moreover, knowledge of U_r can also be important in designing the size and spacing of orifices in the commercial contactors. This is discussed in Section 9.5.4.

9.5 APPLICATION TO DESIGN

9.5.1 Hold-up and Flooding Studies

Methods of determining the hold-up of centrifugal contactor have been investigated and have provided a correlation for hold-up in terms of P_{LO},

$$V_H = a_1 + m_1 P_{LO}$$
$$V_E = a_2 + m_2 P_{LO} \quad (9.3)$$

These equations, although empirical, are based on equations 6.14 and 9.2, both of which were derived from the following, i.e.

$$P_{HLO} = P_{LLI} = 0.513 \times 10^{-6} (P_{LLI})^2 \omega^2 \quad (6.2)$$

Therefore equation 6.2 provides a useful means of predicting the pressure requirement from system physical properties. The pressure losses across the contactor can also be estimated from equation 9.4. A combination of equation 9.3 and 6.2, therefore provides design equations for the prediction of the pressure limitations of a centrifugal contactor.

9.5.2 The Discharge Rate Studies

A procedure for predicting which discharge regime exists

in centrifugal conditions was described in section 9.2. Its application to the design of contactors will now be discussed. The commercail continuous differential type centrifugal contactors differ from the one developed in this work only, since their internals are more complex. Whereas jetting occurred in this contactor, its existence in commercial contactors will therefore depend entirely on the complexity of its internal and on the flow rate of the dispersed phase.

In all commercial contactors there are numerous orifices or trays or bands which may be either concentric or placed at decreasing intervals from the centre of the periphery. The orifices may be of three arrangements, i.e. constant diameter, or increasing or decreasing diameters from the central to the peripheral band. In such situations a drop is initially formed on the peripheral band, and will traverse to the next band, coalesce and a new drop is form at this band. This is repeated until the fluid from the initial droplet reaches the principal interface and coalesces. By this process of repeated formation at new orifices/nozzles, the droplet regime is the predominant discharge regime in commercial contactors. In this contactor the predominant state was also droplet type, with the significant difference being the absence of the process of repeated droplet formation from the periphery to the centre.

Equations 9.6 and 9.7 enable the prediction of band intervals and the flow rate requirements:-

$$C_{od} = 3.73 \left(\frac{\rho_d U_N}{\Delta\rho\omega R}\right)^{1.52} \qquad (9.6)$$

$$C_{od} = 0.63 \left(\frac{\rho_d U_N}{\Delta\rho\omega R}\right)^{0.031} \qquad (9.7)$$

The Q/R ratio can be determined from a knowledge of the state of flow discharges, the system properties and speed of rotation ω, and using the appropriate correlation. Fixing the total radius of the contactor R can determine the flow rate of the dispersed phase near the periphery. Hence the number and size of orifices on the peripheral band can be computed.

9.5.3 The Droplet Formation Studies

Droplet size although of prime importance for mass transfer efficiency, has only an indirect application in designing the dimensions of the centrifugal contactor. The basic dimensions are not determined by the drop size but by capacity, and which can be estimated from the procedure outlined in Section 9.1. For centrifugal contactors the concept of a mass transfer stage is, as in gravity extraction equipment, e.g. the number of theoretical stages as discussed in Chapter 6 do not necessarily equal the number of concentric bands in the contactor.

However, analysis of mass transfer in terms of individual coefficient requires drop size as described by the equations in Chapter 5. In analogous manner to these equations, correlations for mass transfer constant in terms of droplet size are possible for centrifugal contactors. Thus for example, the Skelland and Minhas[151] treatment can be extended by taking speed of rotation ω

into account, i.e.

$$k_{df} = f(\omega, D_d, \mu_o, \mu_c, d, D_N, V_m, t_f, U_r)$$

Dimensionless groups can be arranged, i.e.

$$\left(\frac{k_{df}}{d} \cdot t_f\right) = f\left(\frac{V_m}{dg}\right)^a \left(\frac{d^2}{t_f \cdot D_d}\right)^b \left(\frac{\mu}{\rho_d \cdot d \cdot \sigma}\right)^c \left(\frac{\omega R}{U_r}\right)^d$$

The group $\left(\frac{\omega R}{U_r}\right)$ is included to account for centrifugal velocity R and the radial velocity U_r.

9.5.4 Droplet Velocity Studies

A fundamental feature of the centrifugal contactor is the accelerated settling of droplets by the centripetal force. The droplet velocities are therefore important in design work. If for a process the residence time is important as in solutions that rapidly deteriorate, then this can be estimated from a knowledge of the droplet velocities.

Aside from being able to predict the residence times, these correlations can also be used in mass transfer coefficient calculation. This can be seen from equation (9.9) which includes a group $\left(\frac{\omega R}{U_r}\right)$ which is a ratio of the velocity of rotation and droplet radial velocity.

CHAPTER 10

CONCLUSIONS

The main conclusions of this work can be summarised as:-

(a) the total contactor volume V_E is 5.03 litres and comprises a rotor volume V_C of 4.5 litres and seal volume of 0·5 litres. It is related to the light-liquid-out pressure P_{LO} viz:

$$V_E = V_H + V_L$$

and

$$V_H = a_1 + m_1 P_{LO}$$

$$V_L = a_2 + m_2, P_{LO}$$

where the values of a_1, a_2 and m_1, m_2 are given in Table 9.

(b) Flooding in centrifugal contactors can be of three types, i.e. shaft flooding, rim flooding and capacity flooding, depending upon the back pressure applied and the flow rate of the phases. The operating limits for the contactor are shown by Figs.9.3,9.4,9.5 Flooding is discussed in detail in section 9.1.2.

(c) Pressure losses across the contactor, which influence the drop size is correlated to the flow rate Q and the speed of rotation, i.e.

$$\Delta\rho_\omega = \Delta\rho_o + 1.506 \times 10^{-3} Q\omega \qquad (9.4)$$

These losses are discussed in detail in section 9.1.3.

(d) Flow from a nozzle in a centrifugal contactor may occur in droplet form, jet form or a transition regime. In section 9.2 it is shown that each type of flow can be characterised

by a coefficient of discharge C_{od} and a dimensionless number $(\frac{\rho_d U_N}{\Delta\rho\omega R})$ viz:

For droplet flow, i.e. $C_{od} \leqslant 0.30$

$$C_{od} = 3.73 \left(\frac{\rho_d U_N}{\Delta\rho\omega R}\right)^{1.52} \qquad (9.6)$$

For jet flow, i.e. $C_{od} \geqslant 0.51$

$$C_{od} = 0.63 \left(\frac{\rho_d U_N}{\Delta\rho\omega R}\right)^{0.031} \qquad (9.7)$$

It is also shown that these equations can be used to calculate radius of the contactor and the concentric band spacing.

(e) The mechanism of single droplet formation in the centrifugal contactor is a two stage process, i.e.

(a) Growth of droplet , and

(b) Detachment of the droplet by the action of the centrifugal force.

Assuming this mechanism of droplet formation, a model is derived in section 8.1, viz:

$$V_F = F \left\{\frac{\pi\sigma D_N}{\Delta\rho g} + \frac{10.8\mu_d D_N Q}{D_F^2 \Delta\rho g} - \frac{3.1 Q U_N}{\Delta\rho g} - \frac{\omega^2 R}{\Delta\rho g}\right\} \qquad (9.9)$$

The model showed good agreement when the mechanism of formation is of single/multiple droplet form. For this mechanism the error between the model and experimental results is up to 15%. However, when the jet state exists, where the mechanism is no longer as assumed in the model,

errors of up to 66% are possible.

In this study rigid and non-rigid drops were observed and some of the latter showed high degree of oscillation. The frequency of oscillation could not be measured by the existing techniques.

The droplet volume V_F in the contactor is shown to:

(a) Decrease as the nozzle D_N decreases;

(b) Decrease with decreasing speed of rotation ω, but a point is reached beyond which an increase in ω does not produce proportional decrease in V_F. For this contactor this is at ω = 5000 r.p.m.

(c) Decrease with low viscosity systems , i.e. with decreasing μ_d.

(f) Study of droplet motion in the centrifugal contactor leads to a set of differential equations the resolution of which gives the component velocities of droplets. For the sake of mathematical convenience these are expressed as dimensionless velocities X and Y, viz

$$\frac{dX}{dt} - \omega(Y^2 - X^2) + k_1X + k_2 = 0 \qquad (8.26)$$

$$\frac{dY}{dt} + k_1(Y - 1) + 2X(Y - 1)\omega = 0 \qquad (8.30)$$

Two possible methods of solution are also given. A computer programme using the language SLAM is used to compute the radial velocities. Comparison of the experimental and calculated velocities shows excellent agreement. The error

is approximately 8% and 15% for values of k_1 lower than 4.0 and 7.0 respectively.

Although Stokes's formula is modified to account for the centrifugal force, theoretical velocities calculated from it vary considerably from the experimental values. The modified equation is given by,

$$U_r = k_1 \frac{\Delta\rho}{D\pi\rho_d} \tag{9.26}$$

where

$$k_1 = \left(\frac{18v_c}{\pi D^2 \omega R}\right)$$

Finally, the radial velocities of droplets are extremely high compared to those in gravity equipment, e.g. 0.8 m/s compared to 0.01 m/s. Hence the settling rates are substantially greater in centrifugal contactors.

CHAPTER 11

RECOMMENDATION FOR FUTURE WORK

This work can be extended along two distinct lines, i.e. hydrodynamic and mass transfer studies. For both cases a new contactor should be designed so that

(a) That the contactor offers greater visibility. It is therefor suggested that α -Laval type should be used since the axis of rotation is vertical and the bearings do not hindervision. However, this would require new techniques of equipment fabrication.

(b) Constructing the internals such that any number of concentric bands could be used. For hydrodynamic studies, this would enable the study of drops coalescing at a band, forming again and travelling to the next. For mass transfer studies, it may enable better understanding of the mass transfer to/from the various stages of droplets life.

(c) The apparatus should be designed to operate under pressure. This should make it possible for hold-up of the contactor to be studied at light-liquid-out pressures P_{LO}. It should also enable easier operations of the contactor.

(d) Low speeds of rotation, e.g. 100 r.p.m., could be achieved equally well as the high speeds, e.g. 5000 r.p.m.

Using the new contactor, the following should be investigated:

(i) Mechanism of jet formation. This is probably best investigated at low speeds of rotation.

(ii) Coalescence of droplets at the concentric bands.

(iii) Droplet rupture.

(iv) Mass transfer rates. For this the end-plates will have to be changed every few runs if Macrolon is the material of construction.

APPENDIX A

THE PHYSICAL AND CHEMICAL PROPERTIES OF THE FOUR SYSTEMS USED

TABLE A.1

PROPERTIES OF SYSTEMS USED

NAME	Viscosity μ at $2^{o}C$ Cp	Density at 2^{o} C Kg/m^3	Interfacial tension, N/m
Kerosene	1.557	0.7428×10^{-3}	0.0140
B.P. EM.35c OIL	8.613	0.870×10^{-3}	4.50×10^{-2}
B.P. C.S. 40 OIL	12.012	0.8401×10^{-3}	0.0011
PARAFFIN	34.387	0.8704×10^{-3}	0.0385

(a) Viscosity of the liquids was measured using Cannon-Feuske viscometer, type B.S./IP/CF

(b) Density of the liquid was determined by density bottle method.

(c) Interfacial tension with water for each liquid was measured by Torsion balance method.

APPENDIX B

OPERATIONAL CHARACTERISTIC STUDIES

Viz:

B.1 Hold-up Studies Results

B.2 Flooding Results

B.3 Pressure Characteristics

TABLE B.1. HOLD-UP STUDIES BY DISPLACEMENT METHOD

Q_H IN THE RANGE

Q_L IN THE RANGE

SPEED OF ROTATION ω r.p.m.	SYSTEM	LIGHT-LIQUID-OUT PRESSURE P_{LO} Kg/cm^2	VOLUME OF LIGHT PHASE $V_L = V_{CL} + V_{SL}$ cc	VOLUME OF HEAVY PHASE $V_H = V_{CH} + V_{SH}$ cc	TOTAL CONTACTOR VOLUME $V_E = V_H + V_L$ cc
2750	KEROSENE/ WATER	0.583	930.6	4060.8	4991.4
		0.916	1758.2	3186.5	4944.7
		1.012	2236.3	2680.3	4916.6
		1.434	2948.8	2019.8	4968.6
		1.863	3715.1	1141.3	4856.4
		2.137	4328.7	585.9	4914.6
	PARAFFIN/ WATER	0.353	1232.4	3682.7	4915.1
		0.614	1885.3	3045.1	4930.4
		0.899	2749.6	2210.6	4960.2
		1.172	4017.0	878.5	4895.5
		1.392	4661.4	265.3	4926.7
4600	KEROSENE/ WATER	0.752	521.8	4410.6	4932.4
		1.691	1146.3	3795.5	4941.8
		2.749	2337.4	2570.9	4908.3
		3.614	3069.5	1883.1	4952.6
		4.061	3744.2	1170.8	4915.0
		4.912	4513.2	415.4	4928.6
	PARAFFIN/ WATER	0.603	752.2	4139.6	4891.8
		1.254	1729.3	3206.3	4935.6
		2.008	2727.3	2214.5	4941.8
		2.554	3713.4	1225.3	4938.7
		3.138	4675.8	255.8	4931.6

APPENDIX B.2 FLOODING STUDIES

SPEED OF ROTATION ω (r.p.m.)	PHASE RATIO $(\frac{Q_K}{Q_W})$	COMBINED FLOW RATES L/min	BACK PRESSURE $P_{LLO} = P_{LO}\ P_{HO}$ 0.01335 x Kg/cm^2
4600	0.5	0.63	1.9
		0.94	3.6
		1.25	3.4
		1.54	6.6
		1.76	16.0
		1.54	28.4
		0.56	32.3
	2.0	1.26	3.1
		1.55	2.8
		1.78	5.9
		1.89	16.2
		1.53	25.5
		0.54	28.6
3460	0.5	0.53	1.9
		0.94	2.7
		1.24	4.1
		1.40	15.9
		1.26	24.1
		0.65	25.4
	2.0	0.55	2.3
		0.94	1.6
		1.23	3.8
		1.54	13.0
		1.39	18.1
		0.95	19.9
		0.56	20.8
2750	0.5	0.63	2.1
		0.92	2.4
		1.25	6.0
		1.24	14.2
		0.93	19.5
		0.56	20.3
	2.0	0.95	1.8
		1.24	8.1
		1.26	13.2
		0.93	14.7
		0.56	16.3

APPENDIX B.3 PRESSURE LOSS RESULTS

SPEED OF ROTATION (r.p.m.)	FLOW RATE Q L/m	PRESS DROP 0.01335xKg/cm^2	
0	0.62	0.3	
	1.09	0.9	
	1.69	1.9	
	2.35	2.3	
	3.08	6.4	
	4.72	11.8	
2750	0.64	4.3	
	0.81	3.8	
	0.93	3.7	
	1.07	3.4	
	1.25	3.7	
	1.55	5.6	
	1.89	9.1	
	2.18	14.0	
	2.50	14.1	
	3.24	16.4	
	3.61	19.1	
	4.0	22.8	
	4.61	29.7	
3460	0.62	6.3	
	0.79	5.5	
	0.91	6.0	
	1.08	5.7	
	1.24	6.8	
	1.54	8.8	
	1.89	10.6	
	2.18	12.8	
	3.25	24.0	
	4.0	27.2	
4600	0.94	8.1	
	1.24	8.8	
	1.54	10.9	
	1.90	13.8	
	2.18	16.3	
	2.50	16.3	
	2.87	19.9	
	3.25	26.1	
	3.63	29.6	
	4.06	34.0	

APPENDIX C

DISCHARGE RATE STUDIES

TABLE C.1

ω = 1750 r.p.m.

C.1.1 KEROSENE/WATER SYSTEM

Nozzle Diameter D_N cm	Nozzle Velocity U_N cm/s	Flow Rate Q_a cc/s	Theoretical Flowrate $Q_T=\omega A_o(\frac{\Delta\rho}{\rho}(R_c^2-R_i^2))^{\frac{1}{2}}$	$C_{od}=\frac{Q_T}{Q_a}$	$\frac{\rho_d U_N}{\Delta\rho\omega R}$
0.856	16.71	9.62	2.0813	0.2164	0.1513
	23.43	13.48	4.63260	0.3436	0.2121
	32.43	18.66	9.7347	0.5216	0.2936
	35.75	20.58	14.0559	0.6831	0.3237
	39.55	22.76	14.8553	0.6526	0.3581
	42.33	24.36	14.6616	0.6019	0.3832
	44.30	25.50	16.9068	0.6631	0.4011
	50.46	29.04	17.1553	0.5908	0.4568
	56.54	32.54	21.2713	0.6537	0.5119
	61.08	35.15	21.8473	0.6215	0.5530
	83.52	48.06	31.8224	0.6621	0.7561
0.50	18.03	3.54	0.7635	0.2157	0.1632
	21.55	4.23	1.4158	0.3346	0.1951
	32.54	6.39	3.1455	0.4923	0.2946
	34.30	6.73	4.1267	0.6128	0.3105
	43.65	8.57	4.9061	0.5724	0.3952
	47.60	9.35	6.3577	0.6803	0.4309
	54.80	10.76	6.5289	0.6068	0.4961
	71.50	14.04	8.8669	0.6316	0.6473
	87.68	17.22	11.3488	0.6592	0.7938
0.350	16.05	1.54	0.3493	0.2262	0.1453
	23.89	2.30	0.9121	0.3968	0.2163
	33.20	3.20	1.8477	0.5784	0.3006
	38.88	3.74	2.5411	0.6793	0.3520
	44.13	4.25	2.5584	0.6026	0.3995
	52.94	5.09	3.1840	0.6251	0.4793
	60.71	5.84	3.6201	0.6198	0.5496
	73.28	7.05	4.5346	0.6432	0.6634
	88.01	8.47	5.3982	0.6375	0.7968

TABLE C.1.2

ω = 1750 r.p.m.

PARAFFIN/WATER SYSTEM

Nozzle Diameter D_N cm	Nozzle Velocity U_N cm/s	Flow Rate Q_a cc/s	Theoretical Flow rate $Q_T=\omega A_o(\frac{\Delta\rho}{\rho}(R_c^2-R_i^2))^{\frac{1}{2}}$ cc	$C_{od}=\frac{Q_T}{Q_a}$	$(\frac{\rho_d U_N}{\Delta\rho\omega R})$
0.856	6.64	3.82	0.8066	0.2112	0.1613
	8.73	5.02	1.6150	0.3216	0.2121
	10.02	5.77	2.1012	0.3643	0.2436
	11.99	6.90	3.7463	0.5428	0.2915
	14.27	8.21	5.7584	0.7011	0.3469
	15.09	8.68	5.6660	0.6526	0.3667
	16.15	9.30	6.4538	0.6943	0.3926
	17.33	9.97	6.0743	0.6091	0.4212
	20.29	11.68	7.3968	0.6333	0.4933
	25.18	14.49	9.3578	0.6457	0.6121
	31.56	18.16	11.8422	0.6521	0.7670
0.50	7.59	1.49	0.3031	0.2033	0.1609
	9.26	1.82	0.5540	0.3046	0.1963
	12.03	2.36	0.9737	0.4123	0.2549
	13.88	2.73	1.5071	0.5531	0.2941
	14.52	2.85	1.7516	0.6142	0.3078
	16.74	3.29	2.1400	0.6510	0.3548
	18.87	3.70	1.9210	0.5186	0.3998
	23.09	4.53	2.8080	0.6194	0.4893
	28.77	5.65	3.8023	0.6731	0.6097
	40.03	7.86	5.2511	0.6681	0.8483
0.350	7.94	0.76	0.1645	0.2153	0.1683
	10.60	1.02	0.3628	0.3558	0.2246
	13.15	1.27	0.6749	0.5336	0.2786
	17.32	1.67	0.0380	0.6228	0.3671
	21.37	2.06	1.2094	0.5883	0.4528
	24.02	2.31	1.5123	0.6543	0.5091
	31.78	3.06	2.0633	0.6749	0.6734
	43.05	4.14	2.7920	0.6741	0.9123

TABLE C.2.1

ω = 2750 r.p.m.

KEROSENE/WATER SYSTEM

Nozzle Diameter D_N cm	Nozzle Velocity U_N cm/s	Flowrate Q_a cc/s	Theoretical Flowrate $Q_T=\omega A_o(\frac{\Delta\rho}{\rho}(R_c^2-R_i^2))^{\frac{1}{2}}$ cc	$C_{od}=\frac{Q_T}{Q_a}$	$\frac{\rho_d U_N}{\Delta\rho\omega R}$
0.856	15.99	27.79	3.1393	0.1963	0.1601
	20.10	34.92	7.4343	0.3699	0.2012
	25.10	43.62	10.5531	0.4204	0.2513
	30.88	53.65	22.8453	0.7399	0.3091
	33.05	57.44	20.0438	0.6064	0.3309
	37.10	64.47	25.2202	0.6798	0.3714
	40.32	70.05	25.3950	0.6299	0.4036
	44.05	76.55	27.3165	0.6201	0.4410
	44.87	77.97	31.0776	0.6926	0.4492
	49.95	86.79	30.7564	0.6158	0.5019
0.50	5.63	28.69	1.1684	0.2074	0.1653
	6.21	31.61	1.7042	0.2746	0.1821
	7.56	38.48	2.7856	0.3651	0.2217
	10.25	52.21	5.8055	0.5663	0.3008
	13.34	67.94	8.9148	0.6683	0.3914
	16.99	86.51	10.5841	0.6231	0.4984
0.350	2.67	27.74	0.5543	0.2077	0.1598
	3.57	37.08	1.3619	0.3818	0.2136
	4.93	51.27	2.8578	0.5793	0.2954
	5.69	59.15	3.8627	0.6787	0.3408
	6.97	72.47	4.2712	0.6126	0.4175
	7.15	74.34	4.2830	0.5988	0.4283
	8.15	84.72	5.0725	0.6223	0.4881
	8.66	89.96	5.2738	0.6093	0.5183

TABLE C.2.2

ω = 2750 r.p.m.

PARAFFIN/WATER SYSTEM

Nozzle Diameter D_N cm	Nozzle Velocity U_N cm/s	Flowrate Q_a cc/s	Theoretical flowrate $Q_T=\omega A_o(\frac{\Delta\rho}{\rho}(R_c^2-R_i^2))^{\frac{1}{2}}$	$C_{od}=\frac{Q_T}{Q_a}$	$\frac{\rho_d U_N}{\Delta\rho\omega R}$
0.856	11.34	6.52	1.3996	0.2145	0.1529
	14.96	8.61	2.9994	0.3483	0.2018
	17.97	10.34	4.3034	0.4162	0.2423
	20.99	12.08	6.2253	0.5153	0.2831
	23.09	13.29	8.7943	0.6618	0.3114
	26.35	15.16	11.5549	0.7621	0.3553
	28.59	16.45	11.6929	0.7100	0.3856
	29.17	16.79	9.8578	0.5872	0.3934
	33.67	19.38	12.5860	0.6495	0.4541
	37.09	21.35	13.6097	0.6376	0.5002
	44.00	25.32	16.0392	0.6334	0.5934
	49.18	28.30	17.3231	0.6121	0.6632
	58.59	33.72	20.4152	0.6055	0.7901
0.50	10.11	1.99	0.4270	0.2150	0.1364
	16.95	3.33	1.3699	0.4116	0.2286
	20.49	4.02	1.9060	0.4738	0.2763
	22.03	4.33	2.4349	0.5629	0.2971
	25.29	4.97	3.2857	0.6618	0.3410
	30.20	5.93	3.6085	0.6085	0.4073
	32.75	6.43	4.6058	0.7162	0.4417
	38.31	7.52	4.7688	0.6339	0.5167
	47.32	9.29	5.8075	0.6251	0.6381
	60.35	11.85	7.2155	0.6098	0.8139
0.350	10.55	1.02	0.2067	0.2036	0.1423
	15.48	1.49	0.4642	0.3116	0.2088
	20.34	1.96	0.9649	0.4931	0.2743
	21.97	2.11	1.1451	0.5417	0.2963
	25.40	2.44	1.6699	0.6834	0.3425
	28.38	2.73	1.6917	0.6196	0.3827
	32.75	3.15	1.9080	0.6055	0.4417
	45.49	4.38	2.6441	0.6041	0.6135

TABLE C.3.1

ω = 3460 r.p.m.

KEROSENE/WATER SYSTEM

Nozzle Diameter D_N cm	Nozzle Velocity U_N cm/s	Flowrate Q_a cc/s	Theoretical flowrate $Q_T=\omega A_o(\frac{\Delta\rho}{\rho}(R_c^2-R_i^2))^{\frac{1}{2}}$ cc	$C_{od}=\frac{Q_T}{Q_a}$	$\frac{\rho_d U_N}{\Delta\rho\omega R}$
0.856	29.75	17.12	2.9579	0.1728	0.1362
	43.62	24.90	7.0559	0.2834	0.1981
	62.66	36.06	19.5145	0.5412	0.2869
	72.16	41.52	30.7367	0.7409	0.3304
	77.29	44.43	31.7084	0.7137	0.3535
	89.15	51.30	37.9385	0.7395	0.4082
	98.73	56.82	44.8482	0.7893	0.4521
	107.43	61.82	40.6852	0.6581	0.4919
0.50	30.75	6.04	1.1254	0.1864	0.1408
	38.76	7.61	1.4903	0.1958	0.1775
	59.64	11.71	5.9057	0.5043	0.2731
	64.73	12.71	7.7009	0.6059	0.2964
	68.62	13.47	10.0783	0.7482	0.3142
	81.85	16.07	10.1139	0.6293	0.3748
	108.82	21.37	12.9508	0.6061	0.4983
0.350	29.98	2.88	0.5092	0.1765	0.1373
	41.41	3.98	1.2417	0.3117	0.1896
	51.26	4.93	2.0357	0.4128	0.2347
	58.42	5.62	3.3336	0.5931	0.2675
	74.60	7.18	4.8656	0.6779	0.3416
	94.28	9.07	5.4855	0.6048	0.4317
	107.60	10.35	6.3528	0.6138	0.4927

TABLE C.3.2

ω = 3460 r.p.m.

PARAFFIN/WATER SYSTEM

Nozzle Diameter D_N cm	Nozzle Velocity U_N cm/s	Flowrate Q_a cc/s	Theoretical Flowrate $Q_T = \omega A_o \left(\frac{\Delta\rho}{\rho}(R_c^2 - R_i^2)\right)^{\frac{1}{2}}$ cc	$C_{od} = \frac{Q_T}{Q_a}$	$\frac{\rho_d U_N}{\Delta\rho\, \omega R}$
0.856	13.36	7.69	1.3286	0.1728	0.1432
	18.32	10.54	3.3100	0.3139	0.1964
	22.97	13.22	6.0991	0.4614	0.2462
	27.74	15.96	9.8248	0.6155	0.2973
	32.53	18.72	13.7832	0.7362	0.3487
	34.64	19.94	13.5023	0.6773	0.3713
	37.33	21.48	15.7977	0.7354	0.4001
	40.71	23.43	15.2323	0.6501	0.4364
	45.64	26.27	15.5125	0.5906	0.4892
	56.57	32.55	19.0564	0.5854	0.6053
	75.30	43.33	26.9407	0.6217	0.8071
0.50	12.73	2.50	0.4565	0.1827	0.1364
	20.39	4.00	1.4606	0.3649	0.2185
	23.80	4.67	2.5735	0.5507	0.2551
	27.65	5.43	3.5271	0.6496	0.2964
	31.35	6.15	4.7604	0.7741	0.3357
	32.77	6.43	4.1708	0.6483	0.3512
	46.42	9.11	5.6249	0.6172	0.4975
	65.48	12.86	8.0762	0.6282	0.7018
	79.46	15.60	10.0102	0.6416	0.8517
0.350	13.41	1.29	0.2409	0.1868	0.1437
	19.89	1.91	0.6736	0.3520	0.2132
	21.73	2.09	0.9892	0.4732	0.2329
	28.15	2.71	0.5959	0.5893	0.3017
	29.55	2.84	2.0283	0.7135	0.3167
	33.30	3.20	2.2194	0.6928	0.3596
	47.94	4.61	2.8968	0.6281	0.5138
	67.32	6.48	4.0878	0.6311	0.7216
	77.69	7.47	4.8038	0.6427	0.8327

TABLE C.4.1

ω = 4600 r.p.m.

KEROSENE/WATER SYSTEM

Nozzle Diameter D_N cm	Nozzle Velocity U_N cm/s	Flowrate Q_a cc/s	Theoretical flowrate $Q_T = \omega A_o(\frac{\Delta\rho}{\rho}(R_c^2 - R_i^2))^{\frac{1}{2}}$	$C_{od} = \frac{Q_T}{Q_a}$	$\frac{\rho_d U_N}{\Delta\rho\omega R}$
	41.69	23.99	4.2518	0.1772	0.1436
	58.30	33.55	10.9278	0.3257	0.2008
	86.03	49.51	32.7896	0.6623	0.2963
	98.46	56.66	40.4043	0.7131	0.3391
	100.37	57.76	44.1252	0.7639	0.3457
0.856	113.99	65.60	44.7192	0.6817	0.3926
	42.74	8.39	1.4836	0.1768	0.1472
	52.35	10.28	2.7166	0.2643	0.1803
	78.33	15.38	7.4121	0.4819	0.2698
0.50	86.75	17.03	10.1541	0.5961	0.2988
	93.66	18.39	14.4095	0.7835	0.3226
	102.11	20.05	13.4816	0.6724	0.3517
	118.61	23.29	14.1499	0.6076	0.4084
	42.88	4.13	0.7682	0.1862	0.1477
	65.44	6.30	2.1949	0.3486	0.2254
	78.95	7.60	4.3521	0.5734	0.2719
0.350	87.34	8.40	5.7289	0.6818	0.3008
	109.78	10.56	6.3287	0.5992	0.3781
	116.63	11.52	6.8326	0.6089	0.4017

TABLE C.4.2

ω = 4600 r.p.m.

PARAFFIN/WATER SYSTEM

Nozzle Diameter D_N cm	Nozzle Velocity U_N cm/s	Flowrate Q_a cc/s	Theoretical Flowrate $Q_T=\omega A_o(\frac{\Delta\rho}{\rho}(R_c^2-R_i^2))^{\frac{1}{2}}$	$C_{od}=\frac{Q_T}{Q_a}$	$\frac{\rho_d U_N}{\Delta\rho\omega R}$
0.856	19.13	11.01	1.7864	0.1623	0.1542
	21.00	12.08	3.1088	0.2574	0.1692
	24.65	14.18	5.4124	0.3816	0.1987
	37.16	21.39	11.4671	0.5362	0.2996
	42.71	24.58	17.5181	0.7128	0.3443
	45.45	26.15	20.1778	0.7715	0.3664
	53.25	30.64	19.3945	0.6329	0.4293
	61.22	35.23	22.2712	0.6321	0.4936
	73.59	42.35	25.7998	0.6092	0.5933
	97.05	55.85	34.9109	0.6251	0.7824
	112.39	64.68	41.6205	0.6435	0.9061
0.50	17.63	3.46	0.5406	0.1562	0.1421
	20.32	3.99	0.9865	0.2473	0.1638
	27.49	5.40	2.2338	0.4139	0.2216
	37.16	7.30	4.6603	0.6387	0.2996
	44.14	8.67	5.5690	0.6425	0.3569
	50.77	9.97	7.0797	0.7101	0.4093
	64.09	12.58	8.2236	0.6535	0.5167
	75.48	14.82	9.6046	0.6481	0.6085
	106.88	20.99	13.9180	0.6632	0.8617
0.350	18.77	1.81	0.3019	0.1672	0.1513
	23.43	2.25	0.6134	0.2721	0.1889
	28.74	2.77	1.4035	0.5076	0.2317
	36.31	3.49	2.2446	0.6426	0.2927
	46.74	4.50	3.2613	0.7253	0.3768
	52.11	5.01	2.8696	0.5724	0.4201
	63.03	6.06	3.8189	0.6297	0.5082
	78.56	7.56	4.9532	0.6553	0.6334
	102.89	9.90	6.5640	0.6631	0.8295

APPENDIX D

DROPLET FORMATION STUDIES

(a) TABLES D_1 to D_4 GIVE MATHEMATICAL MODEL VALUES.

(b) TABLES D_5 to D_8 GIVE EXPERIMENTAL VALUES

TABLE D.1-I KEROSENE/WATER SYSTEM ω = 1750 r.p.m.

D_N cm	FLOW RATE $Q_{cc/s}$	NOZZLE VELOCITY U_N cm/s	$F_S = \frac{\pi\sigma D_N}{g\Delta\rho}$	$F_D = \frac{10.8\mu D_N}{D_F^2 g\Delta\rho} \cdot Q$	$F_{CE} = \frac{\omega^2 R}{g}$	$F_K = \frac{3.1\rho_d}{g\Delta\rho} \cdot QU_N$	$F_S + F_D - F_{CE} - F_K$	PREDICTED VOLUME V_F cc
.856	19.11	33.21	0.1502	18.2933	9.5475	5.8305	3.0655	0.7432
	22.80	39.62	0.1502	21.8256	9.5475	8.2989	4.1294	2.6841
	26.37	45.83	0.1502	25.2430	9.5475	11.1028	4.7429	3.1601
	28.31	49.19	0.1502	27.1001	9.5475	12.7935	4.9093	3.7607
	31.83	55.31	0.1502	30.4696	9.5475	16.1739	4.8984	4.6632
	34.58	60.08	0.1502	33.1021	9.5475	19.0866	4.6182	4.6082
0.50	6.60	33.61	0.0877	11.6538	9.5475	2.0379	0.1561	0.1249
	7.93	40.38	0.0877	14.0023	9.5475	2.9418	1.6007	0.8639
	9.66	49.19	0.0877	17.0570	9.5475	4.3654	3.2318	1.9391
	10.25	52.18	0.0877	18.0987	9.5475	4.9136	3.7253	2.2352
	11.02	56.13	0.0877	19.4584	9.5475	5.6826	4.3160	2.5896
	11.78	60.0	0.0877	20.8003	9.5475	6.4934	4.8471	2.9050
0.350	3.95	41.10	0.06142	11.2449	9.5475	1.4915	0.2674	0.2139
	4.27	44.38	0.06142	12.1559	9.5475	1.7410	0.9288	0.6235
	4.73	49.19	0.06142	13.4654	9.5475	2.1375	1.8418	1.1972
	5.47	56.81	0.06142	15.5721	9.5475	2.8549	3.2311	1.9386
	5.78	60.08	0.06142	16.4546	9.5475	3.1903	3.7782	2.2669
	6.27	65.16	0.06142	17.8495	9.5475	3.7534	4.6100	2.7660

TABLE D.1.2 E.M.35C OIL/WATER SYSTEM

ω = 1750 r.p.m.

NOZZLE DIAMETER D_N m	FLOW RATE Q cc/s	NOZZLE VELOCITY U_N	$F_S = \frac{\sigma \pi D_N}{g \Delta \rho}$	$F_D = \frac{10.8 \mu D_N}{D_F^2 g \Delta \rho} . Q$	$F_{CE} = \frac{\omega^2 R}{g}$	$F_K = \frac{3.1 \rho_d}{g \Delta \rho} . Q U_N$	$F_1 + F_D - F_{CE} - F_K$	PREDICTED VOLUME V_F cc
.856	12.66	22.0	0.09619	16.2281	9.5475	5.9706	0.8062	0.6853
	15.54	27.0	0.09619	21.0496	9.5475	8.9945	2.6038	2.2132
	17.61	30.6	0.09619	26.4926	9.5475	11.5516	5.4897	3.5683
	18.99	33.0	0.09619	30.2051	9.5475	13.4338	7.3200	4.3920
	21.81	37.9	0.09619	35.8113	9.5475	17.7197	8.6403	5.1842
	24.17	42.0	0.09619	40.2103	9.5475	21.7615	8.9975	5.3985
.050	4.59	23.4	0.05618	12.5874	9.5475	2.3025	0.7936	0.6745
	5.89	30.0	0.05618	16.0975	9.5475	3.7879	2.8183	2.1137
	7.07	36.0	0.05618	20.4962	9.5475	5.4561	5.5487	3.3293
	8.25	42.0	0.05618	23.8349	9.5475	7.4279	6.9157	4.1494
0.350	2.41	25.0	0.03933	11.5219	9.5475	1.2916	0.7221	0.6138
	2.89	30.0	0.03933	13.7963	9.5475	1.8586	2.4295	1.5792
	3.46	36.0	0.03933	16.6934	9.5475	2.6702	4.5150	2.7090
	4.04	42.0	0.03933	18.6458	9.5475	3.6374	5.5002	3.3001

TABLE D.1.3 C.S. 40 OIL/WATER SYSTEM ω = 1750 r.p.m.

D_N cm	FLOW RATE Q cc/s	NOZZLE VELOCITY U_N cm/s	$F = \frac{\pi\sigma D_N}{g\Delta\rho}$	$F_D = \frac{10.8\mu D_N}{D_F^2 g\Delta\rho}.Q$	$F_{CE} = \frac{\omega^2 R}{g}$	$F_K = \frac{3.1\rho_d}{g\Delta\rho}.QU_N$	$F_1+F_D-F_{CE}-F_K$	PREDICTED VOLUME.V_F cc
.856	12.66	22.0	0.01906	15.1797	9.5475	4.6722	0.9791	0.8322
	14.96	26.0	0.01906	19.2224	9.5475	6.5249	3.1691	2.3768
	16.06	27.9	0.01906	21.0742	9.5475	7.5165	4.0293	2.8205
	19.57	34.0	0.01906	28.2594	9.5475	11.1619	7.5691	4.5415
	22.90	39.8	0.01906	33.4698	9.5475	15.2893	8.6521	5.1912
0.50	4.81	24.5	0.01113	12.3946	9.5475	1.9769	0.8813	0.7932
	5.97	30.4	0.01113	15.5254	9.5475	3.0445	2.9445	2.3556
	6.73	34.3	0.01113	17.7201	9.5475	2.8724	4.3113	3.2335
	7.78	39.6	0.01113	20.8532	9.5475	5.1682	6.1375	3.9894
0.350	2.69	28.0	0.007792	11.6184	9.5475	1.8635	0.8152	0.6521
	3.22	33.5	0.007792	13.7618	9.5475	1.8095	2.4126	1.6888
	3.56	37.0	0.007792	15.6071	9.5475	2.2096	3.8578	2.3147
	3.90	40.5	0.007792	16.7875	9.5475	2.6496	4.5982	2.7589

TABLE D.1.4 PARAFFIN/WATER SYSTEM ω = 1750 r.p.m.

D_N cm	FLOWRATE Q cc/s	NOZZLE VELOCITY U_N cm/s	$F_S = \frac{\pi\rho D_N}{g\Delta\rho}$	$F_D = \frac{10.8\mu D_N}{D_F^2 g\Delta\rho}.Q$	$F_{CE} = \frac{\omega^2 R}{g}$	$F_K = \frac{3.1\rho_d}{g\Delta\rho}.QU_N$	$F_S+F_D-F_{CE}-F_K$	PREDICTED VOLUME $-V_F$
	11.51	20.0	0.8252	18.6576	9.5475	4.9505	4.9848	2.0438
	13.81	24.0	0.8252	22.3859	9.5475	7.1276	6.5361	3.2681
	16.11	28.0	0.8252	26.1142	9.5475	9.7005	7.6914	4.2533
.856	18.42	32.0	0.8252	29.8586	9.5475	12.6760	8.4604	5.0762
	20.72	36.0	0.8252	33.5869	9.5475	16.0411	8.8235	5.2941
	23.02	40.0	0.8252	37.3152	9.5475	19.8018	8.6553	5.4096
	6.28	32.0	0.4820	15.7610	9.5475	4.3239	2.3716	1.4230
	7.07	36.0	0.4820	17.7346	9.5475	5.4727	3.1964	2.1736
	7.85	40.0	0.4820	19.6912	9.5475	6.7526	3.8731	3.0597
0.50	8.64	44.0	0.4820	21.6729	9.5475	8.1754	4.4320	3.8558
	9.43	48.0	0.4820	23.6545	9.5475	9.7341	4.8549	4.4665
	10.21	52.0	0.4820	25.6111	9.5475	11.4175	5.1281	4.8204
	3.37	35.0	0.3374	13.9651	9.5475	2.5365	2.2185	1.3311
	3.66	38.0	0.3374	15.1668	9.5475	2.9909	2.9658	1.7795
	4.04	42.0	0.3374	16.7415	9.5475	3.6490	3.8824	2.3294
0.350	4.52	47.0	0.3374	18.7306	9.5475	4.5685	4.9520	2.9712
	5.39	56.0	0.3374	22.3358	9.5475	6.4911	6.6346	3.9808
	5.97	62.0	0.3374	24.7393	9.5475	7.9600	7.5692	4.1920

TABLE D.2.1 KEROSENE/WATER SYSTEM ω = 2750 r.p.m.

D_N cm	FLOWRATE Q cc/s	NOZZLE VELOCITY U_N cm/s	$F_S = \frac{\pi\sigma D_N}{g\Delta\rho}$	$F_D = \frac{10.8\mu D_N}{D_F^2 g\Delta\rho}.Q$	$F_{CE} = \frac{\omega^2 R}{g}$	$F_K = \frac{3.1\rho_d}{g\Delta\rho}.QU_N$	$F_S+F_D-F_{CE}-F_K$	PREDICTED VOLUME - V_F cc
.856	21.91	38.07	0.1502	31.5221	23.5766	7.6630	0.4324	0.4324
	24.65	42.83	0.1502	35.4614	23.5766	9.6993	2.3375	1.4025
	28.31	49.19	0.1502	41.0265	23.5766	12.7935	4.8066	2.8839
	33.96	59.01	0.1502	48.8585	23.5766	18.4106	6.8703	4.122
	36.39	63.23	0.1502	52.736	23.5766	21.1387	8.1708	4.82
	39.99	69.48	0.1502	57.4214	23.5766	25.5261	8.3176	4.86
0.50	6.9	35.14	0.0877	25.6495	23.5766	2.1275	0.0331	0.01986
	7.0	35.65	0.0877	26.0213	23.5766	2.2926	0.2398	
	7.5	38.20	0.0877	27.8799	23.5766	2.6321	1.7589	
	7.8	39.73	0.0877	28.9952	23.5766	2.847	2.6593	1.5956
	8.12	41.35	0.0877	30.1847	23.5766	3.0846	3.6112	2.1667
	9.19	46.81	0.0877	34.1623	23.5766	3.9521	6.7194	4.0316
0.350	6.12	63.61	0.06142	27.3433	23.5766	3.5764	0.2517	
	6.73	69.95	0.06142	30.0687	23.5766	4.3249	2.2286	
	7.09	73.69	0.06142	31.6772	23.5766	4.7998	3.3622	2.0173
	7.69	79.92	0.06142	34.3578	23.5766	5.6462	5.1964	3.116
	7.91	82.21	0.06142	35.3408	23.5766	5.9741	5.8515	3.5109

TABLE D.2.2 E.M.35C OIL/WATER SYSTEM

$\omega = 2750$ r.p.m.

NOZZLE DIAMETER D_N m	FLOW RATE Q cc/s	NOZZLE VELOCITY U_N cm/s	$F_S = \frac{\sigma \pi D_N}{g \Delta \rho}$	$F_D = \frac{10.8 \mu D_N}{D_F^2 g \Delta \rho} . Q$	$F_{CE} = \frac{\omega^2 R}{g}$	$F_K = \frac{3.1 \rho_d}{\Delta \rho g} . Q U_{UN}$	$F_1 + F_D - F_{CE} - F_K$	PREDICTED VOLUME. V_F cc
0.856	13.81	24.0	0.09619	31.4361	23.5766	7.1051	0.8506	0.6804
	17.26	30.0	0.09619	37.6795	23.5766	11.1000	3.0991	2.0143
	20.72	36.0	0.09619	45.3986	23.5766	15.9902	5.9280	3.5568
	24.17	42.0	0.09619	52.2408	23.5766	21.7615	6.9989	4.1993
0.50	5.11	26.0	0.05618	27.0831	23.5766	2.8481	0.7146	0.5717
	6.28	32.0	0.05618	30.6453	23.5766	4.3080	2.8167	1.8310
	7.46	38.0	0.05618	34.3028	23.5766	6.0769	4.7055	2.8233
	8.64	44.0	0.05618	36.8864	23.5766	8.1495	5.21611	3.1298
0.350	2.69	28.0	0.03933	25.8695	23.5766	1.6146	0.7176	0.5382
	3.17	33.0	0.03933	27.6437	23.5766	2.2425	1.8639	1.2116
	3.75	39.0	0.03933	30.1098	23.5766	3.1351	3.4374	2.0625
	3.85	40.0	0.03933	30.8752	23.5766	3.3013	4.0366	2.4220

TABLE D.2.3 C.S.40 OIL/WATER SYSTEM ω = 2750 r.p.m.

D_N cm	FLOWRATE Q cc/s	NOZZLE VELOCITY U_N cm/s	$F = \frac{\pi \sigma D_N}{g \Delta\rho}$	$F_D = \frac{10.8 \mu D_N}{D_F^2 g \Delta\rho} . Q$	$F_{CE} = \frac{\omega^2 R}{g}$	$F_K = \frac{3.1 \rho_d}{g \Delta\rho} . QU_N$	$F_1 + F_D - F_{CE} - F_K$	PREDICTED VOLUME - V_F cc
.856	13.75	23.9	0.01906	29.8453	23.5766	5.5128	0.7111	0.6186
	16.69	29.0	0.01906	34.3569	23.5766	8.1194	2.6799	2.0099
	18.70	32.5	0.01906	38.3826	23.5766	10.1951	4.6299	2.7780
	20.60	35.8	0.01906	41.9589	23.5766	12.3714	6.0299	3.6179
	23.83	41.4	0.01906	47.7573	23.5766	16.5498	7.6496	4.590
0.50	5.01	25.5	0.01113	26.2277	23.5766	2.1431	0.5191	0.4412
	6.16	31.4	0.01113	30.2902	23.5766	3.2447	3.4800	2.6101
	6.83	34.8	0.01113	31.2616	23.5766	3.9872	3.7089	2.2253
	7.54	38.4	0.01113	33.1206	23.5766	4.8441	4.7110	2.8266
	8.29	42.2	0.01113	34.8623	23.5766	5.8686	5.4282	3.2569
0.350	2.87	29.8	0.00779	25.4916	23.5766	1.4347	0.4881	0.4149
	3.45	35.9	0.00779	27.5043	23.5766	2.0777	1.8578	1.3934
	3.87	40.2	0.00779	28.8846	23.5766	2.6098	2.7060	1.8942
	4.17	43.4	0.00779	30.2325	23.5766	3.0359	2.6278	2.1767

TABLE D.2.4 PARAFFIN/WATER SYSTEM

ω = 2750

NOZZLE DIAMETER D_N m	FLOWRATE Q cc/s	NOZZLE VELOCITY U_N cm/s	$F_S = \frac{\pi\sigma D_N}{g\Delta\rho}$	$F_D = \frac{10.8\mu D_N}{D_F^2 g\Delta\rho} \cdot Q$	$F_{CE} = \frac{\omega^2 R}{g}$	$F_K = \frac{3.1\rho_d}{g\Delta\rho} \cdot QU_N$	$F_S+F_D-F_{CE}-F_K$	PREDICTED VOLUME-V_F cc
.856	14.32	24.88	0.8252	31.2085	23.5766	7.6619	0.7952	0.4771
	16.11	27.99	0.8252	35.1095	23.5766	9.6971	2,6610	1.5966
	18.50	32.15	0.8252	40.3182	23.5766	12.7907	4.7698	2.8619
	22.20	38.57	0.8252	48.3819	23.5766	18.4138	7.2167	4.3300
	23.78	41.32	0.8252	51.8253	23.5766	21.1307	7.9423	4.7659
	26.13	45.41	0.8252	56.9468	23.5766	25.5171	8.6783	5.207
0.50	7.79	39.65	0.4820	30.7440	23.5766	7.6137	0.03575	0.02824
	8.19	41.71	0.4820	32.3227	23.5766	8.4259	0.8021	0.5454
	9.09	46.32	0.4820	35.8746	23.5766	10.3852	2.3948	1.4368
	9.76	49.71	0.4820	38.5189	23.5766	11.9661	3.4582	2.0749
	10.24	52.15	0.4820	40.4132	23.5766	13.1720	4.1466	2.4879
	11.45	58.31	0.4820	45.1886	23.5766	16.4676	5.6264	3.3758
	11.99	61.06	0.4820	47.3198	23.5766	18.0588	6.1664	3.6998
0.350	5.54	57.61	0.3374	31.0388	23.5766	7.3382	0.4614	0.3645
	5.91	61.38	0.3374	33.0955	23.5766	8.9474	0.9089	0.6817
	6.69	69.61	0.3374	37.4634	23.5766	11.4863	2.7379	1.6427
	6.95	72.22	0.3374	38.9194	23.5766	12.3801	3.3001	1.9801
	7.25	75.31	0.3374	40.5994	23.5766	13.4670	3.892	2.3353
	7.49	77.81	0.3374	41.9433	23.5766	14.3747	4.3294	2.5977

TABLE D.3.1 KEROSENE/WATER SYSTEM

ω = 3460 r.p.m.

NOZZLE DIAMETER D_N m	FLOW RATE Q cc/s	NOZZLE VELOCITY U_N cm/s	$F_S = \frac{\pi\sigma D_N}{g\Delta\rho}$	$F_D = \frac{10.8\mu D_N}{D_F^2 g\Delta\rho}.Q$	$F_{CE} = \frac{\omega^2 R}{g}$	$F_K = \frac{3.1\rho_d}{g\Delta\rho}.QU_N$	$F_S+F_D-F_{CE}-F_K$	PREDICTED VOLUME-V_F cc
.856	23.02	40.0	0.1502	46.0205	37.3223	8.4594	0.3891	0.3113
	26.47	46.0	0.1502	50.4086	37.3223	11.1863	2.0502	1.2301
	28.31	49.19	0.1502	53.0854	37.3223	12.7935	3.1198	1.8719
	31.08	54.0	0.1502	56.9102	37.3223	15.4187	4.3194	2.5916
	33.38	58.0	0.1502	60.1759	37.3223	17.7864	5.2174	3.1304
	35.65	62.0	0.1502	63.9870	37.3223	20.3231	6.4918	3.8951
	40.28	70.0	0.1502	69.6086	37.3223	25.9037	6.5328	3.9196
0.50	8.25	42.0	0.0877	40.6072	37.3223	3.1833	0.1893	0.1514
	9.03	46.0	0.0877	42.2225	37.3223	3.8161	1.1718	0.7617
	9.82	50.0	0.0877	44.0147	37.3223	4.5108	2.2694	1.8616
	10.60	54.0	0.0877	45.6623	37.3223	5.2586	3.1692	1.9015
	11.39	58.0	0.0877	47.4682	37.3223	6.0691	4.1649	2.4984
	12.17	62.0	0.0877	49.0321	37.3223	6.9320	4.8655	2.9194
	12.57	64.0	0.0877	49.6948	37.3223	7.3908	5.0694	3.046
0.350	4.23	44.0	0.06142	39.0634	37.3223	1.07099	0.0927	0.0788
	4.62	48.0	0.06142	40.0211	37.3223	2.0373	0.7229	0.5422
	5.00	52.0	0.06142	41.2004	37.3223	2.3886	1.5509	1.008
	5.39	56.0	0.06142	42.5336	37.3223	2.7730	2.4998	1.4998
	5.77	60.0	0.06142	43.5704	37.3223	3.1805	3.1291	1.8774
	6.35	66.0	0.06142	44.7822	37.3223	3.8503	3.6711	2.2026

TABLE D.3.2 E.M.35.C OIL/WATER SYSTEM

ω = 3460 r.p.m.

NOZZLE DIAMETER D_N m	FLOW RATE Q cc/s	NOZZLE VELOCITY U_N cm/s	$F_S = \frac{\sigma \pi D_N}{g \Delta \rho}$	$F_D = \frac{10.8 \mu D_N}{D_F^2 g \Delta \rho} . Q$	$F_{CE} = \frac{\omega^2 R}{g}$	$F_K = \frac{3.1 \rho_d}{g \Delta \rho} . Q U_N$	$F_1 + F_D - F_{CE} - F_K$	PREDICTED VOLUME. V_F cc
.856	16.11	28.00	0.09619	47.6921	37.3223	9.6698	0.7962	0.6369
	19.57	34.00	0.09619	54.0861	37.3223	14.2637	2.5963	1.6876
	22.44	39.00	0.09619	60.6397	37.3223	18.7607	4.6529	2.7917
	25.90	45.00	0.09619	68.3023	37.3223	24.9847	6.0915	3.6549
0.50	5.89	30.0	0.05618	41.7102	37.3223	3.7879	0.6562	0.4921
	7.07	36.0	0.05618	44.6881	37.3223	5.4561	1.9659	1.3761
	8.44	43.0	0.05618	48.5123	37.3223	7.7799	3.4663	2.2530
	9.43	48.0	0.05618	51.1697	37.3223	9.7032	4.2004	2.7302
0.350	3.08	32.0	0.03933	39.8796	37.3223	2.1228	0.4838	0.4113
	3.66	38.0	0.03933	41.6129	37.3223	2.9814	1.3486	1.0114
	4.43	46.0	0.03933	44.3927	37.3223	4.3684	2.7413	1.7818
	4.91	51.0	0.03933	45.7014	37.3223	5.3680	3.0504	1.9828

TABLE D.3.3 CS40 OIL/WATER SYSTEM

ω = 3460 r.p.m.

NOZZLE VELOCITY D_N m	FLOW RATE Q cc/s	NOZZLE VELOCITY U_N cm/s	$F_S = \frac{\pi\sigma D_N}{g\Delta\rho}$	$F_D = \frac{10.8\mu D_N}{D_F^2 g\Delta\rho}.Q$	$F_{CE} = \frac{\omega^2 R}{g}$	$F_K = \frac{3.1\rho_d}{g\Delta\rho}.QU_N$	$F_1+F_D-F_{CE}-F_K$	PREDICTED VOLUME. V_F cc
.856	14.50	25.2	0.01906	44.0526	37.3223	6.1297	0.6197	0.5267
	17.21	29.9	0.01906	48.0345	37.3223	8.6322	2.0991	1.5743
	19.57	34.0	0.01906	51.8842	37.3223	11.1619	3.4191	2.3933
	24.52	42.6	0.01906	60.6749	37.3223	17.5226	5.8489	3.8018
0.50	5.34	27.2	0.01113	40.2289	37.3223	2.4366	0.4811	0.4330
	6.36	32.4	0.01113	42.2871	37.3223	3.4568	1.5211	1.2169
	7.32	37.3	0.01113	44.6905	37.3223	4.5802	2.7993	1.8195
	8.54	43.5	0.01113	47.4237	37.3223	6.2318	3.8807	2.5224
0.350	2.81	29.2	0.00779	39.2316	37.3223	1.3764	0.5407	0.4326
	3.27	34.0	0.00779	40.3297	37.3223	1.8651	1.1501	0.8627
	3.94	40.9	0.00779	42.3614	37.3223	2.7032	2.3437	1.5234
	4.62	48.0	0.00779	44.3269	37.3223	3.7201	3.2923	1.9754

TABLE D.3.4 PARAFFIN/WATER SYSTEM

ω = 3460 r.p.m.

NOZZLE DIAMETER D_N m	FLOWRATE Q cc/s	NOZZLE VELOCITY U_N cm/s	$F_S = \frac{\pi\sigma D_N}{g\,\Delta\rho}$	$F_D = \frac{10.8\mu D_N}{D_F^2 g\Delta\rho}.Q$	$F_{CE} = \frac{\omega^2 R}{g}$	$F_K = \frac{3.1\rho_d}{g\,\Delta\rho}.QU_N$	$F_S+F_D-F_{CE}-F_K$	PREDICTED VOLUME. V_F cc
.856	17.26	30.0	0.8252	48.2321	37.3223	11.1353	0.5997	0.4798
	19.57	34.0	0.8252	53.0433	37.3223	14.3091	2.2372	1.6779
	21.87	38.0	0.8252	58.7681	37.3223	17.8720	4.3990	2.6394
	24.17	42.0	0.8252	63.9582	37.3223	21.8307	5.6305	3.3783
	24.47	46.0	0.8252	69.1418	37.3223	26.1850	6.4598	3.8748
	28.77	50.0	0.8252	74.3676	37.3223	30.9351	6.9354	4.1613
0.50	6.28	32.0	0.4820	41.4922	37.3223	4.3217	0.3302	0.2642
	7.07	36.0	0.4820	43.9825	37.3223	5.4735	1.6687	1.1681
	7.85	40.0	0.4820	47.0547	37.3223	6.7526	3.4619	2.0771
	8.64	44.0	0.4820	49.8130	37.3223	8.1754	4.7973	2.8784
	9.23	47.0	0.4820	51.6063	37.3223	9.3291	5.4369	3.2621
	9.82	50.0	0.4820	53.3335	37.3223	10.5590	5.9341	3.5605
0.350	3.27	34.0	0.3374	39.5663	37.3223	2.3909	0.1905	0.1619
	3.66	38.0	0.3374	41.0980	37.3223	2.9909	1.1222	0.8417
	3.85	40.0	0.3374	42.8783	37.3223	3.3118	2.5816	1.5489
	4.14	43.0	0.3374	44.1117	37.3223	3.8283	3.2984	1.9791
	4.33	45.0	0.3374	44.9750	37.3223	4.1903	3.8000	2.2799
	4.81	50.0	0.3374	46.2682	37.3223	5.1720	4.1112	2.4668

TABLE D.4.1 KEROSENE/WATER SYSTEM

ω = 4600 r.p.m.

NOZZLE DIAMETER D_N m	FLOW RATE Q cc/s	NOZZLE VELOCITY U_N cm/s	$F_S = \frac{\pi\sigma D_N}{g\,\Delta\rho}$	$F_D = \frac{10.8\mu D_N}{D_F^2 g\Delta\rho}.Q$	$F_{CE} = \frac{\omega^2 R}{g}$	$F_K = \frac{3.1\rho_d}{g\Delta\rho}.QU_N$	$F_S+F_D-F_{CE}-F_K$	PREDICTED VOLUME. V_F cc
.856	25.32	44.0	0.1502	76.3397	65.9677	10.2351	0.2871	0.2153
	28.31	49.19	0.1502	79.9020	65.9677	12.7935	1.2910	0.7746
	31.08	54.0	0.1502	83.7290	65.9677	15.4187	2.4928	1.4957
	33.78	58.0	0.1502	87.1599	65.9677	17.9995	3.3429	2.0057
	35.68	62.0	0.1502	90.4372	65.9677	20.3231	4.2966	2.5779
	37.98	66.0	0.1502	93.7031	65.9677	23.0289	4.8567	2.9140
	40.28	70.0	0.1502	96.7996	65.9677	25.9037	5.0784	3.0470
0.50	9.03	46.0	0.0877	69.8516	65.9677	3.8161	0.1555	0.1322
	9.82	50.0	0.0877	71.1095	65.9677	4.5108	0.7187	0.5390
	10.60	54.0	0.0877	72.5160	65.9677	5.2586	1.3774	0.9642
	11.39	58.0	0.0877	74.2273	65.9677	6.0691	2.2782	1.3669
	12.17	62.0	0.0877	75.8058	65.9677	6.9320	2.9938	1.7963
	12.96	66.0	0.0877	77.2006	65.9677	7.8582	3.4624	2.0771
	13.74	70.0	0.0877	78.5151	65.9677	8.8361	3.7989	2.2794
0.350	4.81	50.0	0.06142	68.2120	65.9677	2.2095	0.09626	0.08182
	5.20	54.0	0.06142	69.1495	65.9677	2.5797	0.6635	0.4313
	5.58	58.0	0.06142	70.2261	65.9677	2.9733	1.3466	0.8079
	5.97	62.0	0.06142	71.2041	65.9677	3.4005	1.8973	1.1384
	6.35	66.0	0.06142	72.0758	65.9677	3.8503	2.3192	1.3915
	6.73	70.0	0.06142	72.7330	65.9677	4.3280	2.4987	1.4992

TABLE D.4.2 PARAFFIN/WATER SYSTEM

ω = 4600 r.p.m.

NOZZLE DIAMETER D_N m	FLOW RATE Q cc/s	NOZZLE VELOCITY U_N cm/s	$F_S = \frac{\pi\sigma D_N}{g\Delta\rho}$	$F_D = \frac{10.8\mu D_N}{D_F^2 g\Delta\rho}.Q$	$F_{CE} = \frac{\omega^2 R}{g}$	$F_K = \frac{3.1\rho_d}{g\Delta\rho}.QU_N$	$F_S+F_D-F_{CE}-F_K$	PREDICTED VOLUME. V_F cc
.856	17.26	30.0	0.8252	76.4278	65.9677	11.1353	0.1500	0.1200
	19.57	34.0	0.8252	80.6652	65.9677	14.3091	1.2136	0.9120
	21.87	38.0	0.8252	85.8176	65.9677	17.8720	2.8031	1.6819
	24.17	42.0	0.8252	90.8336	65.9677	21.8307	3.8604	2.3162
	26.47	46.0	0.8252	95.8108	65.9677	26.1850	4.4833	2.6900
	28.77	50.0	0.8252	100.7813	65.9677	30.9351	4.7037	2.8221
0.50	6.68	34.0	0.4820	70.6160	65.9677	4.8842	0.1921	0.1537
	7.46	38.0	0.4820	72.4450	65.9677	6.0963	0.8630	0.6473
	8.25	42.0	0.4820	74.9068	65.9677	7.4515	1.9696	1.1818
	8.84	45.0	0.4820	76.6881	65.9677	8.5547	2.6477	1.5886
	9.43	48.0	0.4820	78.3615	65.9677	9.7341	3.1417	1.8850
	10.21	52.0	0.4820	80.4609	65.9677	11.4175	3.5577	2.1346
0.350	3.46	36.0	0.3374	68.4457	65.9677	2.6787	0.1367	0.1162
	3.75	39.0	0.3374	69.3244	65.9677	3.1451	0.5490	0.4118
	4.04	42.0	0.3374	70.4846	65.9677	3.6490	1.2053	0.7232
	4.33	45.0	0.3374	71.4984	65.9677	4.1903	1.6778	1.0067
	4.62	48.0	0.3374	72.5958	65.9677	4.7690	2.1965	1.3179
	5.00	52.0	0.3374	73.7670	65.9677	5.5913	2.5454	1.5272

TABLES D.5 to D.8

The following tables contain experimental values of droplet volumes under different conditions for the four liquid systems, viz:

(a) Kerosene-water

(b) EM35C oil-water

(c) C.S.40 oil-water

(d) Paraffin-water

Parameters studied for each system are,

(i) Speed of rotation (ω)

(ii) Nozzle diameter (D_N)

(iii) Nozzle velocities (U_N)

The volumes of droplets are calculated as follows:-

Droplet diameters were taken as mean of major and minor axis for a sample and the mean and the standard deviations were calculated as

$$\overline{D} = \frac{\sum_{1}^{n} d}{n}, \quad \text{Stand.Dev.} = \frac{\sum_{1}^{n} (D_i - \overline{D})}{n - 1}$$

The volumes are calculated assuming spherical shape.

TABLE D.5. KEROSENE/WATER SYSTEM

SPEED OF ROTATION ω r.p.m.	NOZZLE DIAMETER D_N cm	NOZZLE VELOCITY U_N cm/s	DROPLET VOLUME V_F cc
1750	0.856	32.8	0.546
		38.4	1.893
		44.5	2.574
		54.2	3.047
	0.50	34.3	0.348
		37.6	0.431
		54.0	1.788
2750	0.35	42.3	0.246
		47.4	0.562
		58.6	0.613
	0.856	34.0	0.244
		36.1	0.659
		42.7	1.826
		49.4	2.107
	0.50	36.9	0.298
		40.4	1.332
		50.2	2.594
		59.8	3.256
	0.350	60.4	0.173
		67.1	1.050
		72.8	1.081
3460	0.856	41.7	0.436
		45.3	1.405
		54.0	2.403

continued overleaf ....

TABLE D.5 (Cont...)

SPEED OF ROTATION ω r.p.m.	NOZZLE DIAMETER D_N cm	NOZZLE VELOCITY U_N cm/s	DROPLET VOLUME V_F cc
3460	0.50	44.7	0.396
		51.6	1.381
		55.9	1.625
	0.35	45.2	0.264
		55.7	0.983
		61.3	0.745
4600	0.856	44.3	0.314
		50.2	0.918
		53.6	1.349
		60.0	1.804
	0.50	47.0	0.158
		52.1	0.664
		60.2	1.315

TABLE D.6 EM3 SC OIL/WATER SYSTEM

SPEED OF ROTATION ω r.p.m.	NOZZLE DIAMETER D_N cm	NOZZLE VELOCITY U_N cm/s	DROPLET VOLUME V_F cc
1750	0.856	21.8 25.2 27.1 32.0 35.9	0.806 1.813 2.008 3.414 4.197
	0.50	23.2 29.1 34.5 35.9	0.723 1.818 2.891 4.216
2750	0.856	23.4 29.1 32.6 37.4	0.648 1.527 2.075 2.794
	0.50	25.5 30.2 36.1 40.2	0.633 1.347 2.283 2.461
3460	0.50	29.9 34.7 40.6 44.2	0.684 1.067 1.483 1.876
	0.856	26.8 31.5 37.1 42.1	0.572 1.445 1.873 2.386

TABLE D.7 C.S. 40 OIL/WATER SYSTEMS

SPEED OF ROTATION ω r.p.m.	NOZZLE DIAMETER D_N cm	NOZZLE VELOCITY U_N cm/s	DROPLET VOLUME V_F cc
1750	0.856	20.9	0.80
		28.9	1.94
		29.8	2.96
		34.1	3.60
2750	0.856	23.4	0.71
		29.1	1.68
		31.8	2.37
		37.3	2.99
3460	0.856	25.8	0.53
		31.5	1.30
		35.2	2.04
		39.4	2.28

TABLE D.8 Cont....

SPEED OF ROTATION ω r.p.m.	NOZZLE DIAMETER D_N cm	NOZZLE VELOCITY U_N cm/s	DROPLET VOLUME V_F cc
4600	0.856	32.0	0.189
		38.6	1.346
		47.3	1.957
	0.50	34.1	0.248
		43.7	1.235
		53.0	1.743
	0.350	37.0	0.142
		43.5	0.714
		52.9	1.146

APPENDIX E

DROPLET VELOCITY STUDIES

The results in this section show droplet velocities in terms of constant $K_1 = \frac{18v_c}{\pi D^2 \omega R}$, which has been calculated for various chemical systems and speeds of rotation (ω).

(i) Tables E_1 to E_3. These give calculated values of U_r from the mathematical model.

(ii) Tables E_4 to E_6. These give experimental values of U_r.

TABLE E.1

ω = 1750 r.p.m.

SYSTEM	CONSTANT K_1	RADIAL VELOCITY U_r m/s
KEROSENE	0.48	20.06
	0.88	37.41
	1.92	58.79
	3.21	65.27
	4.95	55.18
C.S. 40 OIL	0.66	17.38
	2.09	40.89
	3.34	46.51
	5.98	33.43
PARAFFIN	1.12	18.27
	3.06	33.89
	4.94	27.61
	7.18	15.34

TABLE E.2

ω = 2750 r.p.m.

SYSTEM	CONSTANT K_1	RADIAL VELOCITY U_r m/s
KEROSENE	0.15	18.87
	0.93	4.92
	1.73	6.73
	2.81	7.24
	3.26	7.18
C.S. 40 OIL	0.67	26.74
	2.64	55.07
	4.56	52.11
PARAFFIN	0.53	14.20
	1.68	29.52
	2.74	39.76
	5.19	34.69
	7.08	28.47

TABLE E.3

ω = 3460 r.p.m.

SYSTEM	CONSTANT K_1	RADIAL VELOCITY U_r m/s
KEROSENE	0.10	14.87
	0.58	36.38
	1.27	62.92
	2.64	78.81
	3.59	80.09
C.S.40 OIL	0.74	26.37
	1.49	42.65
	2.30	59.91
	3.18	63.26
	5.59	54.42
PARAFFIN	0.86	17.94
	1.94	30.02
	3.73	44.39
	5.82	37.68
	7.59	30.97

TABLE E.4 ω = 1750 r.p.m.

SYSTEM	DROPLET DIAMETER (D) cm	DISTANCE TRAVELLED (1) cm	TIME t_f sec	DROPLET VELOCITY $U_r=(\frac{1N_f}{t_f N_p})$	CONSTANT (K_1)
KEROSENE/ WATER	0.87	0.44	3.4	21.5	0.49
	1.01	0.53	2.1	42.4	0.7
	1.53	0.66	1.9	58.0	1.5
	1.68	0.57	1.5	63.2	2.86
	1.79	0.66	2.0	54.9	4.90
C.S. 40 OIL/WATER	1.15	0.26	3.3	27.6	1.10
	1.55	0.37	3.1	38.2	1.61
	1.78	0.30	2.2	45.4	2.88
	1.90	0.31	3.2	32.3	5.60
PARAFFIN/ WATER	1.33	0.36	4.1	1.47	0.82
	1.42	0.71	3.6	33.1	2.17
	1.66	0.71	3.5	33.8	3.98
	1.89	0.49	3.3	24.9	5.43

TABLE E.5 ω = 2750 r.p.m.

SYSTEM	DROPLET DIAMETER D cm	DISTANCE TRAVELLED (1) cm	TIME t_f (sec)	DROPLET VELOCITY $U_r=(\frac{1.N_f}{t_f N_p})$	CONSTANT K_1
KEROSENE/ WATER	0.78	1.37	3.3	18.7	0.18
	1.08	0.54	2.0	49.2	0.93
	1.51	0.57	1.4	67.8	18.5
	1.59	0.95	2.2	71.9	2.86
	1.83	0.67	1.6	69.8	3.30
C.S.40 OIL/WATER	1.11	0.23	3.4	22.5	0.66
	1.47	0.32	2.9	36.8	0.95
	1.65	0.52	3.1	56.0	2.31
	1.78	0.40	3.2	50.2	3.98
PARAFFIN/ WATER	0.77	0.30	5.0	10.0	0.53
	1.25	0.70	2.8	41.7	2.24
	1.60	0.49	2.1	38.8	4.88
	1.82	0.68	3.7	31.6	7.3

TABLE.6 ω = 3460 r.p.m.

E 6

SYSTEM	DROPLET DIAMETER D cm	DISTANCE TRAVELLED (1) cm	TIME t_f (sec)	DROPLET VELOCITY $U_r=(\frac{1N_f}{t_f N_p})$ cm/s	CONSTANT K_1
KEROSENE/ WATER	0.91	0.56	3.6	25.9	0.27
	1.13	1.05	2.5	70.0	1.43
	1.23	0.92	1.9	80.7	2.14
	1.45	0.545	1.1	82.5	3.26
C.S.40 OIL/WATER	1.00	0.24	2.53	32.0	0.63
	1.35	0.305	2.0	50.8	1.50
	1.57	0.37	1.9	64.8	2.81
	1.63	0.34	2.1	53.21	5.64
PARAFFIN/ WATER	0.97	0.28	4.8	9.7	0.75
	1.38	0.69	2.7	42.6	2.42
	1.47	0.76	2.5	50.8	3.60
	1.70	0.59	3.1	31.7	7.36

APPENDIX F

```
 0 'BEGIN''COMMENT'LEASTSQUARE LINEAR FIT.
 1         GEORGE E. FORSYTHE'S METHOD;
 2       'INTRGER' V,U;
 3       'PROCEDURE'LSQ(N,M,X,Y,A); 'VALUE'N,M;
 4       'INTEGER'N,M; 'ARRAY'X,Y,A;
 5       'BEGIN''INTEGER'I,J,K;'REAL'SUM,SUMSQ;
 6             'ARRAY'P[0:M,1:N],ALFA[1:M];
 7             'FOR'I:=0'STEP'1'UNTIL'N'DO'P[0,I]:=1.0;
 8             'FOR'I:=1'DO'
 9             'BEGIN'SUM:=SUMSQ:=0.0;K:=0;
10                   'FOR'J:=0'STEP'1'UNTIL'N'DO'
11                   'BEGIN'SUM:=SUM+X[J]*P[K,J]↑2;
12                         SUMSQ:=SUMSQ+P[K,J]↑2;
13                   'END';
14                   ALFA[I]:=SUM/SUMSQ;
15                   WRITETEXT('('''('1C')'ALFA(I)=')');
16                   PRINT(ALFA[I],2,3);
17                   'FOR'J:=0'STEP'1'UNTIL'N'DO'
18                   P[I,J]:=X[J]*P[K,J]-ALFA[I]*P[K,J];
19              'END';
20              'FOR'I:=0'STEP'1'UNTIL'M'DO'
21              'BEGIN'SUM:=0.0;SUMSQ:=0.0;
22                   'FOR'J:=0'STEP'1'UNTIL'N'DO'
23                   'BEGIN'SUM:=SUM+Y[J]*P[I,J];
24                         SUMSQ:=SUMSQ+P[I,J]↑2;
25                   'END';
26                   A[I]:=SUM/SUMSQ;
27              'END';
28        'END' OF PROC LSQ;
29
30        V:=READ; U:=READ;
31         'BEGIN''ARRAY'XX,YY[0:V],AA[0:U];'INTEGER'I;
32               'FOR'I:=0'STEP'1'UNTIL'V'DO'XX[I]:=READ;
33               'FOR'I:=0'STEP'1'UNTIL'V'DO'YY[I]:=READ;
34               WRITETEXT('('''('3C')'NUMBER%OF%GIVEN%DATA%
35               POINTS=')');PRINT(V+1,2,0);
36               WRITETEXT('('''('1C')'DEGREE%OF%POLYNOMIAL=')');
37               PRINT(U,1,0); LSQ(V,U,XX,YY,AA);
38                WRITETEXT('('''('3C')'THE%REQUIRED%OUTPUT%
39               PARAMETERS:'('1C')''')');
40              'FOR'I:=0'STEP'1'UNTIL'U'DO'PRINT(AA[I],2,3);
41         'END'; NEWLINE(3);
42 'END' OF PROGRAM;
```

APPENDIX G

TEXT CUT OFF IN ORIGINAL

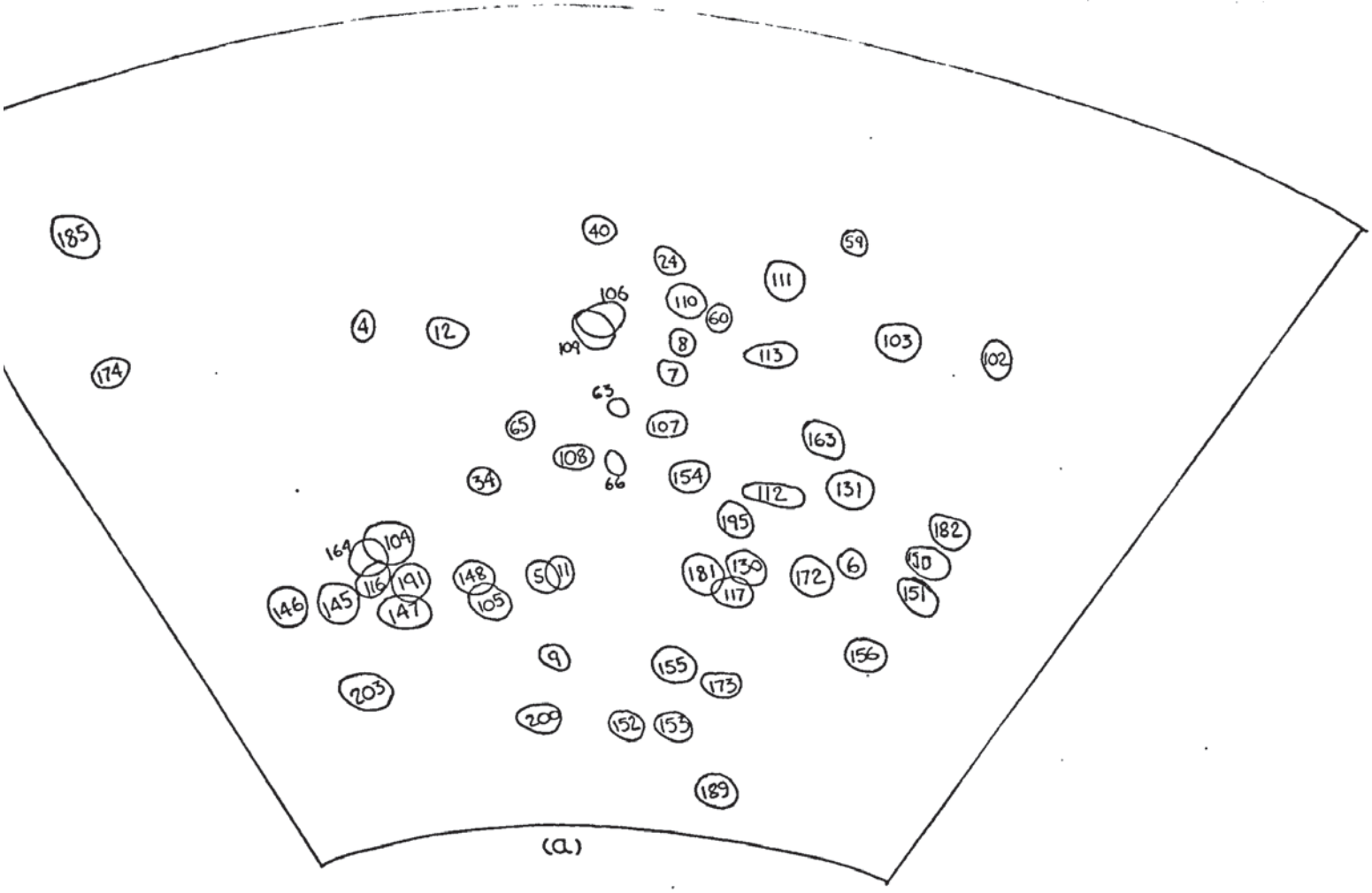

DROPLETS COUNTED AND TRACED ON FILM 10 TAKEN WITH HYPERSPEED CAMERA.

(a) REPRESENTS ONE FRAME PRECEEDING FRAME (b). NUMBERS INDICATE DROPLET NUMBER

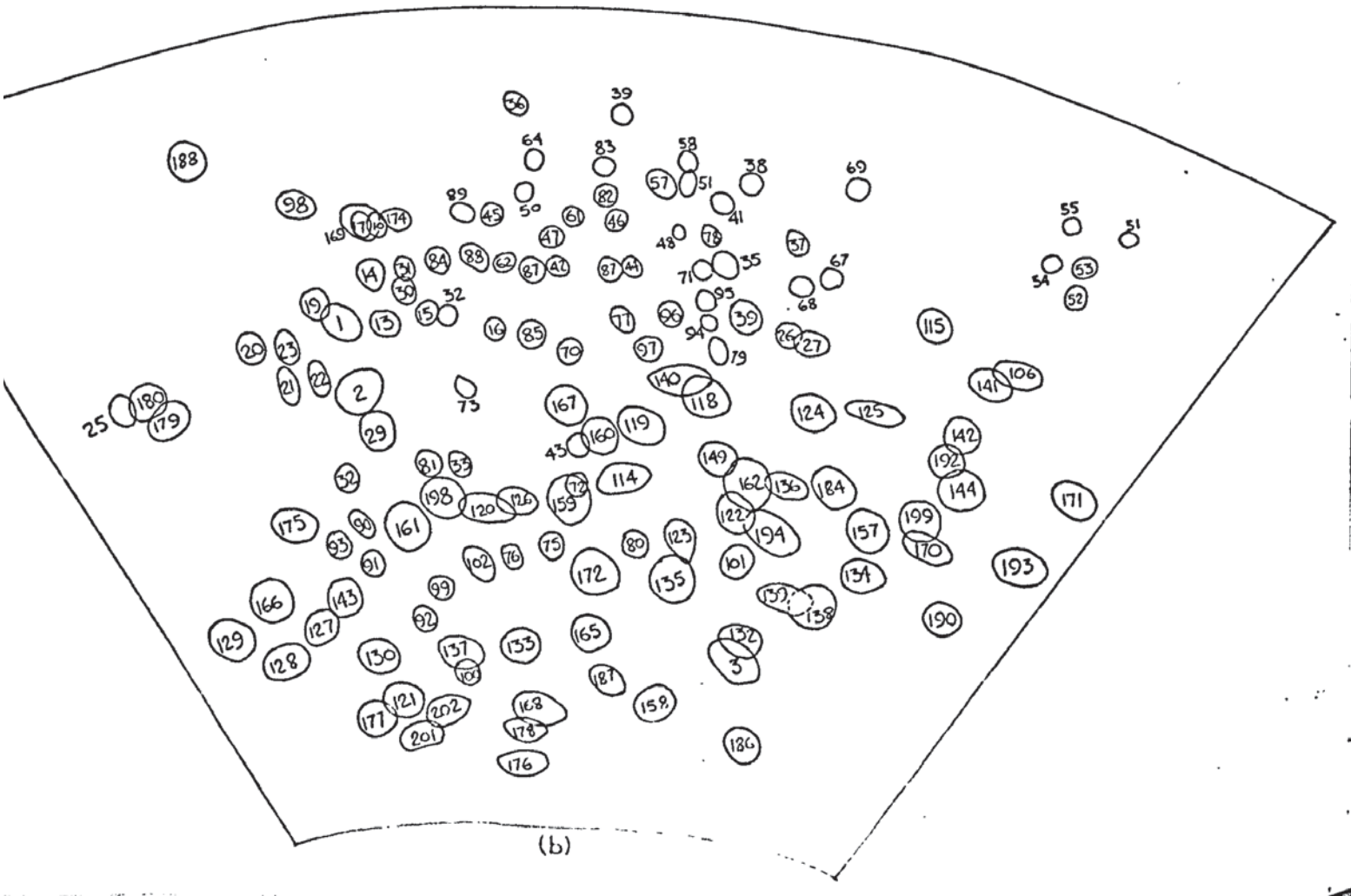

APPENDIX.C. Film number 9.

D_n.nozzle diameter, ω-speed of rotation, U_N- nozzle velocity

Paraffin/water system.

D_N cm.	ω RPM	U_N cm/s.	Minor axis	Major axis.	Mean value.	Actual size. (cc
			0.8	0,9	0.85	
			0.9	I.I	I.0	
			0.9	I.3	I.I	
			0.5	0.7	0.6	
			0.7	0.7	0.7	Mean val
			0.6	0.7	0.65	
			0.5	0.7	0.6	-0.6775
			0.4	0.6	0.5	V_F-I.I5
			0.6	0.7	0.65	
			0.6	0.7	0.65	standard
			0.6	0.8	0.7	deviation
			0.6	0.7	0.65	-0.I5
			0.6	0.7	0.65	
0.35	4600	52.9	0.6	0.6	0.6	
			0.4	0.6	0.5	
			0.5	0.6	0.55	
			0.5	0.6	0.55	
			0.7	0.7	0.7	
			0.6	0.8	0.7	
			0.4	0.9	0.65	
			0.4	0.9	0.65	
			0,5	0.8	0.65	
			0.75	0.8	0.75	
			0.5	0.7	0.6	Mean
			0.5	0.6	0.55	value
			0.5	0.8	0.65	=0.6825
			0.8	0.9	0.85	
	4600	43.5	0.5	0.6	0.55	standard
			0.4	0.5	0.45	deviation
			0.5	0.6	0.55	
			0.5	0.6	0.55	-0.I07
			0.6	0.7	0.65	
			0.6	0,7	0.65	Volume
			0.5	0.6	0.55	
			0.5	0.6	0.55	V_F=0.7I4
			0.5	0.5	0.5	
			0.4	0.5	0.45	
			0.8	0.8	0.80	
			0.5	0.7	0.6	
			0.5	0.5	0.5	
			0.5	0.5	0.5	
			0.5	0.5	0.5	
			0,4	0.6	0.5	
			0.5	0.5	0.5	
			0.5	0.5	0.5	
			0.5	0,6	0.55	Mean
			0.3	0.4	0.35	Value
	4600	37.0	0.4	0.4	0.4	=0.4286
			0.4	0.6	0.5	
			0.5	0.5	0.5	
			0.4	0.4	0.4	standard
			0.4	0.4	0.4	deviation
			0.3	0.3	0.3	=0.006
			0.3	0.3	0.3	Vol-0.I42

D_N cm	ω rpm	U_N cm s	Minor axis	Major axis	Mean value	Actual size cc
			0.6	0.8	0.7	
			0.3	0.5	0.4	
			0.5	0.5	0.5	
			0.5	0.5	0.5	
			0.5	0.5	0.5	
			0.4	0.5	0.45	Mean
			0.4	0.5	0.45	value
			0.4	0.5	0.45	
			0.6	0.6	0.6	=0.5038
			0.4	0.5	0.45	
0.35	3460	35.0	0.5	0.5	0.5	
			0.5	0.6	0.55	stand
			0.5	0.5	0.5	dev.=
			0.5	0.5	0.5	0.077
			0.5	0.5	0.5	
			0.5	0.5	0.5	Vol.V_F =0.376
			0.4	0.5	0.45	
			0.6	0.6	0.6	
			0.6	0.7	0.65	
			0.4	0.6	0.5	
			0.4	0.7	0.55	Mean
			0.5	0.6	0.55	value
			0.4	0.6	0.5	=0.56
			0.6	0.7	0.65	
		42.4	0.5	0.6	0.55	Stand
			0.6	0.6	0.6	dev.=
			0.5	0.5	0.5	
			0.5	0.5	0.5	0.060
			0.6	0.6	0.6	
			0.6	0.6	0.6	Vol .V_F=
			0.6	0.6	0.6	I.38
			0.6	0.7	0.65	
			0.5	0.6	0.55	
			0.4	0.8	0.6	
			0.5	0.6	0.55	Mean
			0.6	0.6	0.6	value=
			0.6	0.6	0.6	
			0.4	0.4	0.4	0.656
			0.5	0.5	0.5	
			0.5	0.6	0.55	Stand
	3460	47.5	0.6	0.7	0.65	dev.=
			0.7	0.9	0.8	0.I72
			0.5	0.5	0.5	
			0.6	0.6	0.6	Vol.V_F=
			0.7	0.8	0.75	I.659
			0.6	0.9	0.75	
			0.6	0.7	0.65	
			0.8	I.0	0.9	
			0.9	I.2	I.I	
			0.8	I.0	0.9	
			0.6	I.I	0.85	
			0.6	0.9	0.75	
			0.8	0.8	0.8	
	2750	64.2	0.8	0.9	0.85	

D_N cm	ω t.p.m.	U_N cm/s	Minor axis	Major axis	Mean value	Actual size(cc)
			0.9	0.9	0.9	Mean.val
			0.4	I.5	0.95	=0.8706
			0.4	I.2	0.8	
			0.7	I.3	I.0	Stand.
			0.8	0.8	0.8	dev.=
			0.7	0.9	0.8	
			0.7	I.0	0.85	0.08303
0.35	2750	64.2	0.9	I.I	I.0	
			0.8	I.0	0.9	Vol.V_F
			0.6	I.2	0.9	=
			0.9	I.0	0.95	I.036
			0.9	0. 9	0.9	
			0.7	I.0	0.85	
			0.9	I.0	0.95	
			0.6	I.4	0.95	Mean.val
			0.6	I.0	0.8	=0.9I07
			0.8	0.9	0.85	Stand.dev
		88.5	0.8	I.I	0.95	0.0738
			0.9	I.0	0.95	
			0.8	I.0	0.9	Vol.V_F=
			0.8	0.9	0.85	I.263
			0.9	I.I	I.0	
			0.7	0.9	0.8	
			0.8	I.0	0.9	
			0.9	I.I	I.0	
			I.0	I.I	I.05	
			0.6	I.0	0.8	
			0.8	I.I	0.95	
			I.0	I.I	I.05	
			0.7	I.3	I.0	
			0.6	I.5	I.05	
			0.8	I.0	0.85	
			0.8	0.8	0.8	
			0.8	0.9	0.85	Mean val
			0.9	I.0	0.95	0.875
			0.9	0.9	0.9	
			0.9	0.9	0.9	Stand.
			0.8	I.I	0.95	dev.=
			0.7	0.8	0.75	0.0856
			0.8	0.9	0.85	
			0.7	I.0	0.85	Vol.V_F
0.35	2750	76.0	0.5	I.I	0.8	=I.429
			0.6	0.8	0.7	
			0.7	0.9	0.8	
			0.8	0.9	0.85	
			0.8	I.0	0.9	
			0.8	I.0	0.9	
			0.9	I.0	0.95	
			0.8	0.9	0.85	
			0.8	0.8	0.8	
			I.0	I.0	I.0	
			I.I	I.I	I.I	
			I.0	I.I	I.05	
			0.8	I.I	0.95	

D_N cm	ω r.p.	U_N cm/s	Minor axis	Major axis	Mean value	Actual size (cc
			0.9	0.9	0.9	Mean
			0.9	0.9	0.9	value=
			0.9	I.0	0.95	0.442
			0.9	0.9	0.9	Stand
			0.8	I.3	I.05	dev.=
0.35	1750	44.3	0.8	0.9	0.85	0.0763
			0.6	I.2	0.9	
			0.8	I.I	0.95	Vol.V_F
			0.9	I.0	0.95	= 2.418
			I.0	I.I	I.05	
			0.6	0.9	0.75	
			0.6	0.9	0.75	
			0.8	I.I	0.95	
			0.7	I.I	0.9	Mean
			0.8	0.8	0.8	value
			0.6	I.0	0.8	=0.863
			0.7	I.I	0.9	
		53.4	0.7	0.9	0.8	Stand
0.35	1750		I.0	I.0	I.0	dev.
			0.8	I.0	0.9	=0.1008
			0.9	I.0	0.95	
			0.9	I.I	I.0	VOL.V_F
			0.8	0.8	0.8	= 1.226
			0.5	0.8	0.65	
			0.8	0.9	0.85	
			0.7	I.0	0.85	
			0.8	0.9	0.85	
			0.8	0.9	0.85	
			0.7	0.7	0.7	
			0.9	I.2	I.05	
			0.8	I.2	I.05	
			0.8	0.9	0.85	
0.35	1750	51.0	0.7	I.I	0.9	Mean
			0.9	I.I	I.0	value
			I.0	I.0	I.0	=0.9036
			0.7	I.0	0.85	Stand
			0.6	I.0	0.8	dev.
			0.7	I.0	0.85	=0.1082.
			0.9	I.2	I.05	Vol.V_F
						= 2.315

NOMENCLATURE

CAPITAL LETTERS

A	a constant in equation 3.6, = $(6\pi r\mu/M)$
A_c, A_D	areas in equation 6.19, cm^2
A_o	constant used in equation 4.10 that characterises disturbance in coalescence
A_i	Interfacial area, cm^2
A_n	coefficient in series of the equations 5.21, 5.23.
A_{max}	length of the major axis of deformed drop, cm.
Ap	amplitude of oscillation of drop.
Ard	interfacial area of a rest drop, cm^2
B	an empirical constant in equation 3.18, cm^{-1}.
B	constant in equations 3.6 and 3.7, = $(\frac{Q(\rho_c - \rho_d)g}{M})$
C	concentration g/cm^3
C	constant in equations 3.6, 3.7 = $(QU_N\rho_d/M)$
C_o, C_i	initial concentration, g/cm^3
C*	concentration at equilibrium, g/cm^3
C_s	saturation concentration, g/cm^3
C_f	fural concentration, g/cm^3
C	constant used in equation 4.10
C	constant used in equation 4.5 ($\neq$ that in 4.10).
C_1, C_2	constants used in euqations 4.2 and 4.3.
C_3, C_4	empirical constants in equation 6.6c.
C_D	correction factor for variation in diffusion coefficient of equation 5.18
C_D	coefficient of resistance to flow in equation 8.

C_{od}	coefficient of discharge defined as $(\frac{Q_T}{Q_a})$
D	droplet diameter, cm
D_{cs}	diffusion coefficient in saturated liquid, cm^2/s
D_d	diffusivity of the dispersed phase, cm/s
D_e	equilibrium drop diameter, cm.
DE	effective diffusivity in equation 5.24, cm/s
D_{FS}	diameter of static droplet, cm
D_{max}	maximum droplet diameter before break-up, cm
D_N	nozzle diameter, cm
D_S	equivalent static droplet diameter, cm
D_{OUT}	outer diameter of nozzle, cm.
E	fraction extraction, i.e. $(\frac{c_o-c_f}{c_o-c^*})$
E_o	εovotos number, $\frac{\Delta\rho g\phi^2}{\sigma}$
E_{cc}	countercurrent efficiency
E_f	mass transfer during droplet formation
E_f	extraction factor in equation 6.43.
E_k	kinetic energy, $g\frac{cm^2}{s^2}$
E_{ov}	overall mass transfer efficiency
F	Harkin-Brown factor used in the droplet formation correlations
F	a constant in equations 4.15 to 4.20
F	a constant in equation 6.28
F_B	buoyancy force acting on a drop
F_{CE}	centripetal force acting on a drop
F_{CO}	Corolois force acting on a drop
F_K	kinetic force acting on a drop

$(F_m)_{mod}$	a modified Froude number $(\rho_d Q/\Delta\rho\omega R)$
F_s	interfacial tension force acting on a drop
F_{net}	summation of all the forces acting on a drop
G	specific gravity
G	constant defined as $(1-(\frac{D}{A})^6)^{\frac{1}{2}}$
J	is a form defined as = $\omega^2 R$
k	constant in equation 3.23
K	overall mass transfer coefficient
K_c	continuous phase mass transfer coefficient
K_d	dispersed phase mass transfer coefficient
K_{dc}	average mass transfer coefficient for the droplet coalescence, cm/s
K_{df}	average mass transfer coefficient for the droplet formation, cm/s
K_D, K_f	empircal constants in equation 8.19
L	distance of fall of drop to interface, cm
L	scale of maniflow, cm
M	virtual mass of the drop, gm
N, N_A	state of mass transfer, $g/cm^2 s$
N	factor in equation 6.32 to account for wave splitting
N	in equations 4.9, 4.10, 4.11 mean number of drops coalescing in time (t)
N_o	total number of drops considered
N_1	dimensionless number $(\rho_d Q/\Delta\rho\omega R)$
N_{cd}	a dimensionless number defined in (3.33)
N_p	a dimensionless number

N_{Re}	Reynolds number, $(\rho UD/\mu)$
N_{sc}	Schimidt number, $(\mu/\rho D)$
N_{sd}	a dimensionless number defined given in equation 3.24, to 3.26
N_{sh}	Sherwood number, $(\frac{X_c D}{D_e})$
N_{we}	Weber number, $(T/(\delta/D))$ or $(\rho_c U^2 D/\sigma)$
$(N_{we})_{crit}$	the critical value for droplet break-up
P	pressure readings of the centrifugal contactor, kg/cm^2
Q	flow rate, cm^3/s
Q_{we}	flow rate over a weir, cm^3/s
R	distance of nozzle from the centre of the rotor shaft, cm
Rc	radius of the cylinder around the shaft, cm
Re	radius of the interface, cm
R_N	radius of nozzle, cm
T	Temperature, ^oC
T_1 to T_9	constants in equation 3.8 and defined in reference (70)
U	velocity of flow from nozzle with appropriate subscripts, cm/s
U	droplet velocity, cm/s
U_r	radial velocity of a droplet, cm/s
U_T	terminal velocity of drop, cm/s
U_ψ	velocity of droplet in ψ direction, cm/s
$\bar{U}^2$	root mean square velocity, cm/s
$U(r_1), U(r_2)$	velocity vectors of points r_1, r_2
U	droplet velocity after infinite time, cm/s
V	contactor volumes with appropriate subscripts, cm^3
V_{eq}	volume of drop at equilibrium, cm^3

V_F final droplet volume, cm^3

V_{FS}, V_S static droplet volume, cm^3

V_i volume of droplet above horizontal section at increment i, cm^3

V_{nL} volume added during drop release, cm^3

X a coefficient in equation 8.33 to account for the effect of "added mass"

X dimensionless velocity, $(U_r/\omega R)$

X_i, X_{max} X-co-ordinate values at increment i and at maximum, cm

Y dimensionless velocity, $(1 + U_\psi/\omega R)$

Small letters

a radius or half axis length in equations 5.20 to 5.24 and 3.36, cm

a jet radius one drop diameter from the end of the jet, cm

a_o surface area of a rest drop, cm^2

a_n nozzle radius = R_N, cm

ap = Ap amplitude of oscillation

a_r surface area of drop, cm^2

b amplitude coefficient

b "effective width" of a centrifugal contactor, cm

d equivalent drop diameter, cm

dn-D_N nozzle diameter, cm

f constant in equation 6.27

g acceleration due to gravity, 980.6 cm/s^2

h	film thickness, with h_1 and h_2 being the initial and final thickness, cm
h_{max}	maximum film thickness, cm
k	a constant in equation 4.19 and 4.10
k_1	constant in equation 5.15
$(ka)_{max}$	dimensionless wave number of the dominant symmetrical wave in equation 6.32
m	mass input of dispersed phase through nozzle in equation 3.9, gm/s
m	distribution coefficient
n	mode of oscillation in equation 3.36
n	index in equation 5.24
p	dynamic pressure on droplet, g/cm^2
r	radius of droplets, cm
r	radius vector between two points $r_1 r_2$, in equation cm.
t_e	time for droplet coalescence, sec.
t_f	droplet formation time, sec.
t_{eq}	time until drop release starts, sec.
t_i	time for interrupted droplet formation, sec.
t_r	time of rest for interrupted droplet formation, sec.
t_r	time for drop release, sec.
$t_{\frac{1}{2}}$	half-life of droplet in coalescence, sec.
$\overline{v}^2$	root mean square velocity in the y direction, cm/s
v	kinematic viscosity in equations 4.3 and 4.4, 6.35 and 6.36.

v	settling velocity of drops, cm/s
v_c	velocity of the dispersed phase = U_N, cm/s
x_1, x_2	solute concentration in dispersed phase
y	co-ordinate of y-axis, cm
y_1, y_2	solute concentration in continuous phase
z	co-ordinate of z-axis, cm
$\overline{z}^2$	root mean square velocity in z direction, cm/s

GREEK LETTERS

ρ_c	density of the continuous phase, g/cm^3
ρ_d	density of the dispersed phase g/cm^3
$\Delta\rho$	the difference between the densities = $\rho_c - \rho_d$, g/cm^3
μ_c, μ_d	dynamic viscosity of continuous and dispersed phases respectively, cp
σ, γ	interfacial tension, dynes/cm
ϕ	volumetric dispersed phase hold-up fraction
ω	speed of rotation, rpm
ω	frequency of oscillation, as in equation 3.36
τ	viscous stress on a droplet
ε	rate of energy dissipation per unit mass
ξ	coefficient of resistance for a drop in centrifugal fields
η	parameter defined by Kolomagoroff as microscale of turbulence
α	parameter in equation
ϕ_i	angle between vertical axis and normal to meridian profile at point (x,z), radians

λ_n	nth eigen value in equations 5.23 and 5.24.
γ	a factor defined as $(3\frac{n^2}{8})^{-\frac{1}{2}}$

Subscripts

N	nozzle
s	static
F	final
J	jetting
H	heavy phase
L	light phase
LLO	light liquid out
LLI	light liquid in
HLO	heavy liquid out
HLI	heavy liquid in
E	total extractor reading
S	seals
C	rotor

BIBLIOGRAPHY

1. Goerring — As mentioned in Chem. Eng. 61(5), 69, 1965
2. Treybal, R.E. — 'Liquid Extraction', Mc Graw Hill, 3rd edition.
3. Arnold, D. — Ph.D. Thesis, Aston University, 1974.
4. Miner, C. — Podbielniak Centrifugal Super Cont. Circular No.13.
5. Banks, N.K. — Mining Congr. J. 45(1), 44-7, (1959).
6. Mumford, C.J. — Brit. Chem. Engineering, 13, 7, 341 (1968).
7. Production of Chloromycetin; Chem. Eng. 56 (10), 108,-11,(1949).
8. Pencillin; ibid. 58 (4) 174, (1951)
9. Inskeep, G.C. et al. Ind. Eng. Chem. 43, 1488 , (1951).
10. Bartels, C.R., Kleniman G; Chem. Eng. Prog. 45, 589, (1949).
11. Anderson, D.W., Lau, E.F. ibid 51, 507, (1955).
12. Jennings, A.S., U.S. Atomic Energy Comm. Report D.P. 680 (1962).
13. Clark A.T. Ibid Report A.T. (07-2)-1, 1962.
14. Miachon, J.P, I.S.E.C. (1971).
15. Jones, H.H.M. Soc. Chem. Ind. Conf. October, 1967, Bradford University.
16. Alexandre, M., Gentiline, P., 'Determination de L'Efficaite dun Appareil Semi-ind. d'extr. par Solvents. Revue IFP, 11, (3), 389, (1956).
17. Todd, D.B., Hopper, C.A., Chem. Eng. Prog. 67, (9), 60-62,(1971).
18. Fox, J.M. Hydrocarbon. Process, 42, (9), 133, (1963).
19. Liquid Dynamics Inc., U.S.A., Bulletin No.15.
20. Podbielniak, W.J. U.S. Pat. 2,004,001 (1935).

21. Podbielniak, W.J., (To L.W.G. Podbielniak), U.S.Pat.2,044,996 (1935)

22. Podbielniak, W.J., French Pat. 802,701, (1936).

23. Podbielniak, W.J., U.S. Pat. 2,093,645, (1936).

24. Podbielniak, W.J., British Pat. 454,994, (1936).

25. Podbielniak, W.J., (to B.B. Schneider), U.S.Pat.2,153,640,(1938).

26. Podbielniak, W.J., (to B.B. Schneider), U.S.Pat.2,209,577,(1940).

27. Cautor, C., (to Establissments Lambiotte Freres), U.S. Pat. 2,036,924, (1936).

28. Establissments Lambiotte Freres, French Pat. 769,254, (1934).

29. Sheldon, H.W., Fahnestook, F.C., U.S. Pat. 2,189,230, (1940).

30. Thayer, G., U.S. Pat. 2,176,982, (1939).

31. Placek, A. U.S. Pat. 1,036,523, (1933).

32. Placek, A., U.S. Pat. 1,936,524, (1933).

33. Doyle, C.M. U.S. Pat. 3,1007,218, (1963).

34. Doyle, W.G. U.S. Pat. 3,114,706, (1963).

35. Doyle, W.G. U.S. Pat. 2,116,246, (1963).

36. Doyle, W.G. U.S. Pat. 3,132,100, (1964).

37. Doyle, W.G. et al. U.S. Pat. 3,217,980, (1965).

38. Doyle, W.G. et al. U.S. Pat. 3,254,832, (1966).

39. Doyle, C.M. U.S. Pat. 3,292,850, (1966).

40. Netherlands Pat. 297693.

41. Palmquist, F.E., Beskow, S. Brit. Pat. 941,939, (1963).

42. Garfullin et al Zhidk. Ekstr. Tr. Vses, Nauch-Tekh. Soves. (19-25), (1969).

43. Ponikarov, I.I. et al. Sh. Prikl. Khim. (Leningrad), 44 (8), 1803-4), (1971).

44. Jacobsen, F.M. Beyer, G.H., A.I.Ch.E. Jnrl. 2, 3, 283 (1956).

45. Todd, D.B. Chem. Eng. Prog. 62, (8), 119, (1966).

46. Lyskotsov, T.B., Khim. Makhina Skroenie, 4 (1961).

47. Soviet export, 32, 38. (1964)

48. Barker, T.A., I.S.E.C. (1969).

49. Todd, D.B., Podbielniak, W.J., Chem. Eng. Prog. 61, (5), 69 (1965).

50. Bauer, E., I.S.E.C. (1969).

51. "Shidkostnaya Skstraktsiya", Edited by P. Romankova, M.J.Kurochkino, (1969)

52. Ibid

53. Webster, D.S. et al,A.E.C. Research Develop. Report. D.P.371 (1961).

54. Webster, D.S. et al, ibid D.P.370 (1961).

55. Cited in reference 2.

56. Harkins, W.D., Brown, F.E., J.Am. Chem. Soc. 41, 449 (1919).

57. Hauser, E.A, Edgerton, H.E., J. Phy. Chem. 40, 973 (1916).

58. Dixon, B.E., Russell, A.A.W., J. Soc. Chem. Ind. Lond. 47, 258, (1955)

59. Keith, F.W., Hixon, A.N., Ind. Eng. Chem. 47, 258, (1955).

60. Tanweer, A.K., Imp. Coll. Chem. Eng. Soc. Jnl., 10, 51 (1956).

61. Haynes, L.G. et al, Ind. E.C. Process Design. Dev. 1, 508,(1968).

62. Juma, S.M., M.Sc. Thesis, University of Manchester (1969).

63. Jeffreys, G.V., Chem. and Proc. Eng., 49, 111 (1968).

64. Treybal, R.E., Hayworth, C.B., Ind. Eng. Chem. 42, 1174 (1950).

65. Null, R., Johnson, H.E., Am. Inst. Chem. Eng. J. 4, 273 (1958).

66. Brown, W.D. et al. Am. Chem. Soc. Jnl. 41, 499, (1919).

67. Ryan, J.T., Ph.D. Thesis, Univ. of Missouri, (1966).

68. Kintner, R.C., Hu, S., Am. Inst. Chem. Eng. J. 1, 42, (1955).

69. Rao, E.V.L.N. et al, Chem. Eng. Sci. 21, 867, (1966).

70. Heertjes, P.M., De-Nie, L.H., De Vries, H.J., Ibid. 26, 441,(1971).

71. Izard, J.A., Am. Inst. Chem. Eng. J. 18, 1634, (1972).

72. Scheele, G.F., Meister, B.J. Ibid, 14, 9, (1968).

73. Vashist, P.N., Ph.D. Thesis, Univ. of Maryland, (1970).

74. Reman, G.H., Chem. Eng. Prog. 62, 56, (1966).

75. Kallansandram, C.V. et al, Tech. Report No.CE/673, Ind. Inst. of Bauglore (1967).

76. Al-Hemeri, A.A., Ph.D. Thesis, University of Aston (1973).

77. Smith, S.W.J., Moss, H., Proc. Roy. Soc. A.93, 373, (1917).

78. Tyler, E., Watkins, F., Phil. Mag. 14, 849, (1932).

79. Onnesorge, G., S. Angew Math. U. Mech. 16, 355, (1936).

80. Merrington, A.C., Richardson, E.G., Pro. Phy. Soc. 59, 1,(1947).

81. Funijawa, A.K. et al, Kagaku Kikai (Japan), 21, 21 (1957).

82. Christiansen, R.M., Hixon, N., Ind. Eng. Chem. 49, (6),1017,(1957).

83. Rayleigh, Lord, Proc. Roy. Soc. (London), 29, 71, (1879).

84. Ibid 49, 321,(1899)

85. Perrut, M., Loutaty, R., Chem. Eng. J., 3, 286, (1972).

86. Scheele, G.F., Meister, B.J., Am. Inst. Chem.Eng. J., 15, (5), 700, (1969).

87. Shiffler, D.A., Ph.D. Thesis, Cornell University (New York),(1965)

88. Allak, A.M.A., Ph.D. Thesis,Aston University (1973).

89. Licht, N., Conway, J.B., Ind. Eng. Chem. 42, 1151, (1950).

90. Hadmard, J.S., Compt. Rend. Acad. Sci., 152, 1735, (1911).

91. Rybczinski, W., Bull. Acad. Sci. Cracovie. Scr.A. 40, (1911).

92. Bond, W.N., Phil. Mag. 4 (7), 24, 889-98, (1927).

93. Bond, W.N., Newton, D.A., ibid, 5, 794-800, (1928).

94. Hughes, R.R., Gilliland, E.R., Chem. Eng. Prog. 48, 497-504 (1952).

95. Spells, K.E., Proc. Roy. Soc. (London), 65B, 541 (1952).

96. Johnson, A.I., Braid, L., Canada J. Chem. Eng., 35, 165-72, (1957).

97. Light, W., Narasimhamurty, G.S.R., A.I.Ch.E. Jnl., 1, 336-73, (1955).

98. Klee, A.J., Treybal, R.E., Ibid, 2, 444-7, (1956).

99. Strom, J.R., Kintner, R.C., A.I.Ch.E. Jnl., 4, 153-6 (1958).

100. Krishna, P.M. et al, J. Chem. Eng. Data, 4, 336 (1959), 4, 340, (1959).

101. Elizinga, E.R., Banchero, J.T., A.I. Ch.E. Jnl., 7, 394-9, (1961).

102. Hu, S., Kintner, R.C., ibid, 1, 42-8, (1955).

103. Hamieliee, A.E., Johnson, A.I., Canada. J. Chem. Eng., 40, 51-5, (1962).

104. Ibid, A.I. Ch. E. Jnl., 13, (2), 220-61, (1967).

105. Thorsen, G. et al, Chem. Eng. Sci., 23, 413-26, (1968).

106. Acrivos, A., Taylor, T.D., ibid, 19, 445-51, (1964).

107. Brenner, H., Ibid., 19, 519-39, (1964).

108. Hendrix, C.D. et al, A.I.Ch.E. Jnl., 13, 1072-7, (1967).

109. Warshay, M.E. et al, Canada. J. Chem. Eng. 37, 29-36, (1959).

110. Harris, D.K., Ph.D. Thesis, Univ. of Maryland, U.S.A. (1970).

111. Ragchavendra, N.M., Rao, M.N., Indian J. Tech. 3, (10), 303, (1965).

112. Gal, O.A.B., Waslo, S., Chem. Eng. Sci. 23, 1431, (1968).

113. Mhatre, M.V., Kintner, R.C., Ind. Eng. Chem. 51, 865, (1959).

114. Kintner, R.C., Advances in Chem. Eng., 4, 52.92, (1963).

115. Schroeder, R.R., Kintner, R.C., A.I. Chem. Jnl., 11, (5), (1965).

116. Kintener, R.C., ibid, 530-34.

117. Lamb, H., "Hydrodynamics", 6th Edit., 473, Dover, N.Y.

118. Rose, P.M., Ph.D. Thesis, Ill. Inst. of Tech., (1965).

119. Brunson, R.J., A.I. Ch. E. Jnl., 19, (4), 858, (1973).

120. Hinze, J.O., Am. Inst. Ch.E. Jnl, 1, (3), 289, (1955).

121. Kolmogoroff, A.N., Compt. Rend. Acad. Sci. USSR, 30, 301, (1941).

122. Ibid, Dokabidy Akad. Nauk, USSR, 66, 1825, (1949).

123. Heertjes, P.M., Chem. Eng. Sci. 3, 122, (1954).

124. Jeffreys, G.V., Lawson, G.B., Trans. Instn. Chem. Eng. 43, 1294, (1965).

125. Shinnar, R., Church, J.M., Ind. And. Eng. Chem. 52, (3), 255, (1969).

126. Tomotika, S., Proc. Roy. Soc.(Lond)., A.153, 302, (1936).

127. Cockbain, E.G., Roberts, T.S., J. Colloid Sc. 8, 440, (1953).

128. Gillespie, T., Rideal, E.V., Trans. Faraday Soc., 52, 173, (1956).

129. Elton, G.A.H., Picknett, R.G., "Proc. 2nd Int. Eng. Surface Activity", 1, 288, (1957).

130. Jeffreys, G.V., Hawksley, J.L., Am. Inst. Chem. Eng. Jnl. 11, 413, (1965).

131. Jeffreys, G.V., Lawson, G.B., Trans. Instn. Chem. Engnrs., 43, 294, (1965).

132. Davies, J.T., Advances in Chemical Eng., Academic Press, 4 , (1963).

133. Hittit, A., Ph.D. Thesis, Aston University, (1972).

134. Mc Avoy, P.H., Kintner, R.C., J. Colloid Sc. 20, 188 (1965).

135. Jeffreys, G.V., Davies, G.A., "Advances in L/L Extraction", Edited by Hanson.

136. MacKay, G.D.M., Mason, S.G., J. Colloid Sci. 18, 674, (1963).

137. Princen, H.M.,J. Colloid Sci., 18, 178, (1963).

138. Murdoch, P.G., Leng, D.E., Chem. Eng. Sci. 26, 1881, (1971).

139. Scheele, G.F., Leng, D.E., Chem. Eng. Sci., 26, 1867, (1971).

140. Robinson, J., Hartland, S., I.S.E.C. Paper, No.56, (1971).

141. Cited in reference 76.

142. Sherwood, T.K. et al, ibid, 31, 1144, (1939).

143. West, F.B. et al, ibid, 43, 234, (1951).

144. Angelo, B. et al, A.I. Ch.E. Jnl., 12, (4), 751, (1966).

145. Heertjes, P.M., De Nie, L.H., Chem. Eng. Sc., 21, 755, (1966).

146. Sawistowski, H.,Goltz, G.E., (1963), Trans. Instn. Chem. Engrs. 41, 174, (1963).

147. Light, W., Pansing, W.F., Ind. Eng. Chem. 45, 1885, (1953).

148. Ilkovic, D., Coll. Czech. Chem. Commun., 6, 498, (1934).

149. Coulson, J.M., Skinner, S.J. Ibid, 1, 197, (1952).

150. Groothius, H., Kramer, H.,ibid, 4, 17, (1955).

151. Skelland, A.H.P., Minhas, S.S., A.I.Ch.E. Jnl., 17, (6), 1316, (1971)

152. Heertjes, P.M., De Nie, L.H., Recent Advances in L/L Extraction, Edited by Hanson, (1971).

153. Rajan, S.M., Heideger, W.J., Aiche E Jnl. 17, (1), 202, (1971).

154. Popovich, A.T., Jarvis, R.E., Trans. O Chem. Eng. Sci. 19, 357, (1964).

155. Heertjes, P.M. De Nie, L.H., Chem. Eng. Sci., 26, 697, (1971).

156. Johnson, Cited in Ref. 76.

157. Marsh, B.D., Heideger, W.J., Ind. Eng. Chem. Fundtls. 4, 129, (1965).

158. Newman, A.B., Trans. Am. Inst. Chem. Engrs. 27, 310, (1931).

159. Kroing, R., Brink, J.C., Appl. Scient. Res. A2, 142, (1960).

160. Handlos, A.E., Baron, T., A.I. Ch.E., Jnl., 3, 127, (1957).

161. Rose, Kintner, R.C., ibid 12, 3, 531 (1966)

162. Johnson, A.J., Hamielec, A.E., (1960), A.I.Ch.E. Jnl. 6,(1),145, (1960).

163. Linton, M., Sutherland, K.L., Chem. Eng. Sci., 12, 214, (1960).

164. Rowe, P.N. et al, Trans. Instn. Chem. Engnrs. 43, 14, (1965).

165. Kinard, G.E. et al, Brit. Chem. Eng. 8, 326, (1963).

166. Griffiths, R.M., Chem. Eng. Science, 12, 198, (1960).

167. Tayeban, H., Garner, F.H., An. Roy. Soc. Esp. Fis. Quinn 56B, 37, 479, (1960).

168. Garner, F.H., Lane, I.J., Trans. Instn. Chem. Engnrs. A62, (1959).

169. Hughmark, G.A., Ind. Eng. Chem. Fund, 6, 408, (1967).

170. Elzinga, E.R., Banchero, J.T., A.I. Ch.E. Jnl. 7, 1394, (1961).

171. Hendrix, C.D. et al, ibid, 13, 1072, (1967).

172. Angelo, J.B., Lightfoot, E.N., ibid, 14, (4), 531, (1968).

173. Baynens, C.A., Laurence, R.L., Ind. Eng. Chem. Fund., 8, 71,(1969).

174. El-Defrawi, Heideger, W.J., A.I.Ch.E. Jnls, 9, (1), 180, (1973).

175. Todd, D.B., Chemical Eng. July 24, 156, (1972).

176. Todd, D.B., I.S.E.C. (1974).

177. Barson, N., Beyer, G.H., Chem. Eng. Prog. 9, 5, 243 (1953).

178. Morgenthaler, J.H., et al, Atomic Energy Comm. Rept. KT110 (1951).

179. Takamatsu, Takahashi, Shofi, Chem. Eng. (Japan) 20, 9 (1958).

180. ibid 20,92,297, (1956).

181. Safanov, A.I., Krylov, V.S., Teoreticheskie, Osnovy. Khim. Tekh, 7, 238, (1953).

182. Kochin, N.E., et al. Theoretical Hydromechanics (in Russian), Part 1, Gostekhizdat, Moscow (1948).

183. Hayes, W.D. et al, A.I.Ch.E. Jnl. 5, 319, (1959).

184. Doyle, C.M. et al, A.I. Ch.E. Meeting, St. Louis Mo. (1968).